Optimum lay-up design of variable stiffness composite structures

Optimum lay-up design of variable stiffness composite structures

Proefschrift

ter verkrijging van de graad van doctor
aan de Technische Universiteit Delft,
op gezag van de Rector Magnificus, Prof. ir. K.C.A.M. Luyben,
voorzitter van het College voor Promoties,
in het openbaar te verdedigen op maandag 14 november 2011 om 15:00 uur

door
Julien Marie Jan Ferdinand VAN CAMPEN
ingenieur Luchtvaart en Ruimtevaart
geboren te Nijmegen

Dit proefschrift is goedgekeurd door de promotor:

Prof. dr. Z. Gürdal

Copromotor: C. Kassapoglou, M.Sc.

Samenstelling promotiecommissie:

Rector Magnificus	Voorzitter
Prof. dr. Z. Gürdal	Technische Universiteit Delft, promotor
C. Kassapoglou, M.Sc.	Technische Universiteit Delft, copromotor
Prof. dr. ir. F. van Keulen	Technische Universiteit Delft
Prof. dr. V. Toropov	University of Leeds
Prof. dr. P. Ermanni	Eidgenössische Technische Hochschule Zürich
Prof. dr. O.T. Thomsen	Aalborg University
Prof. dr. S. Hernández	University of La Coruña
Emeritus Prof. dr. A. Rothwell	Technische Universiteit Delft, reservelid

KEYWORDS:

Automated Fibre Placement, Design Tailoring, Laminate Blending, Laminated Composites, Stacking Sequence Design, Variable Stiffness Composites

This work was financially supported by the AUTOW project, part of the European Union Sixth Framework Programme, Project no. 030771.

ISBN: 978-90-9026426-4

Printed by: Wöhrmann Print Service, Zutphen, the Netherlands

To my loving parents

PREFACE

The work presented in this thesis forms part of a larger research effort at the Aerospace Structures and Computational Mechanics (ASCM) group, of the faculty of Aerospace Engineering at the TU Delft, to develop design and optimisation techniques for variable stiffness (VS) fibre-placed composite laminates. One of the techniques under development is a two-step optimization approach for VS composite laminates. The first step of this approach is to optimise a VS composite structure in terms of lamination parameters (LP), in the second step the LP design is converted into a lay-up design. A possible second step, to convert an LP design into a lay-up design, is presented in this thesis. The objective of this work was to investigate the methods available in the literature and to develop new methods to obtain the optimal VS lay-up design for a given LP design of a VS composite laminate that satisfies prescribed manufacturing constraints. The work presented in this thesis is divided into three parts to fulfil this objective:

- the conversion of LPs into a lay-up design
- the design of blended composite lay-ups
- the design of fibre-steered composite lay-ups

The reasoning behind this division is that, after a design in terms of LPs is converted into a design in terms of fibre angles, there are two possible ways to arrive at a variable stiffness laminate design: laminate blending or fibre steering. Eventually laminate blending and fibre steering may be combined, but this is beyond the scope of the present work.

ACKNOWLEDGMENTS

I am writing these acknowledgements after reaching the end of a more than four year long journey, which officially started on 1 March 2007. It has been a bumpy ride at times, which in retrospect, made the experience all the more worthwhile and valuable; I would not have learned as much if it had been a walk in the park. I am very fortunate to have had Zafer Gürdal as my advisor, the man who inspired me to pursue a Ph.D. degree in the first place. The experience has been exhilarating, both on a professional and a personal level. I am also very thankful for the guidance and support of Christos Kassapoglou, both as a colleague and a friend. His feedback proved very valuable for the work presented in this thesis and our cooperation was very pleasant. I would also like to thank Professor Hernández, Professor Thomsen, Professor Ermanni, Professor Toropov and Professor Van Keulen for their serving on my committee. I would like to thank Professor Rothwell for being a reserve member for my committee and Professor Fokkema for chairing my committee. Furthermore, I would like to acknowledge that part of the work presented in this thesis has been financially supported by the AUTOW project, part of the European Union Sixth Framework Programme, Project no. 030771.

My time with the Aerospace Structures group started at the end of 2003 when I enrolled for the Master's programme (before prof. Gürdal entered the scene). It is a strange feeling to be leaving the group after almost eight years, and there are many people I would thank for the pleasant times we spent together. First and foremost the secretaries: Annemarie, Angela, Colette, and of course Laura, it has been my pleasure working with them, if anything they made me appreciate the value of having a good secretary at your side. Then the staff members: professor Arbocz, thank you for the nice talks we had together. To Jan, thank you for his time and patience. To Gillian, thank you for her interesting insights into faculty politics. To Mostafa, thank you for all the Monty Python videos. To Louis, thank you for all the jokes. To Eddy, thank you for the nice chats and the music. To Roeland, I believe I still owe him a crate of beer, for Belgium still has not fallen apart . . . yet. To Markus, thank you for the nice chats. To Sergio, thank you for the lively discussions over lunch, and to Akke, thank you for the good advice. My partner in crime and office mate, Sam, I really enjoyed our cooperation. Then for my other office mates: Ahmad, Christian, Attila, Ali, Sonell, it was my pleasure to share an office with you, we definitely had some good times. And not to forget all of my other (former) fellow Ph.D. students: Agnes, Claudio, Glenn, Mathieu, Terry, Johannes, Pooria, Sourena, Mohamed, Noah, Farid and Martin, some of whom became good friends over the years.

With my Ph.D. also my time in Delft comes to an end. I am definitely going to miss the town of Delft, and it definitely would not have been the same without my housemates: Laurens, Robin, DJ, Vincent, "Andreas", Frank and Michele. It

also would not have been the same without Formula Student, first as a member of the DUT Racing team, and later as one of the volunteers for Formula Student Germany (it is a virus you cannot get rid off once you become infected).

After four years of absence, I have now returned to Ulm. My sincere gratitude goes out to Robert Bjekovic for convincing me to follow "my own star" and to Jan Krüger for making it happen. Thomas, Klaus, Martin, Ines, Joachim and Daniel, thank you for making me feel right at home.

I am eternally indebted to my parents, without their love and support I would not be where I am today. This thesis is for them. Also I would like to thank my sister and brother, Jasmijn and Laurens, for serving as "paranimfs" during my thesis defence, and also for their unconditional support. If knew no better, I could almost say I infected both of them with the Ph.D. virus. At this point I would like to acknowledge my brother in law Thijs and of course my niece Bente. I cannot express how very proud I am to be her godfather. I had hoped to be able to give a copy of my thesis to my grandfather Jan. Alas this was a bridge too far.

Finally, I would like to thank Miranda Aldham-Breary for reading and re-reading my thesis and for correcting my English, but above all for teaching me how to write good scientific English. A very special thanks goes to Alia Pierce for correcting these acknowledgements.

Ulm, October 2011

SUMMARY

In contemporary composite design researchers are striving to find the arrangement of material constituents that best satisfies a posted set of requirements with respect to strength, stiffness, cost and/or weight. Conventionally in composite laminate design the fibre orientation angles are taken from the set $\{0°/+45°/-45°/90°\}$ and kept constant throughout an entire ply of the laminate. Additionally, the number of plies in the laminate is limited to a discrete number, and design rules like the 10%-rule must be obeyed. As a result, the directional properties of a laminate are not used to their full potential in most design cases, i.e the performance of the laminate can be improved in terms of e.g. weight, cost, stiffness and/or strength. Improvements can be brought about by modification of the stacking sequence within the bounds of conventional design rules, this is referred to as laminate tailoring. This classical form of laminate tailoring can be aided by increasing the range of fibre orientation angles that can be used.

The advent of advanced fibre-placement (AFP) technology makes it possible to take laminate tailoring further than just stacking sequence optimisation; it enables the designer to vary the fibre orientation angle within each ply of the laminate spatially. Spatial variation of fibre orientation angles results in a variable stiffness (VS) laminate. The work presented in this thesis constitutes a possible second step of a two step design process to design VS composite structures. The first step of this approach is to optimise a VS composite structure in terms of lamination parameters (LP), in the second step the LP design is converted into a lay-up design. The objective of the work presented here was to investigate the methods available in the literature to convert LPs into lay-up designs and to develop new methods to obtain an optimal VS lay-up design for a given LP design of a VS composite laminate that satisfies prescribed manufacturing constraints. The work presented in this thesis was divided into three parts as a means to achieve the above objective:

- the conversion of LPs into a lay-up design
- the design of blended composite lay-ups
- the design of fibre-steered composite lay-ups

Composite lay-ups with a discrete number of equally thick layers were considered in this thesis. The mathematical definition of the lamination parameters description was used to determine which part of the feasible LP domain could be described by a laminate of a given discrete number of equally thick layers and a lay-up configuration. It was shown that this part of the feasible LP domain converges to the full theoretical feasible domain as the number of layers in the laminate goes to infinity. The rate of convergence towards the full feasible domain

was found to be larger for flexural LPs than for in-plane LPs. It was proven that the part of the feasible domain that can be described by this lay-up is a fractal, which is additional proof that the part of the feasible domain described by such a practical laminate converges to the full theoretical feasible LP envelope.

A semi-analytical approach was developed to convert LPs into a lay-up design, but it was concluded that this approach could not be expanded to more than two designed fibre orientations in the laminate, which would exclude a larger part of the feasible LP domain from the conversion process. Therefore, a two-step approach to convert LPs into a lay-up design was developed which could be expanded to deal with any arbitrary number of designed fibre orientation in the laminate. The developed two-step approach consisted of a genetic algorithm (GA) used to explore the design space and a gradient-based optimiser used to converge the outcome of the GA to a final lay-up design. The design objective used for the GA and the gradient-based optimiser was the least-squared distance in LP-space between the desired set of LP-values and the LP-values computed for the laminate. Constraints on e.g. the 10%-rule for robustness of the laminate design, could be implemented using an augmented objective function formulation. The two-step approach was proven to be able to match any set of LP values with a laminate design, provided the number of layers in the laminate was chosen to be large enough. The approach was tested for several combinations of LPs, and consistently better results were found for larger values of the number of layers in the laminate.

One way to create a variable stiffness laminate is to divide a structure into several segments and then determine the optimum lay-up for each segment. The manufacturing constraints which are quintessential to multi-segment laminate design are discussed and the concept of laminate blending is presented, laminate blending is needed to guarantee the structural integrity of the laminate design. A non-intrinsically blended, multi-step blending implementation was developed for the implementation of two new blending definitions: generalised blending and relaxed generalised blending. The implementation used a multi-chromosomal genetic algorithm (GA), following the principle of guide-based blending. A guiding laminate stack was encoded using one chromosome. Determining which plies are taken from the guiding stack is done by an additional chromosome for each segment in the structure. The fact that the designs could be represented using the multi-chromosomal GA, which are not blended, made the implementation non-intrinsically blended. Therefore, it was proposed that a repair strategy for the GA was implemented to guarantee that fully blended laminate designs would be obtained.

The proposed blending definitions were then used to design an 18-panel structure with a horseshoe configuration, a panel with two concentric lay-ups loaded in compression and a square VS panel which was designed using LPs. No satisfactory results could be obtained for the horseshoe panel configuration, which was suggested to be an artefact of the use of a single objective function value

to capture a laminate design with many segments. The repair strategy used to enforce laminate blending was identified as an other likely cause of the observed behaviour. The results obtained for the VS panel verified that the performance of the optimiser deteriorates when the number of segments in the structure was increased. A negative effect of the repair strategy of the genetic coding to enforce blending could not be verified, and further investigation of the implementation of the two new blending definitions was recommended.

Varying the in-plane fibre orientation angles within a laminate is a more refined way to design VS composite structures than using laminate blending. All the LP distributions considered for conversion into a lay-up design discussed in this thesis were defined on a finite element (FE) grid. Direct conversion from LPs into stacking sequence designs, led to a stacking sequence design for each node of the FE grid. Therefore, a method was developed to estimate the in-plane curvature of such a nodal fibre angle distribution, such that fibre angle curvature could be subsequently constrained.

A cellular automaton (CA) was developed to enforce manufacturing constraints, like the constraint on in-plane curvature on the initial fibre angle design obtained by converting a given optimum LP distribution into a least-square optimal stacking sequence distribution. The CA used Jacobi iteration to conserve the possible symmetry of the initial fibre angle design, or seed. Two objective functions were used in combination with the CA, the average least-square error in LP space between the obtained VS lay-up and the optimum LP distribution, and an objective function based on an estimate of the buckling load of the structure obtained via sensitivity information, if available. Manufacturing constraints were entered into the CA via an augmented objective function formulation. The results obtained using the CA were found to be consistent and scalable, and that, for small values of the constraint on curvature, the design would converge towards the best-known constant stiffness (CS) design.

How the nodal fibre angle distribution per ply in the laminate can be converted into fibre paths which are fit for production using automated fibre placement (AFP) technology was discussed. A streamline approach was adopted for the work presented in this thesis after a survey of the available literature on the subject of path generation. The advantage of the streamline analogy was that it also provides an estimate of the smeared thickness of the laminate, based on the notion that thickness variation in the laminate results from overlapping fibre paths. It was shown how the LP distribution of the laminate, including the effect of thickness variation and the change in volume of the laminate due to thickness variation, could be computed. The fibre path designs obtained appeared to be manufacturable.

The method developed to convert an optimum LP design for a structure into an optimum VS lay-up design that satisfies a constraint on curvature was discussed using four exemplar structures. Results were generated for two different design

objectives: the average least-square error in LP-space and a sensitivity-based estimate of the buckling load of the structure. The results showed that the proposed conversion process generated consistent designs for different geometries and loading conditions, and nearly identical results were found for both design objectives. It was observed that relative differences between the in-plane distributions of the in-plane and flexural LPs manifest in the relative amount of curvature of the more inward plies in a laminate compared to the curvature of the more outward plies of a laminate, because the in-plane LPs are equally affected by all layers in the laminate, whereas the flexural LPs are more strongly affected by the outward plies of the laminate. The effect the constraint on in-plane fibre curvature had on the performance of the structure, the maximum thickness of the structure due to overlapping fibre paths, the volume of the structure, and the buckling load of the structure when thickness variation due to overlapping fibre paths was taken into account was studied. The buckling load of a structure was found, as expected, to show an increasing trend as the constraint on in-plane curvature was relaxed. Increasing the number of layers in the laminate also had a positive effect on the buckling load value, which became more pronounced when the constraint on in-plane curvature was relaxed further.

The maximum thickness in the laminate and the normalised volume of the laminate also increased when the constraint on in-plane curvature was relaxed. Significant improvements in buckling load value were found when the thickness variation due to overlapping fibre paths was taken into account with a few exceptions for designs without a constraint on in-plane curvature.

The case where only one designed layer in the laminate was considered, consistently showed slightly different trends from the cases where multiple designed layers in the laminate were considered. The buckling load values that were obtained for small values of the curvature constraint were found to be higher. It was concluded that this resulted from the CA converging to a local optimum, rather than to a global optimum, for the designs where multiple layers were considered.

To conclude, it is possible to convert any given combination of lamination parameters successfully into a lay-up design, provided the number of equally thick plies in the laminate is chosen large enough. When converting the LP distribution for a VS laminate, the structural performance of the lay-up design obtained was found to be very close to the structural performance of the LP optimum.

It was shown how the different lay-ups in a VS composite structure could be combined to form a coherent whole using laminate blending. The design of a VS composite structure was proved to be more successful when fibre steering was used, though the design of fibre paths, such that the performance of the laminate was not negatively affected by thickness build-up in the laminate due to gaps and overlaps between neighbouring tows, remains an issue, and further research is required. A long-term goal would be to combine fibre steering and laminate blending to obtain a unified design approach for variable stiffness composite lay-

ups.

A flexible computational tool set has been developed which can be used to convert a variable stiffness composite design given in terms of lamination parameters into an optimal variable stiffness lay-up design. Test results obtained using the developed tools show that it is possible to convert a lamination parameter design into a fibre angle design which very closely approaches the mechanical properties of the optimum lamination parameter design.

SAMENVATTING

Heden ten dage streven onderzoekers van composietmaterialen ernaar om een materiaalrangschikking te vinden die het beste aan de gestelde eisen wat betreft sterkte, stijfheid, kosten en/of gewicht voldoet. In conventioneel laminaatontwerp wordt de oriëntatie van elke laag gekozen uit de set $\{0°/+45°/-45°/90°\}$, en is deze constant voor de gehele laag. Daarbij komt dat het aantal lagen in een laminaat gelimiteerd is tot een eindig aantal discrete lagen, en dat ontwerpregels, zoals bijvoorbeeld de 10%-regel, gerespecteerd dienen te worden. Dientengevolge worden de eigenschappen van het composiet materiaal in de meeste ontwerpgevallen onvolledig benut; er is ruimte voor verbetering wat betreft bijvoorbeeld gewicht, kosten, stijfheid en/of sterkte. Zulke verbeteringen kunnen bewerkstelligd worden door modificatie van de stapelvolgorde van de lagen binnen de grenzen van de conventionele ontwerpvoorschriften, dit wordt het op maat maken van het laminaat genoemd. Deze klassieke vorm om laminaten op maat te maken kan uitgebreid worden door het vergroten van de set vezeloriëntaties waaruit gekozen kan worden.

De komst van geavanceerde vezelplaatsingstechnologie maakt het mogelijk om met het op maat maken van een laminaat nog een stap verder te gaan dan alleen de optimalisatie van de stapelvolgorde; het stelt de ontwerper in staat om de vezeloriëntatie in elke laag van het laminaat ruimtelijk te variëren. Ruimtelijke variatie van de vezelhoekoriëntatie resulteert in een laminaat met variable stijfheid (VS). Het werk dat in dit proefschrift wordt beschreven vormt een mogelijke tweede stap van een twee-stapsaanpak voor het ontwerp van VS composieten constructies. De eerste stap van deze aanpak is de optimalisatie van een VS composieten constructie met behulp van laminatieparameters (LP), in een tweede stap wordt het LP ontwerp geconverteerd in een ontwerp voor een stapelvolgorde van het laminaat. Het doel van het werk dat hier beschreven wordt, was om de in de literatuur voorhanden methodes om LP's in een stapvolgorde-ontwerp te converteren te onderzoeken en om nieuwe methodes te ontwikkelen voor het verkrijgen van een optimaal VS stapelvolgorde-ontwerp voor een gegeven LP ontwerp van een VS composietlaminaat dat voldoet aan door productiemogelijkheden opgelegde beperkingen. Het in dit proefschrift beschreven werk kan in drie stappen opgedeeld worden die nodig zijn om de bovengenoemde doelstelling te verwezenlijken:

- de conversie van LP's in een stapelvolgorde-ontwerp
- het ontwerp van gemixte laminaten
- het ontwerp van vezelgestuurde stapelvolgorde-ontwerpen

Voor het werk in dit proefschrift werden alleen laminaten met een discreet aantal lagen van gelijke dikte verondersteld. De wiskundige definitie van laminatieparameters werd gebruikt om vast te stellen welk deel van de enveloppe die alle

LP's omsluit beschreven kan worden door een laminaat met een gegeven aantal lagen van gelijke dikte en stapelvolgordeconfiguratie. Het is aangetoond dat het gedeelte van de LP enveloppe dat beschreven kan worden convergeert naar de volledige theoretische enveloppe als het aantal lagen oneindig wordt. De convergentie voor de LP's die buiging beschrijven was sneller dan voor de LP's de laminaateigenschappen in het vlak van het laminaat beschrijven. Het is aangetoond dat het deel van de LP enveloppe dat beschreven kan worden door een dergelijke stapelvolgorde een fractaal is, hetgeen bevestigt dat het gedeelte van de LP enveloppe dat door een dergelijk laminaat beschreven kan worden zal convergeren naar de volledige theoretische enveloppe voor een voldoende aantal lagen.

Een semi-analytische aanpak werd ontwikkeld om LP's in een stapelvolgordeontwerp te converteren, maar hieruit werd geconcludeerd dat deze aanpak niet kon worden uitgebreid voor de conversie van een laminaat met meer dan twee ontworpen vezeloriëntaties, hetgeen een groot gedeelte van de LP enveloppe zou uitsluiten voor conversie in een stapelvolgorde-ontwerp. Daarom is een tweestapsaanpak ontwikkeld die voor elk willekeurig aantal lagen kan worden gebruikt. Deze aanpak bestaat uit een genetisch algoritme (GA) dat gebruikt wordt om het ontwerpdomijn te verkennen, en een op afgeleiden gebaseerd optimalisatie algoritme om het uiteindelijke stapelvolgorde-ontwerp te vinden op basis van de uitkomst van het GA. Voor zowel het GA als de afgeleide gebaseerde optimalisatie is de kleinste-kwadraten afstand gebruikt tussen de gewenste LP waarden en de LP waarden berekend voor het laminaat. Randvoorwaarden, zoals bijvoorbeeld de 10%-regel voor een robuust ontwerp, konden geïmplementeerd worden met behulp van een uitgebreide objectfunctieformulering. De aanpak is getest voor meerdere LP-combinaties, en zonder uitzondering werden betere resultaten gevonden wanneer meer lagen in het laminaat werden verondersteld.

Een manier om een laminaat met variabele stijfheid te ontwerpen is onderverdeling van de constructie in meerdere segmenten waarbij voor elk segment de optimale stapelvolgorde wordt bepaald. De door de productie opgelegde beperkingen die van het grootste belang zijn om een multi-segment laminaat te ontwerpen worden uiteengezet en het concept van laminaatmixen wordt gepresenteerd, laminaatmixen is noodzakelijk om de structurele integriteit van een laminaatontwerp te kunnen garanderen. Een niet-intrinsiek gemixte, meer-staps laminaatmiximplementatie is ontwikkeld om twee nieuwe mixdefinities toe te kunnen passen: algemeen mixen en ontspannen algemeen mixen. De ontwikkelde implementatie maakt gebruik van een multi-chromosoom genetisch algoritme (GA), volgens het principe van gids gebaseerd mixen. Een gids laminaatopbouw wordt hierin gecodeerd door één enkel chromosoom. Door een tweede type chromosoom voor elk segment in de constructie wordt bepaald welke lagen van de gids gebruikt worden voor de laminaatopbouw in het segment in kwestie. Deze methode is niet intrinsiek gemixt omdat de representatie van een constructie in de vorm van een multi-chromosomaal individu ook niet gemixte ontwerpen toestaat. Daarom is een reparatiestrategie ontwikkeld voor het GA om het ontwerp van volledig

gemixte laminaten te kunnen garanderen.

De geïntroduceerde mixdefinities werden gebruikt voor het ontwerp van een constructie met 18 panelen geconfigureerd in de vorm van een hoefijzer, een paneel met twee concentrische segmenten in compressie, en een vierkant VS paneel ontworpen met behulp van LP's. Er konden geen tevredenstemmende resultaten verkregen worden voor het hoefijzerpaneel, hetgeen toegeschreven werd aan het gebruik van een enkele objectfunctie om het gedrag van vele segmenten te vangen. Een andere mogelijke oorzaak werd gevonden in de reparatiestrategie. De waarneming dat de prestaties van de mixoptimalisatie verslechteren naarmate meer segmenten in de constructie worden geïntroduceerd werd bevestigd door de resultaten voor het VS paneel. Een negatief effect van de reparatiestrategie kon niet geverifieerd worden, en verder onderzoek naar de implementatie van de twee nieuwe mixstrategiën wordt aanbevolen.

Vezelhoekvariatie in het vlak is een verfijndere manier dan laminaatmixen om een VS composieten constructie te ontwerpen. Alle LP verdelingen die gebruikt zijn voor conversie in een stapelvolgorde-ontwerp in dit proefschrift, waren gegeven op een eindige elementen (EE) grid. De directe conversie van LP's naar stapelvolgorde-ontwerp, leidde dus tot een stapelvolgorde-ontwerp voor elk knooppunt in het EE grid. Daarom is een methode ontwikkeld om de kromming in het vlak van een op knooppunten gebaseerde vezelhoekverdeling te schatten, en wel zo dat het mogelijk is om achtereenvolgens een randvoorwaarde voor kromming op te kunnen leggen.

Een cellular automaton (CA) is ontwikkeld om randvoorwaarden voor de productie, bijvoorbeeld voor de vezelkromming in het vlak, op te kunnen leggen op het vezelhoek ontwerp dat verkregen was door een directe conversie van LP's naar vezelhoeken. Het CA maakte gebruik van Jacobi iteratie opdat mogelijke symmetrie in de initiële vezelhoekverdeling behouden zou blijven. Voor het CA zijn twee verschillende objectfuncties gebruikt: de gemiddelde kleinste-kwadraten fout in LP's tussen de LP's van het VS laminaat en de optimum LP's, en schatting van de kniklast van de constructie verkregen middels sensitiviteit informatie, indien voorhanden. Productie beperkingen werden in acht genomen door middel van een uitgebreide objectfunctieformulering. De resultaten die met behulp van het CA zijn verkregen zijn consistent en kunnen geschaald worden, en tonen aan dat voor kleine waardes van de toelaatbare vezelhoekkromming het vezelhoekontwerp naar het beste constante stijfheids (CS) ontwerp convergeert.

Een literatuurstudie is uitgevoerd hoe een vezelhoekverdeling per knooppunt omgezet kan worden in vezelpaden die door middel van een geautomatiseerde vezelplaatsingstechnologie geproduceerd kunnen worden. Aan de hand van deze literatuurstudie is voor het werk in dit proefschrift voor een stroomlijnaanpak gekozen. Het voordeel van de stroomlijnanalogie is dat deze ook gebruikt kan worden om de uitgesmeerde dikte van de vezelpaden af te schatten, gebruikmakend van het feit dat diktevariatie een voortvloeisel is van overlappende vezelpaden. Het is

aangetoond hoe de LP-verdeling voor een laminaat, de effecten van dikte-opbouw, berekend kan worden. De verkregen vezelpaden lijken produceerbaar te zijn.

De ontwikkelde methode om een optimaal LP ontwerp voor een constructie te converteren in een optimaal VS laminaatopbouwontwerp dat voldoet aan een randvoorwaarde op kromming in het vlak is bestudeerd voor vier constructies. Voor twee verschillende objectfuncties zijn resultaten gegenereerd: de gemiddelde kleinste-kwadraten fout in LP's en een sensitiviteit-gebaseerde schatting van de kniklast van de constructie. Uit de verkregen resultaten bleek dat het voorgestelde conversieprocedé consistente ontwerpen produceert voor verschillende geometriën en belastingsgevallen, en nagenoeg vergelijkbare resultaten werden gevonden voor beide objectfuncties. Een observatie was dat de relatieve verschillen tussen de verdeling van de LP's die de laminaateigenschappen in het vlak beschrijven en de LP's die buigingseigenschappen beschrijven weerspiegelt in de relatieve mate van kromming van de lagen dichter bij het middenvlak van het laminaat dan de kromming van de verder naar buiten gelegen lagen van het laminaat, omdat de LP's in het vlak een gelijke invloed ondervinden van alle lagen in het laminaat, terwijl de buigings LP's de meeste invloed hebben op de buitenste lagen van het laminaat. Het effect van de toegestane vezelkromming in het vlak op de prestaties, maximum dikte door overlappende vezelpaden, volume en kniklast van de constructie voor het geval dat de dikte-opbouw wordt meegenomen is bestudeerd. De kniklast van de constructie nam, zoals verwacht, toe naar mate grotere waardes voor vezelkroming werden toegestaan. Een toename van het aantal lagen in het laminaat, bij gelijk blijvende totale dikte, had een vergelijkbaar positief effect op de kniklast, hetgeen nadrukkelijker werd voor grotere waardes voor toegestane vezelkromming.

De maximum dikte in het laminaat en het genormaliseerde volume van het laminaat namen ook toe naarmate grotere vezelhoekkromming toegestaan werd. Significante verbeteringen van de kniklast werden gevonden voor het geval dat diktevariatie ten gevolge van overlappende vezelpaden meegenomen werd in de analyse, enkele uitzonderingen daargelaten voor het geval dat er geen randvoorwaarde voor vezelhoekkromming actief was.

De gevonden trends voor het geval met slechts één ontworpen laag in het laminaat zijn consistent anders dan die voor de gevallen met meerdere ontworpen lagen. De kniklastwaarden voor kleine toegestane vezelhoekkrommingswaarden waren hoger. De veronderstelde verklaring voor dit fenomeen is dat het CA geconvergeerd moet zijn naar een lokaal optimum voor de gevallen met meerdere lagen, in plaats van naar een globaal optimum.

In conclusie is het mogelijk om elke gegeven combinatie van laminatieparameters succesvol in een laminaatopbouw ontwerp te converteren, onder de voorwaarde dat het aantal lagen van gelijke dikte in het laminaat groot genoeg gekozen wordt. De prestaties van de constructie, voor het geval dat de LP verdeling voor een VS laminaat geconverteerd werd, lagen erg dicht bij die van het optimum ontwerp in

LP's.

Hoe door middel van laminaatmixen verschillende laminaatopbouwen in een VS composieten constructie met elkaar tot een coherent geheel gevormd kunnen worden is beschreven. Het is aangetoond dat vezelsturen een succesvollere manier is een VS composieten constructie te ontwerpen. Desalniettemin blijft de constructie van vezelpaden, dusdanig dat de prestaties van het laminaat niet negatief beïnvloed worden door dikte-opbouw door gaten en overlappingen tussen aangrenzende vezelpaden een onderwerp voor vervolgonderzoek. Een doelstelling voor de lange termijn zou een combinatie van vezelsturen en laminaatmixen zijn, opdat een geïntegreerde aanpak voor het ontwerp van variabele stijfheids laminaten ontstaat.

Een flexibel numeriek raamwerk is ontwikkeld voor de conversie van een variabel stijfheids composietontwerp beschreven door laminatieparameters in een optimaal laminaatopbouwontwerp. De verkregen resultaten tonen aan dat het mogelijk is om een ontwerp beschreven in laminatieparameters te converteren in een vezelhoekontwerp dat de mechanische eigenschappen van het optimaal veronderstelde LP ontwerp zeer dicht benadert.

List of symbols

Abbreviations

AFP	Automated Fibre Placement
AUTOW	Automated Preform Fabrication by Dry Tow Placement
CA	Cellular Automaton
CLT	Classical Lamination Theory
CS	Constant Stiffness
DVZ	Design Variable Zone
FBB	Fractal Branch and Bound
FE	Finite Element
FPM	Fibre Placement Machine
G	Geometry
GA	Genetic Algorithm
LO	Layerwise Optimisation
LP	Lamination Parameter
QI	Quasi-isotropic
SL	Sub-laminate
SLB	Shared Layers Blending
TM	Tow Material
UD	Unidirectional
VS	Variable Stiffness

Greek symbols

β	Penalty term for augmented objective function
κ	Curvature, chapter 1
κ	In-plane curvature, chapter 5
κ_{all}	Allowable curvature value
λ	Critical buckling load factor
Φ	Augmented objective function, chapter 2
ϕ	Normalised coordinate, chapter 4
Ψ	Augmented objective function
σ	In-plane normal stress
τ	In-plane shear stress
θ	Fibre orientation angle

ε	Bonus term for augmented objective function
ε	In-plane strain, chapter 1
ξ	Normalised coordinate, chapter 4

Latin symbols

Q_{ij}	Components of the reduced lamina stiffness matrix
A_i	Surface area of element i
A_{ij}	Components of the in-plane stiffness matrix
B_{ij}	Components of the bending extension coupling stiffness matrix
c	Coverage ratio, chapter 4
c	Number of continuous layers, chapter 3
D	Drag, chapter 1
D_{ij}	Components of the bending stiffness matrix
E_1	Longitudinal modulus
E_2	Transverse modulus
f	Objective function
g	Constraint margin
G_{12}	Shear modulus
h	Global constraint margins
L	Lift, chapter 1
L	Length
M	Moment resultant, chapter 1
m	Number of half waves in x-direction, chapter 3
m_i	Number of stacking sequences satisfying the optimal LPs
N	Number of parts covering a segment, chapter 2
N	Number of segments in a structure, chapter 3
N	Stress resultant, chapter 1
n	Number of half waves in y-direction, chapter 3
n	Number of layers in the laminate, chapter 2
n_β	Number of violated segments
N_{cr}	Critical buckling load
nc	Number of discontinued layers
R	Loading ratio
r	Radius of curvature
S	Aspect ratio
s	Total number of stacking sequence combinations, chapter 3

T	Thickness ratio
t	Thickness of a laminate
t_c	Constant thickness value of a laminate
t_i	Thickness of element i
U_i	Material invariant properties
$V_i^{\mathbf{A}}$	Flexural lamination parameters
$V_i^{\mathbf{A}}$	In-plane lamination parameters
$V_i^{\mathbf{B}}$	Coupling lamination parameters
W	Weight, chapter 4
W	Width
z	Through-the-thickness coordinate

Subscripts

$_A$	Used to denote lay-up belonging to segment A
$_B$	Used to denote lay-up belonging to segment B
$_c$	Used to denoted corresponding lamination parameters
$_s$	Denotes a symmetric laminate
$_x$	With respect to the x-axis
$_y$	With respect to the y-axis

Superscripts

*	Denotes given optimum lamination parameters
$^{\mathbf{A}}$	Belonging to the **A** - matrix
$^{\mathbf{B}}$	Belonging to the **B** - matrix
$^{\mathbf{D}}$	Belonging to the **D** - matrix

Vectors and matrices

Γ_i	Material invariant matrices to define stiffness matrices
θ	Fibre angle vector
$\mathbf{A}$	In-plane stiffness matrix
$\mathbf{B}$	Bending extension coupling stiffness matrix
$\mathbf{D}$	Bending stiffness matrix
$\mathbf{n}$	Normal vector to local fibre angle direction
$\mathbf{P}$	Matrix to compute partial fibre angle derivatives
$\mathbf{s}$	Tangent vector to local fibre angle direction
$\mathbf{V}$	Vector of lamination parameters

Other symbols

$\mathbf{\Psi}$	Stream function
D	Hausdorf Besicovitch dimension
D_T	Topological dimension
s	Dimension along a curve
X	Metric space

Contents

What we call the beginning is often the end. And to make an end is to make a beginning. The end is where we start from.

T.S. Eliot (1888 – 1965)

1 INTRODUCTION

Structural weight plays an important role in the design of vehicles in general and in the design of aircraft in particular. Each kilogram of the weight in an aircraft must be carried by the lift, L, generated by the wings, body and tail of the aircraft to sustain steady-state flight. The drag experienced by an aircraft is a function of its lift, $D = f(L)$ (John D. Anderson 2001), hence a reduction in structural weight has a direct effect on the thrust required to propel an aircraft. Thus less fuel is needed to transport a given payload over a given distance, or more payload can be transported over the same distance for the same amount of fuel burnt, or the same payload can be transported further for the same amount of fuel burnt. All three options have clear economic advantages and it is these which drive the research of light-weight structures.

Metals have been the material of choice for aircraft for a long time, Since from the 1920's onwards the wooden aircraft was gradually replaced by the all-metal aircraft (Schatzberg 1994). The reason for making this transition from wood to aluminium design was a widespread belief in the superiority of metals over wood. For example, that metals do not splinter, nor do they warp due to changes in humidity, they do not rot, nor are they eaten by termites, their properties are more homogeneous, much better known and can be relied upon. Some of these assumptions proved to be wrong: metals do not rot, or attract termites, but they do corrode. Nevertheless, the advantages of metals outweighed the disadvantages, and over the years the all-metal aircraft was proven to be superior to the wooden.

Some parallels can be drawn between the transition from the wooden to the all-metal aircraft, and the transition from the all-metal to the all-composite aircraft. At the time, the idea of a all-metal aircraft was just as novel a concept as the idea of a full-composite aircraft is today, 2011 (Warner 1922). Many airframes already contained some metal parts before the 1920's, but it was not until the Junkers JL-6, the first all-metal passenger plane (1919), that the full-metal aircraft really took off. The use of composite materials in aircraft, in the form of resin-soaked fabrics, dates back to the very early days of aviation, but it was not until the

1960's that advanced composites appeared in aircraft structures.

Composite materials offer an advantage over metals in terms of strength-to-weight ratio and stiffness-to-weight ratio, but composite parts require a radically different design approach than that used for metal parts, as will be made apparent later in this chapter. The development of composite materials accelerated in the 1960's, and they were soon to be found in structural aircraft components, e.g. horizontal and vertical stabilizers. (Niu 1992). The development of all-composite airframes started at the beginning of the 1980's with small business aircraft, e.g. the Beechcraft Starship (1986).

The advantages offered by composite materials are partially offset by having to take into account material failure modes not known to metals, e.g. delamination; or not known to the same extent,i.e. sensitivity to moisture and heat. This leads to a conservative set of design rules for composite structures. (Kassapoglou 2010) This, in combination with the production difficulties encountered when attempting to manufacture large composite structures, meant it was not until 2005 that the first commercial airliner with a full-composite airframe was announced, the Boeing 787 (Marsh 2009).

Our understanding of composite materials in terms of their mechanical properties can still be improved, for example by exploring what today (2011) are still considered to be unconventional composite laminates in terms of fibre orientation angle and/or stacking sequence. The application of the findings of such research will not be limited to aerospace applications alone, and may benefit many other structural applications using laminated composites within transportation, e.g. cars and ships, and even civil applications, e.g. bridges (Nieto, Hernández and Jurado 2009). The ultimate goal for any composite structure is to use composite materials to their full capacity.

An overview of the available literature on the design of composite structures in general and the design of tailored composite structures in particular is given in this chapter. What laminated composites are is discussed briefly in section 1.1, followed by a discussion of the mechanics of laminated composites in section 1.2. The mechanical description of laminated composite structures can be used for their design and to optimise them for design requirements, on e.g. stiffness, strength and weight. Design and optimisation of laminated composites is the subject of sections 1.3 and 1.4, which cover conventional composite laminate design and design tailoring of laminated composites, respectively. Fibre steering is a form of laminate tailoring which became possible due to the advent of automated fibre-placement (AFP) technology, therefore AFP and the manufacturing constraints associated with it, are presented in section 1.5. The scope of the research presented in this thesis is outlined in section 1.6, and an outline of the thesis is given in section 1.7.

1.1 LAMINATE COMPOSITES

Laminated composites are constructed by layering multiple layers of fibre reinforced polymeric composite materials. These layers, commonly referred to as lamina (pl. laminae), typically consist of woven fabrics and/or unidirectional continuous fibres made out of, e.g. carbon, glass, or boron. The lamina are held together by a polymeric resin and together they form a laminate.

Unidirectional continuous fibres and most woven fabrics display orthotropic material behaviour, i.e. there are two principal material axes perpendicular to each other. The elastic stiffness and strength properties of the lamina are defined along these axes. Composite laminates have three main design variables, the number of layers of a given material, the orientation of each individual layer with respect to a fixed reference orientation, and the through-the-thickness order in which the layers are placed in the laminate, which is known as the stacking sequence of the laminate.

Changing the stacking sequence of a laminate can substantially change the in-plane and bending stiffness of the laminate, without changing its thickness, due to the directional properties of the layers in the laminate. The orientation of individual layers in the laminate with respect to a reference orientation has a direct effect on the in-plane stiffness properties of the laminate. The bending stiffness of a laminate is affected by the orientations of the layers in the laminate, and by the way they are stacked. Shuffling the relative through-the-thickness position of the layers in the laminate can yield different bending stiffness values. The stiffness properties of a laminate can thus be changed, i.e. they can be treated as design variables, this contrasts with the design of structures made of monolithic materials, which cannot be changed once chosen.

1.2 MECHANICS OF LAMINATED COMPOSITES

The basis of laminate stiffness formulation is formed by classical lamination theory (CLT). The assumption made for CLT is that a laminate comprises n orthotropic, and/or isotropic, layers which are bonded perfectly together by an infinitely thin, non-shear-deformable bondline. The bending of such a laminate is defined to follow the Kirchoff-Love pure bending assumptions. Another assumption that is made is that all layer(s) are thin compared to the in-plane dimensions of each of the respective layers in the laminate, and the stress components in the out-of-plane z-direction are assumed to be negligible, i.e it is assumed that an approximate state of plane stress prevails in the laminate. The assumptions described in the above can be used to compute the in-plane stresses for the k^{th} layer in a laminate:

$$\begin{Bmatrix} \sigma_x \\ \sigma_y \\ \tau_{xy} \end{Bmatrix}_k = \begin{bmatrix} \overline{Q}_{11} & \overline{Q}_{12} & \overline{Q}_{16} \\ \overline{Q}_{12} & \overline{Q}_{22} & \overline{Q}_{26} \\ \overline{Q}_{16} & \overline{Q}_{26} & \overline{Q}_{66} \end{bmatrix}_k \begin{Bmatrix} \varepsilon_x^\circ + z\kappa_x \\ \varepsilon_y^\circ + z\kappa_y \\ \gamma_{xy}^\circ + z\kappa_{xy} \end{Bmatrix} \quad \text{where} \quad z_{k-1} < z < z_k \tag{1.1}$$

where the k^{th} layer is positioned at the through-the-thickness location $z_{k-1} < z < z_k$, and the matrices $\overline{Q}_{ij}$ are defined as:

$$\begin{array}{ll} \overline{Q}_{11} = U_1 + U_2\cos 2\theta + U_3 \cos 4\theta & \overline{Q}_{12} = U_4 - U_3 \cos 4\theta \\ \overline{Q}_{22} = U_1 - U_2\cos 2\theta + U_3 \cos 4\theta & \overline{Q}_{66} = U_5 - U_3 \cos 4\theta \\ \overline{Q}_{16} = \frac{1}{2}U_2 \sin 2\theta + U_3 \sin 4\theta & \overline{Q}_{26} = \frac{1}{2}U_2 \sin 2\theta - U_3 \sin 4\theta \end{array} \tag{1.2}$$

The material properties of a particular layer in a laminate enter the above equation through the material invariants U_i, where θ is the angle the main material axis of the layer under consideration with a chosen reference orientation. The stresses in each layer of a laminate will either be constant or linear if the orientation of all layers in the laminate are chosen to be the same, which follows from Eq. 1.1. This stress-strain relation is complicated when several different orientations for the layers in the laminate are chosen. The in-plane stresses will then make discrete jumps at the boundary between two plies, and there is no longer a straightforward relationship between the stresses and strains of the laminate. This can be remedied by integrating in thickness direction over the in-plane stresses in the laminate, which results in the following stress and moment resultants:

$$\begin{array}{lll} N_x = \int_{-\frac{h}{2}}^{\frac{h}{2}} \sigma_x dz & N_y = \int_{-\frac{h}{2}}^{\frac{h}{2}} \sigma_y dz & N_{xy} = \int_{-\frac{h}{2}}^{\frac{h}{2}} \tau_{xy} dz \\ M_x = \int_{-\frac{h}{2}}^{\frac{h}{2}} \sigma_x z dz & M_y = \int_{-\frac{h}{2}}^{\frac{h}{2}} \sigma_y z dz & M_{xy} = \int_{-\frac{h}{2}}^{\frac{h}{2}} \tau_{xy} z dz \end{array} \tag{1.3}$$

The stresses for each layer in the laminate, Eq. 1.1, can be substituted in the above equation to obtain the constitutive relations for the laminate:

$$\begin{Bmatrix} N_x \\ N_y \\ N_{xy} \end{Bmatrix} = \begin{bmatrix} A_{11} & A_{12} & A_{16} \\ A_{12} & A_{22} & A_{26} \\ A_{26} & A_{26} & A_{66} \end{bmatrix} \begin{Bmatrix} \varepsilon_x^0 \\ \varepsilon_y^0 \\ \gamma_{xy}^0 \end{Bmatrix} + \begin{bmatrix} B_{11} & B_{12} & B_{16} \\ B_{12} & B_{22} & B_{26} \\ B_{26} & B_{26} & B_{66} \end{bmatrix} \begin{Bmatrix} \kappa_x \\ \kappa_y \\ \kappa_{xy} \end{Bmatrix} \tag{1.4}$$

$$\begin{Bmatrix} M_x \\ M_y \\ M_{xy} \end{Bmatrix} = \begin{bmatrix} B_{11} & B_{12} & B_{16} \\ B_{12} & B_{22} & B_{26} \\ B_{26} & B_{26} & B_{66} \end{bmatrix} \begin{Bmatrix} \varepsilon_x^0 \\ \varepsilon_y^0 \\ \gamma_{xy}^0 \end{Bmatrix} + \begin{bmatrix} D_{11} & D_{12} & D_{16} \\ D_{12} & D_{22} & D_{26} \\ D_{26} & D_{26} & D_{66} \end{bmatrix} \begin{Bmatrix} \kappa_x \\ \kappa_y \\ \kappa_{xy} \end{Bmatrix} \tag{1.5}$$

which in compact form can be written as the ABD-matrices:

$$\begin{array}{ll} A_{ij} = \sum_{k=1}^{N} \left(\overline{Q}_{ij}\right)_k (z_k - z_{k-1}) & B_{ij} = \frac{1}{2} \sum_{k=1}^{N} \left(\overline{Q}_{ij}\right)_k \left(z_k^2 - z_{k-1}^2\right) \\ D_{ij} = \frac{1}{3} \sum_{k=1}^{N} \left(\overline{Q}_{ij}\right)_k \left(z_k^3 - z_{k-1}^3\right) & \end{array} \tag{1.6}$$

The **A** matrix is the extensional stiffness matrix, which relates the in-plane stress resultants to the mid-plane strains of the laminate. The **B** matrix is the bending-extension coupling matrix which relates the in-plane stress resultants to the curvatures and the moment resultants to the mid-plain strains of a laminate; and the **D** matrix is the flexural (bending) stiffness matrix, which relates the moment resultants to the curvatures of the mid-plane of a laminate.

The coupling between bending and in-plane extension can be very useful, but it is commonly considered undesirable. Therefore, the components of the **B** matrix are removed from the equation by symmetric placement of the layers in the laminate around the mid-plane. It is also considered to be good practice to avoid the coupling terms A_{16}, A_{26}, D_{16} and D_{26} (Caprino and Crivelli Visconti 1982).

1.3 Design and optimisation of laminated composites

The act of designing a structure is an optimisation process. The specific challenge in composite design and optimisation, is that the design problem is discrete in its nature: a laminated composite consists of a discrete number of layers, and for ease of manufacturing the fibre orientation angles of the plies in the laminate are restricted to a discrete set, commonly $\{-45°, 0°, +45°, 90°\}$. An excellent overview of the optimisation tools that can be used for the optimisation of laminated composites is provided in Ghiasi, Pasini and Lessard (2009). Some of these tools are described below in more detail.

1.3.1 Gradient-based optimisation

Early attempts to optimise composite structures apply gradient-based continuous variable optimisation methods to this discrete problem. A gradient-based optimiser uses the gradient of the objective function and constraint function(s), or an approximation thereof if a mathematically closed form is not available. The main advantage of gradient-based optimisers is their fast convergence compared to other optimisation methods, however this comes at the risk of converging toward a local optimum rather than a global optimum.

The stacking sequence of the laminate was kept fixed in these early applications, varying only the thickness values of the 0, ±45, and 90-deg layers in the lam-

inate, because gradient-based optimisers use continuous variables in their basic formulation. Consider a balanced symmetric laminate with the specified stacking sequence $[\pm 45_i/0_j/\ 90_k/0_l/\pm 45_m]_s$ for example, where the indices i, j, k, l, and m are continuous variables which control the thickness of the respective layers in the laminate. After optimisation the values of the indices are rounded off to their nearest integer values. A problem with this approach is that constraints may be violated by rounding off to the nearest integer value. A solution would be to round off to the nearest upper and lower discrete value, however, then there are 2^n designs that should be evaluated. This number will grow out of hand as the number of indices increases, and for large numbers it could even be possible that more function evaluations are required to evaluate all rounded off designs than are needed to arrive at the optimum in terms of continuous design variables. A larger problem is posed by the possibility that after rounding off no feasible design is found for a continuous optimum, and that there is no constraint available that will steer the gradient-based optimiser away from such a point.

1.3.2 Integer Linear Programming

Another possibility to optimise a composite laminate would be to evaluate all of the possible lay-up combinations, assuming that the thickness of the overall laminate is fixed. This is an effective, but a computationally exhaustive method, which will can become prohibitively expensive for a large number of design variables, and many layers in the laminate. An effective way to reduce the number of evaluations required is to use an enumeration tree, in which certain branches of the tree can be truncated, e.g. the branch and bound method (Gürdal, Haftka and Hajela 1999). Such an approach only works for problems which are linear in terms of design variables.

1.3.3 Genetic Algorithms

Genetic algorithms (GA) are the most popular optimisation tool used for stacking sequence design of composite laminates (Ghiasi et al. 2009). We have seen that practical composite laminate design can be reduced to determine the number of layers in a laminate, their respective orientation, chosen from a discrete set, and their stacking sequence. All of these features can easily be caught in the integer coding of a GA. To give an example of such encoding, let us consider a laminate with only angles between 0° and 90° with 15° increments. In terms of genetic encoding this set could be represented simply by the set $\{1, 2, 3, 4, 5, 6, 7\}$. In a GA an individual represents one of the possible designs. For this example, a possible individual could look like 4713542637. There are multiple ways to interpret this coded individual.

Without any assumptions made about the laminate build-up the given string would encode the laminate:

$$[45/90/0/30/60/45/15/75/30/90]$$

This laminate is not symmetric nor is it balanced, and thus it may exhibit an undesired mechanical response. To balance the laminate a solution could be to add a minus sign every second time an orientation is encountered in decoding the string going from left to right. This results in the laminate:

$$[45/90/0/30/60/-45/15/75/-30/90]$$

Still this is not a balanced laminate. The balanced condition can be enforced more strictly by treating all the layers that are not in the 0- or 90 degree orientation as angle-ply:

$$[\pm 45/90/0/\pm 30/\pm 60/\pm 45/\pm 15/\pm 75/\pm 30/90]$$

The resulting laminate now is balanced. Though if, due to genetic operations, a 0- or 90 degree orientation layer is changed into an angle-ply the thickness of the laminate changes. This effect will have a negative impact on the convergence of the GA, and it can be prevented by doubling all 0- or 90 degree orientation layers, effectively doubling the number of layers in the laminate compared to the simplest decoding scheme:

$$[\pm 45/90_2/0_2/\pm 30/\pm 60/\pm 45/\pm 15/\pm 75/\pm 30/90_2]$$

Now it is only a small step to a symmetric laminate, by default the laminate is mirrored about the most right entry of the coded individual:

$$[\pm 45/90_2/0_2/\pm 30/\pm 60/\pm 45/\pm 15/\pm 75/\pm 30/90_2]_s$$

The number of layers in the laminate is now the quadruple of the number for the most simple case of decoding, i.e. each location in the coded individual corresponds to four layers in the actual laminate.

One of the more notable disadvantages of the use of genetic algorithms is the large number of function evaluations associated with them and the computational time involved. A method to alleviate this issue is to use a surrogate model for the objective function. (Gürdal et al. 1999)

1.4 TAILORED COMPOSITE STRUCTURES

In conventional composite laminate design the aim is to find the arrangement of material constituents that best satisfies the posted requirements on, for instance,

strength, stiffness and cost. Fibre orientation angles are usually chosen from the set $\{0°/+45°/-45°/90°\}$ and remain constant throughout an entire ply. Furthermore, laminate designs are limited to a fixed number of plies, n, and have to meet design rules like the 10%-rule. This limits the scope of the optimisation problem, and the directional properties of the composite material cannot be used to their full extent, because there is only a limited number of possible combinations of fibre orientation and stacking sequence that can be used. Hence there is room for improvement of the mechanical properties and/or weight of the structure. Such improvement can be achieved by modification of the stacking sequence within the bounds of conventional design rules, i.e. laminate tailoring. As defined by Jones (Jones 1999) laminate tailoring is the act of meeting *"...particular structural requirements with little waste of material capability."*

There are many ways in which laminate tailoring can be achieved, to name a few:

- relaxation of the set of fibre orientation angles
- choosing thinner ply material
- laminate blending
- fibre steering

The simplest way to tailor a laminate is to relax the set of fibre orientation angles used to design the lay-up. The design space proportionally increases in size with the size of the fibre angle set, see section 1.2. Another approach to increase the design space, thereby facilitating laminate tailoring, is to increase the number of plies in the laminate. This is achieved by choosing a thinner ply material for a laminate of a given thickness.

A more rigorous approach is to subdivide a structure into multiple segments and to design the lay-up for each of these segments individually. A drawback of the aforementioned approach is that structural integrity may be lost. Restoring continuity between the different segments in the laminate is generally referred to as laminate blending (Kristinsdottir and Zabinsky 1994), which is explained below.

The concept of laminate tailoring can be taken further by allowing fibre angle variation within a ply. The latter form of composite laminate tailoring is known as variable stiffness (VS) composite laminate design. It is posited by Jegley *et al.* (Jegley, Tatting and Gürdal 2003) that matching the spatial variation of the stress state in a structure by varying the fibre orientation angle, exploits the direction material properties of fibre-reinforced composite laminates more efficiently both for strength and stiffness. The variation in fibre orientation angle will result in spatially variable stiffness properties, hence the term VS composite laminate.

1.4.1 LAMINATE BLENDING

The term blending was introduced by Zabinsky (1994), and refers to the activity of designing a structure such that for all segments in the structure some or all plies of the stack of the segment continue in the adjacent segment to improve manufacturing. Several methods to design multi-segment blended composite laminates are described in the literature.

Which degree of stacking sequence incompatibility is allowable should be defined before a blended composite laminate can be designed. Several stacking sequence incompatibilities are illustrated in Fig. 1.1. When the laminates in two adjacent segments are the same, they can be said to be perfectly blended, i.e. segments II and III in Fig. 1.1. The outermost ply is dropped between segments I and II, which may be acceptable if the loads, static and fatigue, are low enough for the ply drop not to lead to premature failure, but should be avoided at higher loads. The risk of delamination is smaller for the ply drop between segments III and IV, because the location of the ply drop is covered by another ply. There is a discontinuity in fibre orientation angle for one of the plies between segments IV and V. This discontinuity may lead to stress concentrations. Between panels V and VI there is an overall mismatch in stacking sequence, leading to a total loss of structural integrity at this location.

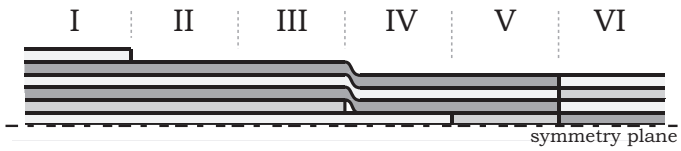

Figure 1.1: *Example of a multi-segment structure.*

A "less-than-or-equal rule" is proposed by Kristinsdottir, Zabinsky, Tuttle and Neogi (2001). The laminate is designed, using this method, such that segments can only contain the same plies as an adjacent segment or less. The blending problem is defined as a constraint problem by Liu and Haftka (2001) who enforce stacking sequence continuity between segments through continuity constraints. The method allows for a trade-off between continuity and structural weight. Results obtained for an 18-panel wing-box structure show that a substantial increase in lay-up continuity can be obtained for only a small weight penalty, but that above a certain degree of continuity the structural weight will increase sharply.

Design variable zones (DVZ) and sub-laminates (SL) are used by Soremekun, Gürdal, Kassapoglou and Toni (2002). The optimisation problem is structured in such a way in their approach that only blended designs can be represented. The weight penalty for blended designs is much smaller, as a result.

A distributed GA within a parallel processing environment with migration is used in Adams, Watson and Gürdal (2003) to obtain blended designs. Segments are designed separately in this approach, and the Levenstein distance (Levenstein 1966) is used to penalise the difference in stacking sequence between adjacent segments. Fully blended designs are obtained using this approach, but the associated computational costs are high.

The issue of excessive computational cost is addressed in Adams, Watson, Gürdal and Anderson-Cook (2004) by simplifying the blending problem by introducing a guiding stack from which all laminates in a structure are obtained by deleting a contiguous series of outermost or innermost plies, i.e. inner and outer blending. The definitions of the inner and outer blending approach produces intrinsically blended designs and is therefore used in an effort to reduce further the computational effort involved in designing optimal blended composite structures (Seresta, Gürdal, Adams and Watson 2007, IJsselmuiden, Abdalla, Seresta and Gürdal 2009*a*). The drawback of the inner and outer blending definitions is that they restrict the optimisation problem to a small region of the design space, excluding a whole range of possibly optimal and manufacturable designs.

A variation on inner and outer blending is proposed by Liu, Toropov, Querin and Barton (2009*b*), shared layers blending (SLB). The SLB algorithm ranks all segments in a structure by the number of layers in each orientation. The minimum number of layers shared by all segments is identified and are placed as the outermost layers in the laminate. The procedure is repeated for the remaining layers in each segment. In contrast to pure inner and outer blending no perfect blending can be guaranteed.

A totally different approach to the blending problem is proposed by Giger, Keller and Ermanni (2007) who use graph theory to define compact and connected fibre patches. This method results in fully blended designs and is more flexible than inner or outer blending. The method is developed further in Keller (2011) where the use of graph theory is relaxed, which leads to a more compact formulation.

1.4.2 Fibre steering

Early work on VS composite laminates was done by Hyer and Lee (1991) and Gürdal and Olmedo (1993). Hyer and Lee (1991) discuss a square plate with a centrally located hole subjected to a uni-axial compressive load. They consider a quarter of this plate for design purposes. This quarter is subdivided into a maximum of eighteen regions, each of which can be assigned a different fibre orientation angle. A sensitivity study per region led to the conclusion that gains in buckling performance can be achieved by introducing a curvilinear fibre angle format. Gürdal and Olmedo (1993) use continuous linear fibre angle variations to study the effect of stiffness variations on the elastic properties of a panel. They show that variable stiffness laminates will generate stress gradients that

induce transverse stresses without the presence of an external transverse load, and shear stresses when no shear-extension coupling is present. They go on to suggest that these effects can be used to the designer's advantage to tailor the stress distribution in a composite plate.

Tatting and Gürdal (2003) present a procedure that can be used to design and analyse VS composite plates using the STAGS finite element (FE) code. Linear fibre angle variation is used in their work, i.e. fibre angles are varied linearly in one direction between two extreme values. The method can be used to assess manufacturability and is flexible enough to include various tow path definitions. Coupled to cellular automata (CA) the method can also be used to design selective reinforcements (Tatting, Setoodeh and Gürdal 2005). Analysis and testing of VS composite panels by Wu, Gürdal and Starnes, Jr. (2002) show that the failure load of VS composite panels optimised for uni-axial compression can be significantly improved compared to a $[\pm 45_5]_s$ baseline design. Panels in which tows are allowed to overlap due to steering, resulting in thickness build up, are found to perform better than panels where tows are cut to keep the thickness of the panel constant. The tested VS panels were found to perform better than the analysis predicted. Pre-stresses due to curing were therefore included in the analysis, and the results were found to agree for the panel without thickness build-up. IJsselmuiden, Abdalla and Gürdal (2010*b*) investigated this further and concluded it is important to include the thermal effect of curing in the optimisation of VS composite structures. They find, that thermal stresses strongly depend on the thickness of the laminate.

There are two ways to design VS composites using fibre angles as design variables: (i) using tow-path definitions, which reduces the number of design variables to a hand full of parameters to define the path, or (ii) using fibre angles directly, which is less restricted, but results in a significant increase of design variables. Blom, Setoodeh, Hol and Gürdal (2008) use different tow path definitions to maximise the fundamental frequencies of conical shells. Once the tow-paths are known, fibre angles and overlaps must be determined at each point of the structure for a finite element analysis (Blom, Tatting, Hol and Gürdal 2009). Setoodeh, Abdalla and Gürdal (2005) use fibre angles directly as design variables within a CA framework. Fibre angles are used as continuous design variables, their orientations are based on minimum compliance. In order to maintain fibre orientation continuity heuristic pattern matching is used in combination with local optimality criteria (Setoodeh, Gürdal and Watson 2006). Substantial gains in compliance can be achieved using this method through placing fibres in an optimal spatial configuration. A separable, reciprocal approximation is introduced by Setoodeh, Abdalla, IJsselmuiden and Gürdal (2009) for the design of VS laminated composites using the fibre angles at the nodes of an FE model as design variables. This approach is adapted in Setoodeh, Abdalla and Gürdal (2006*b*) to use lamination parameters (LP) as design variables instead.

The introduction of strength-based failure criteria in the LP design space (IJsselmuiden,

Abdalla and Gürdal 2008) combined with the approximation of the convex feasible region of the LPs (Setoodeh, Abdalla and Gürdal 2006*a*) gives a set of practical design constraints when using LPs as design variables. IJsselmuiden, Abdalla and Gürdal (2010*a*) use these constraints and a conservative reciprocal approximation scheme to optimise VS composite panels for buckling. They expand the inverse of the buckling load in terms of in-plane stiffness and the inverse of flexural stiffness, which yields an objective function that is convex in terms of LPs. The buckling loads of the obtained VS designs are 100% in excess of the best constant stiffness (CS) design. This method has been developed further for the design of more generic structures described by triangular element FE meshes (IJsselmuiden, Abdalla, Pilaka and Gürdal 2010, IJsselmuiden, Campen, Schön and Carosella 2011, Van Campen and IJsselmuiden 2011).

The conversion of an optimum LP design to a design in terms of fibre angles is described in Setoodeh, Blom, Abdalla and Gürdal (2006) for up to two designed variable stiffness layers of a balanced symmetric laminate, i.e. $[\pm\theta_1/\pm\theta_2]_s$. A more general approach is presented in Van Campen, Kassapoglou and Gürdal (2011).

1.5 AUTOMATED FIBRE PLACEMENT

The manufacture of fibre steered composite parts is enabled by automated fibre placement (AFP) technology. AFP is a fully automated process which combines the compaction and cut-restart capabilities of automated tape laying with the differential payout capability of filament winding. (Blom 2010) Several different types of machines are commercially available for AFP, and there are different types of materials that can be deposited: prepregs (pre-impregnated fibre material), thermoplastics (fibres in thermoplastic resin), and dry fibres held together by a small percentage of binder material. Carbon fibre prepreg is most commonly encountered in the aerospace industry, and the work presented in this thesis was financed by a European Sixth Framework Programme Project, Project no. 030771, that had as an objective to investigate the possibility to place dry fibre material.

The fibre material is placed on the surface of a mandrel in bands of parallel fibres in the form of slit tape (Blom 2010). The bands of parallel fibres are called courses. Typical values for the width of a course are 3.175mm, 6.35mm and 12.7mm (respectively $\frac{1}{2}$in., $\frac{1}{4}$in. and $\frac{1}{8}$in.). A maximum of 32 tows can be placed simultaneously in parallel on the surface for a tow width of 3.175mm, which results in a maximum tow width of 101.6mm (4in.).

Most AFP machines have seven axes of motion: three translational axes of the placement head, three rotational axes of the placement head and one rotational axis of the mandrel supporting the part being manufactured during production.

The tows are moved forward by pinching rollers to start the placement of fibre material. The tows are then heated to increase their tackiness, in case of prepreg and thermoplastic tows, or to activate the binder in dry tows, and placed on the surface of the mandrel. Once there is adhesion between the mandrel and the tow, the pinching wheels are released. The deposited material is compacted by a roller to adhere better to the surface of the mandrel and to remove any trapped air. (Blom 2010) Each tow in a course originates from an individual spool and can be cut and restarted individually.

There are several manufacturing constraints associated with automated fibre placement technology, an overview is given in table 1.1 (Van Campen and IJsselmuiden 2011). These constraints result from structural defects, which arise as a result of limitations on the geometry of the structure, the tow material, and the fibre placement machine (FPM). Note that depending on the chosen application there may be additional manufacturing constraints, e.g. when using core material. Geometrical constraints result from instances where small tensile forces in the

Table 1.1: *Overview of manufacturing criteria and constraints. Sources: G (geometry of the structure), TM (tow material), FPM (fibre placement machine).*

Constraint	**Source**	**Potentially Induced Effect**
Convex[1] Angle/Radius	G, FPM, TM	Bad adhesion, in-plane path defects and wrinkles
Concave[1] Curvature	G, FPM	Contact placement head and tooling surface Fibre bridging
Steering Radius	TM	Buckling due to in-plane bending
Deposited Thickness	TM	Swelling and lack of adhesion between plies
Complex geometry	G, FPM, TM	Contact placement head and tooling surface Fibre bridging

fibres, which is inherent to the placement process, cause tows not to follow an intended tow path exactly. The shear and normal forces required to keep the tow in place might become too large for the material system used, and, as a result, the intended tow-path will not be followed or convex features of the geometry will be partially bridged by the tow material, see Fig. 1.2(a) and 1.2(b). Furthermore,

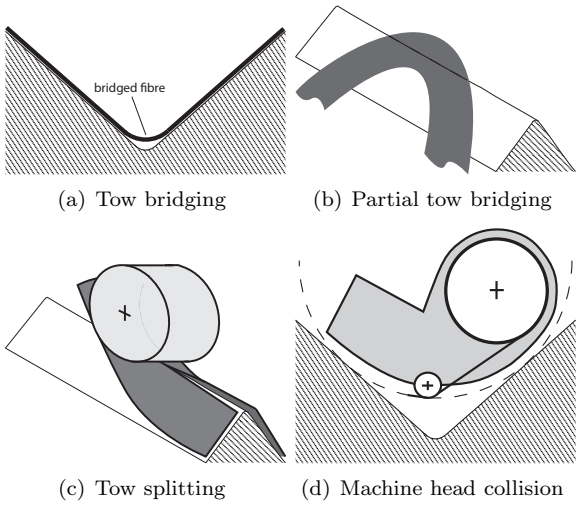

(a) Tow bridging (b) Partial tow bridging

(c) Tow splitting (d) Machine head collision

Figure 1.2: *Geometrical constraints for automated tow-placement.*

tows placed along and just over sharp edges are likely to split as shown in Fig. 1.2(c).

The physical size of the fibre placement head dictates the minimum size convex features in a geometry can have. The machine head cannot be allowed to collide with the tooling surface, or with tow material which has already been deposited, see Fig. 1.2(d). Additionally the machine will only be able to place tow material within a given tolerance, meaning measurement techniques for fibre misalignment is required (Kratmann, Sutcliffe, Lilleheden, Pyrz and Thomsen 2009).

Tow placement of variable stiffness composites relies on the manufacturing ability to steer fibres within the plane of the laminate. To this end there must be adhesion between the tow material and the sub-structure it is placed on, either the tooling surface or previously deposited tows. The amount of adhesion depends on the type of tow material used, pre-impregnated, or dry with some binder material, and on the material system used. (Van Campen and IJsselmuiden 2011) Application of heat just before placing the tows activates the resin or binder and makes the tows tacky, thus realising the adhesion between the placement surface and the tow material. Tows can only accommodate a certain amount of in-plane curvature depending on the material system used.

The manufacturing constraints mentioned above are interrelated. Nevertheless, a distinction can be made between constraints stemming from the use of state-of-the-art manufacturing technology and those stemming from physical limitations. It is assumed, in this work, that the optimal LP distribution has been obtained. Hence, geometrical constraints will not be considered in this thesis, and neither

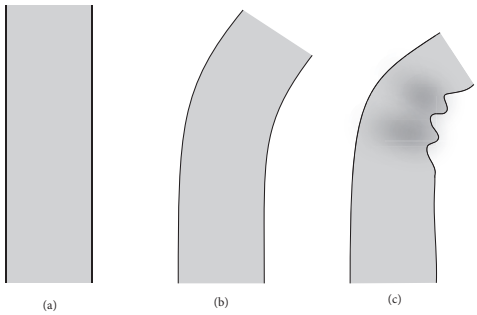

Figure 1.3: *Curvature constraint of a single tow: (a) straight tow (b) curved tow (c) tow curved beyond curvature constraint, wrinkling occurs*

will FPM constraints, as they coincide with geometrical constraints. The constraints on steering radius and thickness constraint are discussed below.

1.5.1 Steering radius

Each tow has a given, finite width. The width of a course being placed is a multiple of this width, i.e. the width of a course with k tows is k times the tow width. When steering a course along a circular arc of a given radius it becomes apparent that as tows become further away from the centre point of the circle they will have to cover a longer distance, and thus require a higher feeding rate from the tow placement machine.

The same holds true for a single tow, however, the material feed cannot be adjusted as a function of the radial coordinate. Instead the side of the tow furthest away from the centre point will be loaded in tension, whereas the side closest to the centre point will be in compression. The tow can only accommodate such in-plane bending up to a certain limit before starting to show out-of-plane deformations.

As soon as the curvature of the innermost tow of a course becomes too severe, the compressed side of the tow will show local buckling and wrinkle. This is detrimental to the mechanical properties of the finished product and should be avoided.

1.5.2 Thickness variation

Multiple tow courses are needed to construct a tow-placed laminate. Here one layer of such a laminate is considered. Assuming the tow courses in this layer are all derived from one reference curve, there are two options that can be used to fill the entire layer with tow courses: (i) parallel paths, or (ii) shifted paths (Tatting and Gürdal 2003).

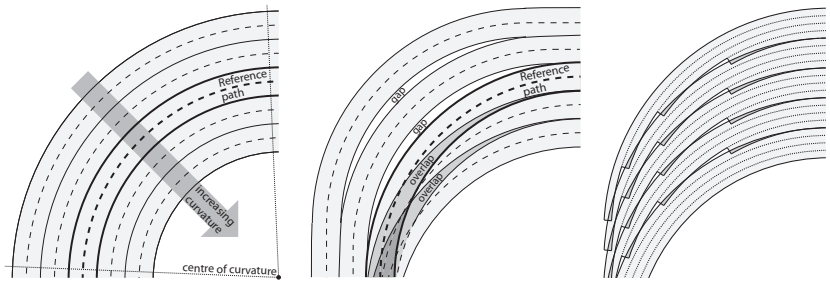

(a) Parallel placement (b) Shifted placement (c) Shifted placement with tow drops

Figure 1.4: *Tow paths derived from a reference curve.*

The advantage of parallel paths is, that no gaps or overlaps between tows will occur, which results in a structure of uniform thickness and, theoretically, without any defects. To its disadvantage, the steering radii of each parallel tow will be different, which at sufficient distance from the reference path will result in a violation of the maximum allowable in-plane curvature, see section 1.5.1, as is demonstrated in Fig. 1.4(a).

The in-plane curvatures of each tow course are equal when they are placed along a path which has been shifted parallel to the reference tow-path, as is demonstrated in Fig. 1.4(b). The parallel shift results in the combination of the two most extreme cases: (i) tows fully overlapping, or (ii) gaps between the tows with no overlaps. These gaps and overlaps cause a change in thickness of the layer under consideration, and thus of the laminate as a whole.

Even when more relaxed tow-path definitions are used it is apparent that gaps and overlaps will occur as a result of neighbouring paths not being fully parallel. Fibre angle variation thus results in thickness variation of the laminate, except for the special case of tangent tow-paths.

Tows can be dropped and restarted, see Fig. 1.4(c), to prevent thickness build-up due to fibre steering. Thickness variation in this case is reduced to a much smaller case, though gaps and overlaps will still be introduced, and with them potential defects in the laminate. A comparison between compression loaded panels of the same lay-up, one with overlaps, the other one with cut tows, shows significant improvement in mechanical performance when tows are not cut (Wu et al. 2002). Explanations for this outcome are the locally increased thickness of the laminate and the induced defects in the panel with tow-cuts. Blom, Lopes, Kromwijk, Gürdal and Camanho (2009) have studied the effect of tow-drop areas on strength and stiffness of the laminate. Their results show that a reduction of strength of a laminate is more pronounced when wider tows are used, i.e. when bigger gaps and overlaps occur, and that staggering the tow courses will have a

more positive effect on strength of the laminate. Nevertheless, excessive thickness build-up in the laminate should be avoided as it makes the manufacturing process more difficult, and it increases the weight of the laminate.

Another way to reduce thickness build-up in a laminate is to use ply staggering. Excessive thickness build-up is avoided by shifting the locations of the occurring overlaps between the plies in the laminate (Tatting and Gürdal 2003). This way the thickness variation will be much more gradual, though the amount of material added to a structure will remain the same.

Thickness build-up due to fibre steering can be used as a measure of the amount of mass added to a structure due to overlaps. In the case where the tows are cut, it is an indication of the amount of extra production time required to cut the tows. When designing VS composite laminates it is important that it is possible to impose constraints on mass or production time when converting an optimised LP design into a fibre angle design .

1.6 Scope and aims

The work presented in this thesis is part of a larger effort at the Aerospace Structures and Computational Mechanics (ASCM) group of the faculty of Aerospace Engineering of the Delft University of Technology (the Netherlands) to develop design and optimisation techniques for variable stiffness (VS) fibre-placed composite laminates. One of the techniques under development is a two-step optimisation approach. The first step of this approach is to optimise a VS composite structure in terms of lamination parameters (LP), in the second step the LP design is converted into a lay-up design. The work presented in this thesis provides a possible second step for the above approach.

The second step of the proposed two-step design approach revolves around the question: *"Given a structure with a known optimal lamination parameter distribution, which lay-up design results in the best possible performance whilst satisfying prescribed manufacturing constraints?"* Therefore, the main objective of the work presented in this thesis was to investigate the methods presented in the literature to obtain a stacking sequence design based on lamination parameters, and to develop new methods to obtain an optimal VS lay-up design for a given LP design of a VS composite laminate that satisfies prescribed manufacturing constraints. To this end, it was necessary to determine what the criteria for a point in lamination parameter space are, such that this point could be matched exactly to a lay-up design rather than be approximated. Thus, the part of the theoretical feasible domain of the lamination parameters that can be described using a given laminate configuration and a discrete number of layers in the laminate was studied. Secondly, it was necessary to identify and develop methods to obtain the best (set of) lay-up design(s) that match a given set of lamination parameter values. The

stacking sequence designs obtained this way was used to design a variable stiffness lay-up, either in the form of a blended laminate structure or fibre steered design. Once a lay-up design has been established for one set of LPs the lay-up designs for neighbouring design points should be combined into one continuous design. How lay-up continuity in the structure can be achieved by laminate blending and by fibre steering is discussed in this thesis. Finally, how fibre paths are determined on the basis of an obtained variable stiffness lay-up design was studied. All these separate research objectives, once combined, contributed to fulfilling the main research objective.

1.7 THESIS OUTLINE

The work presented in this thesis is divided into three parts:

- the conversion of LPs into a lay-up design
- the design of blended composite lay-ups
- the design of steered composite lay-ups

The reasoning behind this division is that, after a design in terms of LPs has been converted into a design in terms of fibre angles, there are two possible ways to arrive at a variable stiffness laminate design: laminate blending or fibre steering. Eventually laminate blending and fibre steering might be combined, but this was beyond the scope of the present work.

The reader is presented with a mathematical description of the lamination parameters in chapter 2. Their theoretical feasible domain will be discussed and the description of the feasible domain for practical laminates is developed further. The conversion from a set of lamination parameters into a lay-up design is also discussed and new tools for the conversion from LPs to a lay-up design are developed. Chapter 2 constitutes the first part of this thesis.

The design of multi-segment blended composite laminates using a guide-based optimisation procedure is described in chapter 3. Multi-segment composite laminate structures and the definition of blending are discussed in more detail, and the quintessential manufacturing constraints associated with blended composite laminate design are discussed. Several blending definitions and implementations are discussed, and the choice made to use the guide-based implementation in this work is explained. A new implementation of guide-based blending using multi-chromosomal genetic encoding is introduced, and implementations of several existing and new blending definitions using this framework are discussed. The results obtained using the new blending definitions introduced in chapter 3 are compared to results obtained using two pre-existing blending definitions for

a benchmark problem taken from the literature, in chapter 4. In this chapter the results obtained for several other example structures are discussed. Chapters 3 and 4 constitute the second part of this thesis.

An in-depth discussion of the design of variable stiffness laminates as part of the framework presented in this thesis is given in chapter 5. One of the manufacturing constraints associated with fibre steering technology, minimum steering radius, and its mathematical implementation are discussed, and a unified approach for the conversion of LPs into a fibre angle design and the implementation of one or multiple manufacturing constraints is presented. The LP distributions considered in this thesis for conversion into a VS lay-up design all are given on a finite element grid. The unified conversion approach presented in chapter 5 produces a VS lay-up design on a finite element grid. How this nodal fibre angle distribution per ply in the laminate can be converted into fibre paths which are fit for production using automated fibre placement technology is discussed in chapter 6. Estimation of laminate thickness build-up due to gaps and overlaps is reviewed in this chapter. The methods used to describe and obtain fibre paths found in the literature are discussed, and a suitable method for the conversion of nodal fibre angle distributions into fibre paths is identified. A method that can be used to estimate thickness build-up in a laminate, based on the nodal fibre angle distribution, and to determine fibre paths for manufacturing is proposed in this thesis based on a review of the literature on fibre path generation and thickness estimation. Four example structures were studied using the developed optimisation tools for the conversion process from LPs to a fibre angle design, this is discussed in chapter 7. The effect the constraint on in-plane curvature of the fibre distribution of a ply has on the buckling performance of the structures considered, and the thickness build-up in the laminate was studied. The effect that laminate thickness variation due to fibre steering has on the buckling load of the four structures was also studied. Chapters 5, 6 and 7 constitute the third part of this thesis.

Finally, the conclusions drawn for each of the parts mentioned above are presented and collated in chapter 8. Recommendations for future work on the subject of this thesis are also given in this chapter.

Note that part of the work presented in this thesis, was developed as part of the AUTOW project, European Union Sixth Framework Programme Project no. 030771, in which the design and engineering of composite parts manufactured using dry tow-placement was investigated.

The more alternatives, the more difficult the choice.

Abbe' D'Allanival

2

LAMINATION PARAMETERS AND LAMINATE CONFIGURATION

The mechanical properties of laminated composite materials were described in section 1.2. The lamination parameters (LP), presented in this chapter, provide a compact description of the material properties of a laminated composite. A set of only twelve dimensionless variables, and in the case of the balanced symmetric assumption as little as four, together with the material invariants are needed to describe the linear mechanical behaviour of a laminated composite fully.

The lamination parameters' compact formulation and continuous nature make them well suited as design variables. Numerous cases can be found in the literature that use LPs as design variables. Some examples of these cases are given in the following list, grouped per optimized response:

- buckling (Fukunaga, Sekine, Sato and Iino 1995, Terada, Todoroki and Shimamura 2001, Diaconu and Sekine 2004, Matsuzaki and Todoroki 2007, Weaver and Nemeth 2007, Todoroki and Sekishiro 2008, IJsselmuiden, Abdalla and Gürdal 2010*b*).
- compliance (Fukunaga and Vanderplaats 1991, Fukunaga and Sekine 1992, Miki and Sugiyama 1993, Setoodeh, Abdalla and Gürdal 2006*b*).
- thermo-mechanical buckling (Autio 2000).
- eigenfrequencies (Diaconu, Sato and Sekine 2002*b*).
- strength (IJsselmuiden et al. 2008, Todoroki and Sekishiro 2008).

Design of a composite structure using LPs requires the capability to convert the resulting set of LPs into a laminate configuration, i.e. fibre orientations and stacking sequence. Only a limited set of references can be found on this topic.

Fukunaga and Sekine (1992) have proposed a method to determine the best laminate configuration from a given set of LPs, however their method is limited to four-layer laminates, and can only be used for in-plane or flexural LPs. Diaconu et al. (2002*b*) have posited the inverse relationship as an optimization problem, allowing layer thickness to be a continuous variable. The assumption that layer thickness is a continuous variable may for practical laminates require rounding of to the nearest commercially available layer thickness.

The focus of this chapter will be to present the reader with a mathematical description of lamination parameters, discuss their theoretical feasible domain and to develop the feasible domain further for practical laminates, and finally to develop and discuss the conversion process. Additionally, laminate configurations with zero or negligible coupling terms that are alternatives to the conventional assumptions of balance and symmetry will be investigated, and the fractal nature of the feasible domain of the LPs will be discussed.

2.1 LAMINATION PARAMETERS

The **ABD**-matrices describing the mechanical stiffness of a laminate, see Eq. 1.6, can be rearranged into the following form:

$$\begin{aligned}\mathbf{A} &= h\left(\mathbf{\Gamma}_0 + \mathbf{\Gamma}_1 V_1^{\mathbf{A}} + \mathbf{\Gamma}_2 V_2^{\mathbf{A}} + \mathbf{\Gamma}_3 V_3^{\mathbf{A}} + \mathbf{\Gamma}_4 V_4^{\mathbf{A}}\right)\\ \mathbf{B} &= \frac{h^2}{4}\left(\mathbf{\Gamma}_1 V_1^{\mathbf{B}} + \mathbf{\Gamma}_2 V_2^{\mathbf{B}} + \mathbf{\Gamma}_3 V_3^{\mathbf{B}} + \mathbf{\Gamma}_4 V_4^{\mathbf{B}}\right)\\ \mathbf{D} &= \frac{h^3}{12}\left(\mathbf{\Gamma}_0 + \mathbf{\Gamma}_1 V_1^{\mathbf{D}} + \mathbf{\Gamma}_2 V_2^{\mathbf{D}} + \mathbf{\Gamma}_3 V_3^{\mathbf{D}} + \mathbf{\Gamma}_4 V_4^{\mathbf{D}}\right)\end{aligned} \tag{2.1}$$

where Γ_i are the matrices of material invariants (IJsselmuiden, Abdalla and Gürdal 2010*a*), see appendix A, and $V_i^{\mathbf{A},\mathbf{B},\mathbf{D}}$, $i = 1 \ldots 4$ are the lamination parameters (LP) introduced by Tsai and Pagano (1968) and Tsai and Hahn (1980).

The LPs are defined as non-dimensional through-the-thickness integrals of the layer orientation angles. Here the LPs are defined as:

$$\begin{aligned}\left(V_1^{\mathbf{A}}, V_2^{\mathbf{A}}, V_3^{\mathbf{A}}, V_4^{\mathbf{A}}\right) &= \int_{-\frac{1}{2}}^{\frac{1}{2}} \left(\cos 2\theta, \sin 2\theta, \cos 4\theta, \sin 4\theta\right) d\overline{z}\\ \left(V_1^{\mathbf{B}}, V_2^{\mathbf{B}}, V_3^{\mathbf{B}}, V_4^{\mathbf{B}}\right) &= 4\int_{-\frac{1}{2}}^{\frac{1}{2}} \overline{z}\left(\cos 2\theta, \sin 2\theta, \cos 4\theta, \sin 4\theta\right) d\overline{z}\\ \left(V_1^{\mathbf{D}}, V_2^{\mathbf{D}}, V_3^{\mathbf{D}}, V_4^{\mathbf{D}}\right) &= 12\int_{-\frac{1}{2}}^{\frac{1}{2}} \overline{z}^2\left(\cos 2\theta, \sin 2\theta, \cos 4\theta, \sin 4\theta\right) d\overline{z}\end{aligned} \tag{2.2}$$

Practical composite laminates are comprised of a discrete number of plies of given

thickness, hence, the layer orientation angles do not vary as a continuous function through the stack but are piece-wise constant in each layer. Thus, the integral expressions in equations 2.2 to 2.3 can be replaced by summations:

$$\left\{V_1^{\mathbf{A}}, V_2^{\mathbf{A}}, V_3^{\mathbf{A}}, V_4^{\mathbf{A}}\right\} = \frac{1}{n}\sum_{i=1}^{n}\left\{\cos 2\theta_i, \sin 2\theta_i, \cos 4\theta_i, \sin 4\theta_i\right\} \quad (2.3)$$

$$\left\{V_1^{\mathbf{B}}, V_2^{\mathbf{B}}, V_3^{\mathbf{B}}, V_4^{\mathbf{B}}\right\} = \frac{2}{n^2}\sum_{i=1}^{n}\left(\left(\frac{n}{2}-i+1\right)^2 - \left(\frac{n}{2}-i\right)^2\right)\left\{\cos 2\theta_i, \sin 2\theta_i, \cos 4\theta_i, \sin 4\theta_i\right\} \quad (2.4)$$

$$\left\{V_1^{\mathbf{D}}, V_2^{\mathbf{D}}, V_3^{\mathbf{D}}, V_4^{\mathbf{D}}\right\} = \frac{4}{n^3}\sum_{i=1}^{n}\left(\left(\frac{n}{2}-i+1\right)^3 - \left(\frac{n}{2}-i\right)^3\right)\left\{\cos 2\theta_i, \sin 2\theta_i, \cos 4\theta_i, \sin 4\theta_i\right\} \quad (2.5)$$

where n is the number of layers in the laminate.

Considering only balanced symmetric laminates the terms $V_2^{\mathbf{A}}$, $V_4^{\mathbf{A}}$, $V_1^{\mathbf{B}}$, $V_2^{\mathbf{B}}$, $V_3^{\mathbf{B}}$ and $V_4^{\mathbf{B}}$ drop out, and the terms $V_2^{\mathbf{D}}$ and $V_4^{\mathbf{D}}$ become negligible, especially for a larger number of layers n. Note, that the actual number of plies in the laminate is $4n$ because of the assumption of symmetry and balance.

2.2 Feasible envelope

Lamination parameters are essentially functionals of the stacking sequence function $\theta(\overline{z})$, which couple with the mechanical properties of a laminate through trigonometric functions. The trigonometric nature of the LPs means that they are intrinsically bound by a feasible domain. Equation 2.2 also implies that the LPs are closely coupled. Thus the numeric values that the LPs can attain are coupled and bound to a feasible domain.

2.2.1 Theoretical envelope

Miki (1982) and Miki and Sugiyama (1993) were the first to describe this feasible domain for balanced symmetric laminates, first for two in-plane LPs, $V_1^{\mathbf{A}}$ and $V_3^{\mathbf{A}}$, and later for two flexural lamination parameters, $V_1^{\mathbf{D}}$ and $V_3^{\mathbf{D}}$. Both domains are two-dimensional, and are shown in figure 2.1. Their shape is a direct result of the trigonometric relations underlying the LPs.

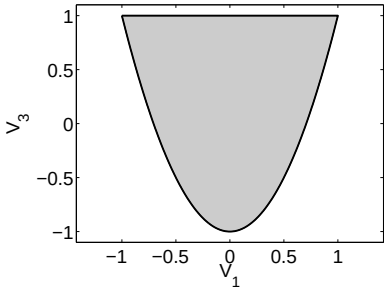

Figure 2.1: *Feasible domain for either the in-plane LPs* $V_1^{\mathbf{A}}$ *and* $V_3^{\mathbf{A}}$ *or only the flexural LPs* $V_1^{\mathbf{D}}$ *and* $V_3^{\mathbf{D}}$.

This work is extended by Fukunaga and Sekine (1992) who describe the analytical relationship between all four in-plane LPs, and the relationship between all four flexural LPs without considering the coupling between in-plane and flexural response. The prescribed domain thus is still limited to symmetric laminate configurations. It turns out that without any assumption on the construction of the laminate for two LPs describing either the **A**-,**B**-, or **D**-matrix the feasible region can be obtained analytically (Diaconu, Sato and Sekine 2002*a*). These feasible domains are shown in figure 2.2 for $V_i^{\mathbf{A},\mathbf{D}}$.

Diaconu et al. (2002*a*) present a variational approach that can be used to determine the feasible domain of all 12 lamination parameters numerically. The feasible LP domain is bound by a 12-dimensional hyperplane. According to Diaconu et al. (2002*a*) this hyperplane is found by determining the lay-up function $\theta(\overline{z})$ that maximizes the functional given in equation 2.6.

$$F\left[\theta(\overline{z})\right] = \sum_{i=1}^{4} k_i^{\mathbf{A}} V_i^{\mathbf{A}} + k_i^{\mathbf{B}} V_i^{\mathbf{B}} + k_i^{\mathbf{D}} V_i^{\mathbf{D}} = \int_0^1 G\left[\overline{z}, \theta(\overline{z})\right] d\overline{z} \tag{2.6}$$

where:

$$G\left[\overline{z}, \theta(\overline{z})\right] = \sum_{i=1}^{4} g_i(\overline{z}) f_i\left[\theta(\overline{z})\right] \tag{2.7}$$

$$g_i(\overline{z}) = \frac{1}{2} k_i^{\mathbf{A}} + k_i^{\mathbf{B}} \overline{z} + \frac{3}{2} k_i^{\mathbf{D}} \overline{z}^2 \tag{2.8}$$

$$f_{[1,2,3,4]} = \left[\theta(\overline{z})\right] = \left[\cos 2\theta(\overline{z}), \sin 2\theta(\overline{z}), \cos 4\theta(\overline{z}), \sin 4\theta(\overline{z})\right] \tag{2.9}$$

$$\sum_{i=1}^{4} \left[\left(k_i^{\mathbf{A}}\right)^2 + \left(k_i^{\mathbf{B}}\right)^2 + \left(k_i^{\mathbf{D}}\right)^2 \right] = 1 \tag{2.10}$$

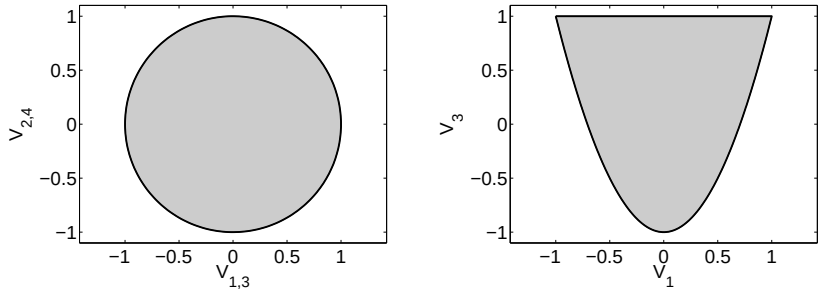

(a) (V_1, V_2), (V_3, V_4) (b) (V_1, V_3)

(c) (V_3, V_2) (d) (V_1, V_4)

Figure 2.2: *Feasible domain for* $V_i^{\mathbf{A},\mathbf{D}}$, $i = 1, \ldots, 4$.

This variational approach can provide the feasible region for any set of lamination parameters, however, it does not give any explicit relationships. Instead the feasible region for the LPs can only be built numerically.

Like Diaconu et al. (2002*a*), Setoodeh, Abdalla and Gürdal (2006*a*) use the fact that the feasible region is known to be convex (Grenestedt and Gudmundson 1993). The numerical method they propose can be used to obtain an approximate feasible region for any combination of lamination parameters. It builds the approximation of the feasible region through convex hulls of feasible points in lamination parameters space. The number of fibre angle orientations and the number of equi-thickness layers in the laminate is increased until the volume of such a convex hull converges to a constant value. The resulting hyperplanes can be treated as linear side constraints, which can be used in standard gradient-based optimisation methods, and formed the basis for work by IJsselmuiden *et al.* (IJsselmuiden et al. 2008, IJsselmuiden et al. 2009*a*, IJsselmuiden, Abdalla and Gürdal 2010*a*, IJsselmuiden, Abdalla and Gürdal 2010*b*). A key feature of the method presented by Setoodeh, Abdalla and Gürdal (2006*a*) is that the set of linear inequality constraints only needs to be obtained once. It can be stored and used in any future design optimisation problem. This approach also does not give any explicit relationships for the feasible region of the lamination parameters. The difficulty in obtaining an analytically closed form of the feasible LP domain stems from the summation of trigonometric functions with variable weighting factors. To the author's knowledge to date (2011) no exact analytical description of the feasible LP domain has been made.

2.2.2 Practical envelope

The fibre orientation angle and ply thickness can be treated as a continuous design variable. However, commercially, ply material is only available in a limited number of gauges. Design of real-life applications requires that ply thickness is chosen from this limited number gauges. Therefore, when designing a laminate to a given thickness, the number of plies in the laminate must be rounded off to the nearest integer value. Constructing a laminate from a limited number of constant thickness plies has its effect on the feasible envelope of the lamination parameters.

Setoodeh, Abdalla, Gürdal and Tatting (2005) report that the upper bound on the feasible domain of the in-plane lamination parameters of a balanced symmetric laminate for a given discrete number of plies of equal thickness takes the form given in Eq. (2.11):

$$V_3^{\mathbf{A}} \leq 2n(V_1^{\mathbf{A}} - \frac{2p}{n})^2 + 4(n-1)(V_1^{\mathbf{A}} - \frac{2p}{n}) + (2n-3) \tag{2.11}$$

where $p = 0, 1, 2, \ldots, n-1$, and n is the number of layers in the laminate.The upper bound of the feasible domain of the flexural lamination parameters for the same laminate is given by Eq. (2.12):

$$V_3^{\mathbf{D}} \leq \frac{2s_n}{a} V_1^{\mathbf{D}\,2} \pm \frac{4b}{a} V_1^{\mathbf{D}} + \frac{2b^2 + as_n - 2a^2}{as_n} \tag{2.12}$$

where:

$$a = \sum_{j=1}^{i} \{p_i\}_j$$

$$b = s_n - a - 2q \sum_{j=1}^{i} \{r_i\}_j$$

and:

$$s_n = \sum_{i=1}^{n} \left(1 + 6 \sum_{j=1}^{i} (j-1) \right) = n^3$$

for $q = \langle 0, 1 \rangle$ and $i = 1, 2, \ldots, n-1$. Here the different ply angles used to construct the laminate are represented by weight factors, gathered in the set $\{k_i\}$:

$$\{k_i\} = 1 + 3i(i-1)$$

for $i = 1, 2, \ldots, n$. In this $\{p_i\}$ represents the set of all the possible permutations picking i from the n weights available in set $\{k_i\}$. $\{r_i\}$ represents the set of all possible permutations of the remaining weights after selecting those for $\{p_i\}$.

To guarantee the convexity of the feasible domain of flexural LPs, the upper boundary on $V_3^{\mathbf{D}}$ of the feasible domain can be restricted to a straight horizontal line, given in Eq. (2.13):

$$\begin{array}{ll} V_3^{\mathbf{D}} \leq \frac{3(n-1)^3 - n^3}{1 + 3(n-1)n} & \text{for} \quad n = 1, \ldots, 4 \\ V_3^{\mathbf{D}} \leq 1 - \frac{1280}{37n^3} & \text{for} \quad n \geq 5 \end{array} \tag{2.13}$$

It can be seen that for $n \to \infty$ the convex feasible domain of the flexural LPs approaches the full theoretical feasible domain faster than the convex feasible domain of the in-plane LPs, illustrated by the horizontal line in figure 2.3(d).

A similar study can be performed for any type of laminate configuration. In the above discussion specifically only balanced symmetric laminates were considered.

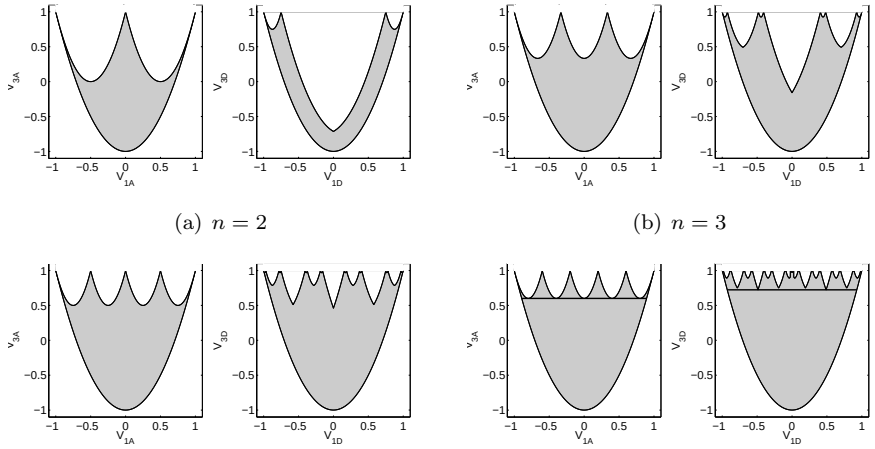

(a) $n = 2$ (b) $n = 3$

(c) $n = 4$ (d) $n = 5$

Figure 2.3: *Feasible domain for in-plane and flexural lamination parameters of balanced symmetric laminates of lay-up* $[\pm\theta_1/\pm\theta_2/\ldots/\pm\theta_n]_s$ *with equal thickness layers. The horizontal line for* $n = 5$ *forms the upperbound of the convex feasible domain.*

2.2.3 Fractal nature of the practical envelope

Each laminate that consists of more than two layers can be interpreted as a laminate consisting of two sub-laminates: a sub-laminate of $n-1$ layers and a sub-laminate of 1 layer. The influence of these sub-laminates on the final LP-value is then weighted accordingly, i.e. $\frac{n-1}{n}$, respectively $\frac{1}{n}$ for the in-plane LPs, and $\left(\frac{n-1}{n}\right)^3$, respectively $\frac{1}{n^3}$ for the flexural LPs.

Closer inspection of the family of graphs in figure 2.3 shows that the upper boundary of the feasible domain for $n-1$ layers repeats in the upper boundary of the feasible domain for n layers. For the in-plane LPs the profile of the upper boundary is scaled down by a factor $\frac{n-1}{n}$. The profile of the upper boundary for the flexural LPs is scaled down by a factor of $\frac{(n-1)^3}{n^3}$. In the limit of $n \to \infty$ both scaling factors will go to 1, i.e. the feasible domain converges to the theoretical feasible domain $2V_1^{\mathbf{AD}\,2} - 1 \leq V_3^{\mathbf{AD}} \leq 1$.

The Hausdorff dimension of metric space X is defined as:

$$\dim_H(X) = \inf\left\{d \geq 0 : C_H^d(X) = 0\right\} \tag{2.14}$$

By definition (Mandelbrot 1999) a fractal is a set for which the Hausdorff Besicovitch dimension strictly exceeds the topological dimension D_T, e.g. for a point $D_T = 0$, for a line $D_T = 1$ and for a surface $D_T = 2$. A more practical

measure is given by the similarity dimension D, equation 2.15, which for self-similar shapes like the practical feasible domains mentioned above, can be used to guess the Hausdorff Besicovitch dimension:

$$D = \frac{\log(N)}{\log(\frac{1}{r})} \tag{2.15}$$

where r is the scaling factor and N is the number of parts covering each segment. Koch's curve, see Fig. 2.4, is used to demonstrate this concept. Consider a line segment of given length, Koch's curve is then constructed by recursively:

1. dividing the line segment into three segments of equal length
2. replacing the middle segment by an upward pointing equilateral triangle
3. removing the base segment of the triangle

The starting point and the first two iterations are shown in Fig. 2.4. The line segment in the first iteration is replaced by 4 line segments each $\frac{1}{3}$ of the length of the original segment, hence $N = 4$ and $r = \frac{1}{3}$. Therefore $D = \frac{\log(4)}{\log(3)}$. $D_T = 1$ for the original line segment. It is thus proven that Koch's curve is a fractal, $D > D_T$.

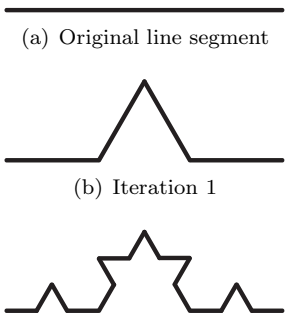

(a) Original line segment

(b) Iteration 1

(c) Iteration 2

Figure 2.4: *Koch's curve.*

There are two permutations for a laminate subdivided into a sub-laminates of $n-1$ layers and 1 layer respectively: the single layer sub-laminate is stacked on top of the $(n-1)$-sub-laminate to form the full laminate, or the other way around. The $(n-1)$-sub-laminate can be described by a single point in LP space. Adding one layer of given orientation to the $(n-1)$-sub-laminate, results in two possible

points in LP-space because there are two permutations: $N = 2$. The weight of the single layer that is added is determined by the scaling factor, for in-plane LPs this is $\frac{n-1}{n}$ and for flexural LPs this is $\frac{(n-1)^3}{n^3}$. The similarity dimension for the case of two sub-laminates then becomes: $D = \frac{\log(2)}{\log(n)}$ for in-plane LPs and $D = \frac{\log(2)}{3\log(n)}$ for flexural LPs. The topological dimension of a point in LP-space is 0 for both in-plane and flexural LPs $D > D_T$ at all times. This serves as proof that the practical feasible LP domain is a fractal. Terada et al. (2001) were the first to observe that the feasible domain of the LPs behaved like a fractal.

The fractal nature of the feasible domain can be used to our advantage when describing it for any number of layers n. At the same time it shows us that the practical feasible envelope of the LPs will converge towards the continuous one, but will never fully coincide.

2.3 Conversion process

The usage of LPs as design variables depends on the presence of a strategy to convert a given point in LP space into a laminate configuration, or where that is not possible, to find a laminate configuration that represents the target LP values best, i.e. which is closest in LP-space and/or minimizes the value of the objective function specified for the optimisation problem.

2.3.1 From LPs to laminate configuration

The approaches to convert LPs into laminate configurations that are found in literature can be divided into three categories:

i. Analytical

ii. Discrete search and optimisation

iii. Continuous optimisation

In the following each of these categories will be discussed.

Analytical approach

An analytical method to determine the best laminate configuration from a given set of in-plane or flexural LPs is proposed by Fukunaga and Sekine (1992). They solve the system of the in-plane LPs $V_i^{\mathbf{A}}$, $i = 1 \ldots 4$ or the flexural LPs $V_i^{\mathbf{D}}$, $i = 1 \ldots 4$. As a consequence, their method is limited to four-layer symmetric

laminates, and can only consider the four in-plane or the four flexural LPs at a time.

Using a three-layered laminate any set of the four in-plane LPs can be obtained as is shown by Hammer, Bendsøe, Lipton and Pedersen (1997), Lipton (1994), and Autio (2001). Only two layers are required to do the same for the flexural LPs.

The above observations are only valid when considering ply thickness as a continuous variable, which makes them not directly suitable for practical application, in which the ply thickness is limited to a discrete set of values.

Balanced symmetric laminates can be described using four LPs ($V_1^{\mathbf{A}}$, $V_3^{\mathbf{A}}$, $V_1^{\mathbf{D}}$, $V_3^{\mathbf{D}}$), ignoring the coupling terms D_{16} and D_{26} of the $\mathbf{D}$-matrix. Equi-thickness plies are assumed by Van Campen and Gürdal (2009), which can be used to uniquely definite the laminate $[\pm\theta_1/\pm\theta_2]_s$ for a combination of $V_1^{\mathbf{A}}$ and $V_3^{\mathbf{A}}$, given their values are within the practical feasible domain, see section 2.2.2. The layers θ_1 and θ_2 can be stacked in two ways, which means that there are two points in the flexural Miki diagram, see Fig. 2.1, that correspond to the given in-plane LPs:

$$\begin{aligned} V_{1_c}^{\mathbf{D}} &= V_1^{\mathbf{A}} \pm \tfrac{3}{8}\sqrt{2(V_3^{\mathbf{A}} - 2\,{V_1^{\mathbf{A}}}^2 + 1)} \\ V_{3_c}^{\mathbf{D}} &= V_3^{\mathbf{A}} \pm \tfrac{3}{2} V_1^{\mathbf{A}} \sqrt{2(V_3^{\mathbf{A}} - 2\,{V_1^{\mathbf{A}}}^2 + 1)} \end{aligned} \tag{2.16}$$

Similarly, for a combination of $V_1^{\mathbf{D}}$ and $V_3^{\mathbf{D}}$ given in the feasible domain, there is at least one and at most two points in the in-plane Miki diagram that correspond to the given flexural LPs:

$$\begin{aligned} V_{1_c}^{\mathbf{A}} &= V_1^{\mathbf{D}} \mp \tfrac{3}{14}\sqrt{14(V_3^{\mathbf{D}} - 2\,{V_1^{\mathbf{D}}}^2 + 1)} \\ V_{3_c}^{\mathbf{A}} &= -\tfrac{36}{7} V_1^{\mathbf{D}} + \tfrac{25}{7} V_3^{\mathbf{D}} \mp \tfrac{6}{7} V_1^{*} \sqrt{14(V_3^{\mathbf{A}} - 2\,{V_1^{\mathbf{A}}}^2 + 1)} + \tfrac{18}{7} \end{aligned} \tag{2.17}$$

For both cases the values for θ_1 and θ_2 are easily computed:

$$\begin{aligned} \theta_1 &= \pm\tfrac{1}{2} \arccos\left(V_1^{\mathbf{D}} \pm \tfrac{1}{14}\sqrt{14(V_3^{\mathbf{D}} - 2\,{V_1^{\mathbf{D}}}^2 + 1)} \right) \\ \theta_2 &= \pm\tfrac{1}{2} \arccos\left(V_1^{\mathbf{D}} \mp \tfrac{1}{2}\sqrt{14(V_3^{\mathbf{D}} - 2\,{V_1^{\mathbf{D}}}^2 + 1)} \right) \end{aligned} \tag{2.18}$$

From Eqs. 2.16 and 2.17 it can be deduced that, given a set of four LPs $V_1^{\mathbf{A}}$, $V_3^{\mathbf{A}}$, $V_1^{\mathbf{D}}$, $V_3^{\mathbf{D}}$, there are cases possible where the balanced symmetric laminate with two designed plies, $[\pm\theta_1/\pm\theta_2]_s$, cannot represent the in-plane and flexural LPs at the same time. Therefore a line-search in θ-space is performed:

$$\theta_{1,2} = (1-s)\theta_{1,2}^{\mathbf{A}} + s\theta_{1,2}^{\mathbf{D}} \quad , \quad 0 \le s \le 1 \tag{2.19}$$

where $\theta_{1,2}^{\mathbf{A}}$ and $\theta_{1,2}^{\mathbf{D}}$ are the lay-ups that satisfy the in-plane and the flexural LPs respectively. The objective of this line search is to minimise the distance in LP-space between the desired LPs and those calculated for the laminate $[\pm\theta_1/\pm\theta_2]_s$. The main drawback of this semi-analytic approach is that it is not expandable to a larger number of designed plies.

Discrete search and optimisation

Layerwise Optimisation (LO) (Narita 2003) is a simple iterative search strategy. The fibre angles which result in the smallest difference between the desired LPs and the actual LPs of the laminate are determined sequentially for each layer. The search algorithm starts from the layer furthest away from the mid-plane of the laminate. Once the orientation of the most outward layer which best satisfies the desired LPs has been determined by scanning the range of $[0°, 90°]$ using a predefined increment, the algorithm moves on to the next most outward layer. This process is repeated until the layer closest to the mid-plane is reached, see Fig. 2.5. Moving from the most outward layer to the most inward layer addresses the larger influence on the flexural behaviour of the laminate that layers positioned further away from the mid-plane have.

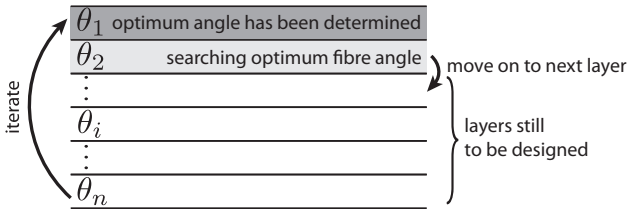

Figure 2.5: *Layerwise Optimisation Approach (Narita and Hodgkinson 2005)*

The algorithm only accounts for a layer in the computation of the LPs once a fibre angle has been assigned to it, because each layer is designed separately, its optimal orientation may change once the orientations of other layers have been determined and are taken into account for the computation of the LPs of the laminate. Therefore, the algorithm requires a small number of iterations before settling into a final design (Narita and Hodgkinson 2005).

A branch and bound method to search for the laminate best matching a predefined set of LPs is applied by Terada et al. (2001). The search algorithm is made more efficient by making use of the fractal nature of the feasible domain of the LPs, see section 2.2.3. This seminal work on the fractal branch and bound (FBB) method is limited to the flexural Miki diagram, i.e. $V_1^{\mathbf{D}}$ and $V_3^{\mathbf{D}}$. The FBB method has been extended to unsymmetrical laminates and therefore to 9 LPs by Matsuzaki and Todoroki (2007). In this case $V_4^{\mathbf{A}} = V_4^{\mathbf{B}} = V_4^{\mathbf{D}} = 0$ because

the fibre orientation angle set is limited to $[0°/\pm 45°/90°]$. The FBB method is extended further in Todoroki and Sekishiro (2008) to include a strength constraint and to make it applicable to structures with more than one region for which the laminate configuration is to be determined, e.g. blade-stiffened panels.

LPs are fitted with a laminate configuration by IJsselmuiden et al. (2009*a*) using an approximation of the desired mechanical response of the laminate. To this end they apply a genetic algorithm (GA), which uses a discrete set of fibre angle orientations to code a laminate configuration. The individuals of the GA are decoded into laminate configurations for evaluation. Laminate encoding using GAs will be discussed in further detail in chapter 3.

Continuous optimisation

The inverse relationship is posited by Diaconu and Sekine (2004) as an optimization problem, allowing layer thickness to be a continuous variable. The main drawback of this approach is that layer thickness for the optimised design must be rounded off to the nearest discrete value, which means moving away from the obtained optimum.

The fibre orientation angle for each layer in the laminate is expanded by Setoodeh, Blom, Abdalla and Gürdal (2006) by using a set of basis functions with unknown coefficients. The coefficients are sought which result in the closest distribution of the lamination parameters to their optimal distribution in a least square sense. The resulting non-linear least square problem is subjected to a constraint on in-plane fibre angle curvature, associated with automated fibre placement technology. The problem is solved using a constrained non-linear least square solver. The results show that the mechanical performance of the fibre angle design approaches the mechanical performance obtained for the LP optimum. The design of variable stiffness composites will be described in more detail in chapter 5.

In this chapter a new methodology is described to convert an optimal set of LPs into a stacking sequence design of a given configuration. First the laminate configuration is specified, e.g. $[\pm\theta_1/\pm\theta_2\ldots/\pm\theta_n]_s$ where n is the number of specifiable fibre orientation angles in the laminate. (Note, that the thickness of the laminate is kept constant.) Then the fibre orientation angles for the laminate are obtained using a two-step optimisation approach (Van Campen et al. 2011). This optimisation formulation will be described in detail in the following section.

2.3.2 Optimisation formulation

From the discussion on the feasible domain of lamination parameters, section 2.2, it can be concluded that there is no closed form solution to convert a point in LP space into a balanced symmetric stacking sequence. Even more so, when

prescribing the number of layers in the laminate, certain points in LP space do not have a corresponding lay-up, and the closest alternative must be found.

Laminate design in terms of fibre angles in most cases is a non-convex optimisation problem (Svanberg 1984). Therefore it is proposed to seed a gradient-based optimiser with multiple starting points in order to reduce the likelihood of getting stuck in a local optimum. The starting points are obtained using the genetic algorithm described in appendix B. The m best designs are passed on to a gradient-based solver. The solver used for the research presented here uses a gradient descent approach, and yields m laminate designs from which the best one is selected to be the result of the conversion process. The two-step optimisation approach is drawn schematically in Fig. 2.6.

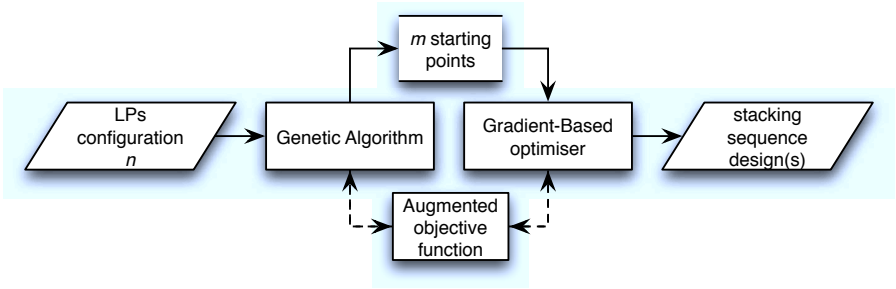

Figure 2.6: *Proposed two-step approach to convert LPs into a stacking sequence design. In the first step a GA is used to determine the best stacking sequence design for a given laminate configuration and a given number of layers n. These designs, limited to a discrete set of fibre orientation angles, are refined in the second gradient-based optimisation step.*

Any objective can be chosen for this optimisation problem. Without any further information the most straight forward objective would be the least square distance of the LPs to the desired optimum point. The distance-based objective function proposed here, takes the form:

$$f = |\mathbf{V} - \mathbf{V}^*| \quad \text{with} \quad \mathbf{V} = \left\{V_1^{\mathbf{A}}, V_3^{\mathbf{A}}, V_1^{\mathbf{D}}, V_3^{\mathbf{D}}\right\} \tag{2.20}$$

where * denotes the given optimum lamination parameters.

The stacking sequence design may be subject to manufacturing constraints and/or engineering guidelines. This necessitates the inclusion of constraints in the optimisation process. In order to facilitate the implementation in the GA an augmented objective function is proposed:

$$\Phi = \begin{cases} f + \varepsilon g_{\max} & \text{if} \quad g_{\max} \leq 0 \\ f + \beta g_{\max} & \text{if} \quad g_{\max} > 0 \end{cases} \tag{2.21}$$

where Φ is to be minimized. Eq. 2.21 is an augmented objective function, in which f describes the actual objective of the optimisation problem, see Eq. 2.20, g are the constraint margins, $g = 0.1$ means a 10% constraint violation, whereas $g = -0.1$ indicates a 10% constraint margin. They are multiplied by bonus term ε, respectively penalty term β.

An important constraint in contemporary laminate design is the requirement for built-in robustness, often referred to as the 10%-rule. The limitation of the feasible LP envelope due to this constraint and the implementation of a constraint margin for it will be described in section 2.3.3.

A drawback of the described approach is that it needs to be repeated each time a set of LPs is converted into a stacking sequence design. This can be prevented by the construction of a database of stacking sequences for which the LPs have been computed and stored. The best fitting stacking sequence(s) are picked from this database by means of a simple search. The advantage is that a database only needs to be constructed once for a given type of laminate configuration.

2.3.3 Robust laminate design

Several empirical design rules are employed in contemporary composite laminate design in order to guarantee the robustness of the laminate against secondary loading that cannot be easily modelled (and/or may not even be known) during the design. These empirical design rules limit the region in LP space that can be used for laminate design.

A commonly applied practical constraint is the ten percent rule. The philosophy behind the ten percent rule is that a laminate has a minimum required amount of fibres in all four directions, $\{-45°, 0°, 45°90°\}$. This should assure a certain stiffness and strength of the laminate in its weakest and most compliant direction. This constraint is mainly concerned with the in-plane behaviour of a laminate.

Abdalla, Kassapoglou and Gürdal (2009) present a description of the constraint on the feasible region of the in-plane LPs for balanced laminate designs based on laminate stiffness, Eq. 2.22:

$$\begin{aligned} &(1-\alpha)^2 + (1-\alpha)V_3^{\mathbf{A}} - 2{V_1^{\mathbf{A}}}^2 \geq 0 \\ &1 - \alpha - V_3^{\mathbf{A}} \geq 0 \end{aligned} \tag{2.22}$$

where:

$$\alpha = 1 - \frac{(1-4p)(\gamma_0+\gamma_1)}{2\gamma_0\gamma_1} \tag{2.23}$$

$$(\gamma_1,\gamma_0) = \begin{cases} (\frac{\gamma^*}{\iota},\gamma^*) & ,\delta \le 1 \\ (\gamma^*,\iota\gamma^*) & ,\delta \ge 1 \end{cases} \tag{2.24}$$

$$\gamma^* = \frac{U_5}{U_3} \tag{2.25}$$

$$\delta = \frac{1}{2\sqrt{2}}\frac{U_2}{U_3}\sqrt{\frac{U_1-U_4}{U_1+U_4}} \tag{2.26}$$

$$\iota = \begin{cases} \frac{\delta}{4}\left(\sqrt{8+\delta^2}+\delta\right) & ,\delta \le 1 \\ \frac{1+\sqrt{1+8\delta^2}}{4\delta^2} & ,\delta \ge 1 \end{cases} \tag{2.27}$$

$$\tag{2.28}$$

Here p is minimum required percentage of volume fraction per direction, 0.1 for the ten percent rule. A definition of the material invariants U_i is given in appendix A.

It is clear that this constraint on the LPs is dependent on the mechanical properties of the material system used, and is different from the conventional ten percent rule, as it does not use any orientation angles. Taking $\alpha = 4p$, a relaxed form of the ten percent rule is obtained. A laminate consisting of only the fibre directions $\{-45°, 0°, 45°90°\}$ would result in the triangular domain presented in Fig. 2.7. Relaxation of the fibre angle orientations results in a scaled-down and translated version of the original bounding parabola $V_3^{\mathbf{A}} + 2\,{V_1^{\mathbf{A}}}^2 \ge 1$, $V_3^{\mathbf{A}} \le 1$, as is also plotted in Fig. 2.7.

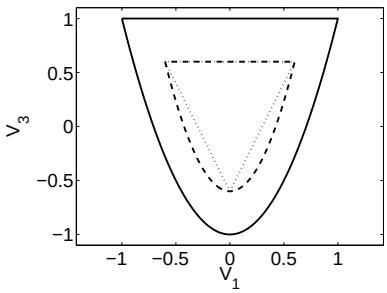

Figure 2.7: *Robust feasible domain for the in-plane LPs* $V_1^{\mathbf{A}}$ *and* $V_3^{\mathbf{A}}$*,* $\alpha = 4p$*,* $p = 0.1$*.*

The robustness constraint described above can be used in the design of composite laminates using LPs. To guarantee that the constraint will still be satisfied after converting such a robust LP design into a laminate configuration, it is important

to include the robustness constraint in the conversion process.

Empirical design rules, like the ten percent rule can be enforced on the conversion process from LPs to a laminate configuration through introduction of a constraint in the optimisation problem, as was described in section 2.3.2. The constraints in Eq. 2.22 are normalised using the relative size of the scaled parabola, $(1-\alpha)$. This results in the constraint margins:

$$g_1 = \frac{2}{1-\alpha}\, {V_1^{\mathbf{A}}}^2 - V_3^{\mathbf{A}} - (1-\alpha) \tag{2.29}$$

$$g_2 = \frac{1}{1-\alpha} V_3^{\mathbf{A}} - 1 \tag{2.30}$$

2.4 VERIFICATION

A selection of assumed optimum points in LP space will be considered in this section to investigate the efficiency of the proposed conversion process from LPs to a stacking sequence design. The effect of the number of layers in the laminate, and the use of different laminate configurations will be considered for an extended definition of the quasi-isotropic laminate, and the enforcement of robust laminate design will be considered for a unidirectional laminate.

2.4.1 EXTENDED QUASI-ISOTROPIC DESIGN

The aim of quasi-isotropic (QI) laminate design is to achieve near isotropic in-plane properties for a composite laminate. Here the definition is extended to achieve a near isotropic response for all mechanical properties of a composite laminate. The lamination parameters (LP) of this extended QI laminate equal the null vector: $\mathbf{V^{ABD}} = \mathbf{0}$. Five different laminate configurations were used to obtain laminate designs close to or satisfying these LPs:

- Plain: $[\theta_1/\ldots/\theta_n]$
- Balanced: $[\pm\theta_1/\ldots/\pm\theta_n]$
- Symmetric: $[\theta_1/\ldots/\theta_n]_s$
- Balanced-symmetric: $[\pm\theta_1/\ldots/\pm\theta_n]_s$
- Special orthotropic: $[[\pm\theta_1/\ldots/\pm\theta_n]_s]_a$
  (Caprino and Crivelli Visconti 1982)

where $_a$ means anti-symmetric. Thickness of the laminate is assumed to be constant and independent of the laminate configuration used.

Results were obtained for $\varepsilon = 0.1$, $\beta = 5$, see Eq. 2.21, and for 1 up to 16 designed layers. The GA, see appendix B, was set to a population size of 50 individuals, with 5 elite individuals. Fibre angles ranged from $-75°$ to $90°$ with $15°$-increments. The probabilities of mutation, permutation and ply swap were set to 5% each, and the probability of crossover to 100%. The GA was considered to have converged after 10 iterations without improvement. Gradient descent was used as gradient-based solver, applying the Jacobian of the objective function, Eq. 2.21. A step-size of $5 \cdot 10^{-3}$ was used, and the solution was considered to be converged after 10 consecutive iterations with improvement of less than 0.1%.

The laminate designs that were obtained for the case when only $V_1^{\mathbf{A}}$ and $V_3^{\mathbf{A}}$ are considered in the conversion process, are presented in table 2.1. The case $V_1^{\mathbf{A}} = V_3^{\mathbf{A}} = 0$ corresponds to conventional QI design. The development of the residual term f, the distance in LP space between the LPs of the laminate and the LP target, as function of designed layers is plotted in Fig. 2.8. The laminate configuration has no effect on the outcome of the conversion process, as was to be expected, because the values of $V_1^{\mathbf{A}}$ and $V_3^{\mathbf{A}}$ are insensitive to stacking sequence or balancing. The insensitivity to stacking sequence is reflected in the obtained designs, see table 2.1. Two complementary fibre angle values were found for $n = 1$. Note that because of the cosine terms used to compute $V_1^{\mathbf{A}}$ and $V_3^{\mathbf{A}}$ the sign of the fibre angle is irrelevant. For $n = 2$ two permutations of the same design were obtained. Four permutations of the same design, and one design very close to the known QI design were found for $n = 4$. The residual terms is near zero for all $n \geq 4$.

Table 2.1: *QI fibre angle designs for several laminate configurations, $V_1^{\mathbf{A}} = V_3^{\mathbf{A}} = 0$. Development of the LP residual is plotted in Fig. 2.8*

Laminate configuration	**Number of designed layers** n		
	$n = 1$	$n = 2$	$n = 4$
$[\theta_1/\ldots/\theta_n]$	$\{26.4\}$	$\{68.1, 21.9\}$	$\{31.4, 76.2, -58.6, 13.8\}$
$[\pm\theta_1/\ldots/\pm\theta_n]$	$\{26.4\}$	$\{-21.9, -68.1\}$	$\{13.8, 31.4, 58.6, -76.2\}$
$[\theta_1/\ldots/\theta_n]_s$	$\{-26.4\}$	$\{-68.1, -21.9\}$	$\{-0.122, 45.1, -45.1, -89.5\}$
$[\pm\theta_1/\ldots/\pm\theta_n]_s$	$\{63.6\}$	$\{68.1, -21.9\}$	$\{13.8, 76.2, -58.6, 31.4\}$
$[[\pm\theta_1/\ldots/\pm\theta_n]_s]_a$	$\{-26.4\}$	$\{-68.1, -21.9\}$	$\{31.4, 58.6, 76.2, -13.8\}$

The requirement that $V_1^{\mathbf{A}} = V_3^{\mathbf{A}} = V_1^{\mathbf{D}} = V_3^{\mathbf{D}} = 0$ is an extension of the conventional definition of QI laminates. The designs that were obtained when only $V_1^{\mathbf{A}}$, $V_3^{\mathbf{A}}$, $V_1^{\mathbf{D}}$ and $V_3^{\mathbf{D}}$ are considered in the conversion process are presented in table 2.2, and the development of the residual term f as a function of designed layers is plotted in Fig. 2.9. It was found that a few more designed layers n

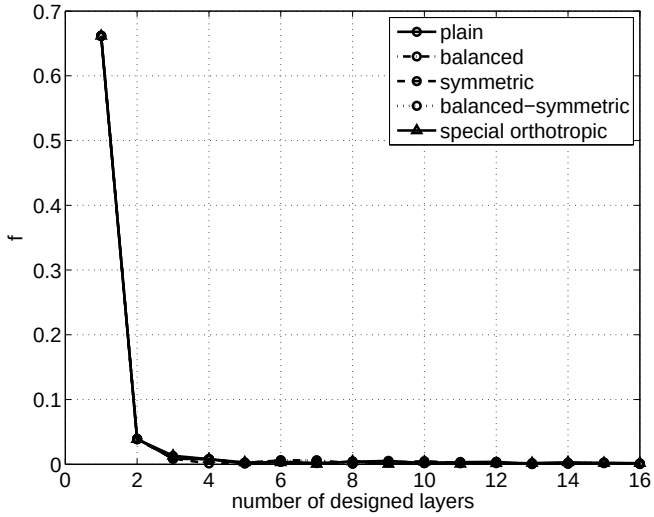

Figure 2.8: *Residual term f as function of the number of designed, $V_1^{\mathbf{A}} = V_3^{\mathbf{A}} = 0$.*

were required before the residual term was near zero, more than was the case when only $V_1^{\mathbf{A}}$ and $V_3^{\mathbf{A}}$ were considered. The rate of convergence of all laminate configurations considered was similar, but not equal, because stacking sequence and thus laminate configuration influence the values of $V_1^{\mathbf{D}}$ and $V_3^{\mathbf{D}}$.

Fibre angle results for $n = 1$ showed two complementary designs. The fibre angle designs for $n = 2$ for the different laminate configurations appeared to be similar, but were no longer permutations of the same design as was the case for $V_1^{\mathbf{A}}$ and $V_3^{\mathbf{A}}$, because $V_1^{\mathbf{D}}$ and $V_3^{\mathbf{D}}$ are taken into account. The differences between the fibre angle designs for the different laminate configurations was increased for $n = 4$.

Table 2.2: *QI fibre angle designs for several laminate configurations, $V_1^{\mathbf{A}} = V_3^{\mathbf{A}} = V_1^{\mathbf{D}} = V_3^{\mathbf{D}} = 0$. Development of the LP residual is plotted in Fig. 2.9*

Laminate configuration	**Number of designed layers** n		
	$n = 1$	$n = 2$	$n = 4$
$[\theta_1/\ldots/\theta_n]$	$\{-26.2\}$	$\{-22.6, 67.4\}$	$\{-67.3, 67.4, 22.6, -22.7\}$
$[\pm\theta_1/\ldots/\pm\theta_n]$	$\{-63.8\}$	$\{22.7, 67.3\}$	$\{67.3, 22.6, -67.4, 22.7\}$
$[\theta_1/\ldots/\theta_n]_s$	$\{-26.2\}$	$\{-26.8, -74.5\}$	$\{62.4, 0, -35.4, -69.9\}$
$[\pm\theta_1/\ldots/\pm\theta_n]_s$	$\{-26.2\}$	$\{-63.2, 15.5\}$	$\{32.2, 88.5, -15.4, 53.7\}$
$[[\pm\theta_1/\ldots/\pm\theta_n]_s]_a$	$\{26.2\}$	$\{-24.9, -70.3\}$	$\{58.3, 4.79, 74.1, -35.1\}$

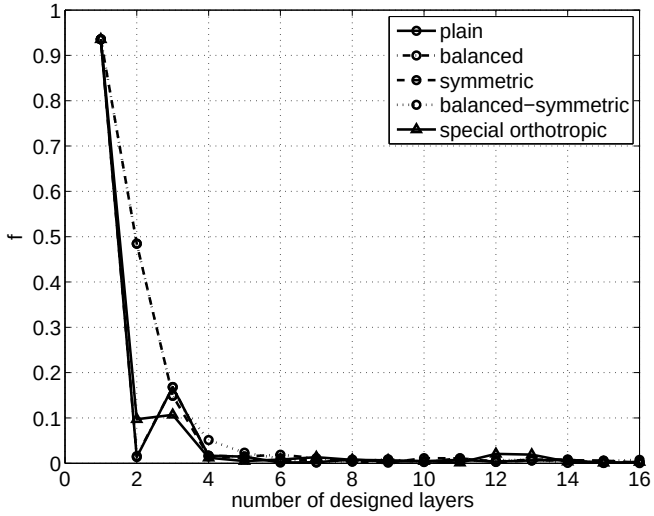

Figure 2.9: *Residual term f as function of the number of designed, $V_1^{\mathbf{A}} = V_3^{\mathbf{A}} = V_1^{\mathbf{D}} = V_3^{\mathbf{D}} = 0$.*

The laminate designs that were obtained for the case when $\mathbf{V}$ are considered, are presented in table 2.3, and the development of the residual term f as a function of designed layers is plotted in Fig. 2.10. The spread of the residual term f for the different laminate configurations was much larger than for the two previously presented design cases. The reason for this is that all LPs are taken into account. Symmetry eliminates the $\mathbf{B}$-matrix, giving symmetric designs an advantage over other designs, and balancing eliminates the coupling terms for the $\mathbf{A}$-matrix and makes them negligibly small for the $\mathbf{D}$-matrix when $+\theta_i$ and $-\theta_i$ are next to each other. Designs which are not balanced or symmetric will require more designed layers in the laminate in order to find a design in which the coupling terms are (nearly) eliminated. All laminate configurations considered in Fig. 2.10 eventually converged to $f \approx 0$. The special-orthotropic and balanced designs were found to converge fastest.

The relation between the total number of layers in a laminate n_t and the number of fibre angles that is designed n_d depends on the chosen laminate configuration. This relationship is $n_t = n_d$ for the plain laminate configuration up to $n_t = 8n_d$ for the special-orthotropic configuration. This relationship can be used to put the results that were found for $\mathbf{V} = \mathbf{0}$ into perspective. When plotting the residual f as function of n_t, see Fig. 2.11, the spread between the different laminate configurations was greatly reduced, and the special-orthotropic configuration appeared to be rather restrictive.

Table 2.3: *QI fibre angle designs for several laminate configurations,* $\mathbf{V} = \mathbf{0}$. *Development of the LP residual is plotted in Fig. 2.10*

Laminate configuration	**Number of designed layers** n		
	$n = 1$	$n = 2$	$n = 4$
$[\theta_1/\ldots/\theta_n]$	$\{45\}$	$\{-29.1, -75.9\}$	$\{15.1, -30.5, -74.5, 59.9\}$
$[\pm\theta_1/\ldots/\pm\theta_n]$	$\{-28.5\}$	$\{21.4, -64.7\}$	$\{-63, -15.6, 90, -28.5\}$
$[\theta_1/\ldots/\theta_n]_s$	$\{-45\}$	$\{-27.9, -77.1\}$	$\{73.8, -56.8, 27.5, -14.5\}$
$[\pm\theta_1/\ldots/\pm\theta_n]_s$	$\{26.9\}$	$\{-26.9, -74.7\}$	$\{-31.8, -87.1, 16.5, 54.6\}$
$[[\pm\theta_1/\ldots/\pm\theta_n]_s]_a$	$\{26.2\}$	$\{-24.9, 70.3\}$	$\{-58, 4.55, 74.4, 35.3\}$

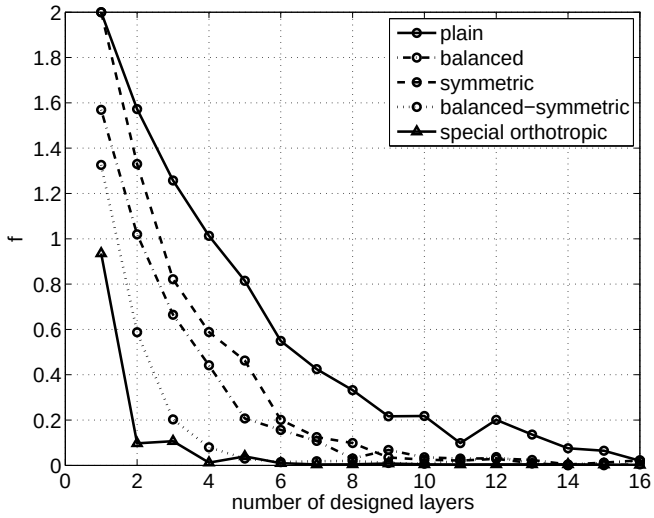

Figure 2.10: *Residual term* f *as function of the number of designed layers,* $\mathbf{V} = \mathbf{0}$.

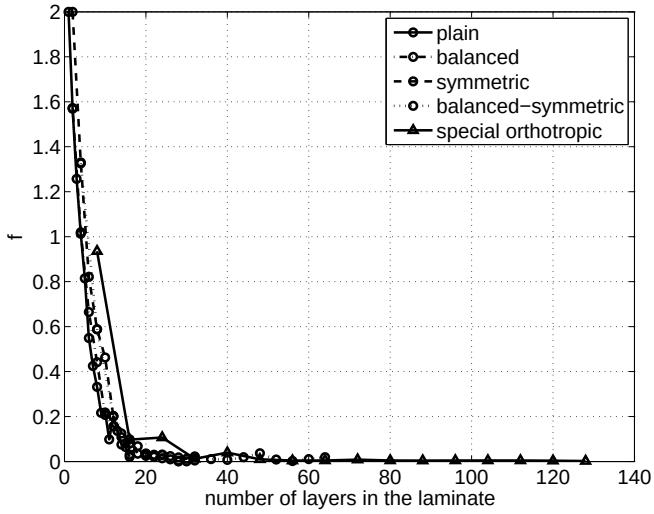

Figure 2.11: *Residual term f as function of the total number of layers in the laminate n_t, $\mathbf{V} = \mathbf{0}$.*

The tool developed to convert LPs into laminate designs was concluded to be capable of satisfying the desired set of LPs for all three design cases, $V_1^{\mathbf{A}} = V_3^{\mathbf{A}} = 0$, $V_1^{\mathbf{A}} = V_3^{\mathbf{A}} = V_1^{\mathbf{D}} = V_3^{\mathbf{D}} = 0$, and $\mathbf{V} = \mathbf{0}$, provided the number of designed layers chosen is large enough and laminate configuration is chosen appropriately. It becomes easier to satisfy the desired point in LP space when the number of LPs considered in the conversion process is reduced.

2.4.2 Robust unidirectional design

A unidirectional (UD) laminate of 0°-orientation is considered: $V_1^{\mathbf{A}}$, $V_3^{\mathbf{A}}$, $V_1^{\mathbf{D}}$, $V_3^{\mathbf{D}}$ equal 1, and all other LPs equal zero. This laminate falls outside the feasible LP envelope for robust laminate design, see section 2.3.3. In order to prove the effectiveness of the robustness constraint this constraint was enforced on the case of UD laminate design.

A balanced-symmetric laminate with four designed fibre orientation angles, $n = 4$ was assumed with the following material properties: $E_1 = 181$GPa (26.25Msi), $E_2 = 10.3$GPa (1.49Msi), $G_{12} = 7.17$GPa (1.04Msi) and $\nu_{12} = 0.28$. Results were obtained for $p = 0.00$ to 0.24 (p is minimum required percentage of volume fraction per direction, 0.1 for the ten percent rule), and the same optimiser settings were applied as used in section 2.4.1. The results are given in table 2.4 and Fig. 2.12 and Fig. 2.13. Only $V_1^{\mathbf{A}}$ and $V_3^{\mathbf{A}}$ were considered for obtaining the results. All

the other LPs were ignored, because robustness is only dependent on the in-plane properties of the laminate.

Table 2.4: *Robust fibre angle designs for several values of p, $p = 0.1$ for the ten percent rule.*

p	α	f	g_1	g_2	θ
0.00	0.2010	0.5082	-0.8746	-0.0068	$\{0, 0, 8.2, 72.4\}$
0.05	0.3608	0.5275	-0.0659	-0.0095	$\{0, 0, 0, 60.5\}$
0.10	0.5206	0.7822	-0.0815	-0.0730	$\{27.7, 3.8, 69.9, 0\}$
0.15	0.6804	0.9973	-0.0894	-0.0650	$\{0, 72.1, 44.8, 7.2\}$
0.20	0.8402	1.2112	-0.0381	-0.1120	$\{29.0, 43.6, 90, 0\}$
0.24	0.9680	1.4006	-0.0131	-0.9596	$\{44.0, 44.0, 0, 90\}$

The robustness constraint for all results was satisfied, i.e. $g_{\max} \leq 0$, and the results for the residual f showed a monotonically increasing trend as the value of p increased. The residual value nearly coincides with the expected value, plotted as a dashed line in Fig. 2.13, for all cases except $p = 0.00$. The reason for this is, that the top right corner of the robust envelope, where the optimum design is expected, falls outside the feasible domain for $n = 4$ when $p = 0$, see Fig. 2.12 and section 2.2.2. The other designs nearly fall onto the top right corner of the robust feasible envelope. It was concluded that the developed tool to convert LPs into stacking sequence designs was capable of satisfying the constraint on laminate robustness presented in section 2.3.3.

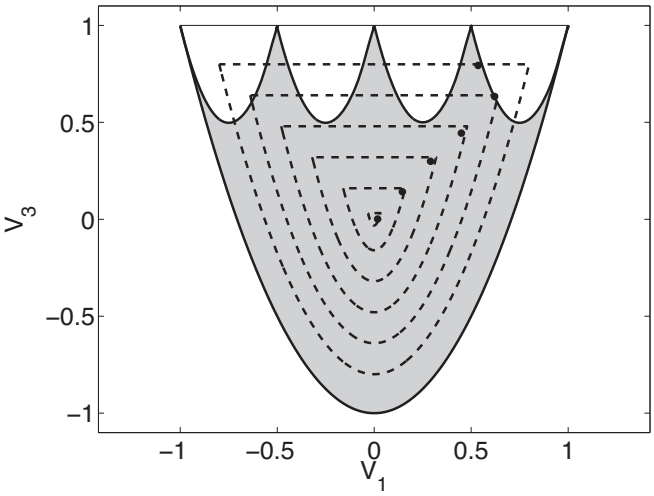

Figure 2.12: *Obtained results in LP space. The robust feasible envelopes are indicated by dashed lines. The largest dashed envelope is for $p = 0$. The feasible domain for $n = 4$ is shaded in grey.*

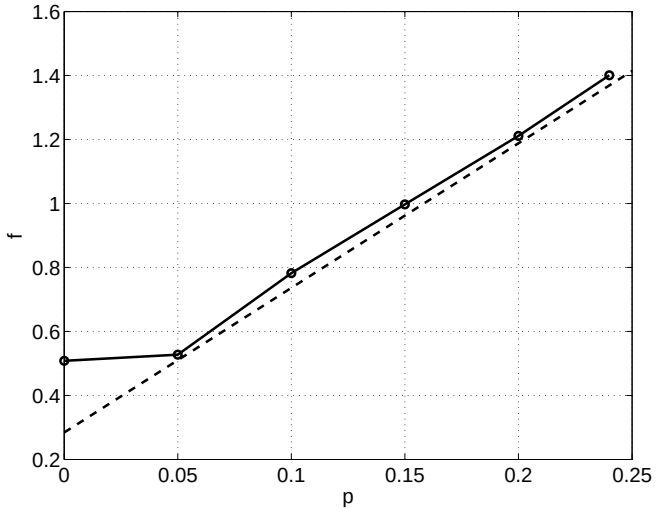

Figure 2.13: *Residual term f as function of p, $p = 0.1$ for the ten percent rule. The dashed line represents the residual term for the ideal case.*

Order, unity and continuity are human inventions just as truly as catalogues and encyclopaedias.

Bertrand Russell (1872 – 1970)

3

MULTI-SEGMENT BLENDED LAMINATE DESIGN

Thin-walled composite structures can be divided into multiple segments, each of which can be subjected to different loading conditions. A single layup that spans across these multiple segments can be designed to satisfy all material and design constraints for these different loading conditions. However, this layup will contain more material than would be required to carry all of the specified loads, even when tailored to meet the most critical loading condition with the smallest possible waste of material capability. The material capability of the laminated composite could be put to more efficient use, if the layup of each segment was tailored to its particular loading condition.

A general problem of designing tailored composite structures with multiple interconnected segments is that, when the segments are designed individually, the stacking sequence that results in the global optimum may not be the same from one segment to another. Inevitably this will lead to incompatibilities in stacking sequence along the edges of adjacent segments. The resulting structure would be at best expensive to manufacture, and in the worst case it will suffer from stress concentrations at the boundaries between segments, or may lack any form of structural integrity. For example, the forces in a ply that is dropped going from one segment to the other need to be transferred through the resin to adjacent plies, and may induce failure of the matrix material. A structure should be designed such that some or all of the plies of the stack of one segment continue in the stacks of the adjacent segments to avoid this undesirable outcome of the design process. Enforcing stacking sequence continuity from one segment to another is generally referred to as *blending*.

Several methods to achieve multi-segment blended composite laminate design can be found in the literature and these include the following:

- "less-than-or-equal rule" (Kristinsdottir et al. 2001): segments can only contain the same plies as an adjacent segment or less

- continuity constraints (Liu and Haftka 2001): continuity is enforced through constraints on the optimisation problem
- design variable zones (DVZ) and sub-laminates (SL) (Soremekun et al. 2002): the optimisation problem is structured in such a way that only blended designs can be represented
- distributed GA within a parallel processing environment with migration: segments are designed separately, and the Levenstein distance (Levenstein 1966) is used to penalise the difference in stacking sequence between adjacent segments. (Adams et al. 2003)
- guide-based blending (Adams et al. 2004, Seresta et al. 2007, Van Campen, Seresta, Abdalla and Gürdal 2008, IJsselmuiden et al. 2009*a*): a guiding string is used from which the stacking sequences of all segments in the structure are derived
- graph-based parametrisation (Giger et al. 2007, Keller 2011): graph theory is used to define compact and connected fibre patches
- shared layers blending (SLB) (Liu et al. 2009*b*): an algorithm ranks all segments in a structure by the number of layers of each orientation, the minimum number of layers shared by all segments is identified and placed as the outermost layers in the laminate, after which the procedure is repeated for the layers remaining in each segment

The design of multi-segment blended composite laminates using a guide-based optimisation procedure is described in this chapter. First, multi-segment composite laminate structures and the definition of blending are discussed in more detail. This is followed by a description of the quintessential manufacturing constraints associated with blended composite laminate design. The manufacturing constraints form the basis of practical blending definitions which can be used in an optimization framework. Several blending definitions and implementations are discussed, and the choice for the guide-based implementation used in this work is explained. Then, a new implementation of guide-based blending using multi-chromosomal genetic encoding is introduced, and the implementations of several existing and new blending definitions using this framework are discussed. The chapter concludes with a demonstration of the proposed blending definition for a simple two-panel example.

3.1 Multi-segment laminate design

An important goal in structural design is to reduce the part count of a structure. Mechanical joints make a significant contribution to structural weight and cost,

and reducing the number of joints leads to weight and cost savings. Advances in laminated composite design have made it possible to replace several metal parts with one composite part. (Ashby 1992). Many examples can be found in contemporary composite laminate design, e.g. an aircraft wing skin (Fig. 3.1).

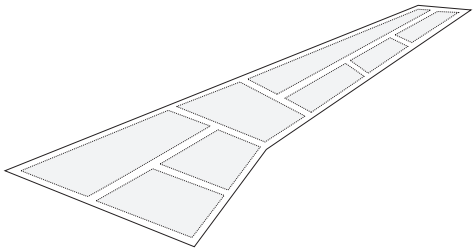

Figure 3.1: *Example of a multi-segment composite structure, wing skin.*

3.1.1 Multi-segment laminates

The integration of multiple parts into a single composite part means that this part will be subject to different loading conditions at different locations on the part. To make effective use of the material properties of the laminated composite, i.e. to tailor a structure (Jones 1999), it is useful to divide the structure into several segments depending on the local loading and/or geometry of the part. Each segment can then be optimised for the specific loading condition(s) it is subjected to. This considerably increases the design space for the part.

A rectangular panel, see Fig. 3.2, can be used to demonstrate this concept. The panel in Fig. 3.2 consists of multiple segments. Assume that p variables are needed to describe the material properties of the lay-up of one segment[1] fully, hence there are at most p design variables if the panel were to be designed as using only a single segment. Dividing the part into q segments of given dimension, see Fig. 3.2, the design space is increased to pq design variables. The increased design space allows for designs that would otherwise be impossible to describe using a single lay-up, and so contributes to the more efficient use of the composite material, at the same time it poses a drawback, as it becomes more complicated to find an optimal design. The definition of optimality depends on the design problem at hand, e.g. whether it is maximisation of buckling load, minimisation of compliance, etc.

The relaxation of the design problem to allow a different layup for each segment in a composite structure is the first step towards variable stiffness (VS) composite

[1] The geometry of the segment is considered to be given and fixed.

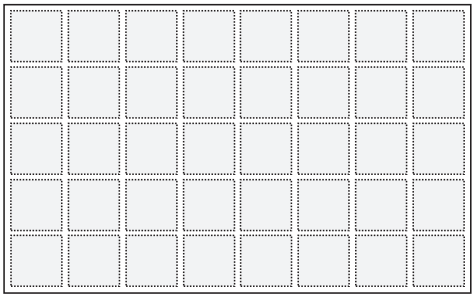

Figure 3.2: *Rectangular panel divided in multiple segments.*

laminate design. It is only under special conditions that the stress state in a structure can be considered to be uniform, thus following this observation segments of a structure can be progressively made smaller, to permit more design freedom, until they eventually converge towards the finite element representation of the structure. Such designs can be accommodated using in-plane fibre steering, as is discussed in chapter 5. In this chapter only straight fibre design is considered.

3.1.2 LAMINATE BLENDING

The activity of designing a structure such that for all segments in the structure some or all plies of the stack of the segment continue in the adjacent segment to improve manufacturing is generally known as *blending*. The term blending was introduced by Zabinsky (1994). The stacking sequence resulting in a global optimum performance may not be the same from one segment to another. Blended composite laminate design tries to avoid incompatibilities in stacking sequence along the edge of adjacent segments that may lead to stress concentrations or lack of structural integrity; this is illustrated in Fig. 3.3.

The laminates in segments II and III in Fig. 3.3 can be said to be perfectly blended, that is they are the same. Between laminates I and II the outermost ply is dropped. This external ply drop is acceptable if the loads (static and fatigue) are low enough for the ply drop not to lead to premature failure. At higher loads, there is the risk of peeling and delamination, and external ply drops should be avoided. Between panels III and IV a ply which is not the outermost ply is dropped, here the risk of peeling and delamination is reduced, because the location of the ply drop is covered by another ply. Between panels IV and V there is a discontinuity in fibre orientation angle in one of the plies, in this case the innermost ply. The discontinuity may lead to stress concentrations locally, but may be deemed acceptable if a sufficient number of plies are used to bridge the discontinuity. Between panels V and VI there is an overall mismatch in stacking

sequence, leading to a total loss of structural integrity at this location.

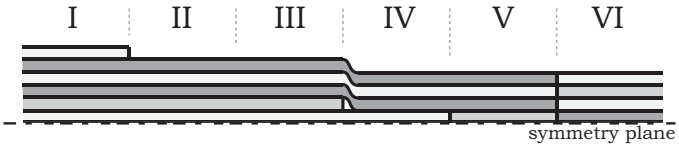

Figure 3.3: *Example of a multi-segment structure.*

3.1.3 Two-step optimisation

The number of design variables is multiplied by the number of segments when designing a multi-segment laminate instead of a single-segment laminate, which will make the optimisation problem overall more complex. Most layup optimisation problems become convex when choosing lamination parameters (LP) as design variables (Svanberg 1984). Therefore, it becomes computationally attractive to pose the design of multi-segment blended composite laminates as a two-step optimisation process (IJsselmuiden et al. 2009*a*), see Fig. 3.4. In the first step each segment is optimised using LPs as design variables. A consequence of designing a laminate in terms of LPs is that the obtained optimum design must be converted into a stacking sequence design, which is done in the second step.

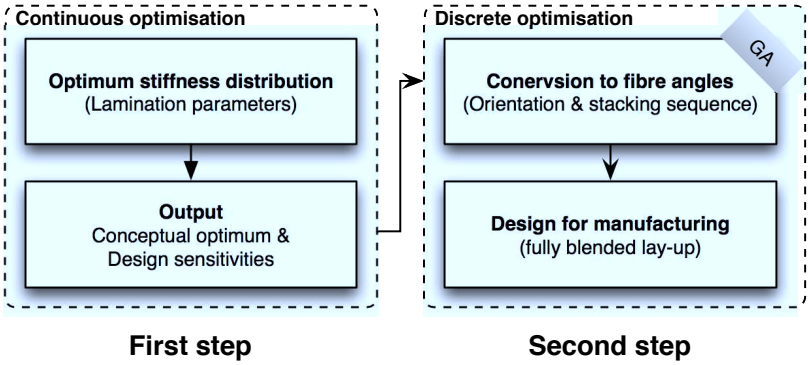

Figure 3.4: *Two-step optimisation process for blended composite laminate design.*

A robust method that can be used to convert a point in lamination parameter space into a laminate configuration was presented in chapter 2. This method can be applied to a segmented structure for which the optimal LPs are given for each segment, and a layup for each segment in the structure is sought which minimises

the local objective function used in the conversion process. The objective function can be either the least-square distance in lamination parameter space, Eq. 2.20 given below:

$$f = |\mathbf{V}^* - \mathbf{V}| \tag{2.20}$$

or an objective function that resembles the objective for which the LPs in each segment were optimised, e.g. maximum buckling load. The layups that result from the conversion process from LPs to fibre angle designs do not necessarily result in a blended design. Therefore blending should be enforced in either the conversion process or once the fibre angles for the given LPs have been retrieved.

The enforcement of blending effectively couples the layup design of all segments in a structure, apart from the coupling that should already occur when the load redistribution over all segments is considered in both design steps: a change in the layup of one segment will directly affect the layups of its neighbouring segments and hence indirectly affect the layups of all other segments in the structure. A stacking sequence design that is optimal for the local[2] segment does not necessarily coincide with the local stacking sequence design that contributes to achieve a global optimum design for the structure. The second step of the two step optimisation process described here can thus be formulated as a global/local optimisation problem, where the global design consists of blending all the local designs. The local optimisation problem can be used to return a number of near optimal stacking sequences, that can then be used to define a surrogate model to be used in the global optimisation problem.

3.2 MANUFACTURING CONSTRAINTS

There are two options when two or more adjacent layups of different stacking sequence occur: layers continue from one layup region into the next, or layers are discontinued/dropped at the edge of the layup region. There is a number of manufacturing constraints that should be considered when layers are dropped:

- no edges of dropped layers may be in physical contact with an edge of an other dropped layer
- the consecutive number of layers dropped at one time and the total number of layers dropped throughout the thickness may not exceed a certain number. These numbers are usually imposed by design rules (e.g. to minimise of the tendency to delaminate) or other considerations (e.g. to maintain a relatively straight neutral axis)

[2]The usage of local and global in this context should not be confused with local and global optima. As used here the terms refer to a single segment, respectively the structure as a whole.

In addition general stacking sequence design guidelines must be adhered to. For example:

- the number of consecutive plies of the same orientation may not exceed a certain number imposed by design guidelines (e.g. to minimise micro-cracking) or other considerations
- the difference in fibre angle orientation between two consecutive plies is kept below a certain value (e.g. to minimise interlaminar stresses)

The aforementioned design guidelines and constraints are discussed in this section.

3.2.1 Edges in physical contact

The fibre angle orientation at the same through-the-thickness coordinate may be different for two adjacent but separately designed layups. The result is a discontinuity in fibre orientation angle at the boundary of the two layup regions. Such a discontinuity can only be accommodated during production by cutting the ply material and having it continue in the different direction specified for the next layup region. However, there are both mechanical and manufacturing issues that need to be overcome using this approach.

The discontinuity of the ply material means that locally stresses need to be transmitted through the matrix material of the laminate from one layup region to the next, and this affects the mechanical properties of the laminate. The stiffness of the matrix material alone is typically much less than that of the fibres and resin combined, thus stiffness is reduced. Strength is reduced likewise, because the matrix material is not as strong as the fibre material, and matrix cracking is likely to occur; the discontinuity can be considered to be a defect. Only if the discontinuity in one layer is bridged on either side by layers that continue from the one region into the other, see Fig. 3.5, might the discontinuity be deemed acceptable from a mechanical point of view.

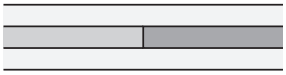

Figure 3.5: *Discontinuity in one ply bridged by continuing layers on either side.*

The laminate can be manufactured by cutting pieces of fibre tape to size and placing them in a mould by hand. Alternatively an automated fibre placement (AFP) machine can be used for the construction of the laminate. Fibre tape can be cut to size and can be placed by hand such that plies in adjacent regions are just touching each other, if due care is applied in production. The risks of defects

at the boundary of two regions when hand layup is used are: improper sizing and placement of the cut fibre material and shifting of the fibres during injection.

The chances on defects due to improper placement or sizing of the tow material are greatly reduced by using AFP, however, the occurrence of gaps and overlaps is an intrinsic feature of AFP. A fibre placement machine (FPM) places bands of uni-directional (UD) ply material, tows, in parallel in order to construct the layer of a laminate. Generally four to thirty-two tows are placed simultaneously in one pass of the machine head, see section 1.5. At the boundary between two layup regions these tow paths are cut perpendicular to the fibre direction, resulting in a zigzag pattern at the boundary. Two zigzag patterns meeting will result in tows overlapping at some points whilst gaps occur at other points, as shown in Fig. 3.6. In summary, a discontinuity in fibre angle direction within one ply should be

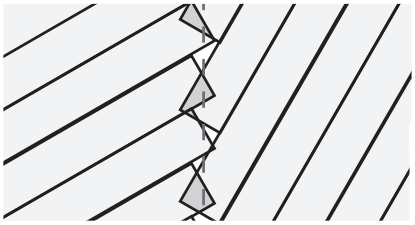

Figure 3.6: *Occurrence of gaps and overlaps for a ply with a discrete change of orientation.*

avoided regardless of the manufacturing method used.

3.2.2 Dropped layers

Dropping a layer between two segments which is not the most outward layer in the layup will lead to the occurrence of a resin pocket as is indicated in Fig. 3.7(a). Such a resin pocket leads to locally higher inter-laminar stresses, and thereby will have a negative effect on the failure response of the laminate (Fagiano 2010).

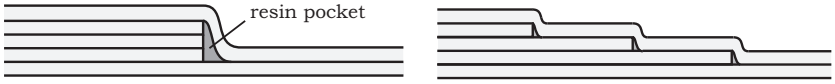

(a) Occurrence of a resin pocket due to dropped plies

(b) Staggered ply drops

Figure 3.7: *Adjacent layup regions with dropped layers.*

Empirical design guidelines to mitigate the negative effects of ply drops can be found in literature (Kassapoglou 2010):

- avoid external ply drops
- drop plies symmetrically w.r.t. the mid-plane of the laminate when more then one ply is dropped
- avoid dropping more than four plies at a single location[3]
- stagger successive ply drops by at least 10/15 times the dropped height

The aim of the first guideline is to prevent delamination; the risk of delamination is high when the ply furthest away from the mid-plane of the laminate is dropped. The other design guidelines mentioned above are designed to reduce inter-laminar shear stresses due to ply drops.

3.2.3 Consecutive ply orientations

UD ply material was the material of choice for the work presented in this thesis. There are some specific design rules that apply to the use of UD material, which have to do with the stacking sequence design of the laminate.

Excessive inter-laminar shear stresses may be induced when the fibre orientations of two consecutive layers are (close to) perpendicular. Large jumps in fibre angle orientation should therefore be avoided. (For example the laminate with stacking sequence $[90/45/0/-45]$ is preferred over the laminate with stacking $[90/0/45/-45]$ sequence.)

A stack of UD layers of the same fibre angle orientation allows for cracks that have formed in the matrix material to grow easily in the through-the-thickness direction of the laminate being arrested (Kassapoglou 2010). Micro-cracks can be arrested by interrupting the stack with layers of a different orientation, preferably at least 45° different from the orientation of the stack. The number of consecutive plies of the same orientation angle should therefore be limited to four or five plies for a typical UD material.

3.3 Blending definition and framework

The design and optimisation of blended composite laminates requires that the manufacturing constraints discussed in the previous section are converted into a mathematical form. The blending definition used determines the mathematical

[3]With proper analysis and testing it may be acceptable to drop more plies.

form the constraints take, and the way they are implemented in an optimisation framework. Both are discussed in this section, but first a categorisation of blending definitions and frameworks is given.

3.3.1 Categorisation of blending definitions and implementations

An extensive review of blending definitions and implementations of the blending problem found in literature was given in section 1.4. The definition of what constitutes a blended laminate and how the optimisation is formulated are closely related. The definitions and their implementations can be categorised by design representation, which is either intrinsically blended or requires extrinsic enforcement of blending, and by how the optimisation problem is defined, either in one step, or in multiple steps. A summary of the blending categories is presented in table 3.1.

The most straightforward solution to the blending problem is to include manufacturing constraints directly in the optimisation problem (Liu and Haftka 2001). However finding a fully blended design this way may be expensive or even impossible. Consequently, design representations are adopted that are intrinsically blended, e.g. guide-based blending (Adams et al. 2004, Seresta et al. 2007), and all computational effort is spent finding the optimal solution within the bounds of the blending definition used. Nonetheless, there is continued interest in extrinsic design representations for the blending problem, because intrinsic representations are found to be too restrictive, excluding possibly manufacturable and optimal designs.

The reason for splitting up the blending problem into multiple levels is to separate the optimisation of mechanical properties from the design for blending, e.g. shared layers blending (SLB) (Liu et al. 2009*a*). The advantage of splitting up the blending problem is that the structural optimisation problem can be solved using a computationally efficient gradient-based optimisation scheme, and the stacking sequence design can be performed using an evolutionary algorithm (EA) using a fitness function based on an approximation of the response of the optimised structure (IJsselmuiden et al. 2009*b*). Overall, a multi-step optimisation framework can be used to improve computational efficiency when designing blended laminates.

A two-step optimisation process was used for the work presented in this thesis, see in Fig. 3.4. The focus of the work presented was the use of generalised guide-based blending definitions which will be discussed next.

Table 3.1: *Categorisation of approaches to laminate blending.*

Representation	Single optimisation	Multi-step optimisation
Extrinsically blended	• Continuity constraints (Liu and Haftka 2001)	• Bi-level optimisation (Liu and Butler 2007)
	• Genetic Algorithm with migration (Adams et al. 2003)	• Shared-layers blending (SLB) (Liu, Toropov, Querin and Barton 2009*a*)
	• Generalised guide-based blending (Van Campen et al. 2008, Van Campen, Kassapoglou and Gürdal 2009)	• Generalised guide-based blending presented in this thesis
		• Competing layups
Intrinsically blended	• "Less-than-or-equal rule" (Kristinsdottir et al. 2001)	• Design variable zones (DVZ) and sub-laminates (SL) (Soremekun et al. 2002)
	• Guide-based blending (Adams et al. 2004, Seresta et al. 2007)	• Guide-based blending (IJsselmuiden, Abdalla, Seresta and Gürdal 2009*b*)
	• Graph-based parametrisation (Giger et al. 2007, Keller 2011)	

3.3.2 GUIDE-BASED BLENDING

Guide-based blending, introduced by Adams et al. (2004), is a computationally efficient way to formulate the blending problem. The optimisation is simplified by introducing a guiding stack from which all laminates in a structure are obtained by deleting a contiguous set of outermost or innermost plies. As a result only one stack needs to be designed for the entire structure, rather than a layup for each segment.

The guide-based blending approach of Adams *et al.* (Adams et al. 2004) cannot be used to trade the degree of blending against weight of the structure, as approaches using continuity constraints do (Liu and Haftka 2001). However, the conventional implementation of the guide-based blending approach inherently satisfies the definitions of inner and outer blending, which is described next.

INNER AND OUTER BLENDING

Inner (outward) and outer (inward) blending of laminate segments are realised by dropping a contiguous set of layers from respectively the outside of the guiding stack or the inside of the guiding stack (Adams et al. 2004), as is shown schematically in Fig. 3.8. Panel I in the figure may be considered to have all the layers in the guide. Panels II and III have one and two layers, respectively, dropped from the guide. Note that only symmetrical laminates are assumed, and that the guiding stack only models one side of the symmetry plane.

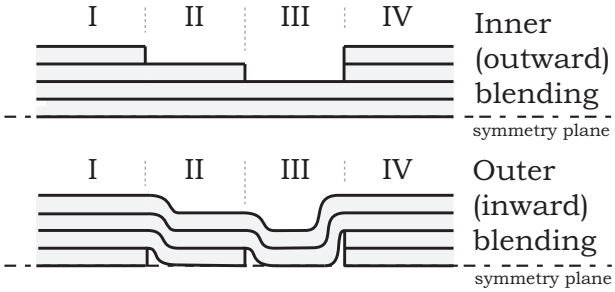

Figure 3.8: *Examples of inner (outward) and outer (inward) blending, after (Adams et al. 2004).*

Inner and outer blending can be successfully used to simplify the optimisation problem. Instead of designing the stack for every segment independently, only the guiding stack and the number of plies per segment need to be designed, which greatly reduces the number of design variables. The definition lends itself very well to a two-step optimisation approach, where the guide is designed globally using

a genetic algorithm (GA)[4] and the number of layers per segment is determined locally (IJsselmuiden et al. 2009*b*).

Generalised blending

The restriction of the design space calls for a relaxation of the blending definition used in conjunction with a guide-based blending implementation. Two such relaxations are introduced by Van Campen et al. (2008): generalised and relaxed generalised blending. Both these definitions are designed to make use of the fact that the computational cost of GA operations are relatively small compared to the computational cost required to evaluate the objective function of the optimisation. An increased level of GA complexity for an equal number of function evaluations results in a relatively small increase of computational effort for the entire optimisation process, because the bulk of the computational cost is associated with the evaluation of the objective function. The implementation of the generalised blending definitions is discussed later in section 3.4.

For the ongoing discussion *generalised blending* is defined as follows:

Definition *Two adjacent laminate segments are considered to be completely blended if all the layers from the thinner panel continue in the thicker one regardless of their position along the thickness of the laminate.*

This definition implies that if two segments have an equal number of plies, they must be the same. Plies can be dropped at any through-the-thickness location in the thicker of the two stacks using this definition, contrary to inner and outer blending where a contiguous set of plies must be dropped. A ply that occurs in the thinner of the two segments without occurring in the thicker of the two segments is called a *mismatched* ply and violates the generalised blending definition. Note that the process of dropping and draping plies remains the same, i.e. irrespective of the number or location of the plies dropped, all the basic physical features of inner and outer blending are shared. Generalised blending is demonstrated in the left side of Fig. 3.9, segments I and II can be considered to be generally blended: segment I is thicker than segment II and all plies in segment II also occur in segment I.

Stacking two blended laminates on top of one another might be called for in some applications of laminate blending. If the result also is to be considered blended, the blending definition needs to be *additive*. The generalised blending definition described above is limited from the point of additivity, because it distinguishes between a thick and a thin segment. It is possible to add together two laminate

[4] The implementation of guide-based blending using a genetic algorithm is explained in section 3.4.

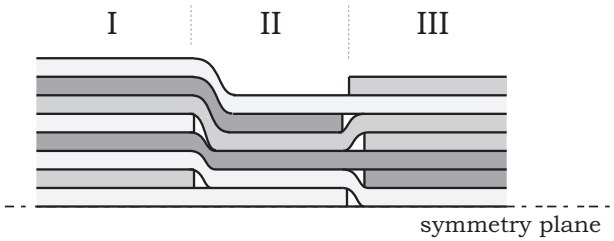

Figure 3.9: *Examples of generalised and relaxed generalised blending.*

designs which are blended according to the generalised blending definition which result in a laminate which is no longer blended according to the generalised blending definition, i.e. plies may occur in the thinner segment which do not occur in the thicker of the two segments.

The generalised blending definition must be relaxed to achieve additivity; the distinction between thick and thin panels needs to be removed. A *relaxed generalised* blending definition is proposed, which is less restrictive than the generalised blending definition:

Definition *Two adjacent laminate segments are considered to be completely blended if there are no dropped edges in physical contact.*

Dropped edges in physical contact are difficult if not impossible to manufacture, as discussed in section 3.2.1, and local gaps and overlaps will occur leading to thickness variations along the edge between two segments. Dropped plies in physical contact are called *butted edges*. Note that the process of dropping and draping plies remains unchanged for relaxed generalised blending. Relaxed generalised blending is demonstrated in the right side of Fig. 3.9, segments II and III can be considered to be blended according to the definition.

Note that features like e.g. the maximum number of contiguous plies that can be dropped do not form an intrinsic part of the generalised and relaxed generalised blending definitions and should be constrained separately. Both generalisations described in this section allow imposing such practical limitations without loss of generality.

3.3.3 Competing layups

A method to convert lamination parameters (LP) into stacking sequence designs was discussed in chapter 2. It was shown that the conversion process has no unique solution, and that as the number of designed plies in the laminate n_d is increased,

the number of alternative layups increases. It can be said that these layups compete to satisfy the desired point in LP-space. The multiplicity in stacking sequence designs per segment can be used to our advantage in relation to the blending problem. Once all possible stacking sequences have been determined for all segments, the combination of stacking sequences which results in the smallest number of violations of the manufacturing constraints mentioned in section 3.2 can be determined. Such a combinatorial problem can be solved using a GA (Adams et al. 2003).

An N-segment structure is considered to demonstrate the concept, see Fig. 3.10. The optimal LPs for each segment are known and for each segment i there are m_i stacking sequences which satisfy the optimal LPs. The total number of stacking sequence combinations then becomes:

$$s = \prod_{i=1}^{N} m_i \tag{3.1}$$

The combination which leads to the smallest amount of manufacturing violations is then subjected to a number of repair operations. The repair operations are designed to eliminate any remaining violation of a manufacturing constraint. Any of the aforementioned blending definitions, inner, outer, generalised and relaxed generalised blending can be used.

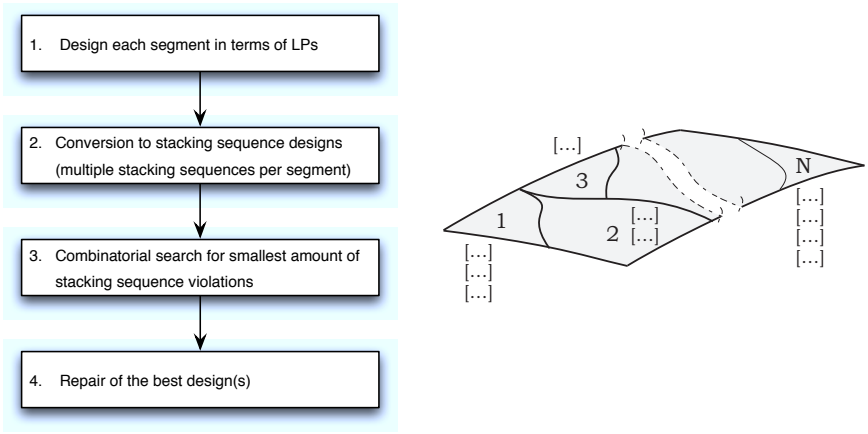

Figure 3.10: *Laminate blending using competing layups.*

Repair strategies involve the elimination of mismatched layers or butted-edges, depending on the blending definition used, as well as the reordering of plies to achieve an inwardly blended or outwardly blended design. The repair of manufac-

turing constraint violations changes the stacking sequence and laminate thickness and thereby its mechanical properties. Therefore a repair operation should be formulated as an optimisation problem to perform the repair which results in the smallest degradation of mechanical properties of the laminate. The overall laminate optimisation thus becomes a multi-step optimisation problem: (i) optimisation in terms of LPs, (ii) conversion from LPs to stacking sequences, (iii) combinatorial optimisation, (iv) repair optimisation, see Fig. 3.10. The implementation of the competing layups framework was not pursued in this thesis, because it was deemed to be less efficient than the guide-based blending approach.

3.4 Design parametrisation

A multi-chromosomal GA was used for the implementation of the blending problem described in this thesis. The parametrisation of guide-based blending using the generalised and the relaxed-generalised blending definitions, the formulation of the objective function, and the computation of parameters related to the generalised and relaxed generalised blending definitions are discussed in this section. The functioning of GAs in general and the choice for the multi-chromosomal GA are explained, followed by the encoding of the laminate designs, the computation of the objective function and the enforcement of blending.

3.4.1 Choice for multi-chromosomal genetic algorithm

Genetic algorithms, first introduced by Holland (1975), are stochastic, population-based search and optimisation heuristics designed to mimic the process of natural selection and evolution found in nature. The design space is explored by a population, where designs are usually encoded in the form of a integer strings called *chromosomes* (Keedwell and Narayanan 2005, Ahn 2006). In most implementation a design, called an *individual* consists of one chromosome. The characters in the integer string are referred to as *genes*.

Individuals (designs) are ranked based on their fitness function value, which is obtained by evaluation of an individual. Designs with a better fitness function value have a better chance of being used for the generation of a new generation. The genetic operators and sorting mechanism used in this thesis are described in appendix B.

GAs are frequently used for stacking sequence design of composite laminate structures (Ghiasi et al. 2009). Laminate design can be reduced to determining the number of layers in a laminate, choosing their respective orientation from a discrete set of orientation values and determining their stacking sequence (Gürdal, IJsselmuiden and Campen 2010). All these features can be straightforwardly incorporated in the integer coding of a GA.

A multi-chromosomal GA, i.e. one design is described by multiple chromosomes grouped together to form an individual, was chosen for the work presented in this thesis. One chromosome was assigned to the design of the guiding stack in the chosen implementation, and a binary chromosome was assigned to each segment in the structure to select layers from the guide. The multi-chromosomal GA used is an adaptation of the multi-chromosomal GA introduced by McMahon, Watson, Soremekun, Gürdal and Haftka (1998) and is described in detail in appendix B.

Generalised guide-based blending expands the design space considerably compared to conventional guide-based blending (Adams et al. 2004, Seresta et al. 2007, IJsselmuiden et al. 2009*b*), but allows for the representation of unblended designs. When a blended design is enforced through constrained optimisation generalised blending should be placed in the top right corner of table 3.1: this gives a multi-step approach where blending is enforced by the optimisation process and not by the representation of the laminate. This will lead to difficulty on the part of the optimiser as blended designs can produce unblended offspring as will be shown in section 3.4.4.

Designs which do not satisfy the blending definition can be rejected by the GA before they are evaluated. This way the relatively modest computational cost of the GA can be exploited to find blended designs. A more aggressive approach would be to eliminate any individual in the GA which does not satisfy the blending definition and repeat the operations that created the "killed" individual until a design is found which satisfies the blending definition (Van Campen et al. 2009). Note that especially for structures with many segments there is the risk that computational cost will become excessive when this replacement procedure is adopted.

A more robust solution would be to repair individuals which do not satisfy the blending definition. This can either be done by repairing the genetic coding of the individual, or by defining an interpretation strategy of the coded individuals that consistently decodes all individuals into laminates that satisfy the blending definition used. Explanation of this blending reinforcement is provided in section 3.4.4.

The identification of blended laminate designs is dependent on the encoding of the laminate. Therefore, laminate encoding is discussed next.

3.4.2 Laminate encoding

The multi-chromosomal GA described in appendix B was used to implement the work on guide-based composite laminate blending presented in this thesis. An encoded design, or individual, consists of a guide chromosome encoding the guiding stack. Layers are chosen from the guiding stack to define the laminate in each segment of the structure. Binary chromosomes are assigned to each segment and

are used to select which layers from the guiding stack are used to construct the laminate of the given segment.

The *guide chromosome* encodes the orientations of the guiding stack, e.g. consider that fibre orientation angles can be varied between 0° and 90° with 15° increments. This fibre angle orientation set can be represented by the coded set $\{1, 2, 3, 4, 5, 6, 7\}$. The guide chromosome of an individual could look like the following: 4125347671. There are multiple ways to interpret this guide chromosome. If a balanced symmetric layup is assumed the guiding stack upon decoding becomes: $[\pm 45°/0°_2/\pm 15°/\pm 60°/\pm 30°/\pm 45°/90°_2/\pm 75°/90°_2/0°_2]_s$

Each segment of a structure is encoded by a *switch chromosome*, this is a binary string which is used to 'switch' layers from the guiding stack on (1) or off (0) for that segment. The length of the switch chromosome is equal to that of the guide chromosome. A possible structure consisting of two segments could be encoded as follows:

Guide chromosome:	4	1	2	5	3	4	7	6	7	1
Switch chromosome segment A:	1	1	0	1	0	1	0	1	1	1
Switch chromosome segment B:	1	0	0	1	0	1	0	0	0	1

This individual encodes the laminate $[\pm 45°/0°_2/\pm 60°/\pm 45°/\pm 75°/90°_2/0°_2]_s$ for segment A and the laminate $[\pm 45°/\pm 60°/\pm 45°/0°_2]_s$ for segment B. This laminate satisfies the definition of generalised blending.

3.4.3 Optimisation formulation

Design of blended composite laminates is commonly focussed on weight reduction whilst satisfying prescribed structural performance (Soremekun et al. 2002, Adams et al. 2003, IJsselmuiden et al. 2009*a*). The weight of the laminate is directly related to its volume, assuming that there are no voids and that density is uniform. The following objective function was used for the work presented in this thesis:

$$\min f = \frac{V_{\text{blended laminate}}}{V_{\text{single laminate}}} \tag{3.2}$$

The volume of the blended laminate $V_{\text{blended laminate}}$ is normalised by the volume of the laminate that satisfies the structural requirements for all segments in the

structure, $V_{\text{single laminate}}$. Both volumes are computed respectively as:

$$V_{\text{blended laminate}} = \sum_{i=1}^{N} A_i t_i \tag{3.3}$$

$$V_{\text{single laminate}} = t \sum_{i=1}^{N} A_i \tag{3.4}$$

$$\tag{3.5}$$

where N is the number of segments in the structure, and A_i and t_i are the surface area and thickness of a laminate segment respectively.

The multi-chromosomal GA used, sorts the individuals in the population based on a single objective function value. The constraints were therefore implemented using an augmented objective function (Soremekun et al. 2002) as was done in section 2.3.2. The constraints were enforced through the use of constraint margins. Here an example is given for a constraint on buckling load:

$$g_{N_{cr}} = 1 - \frac{N_{cr}}{N_{cr_{\min}}} \tag{3.6}$$

where N_{cr} is the critical buckling load of the structure and $N_{cr_{\min}}$ the minimum allowable buckling load. The constraint margin is normalised to yield a value of 0.1 for a 10% violation of $N_{cr_{\min}}$, and a value of -0.1 for a 10% margin. The augmentation procedure is designed always to use the most severe constraint violation $g_{\max}$:

$$\Psi = \begin{cases} f + \varepsilon g_{\max} & \text{if} \quad g_{\max} \leq 0 \\ f + \beta g_{\max} & \text{if} \quad g_{\max} > 0 \end{cases} \tag{2.21}$$

where Ψ is to be minimized, ε is a bonus term and β is a penalty term.

3.4.4 Blending enforcement

Generalised and relaxed generalised blending can be enforced in the form of a constraint on the optimisation problem. Measures must be defined to determine whether a laminate is blended, and if not to determine how far it is away from being blended, to enforce blending in the form of a constraint. Note that blending is considered between two segments at a time.

Consider the switch chromosomes for two adjacent segments: S_A and S_B. Layers which are switched on, i.e. the binary value is 1, in both segments are continuous. The set of continuous layers is defined as the intersection of S_A and S_B: $C = S_A \cap S_B$. This can be used to determine the total number of layers that occur in the thinner of the two laminates, but not in the thicker laminate, which are

referred to as *mismatched layers*:

$$m = \min\left(\sum S_A, \sum S_B\right) - \sum C \tag{3.7}$$

The segments are blended according to the definition for generalised blending if $m = 0$. Any positive integer for m indicates the segments are not blended according to the generalised blending definition. The value of m can be used to assess the degree of change required to make the two segments blended.

The relaxed generalised blending definition requires that no butted edges occur between two adjacent segments. This means that between any consecutive pair of continuous layers, i.e. layers from the guide which are used in both segments under consideration, only in one of the two segments layers may be dropped, i.e. occur in one of the segments but not it the other. The number of butted edges between the segments can thus be defined as:

$$b = \sum_{i=1}^{c+1} \min\left(nc_A^i, nc_B^i\right) \tag{3.8}$$

where c is the number of continuous layers between both segments, and nc_A^i and nc_B^i are the number of discontinued layers between continuous layers $i-1$ and i. A panel is only considered blended according to the relaxed generalised definition if $b = 0$. The value of b can be used to assess the degree of change required to make the two segments blended.

The enforcement of either the generalised or the relaxed generalised blending definition can be left to the selective, or evolutionary, pressure of the multi-chromosomal GA. Unblended designs can simply be rejected for function evaluation to save computational cost, and assigned a fitness value which reflects the amount of change required to create a blended design out of the individual.

The problem that this approach has, is that two parents which satisfy the blending definition can produce offspring which do not. Generalised blending and the crossover operation, see appendix B, are considered to illustrate this, table 3.2.

The two parent individuals in the above example satisfy the generalised blending definition, but for both of their two children $m = 2$.

A solution to this problem would be to reject the outcome of the crossover operation and to repeat it until two blended child individuals result. A more apt choice of the crossover location in the above example would indeed resolve the issue, table 3.3

The number of times the genetic operations need to be repeated before a blended design results will become very large, for more complicated structures. A smarter strategy is thus required.

Table 3.2: *Blended parents producing unblended offspring due to improper choice of crossover location*

Blended parents																				
1	1	1	1	1	1	1	0	0	0	×	0	0	0	0	0	0	1	1	1	1
1	1	1	1	0	0	0	0	0	0		0	0	0	1	1	1	1	1	1	1
⇓																				
Unblended children																				
1	1	1	1	1	0	1	1	1	1	&	0	0	0	0	0	1	1	0	0	0
1	1	1	1	0	1	1	1	1	1		0	0	0	1	1	0	0	0	0	0

Table 3.3: *Blended parents producing blended offspring thanks to proper choice of crossover location*

Blended parents																				
1	1	1	1	1	1	1	0	0	0	×	0	0	0	0	0	0	1	1	1	1
1	1	1	1	0	0	0	0	0	0		0	0	0	1	1	1	1	1	1	1
⇓																				
Blended children																				
1	1	1	0	0	0	1	1	1	1	&	0	0	0	1	1	1	1	0	0	0
1	1	1	1	1	1	1	1	1	1		0	0	0	1	0	0	0	0	0	0

A repair strategy can be devised which consistently converts an unblended design into a blended one. Mismatched layers can be repaired by continuing the layer in the thicker of the two segments, and butted edges can be repaired by replacing the butted edges with continuous layers. The following individual demonstrates the repair of mismatched layers, table 3.4.

Table 3.4: *Repair of mismatched layers*

Unblended individual											Repaired individual									
1	1	1	0	0	0	**1**	1	0	0	⇒	**1**	1	1	0	0	0	**1**	1	0	0
0	1	1	0	1	1	0	1	1	1		**1**	1	1	0	1	1	**1**	1	1	1

where the mismatched layers are indicated in bold. The same example is used to demonstrate the repair of butted edges, table 3.5.

where the butted edges are indicated in bold. Note that designs satisfying the generalised blending definition automatically satisfy the relaxed blending definition.

Table 3.5: *Repair of butted edges*

Unblended individual											Repaired individual									
1	1	1	0	0	0	**1**	1	0	0	⇒	1	1	1	0	**1**	**1**	**1**	1	0	0
0	1	1	0	**1**	**1**	0	1	1	1		0	1	1	0	**1**	**1**	**1**	1	1	1

The aforementioned repair strategies can be used to either repair the genetic coding, or to interpret the genetic coding as a blended design before evaluation of the objective function. The later was chosen for the work presented in this thesis.

3.5 VERIFICATION

The laminate blending implementation using the multi-chromosomal GA is verified in this section using a simple example problem. Generalised and relaxed generalised blending are discussed as well as inner and outer blending to serve as a reference.

3.5.1 TWO-PANEL EXAMPLE

A two-panel structure was used for demonstration purposes, see Fig. 3.11. Each panel was simply supported and loaded using in-plane bi-axial compression. The following material properties were assumed: $E_1 = 181$GPa (26.25Msi), $E_2 = 10.3$GPa (1.49Msi), $G_{12} = 7.17$GPa (1.04Msi), $\nu_{12} = 0.28$ and $t_{\text{ply}} = 1.91 \cdot 10^{-4}$m. The lay-up was assumed to be balanced symmetric, $[\pm\theta_1/\ldots/\pm\theta_n]_s$, and both panels were 1.0m by 0.5m in dimension.

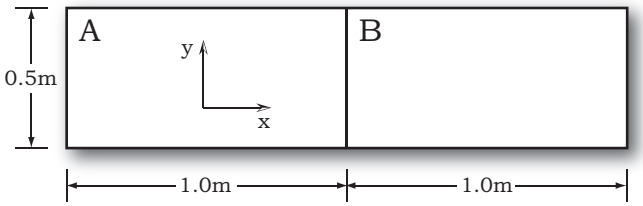

Figure 3.11: *Two-panel example structure. The panels are loaded in in-plane compression.*

Two different load cases were considered, one in which the panels are loaded equally and one where panel A is loaded more heavily in the x-direction than in

the y-direction with the loads in x- and y-direction switched for panel B. The load cases are given in table 3.6. The design objective was to find the lightest laminate that did not buckle under the specified loads. The critical buckling load for a rectangular panel under bi-axial compression was computed using Eq. 3.9.

$$N_{x_{\mathrm{cr}}} = \pi^2 \frac{D_{11}\left(\frac{m}{a}\right)^4 + 2\left(D_{12} + 2D_{66}\right)\left(\frac{m}{a}\right)^2\left(\frac{n}{b}\right)^2 + D_{22}\left(\frac{n}{b}\right)^4}{\left(\frac{m}{a}\right)^2 + R\left(\frac{n}{b}\right)^2} \tag{3.9}$$

where m is the number of half-waves in x-direction and n is the number of half-waves in y-direction, a and b are the x- and y-dimensions of the panel, and R is the loading ratio of the panel: $\frac{N_y}{N_x}$.

Table 3.6: *Load cases for the two-panel structure.*

	Panel A		**Panel B**	
	x-direction	y-direction	x-direction	y-direction
Load case I [N]	5000	5000	5000	5000
Load case II [N]	7000	3000	3000	7000

3.5.2 Results and discussion

The multi-chromosomal GA was set to use 50 individuals and a guide of 20 layers. An elite population of 5 individuals was used and the crossover rate was set to 1. The probabilities for mutation, permutation and ply swap were all 5%. Fibre angles could vary between 0° and 90° with 15° increments. The bonus and penalty terms were set to $\beta = 5$ and $\varepsilon = 1 \cdot 10^{-3}$ respectively. The GA was considered to have converged after 50 iterations without improvement. Blending was enforced through interpretation of the genetic coding, see section 3.4.4.

The optimal layup for when a single layup is considered to cover both segments was considered first, for which a guide length of only 10 layers was used. The volume of this design was used to normalise the volume of the blended designs. The results for the different blending definitions are presented in tables 3.7 and 3.8 for the two load cases respectively.

Naturally, the layups expected (and computed) for panel A and B for load case I were the same in panel A and panel B for all blending definitions, since the panel loads were the same. The layup designs differed slightly for the different blending definitions, but buckling performance was comparable, and differences were attributed to the multiplicity of solutions to the problem and the probabilistic

Table 3.7: *Optimised stacking sequence designs load case I.*

		layup panel A & panel B	$g_{N_{cr}}$ panel A	panel B	**Volume** $[V/V_{sl}]$	**Iterations**
1.	Single layup	$[\pm 75°/\pm 60°/\pm 75°/\pm 90°]_s$	-1.0848	-1.0848	1.0	57
2.	Inner blending	$[\pm 60°/\pm 90°/\pm 60°/\pm 0°]_s$	-1.0879	-1.0879	1.0	103
3.	Outer blending	$[\pm 75°/\pm 60°/\pm 75°/\pm 90°]_s$	-1.0848	-1.0848	1.0	96
4.	Generalised blending	$[\pm 75°/\pm 60°/\pm 90°/\pm 60°]_s$	-1.0879	-1.0879	1.0	94
5.	Relaxed generalised blending	$[\pm 75°/\pm 60°/\pm 75°/\pm 90°]_s$	-1.0848	-1.0848	1.0	103

Table 3.8: *Optimised stacking sequence designs load case II. Dropped layers are underlined.*

		layup panel A	panel B	$g_{N_{cr}}$ panel A	panel B	**Volume** $[V/V_{sl}]$	**Iterations**
1.	Single layup	$[\pm 75°/\pm 75°/\pm 60°/\pm 90°]_s$		-0.7903	-0.7172	1.0	109
2.	Inner blending	$[\pm 60°/\pm 60°/\pm 45°]_s$	$[\underline{\pm 60°}/\pm 60°/\pm 60°/\pm 45°]_s$	-0.0641	-0.5459	0.875	84
3.	Outer blending	$[\pm 60°/\pm 60°/\pm 60°]_s$	$[\pm 60°/\pm 60°/\pm 60°/\underline{\pm 60°}]_s$	-0.0641	-0.5459	0.875	64
4.	Generalised blending	$[\pm 60°/\pm 60°/\pm 60°]_s$	$[\pm 60°/\underline{\pm 75°}/\pm 60°/\pm 60°]_s$	-0.0641	-0.6027	0.875	93
5.	Relaxed generalised blending	$[\pm 60°/\pm 60°/\underline{\pm 60°}]_s$	$[\underline{\pm 90°}/\underline{\pm 90°}/\pm 60°/\pm 60°]_s$	-0.0641	-0.7458	0.875	116

nature of the optimiser. The similar outcome for all blending definitions was to be expected because both panels carry the same compressive loads, and thus prove the proper functioning of the GA implementation of the blending problem for this example. Note that the number of iterations the optimiser needs to converge is in the same order of magnitude for all blending definitions.

The results presented in table 3.8 were obtained for load case II and show that laminate blending can be used to reduce structural volume and thus weight; the volumes of all blended designs are lower than the volume of the single layup design. All blended designs found the same volume, 3 designed layers for panel A and 4 designed layers for panel B. Note that discontinued layers are underlined in the table.

The constraint margin for buckling of panel B was found to improve as the blending definition is relaxed. The margin was equal for inner and outer blending, for generalised blending it was already larger and it was largest for relaxed generalised blending. It is concluded that relaxing the blending definition caused the design space to be enlarged and that the result of the optimisation could be improved.

It is an important and popular fact
that things are not always what they seem.

Douglas Adams (1952 – 2001)

4

RESULTS MULTI-SEGMENT BLENDED LAMINATE DESIGN

How to design multi-segment blended composite laminates was described in chapter 3. A new implementation of guide-based blending using a mutli-chromosomal genetic algorithm (GA) was introduced, and the use of several existing and new definitions of laminate blending were discussed.

In this chapter, the results obtained using the new blending definitions introduced in chapter 3 are compared. Three different structures were used to study the merits of the newly introduced blending definitions:

- an 18-panel horseshoe configuration
- a rectangular panel with two concentric lay-ups
- a square variable stiffness panel

The first example problem, an 18-panel horseshoe configuration, was used to compare the blending definitions under consideration with existing literature on the subject. This configuration is used to represent the floor structure of a helicopter and has been used in a number of studies on blended laminate design (Soremekun et al. 2002, Adams et al. 2003, Adams et al. 2004, Liu et al. 2009*a*, IJsselmuiden et al. 2009*a*).

The second example, a rectangular panel with two concentric lay-ups, was used to see if the buckling load of the panel improved by varying the stiffness properties of the inner and the outer lay-up. As such this example constitutes a simple blending example that takes into consideration the effect of load redistribution.

The last example, a square variable stiffness panel, was used to investigate the possibility of using laminate blending for the design of variable stiffness composite structures, where load redistribution in the structure plays an important role. To

this end, a square plate, for which the optimal lamination parameter (LP) distribution was assumed to be known, was progressively divided into an increasing number of segments. The objective was to match the given LP distribution by varying the stacking sequence design in each segment.

The motivation for the choice of each of these example problems is described more extensively in their respective sections, where each of the example problems and the generated results are discussed in detail. The chapter is concluded with a discussion on the merits of the different blending definitions for the four structures considered.

4.1 18-PANEL HORSESHOE CONFIGURATION

The 18-panel horseshoe configuration has been used multiple times as a benchmark problem for the laminate blending problem (Soremekun et al. 2002, Adams et al. 2003, Adams et al. 2004, IJsselmuiden et al. 2009*a*). In the research reported here it was used to determine the efficacy of the generalised and relaxed generalised blending definition presented in chapter 3. This was done by comparing the results obtained with results found in the literature and the results obtained using pre-existing blending definitions.

4.1.1 PROBLEM DEFINITION

Eighteen panels were configured in a horseshoe configuration, as shown in Fig. 4.1, and these resemble a section of the floor panel of a helicopter. All the panels are assumed to be simply supported at their boundaries and loaded in bi-axial compression, also shown in Fig. 4.1. The design objective for the horseshoe panel was to find the lightest design for which none of the panels buckles under the applied loads. This objective was defined as minimising the summation of the number of layers in all panels:

$$\min_{\theta} f = \frac{1}{f_0} \sum_{i=1}^{n_p} n_i \tag{4.1}$$

where n_i is the total number of plies in a panel, n_p is the total number of panels, and f_0 is the objective function value for the baseline single lay-up design for all panels.

The critical buckling load for a rectangular panel under bi-axial compression was calculated using Eq. 3.9:

$$N_{x_{\mathrm{cr}}} = \pi^2 \frac{D_{11}\left(\frac{m}{a}\right)^4 + 2\left(D_{12}+2D_{66}\right)\left(\frac{m}{a}\right)^2\left(\frac{n}{b}\right)^2 + D_{22}\left(\frac{n}{b}\right)^4}{\left(\frac{m}{a}\right)^2 + R\left(\frac{n}{b}\right)^2} \tag{3.9}$$

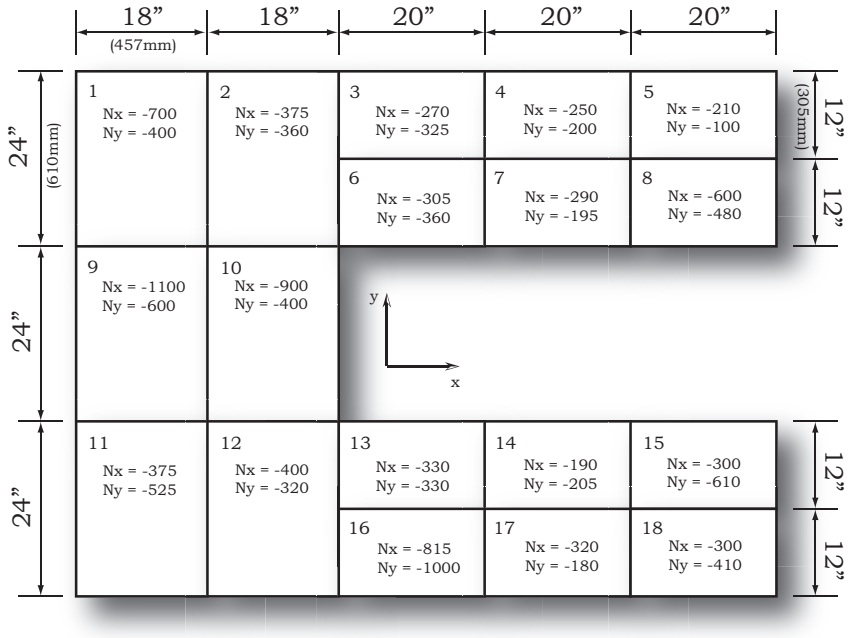

Figure 4.1: *18-panel horseshoe configuration (Soremekun et al. (2002), renumbered following IJsselmuiden et al. (2009a)), all loads in* $^{\mathrm{lbf}}/_{\mathrm{in}}$ *(*$\times 175.1$ *for* $^{\mathrm{N}}/_{\mathrm{m}}$*).*

where m is the number of half-waves in x-direction and n is the number of half-waves in y-direction, a and b are the x- and y-dimensions of the panel, and R is the loading ratio of the panel: $\frac{N_y}{N_x}$. Note that it was assumed that no load redistribution would result from changing the lay-up in one of the panels. The buckling constraint was enforced using an augmented formulation for the objective function:

$$\Psi = \begin{cases} f + \varepsilon g_{\max} & \text{if} \quad g_{\max} \leq 0 \\ f + \beta g_{\max} \sqrt{n_\beta} & \text{if} \quad g_{\max} > 0 \end{cases} \tag{4.2}$$

with f given in Eq. 4.1 and n_β the number of violated segments.

The material properties for a graphite-epoxy (IM7/8552) were used: $E_1 = 141$GPa (20.5Msi), $E_2 = 9.03$GPa (1.31Msi), $G_{12} = 4.72$GPa (0.62Msi), $\nu_{12} = 0.32$ and $t_{\text{ply}} = 1.91 \cdot 10^{-4}$m (0.0075inch). The designed lay-ups were of the form $[\theta_1/\ldots/\theta_n]_s$. Balancing of the laminate was enforced by taking the negative value of every other ply in the laminate, e.g. $[45/30/90/0/45/30/60]_s$ would become $[45/30/90/0/-45/-30/60]_s$. Note that the laminates obtained this way are not strictly balanced.

4.1.2 Generated results

Results for the 18-panel horseshoe configuration were generated for inner and outer blending and the generalised and relaxed generalised blending definitions, see section 3.3.2. The chromosome length for the multi-chromosomal genetic algorithm (GA) was chosen to be 22, 5 sub-populations with 50 individuals each were used, and with every 5 iterations the best individuals of each sub-population migrated to the next sub-population. Ply angles were coded by integers 1 to 7, coding the fibre orientations between 0 and 90 degrees with 15-degree increments, and the multi-chromosomal GA was set to converge after 500 iterations without improvement. The crossover rate of the GA was set to 100%, and mutation, permutation and ply swap rates were set to 5%. More details on the multi-chromosomal GA used can be found in appendix B. Equation 4.2 was used as the objective function of the optimisation, with bonus term $\varepsilon = 0.001$ and penalty term $\beta = 5$.

4.1.3 Results and discussion

There were two bounds inbetween which blended designs were expected to be found in terms of number of layers per panel and thus weight of the overall 18-panel horseshoe configuration. The lower bound is given by the design for which every panel is optimised individually, with no form of blending considered. The single lay-up design, for which all panels have the same lay-up, constitutes the upper bound on structural weight. Results previously reported in the literature

(Soremekun et al. 2002, Adams et al. 2003, Adams et al. 2004, IJsselmuiden et al. 2009*a*) are presented in table 4.1. Note that no balancing of the laminate was enforced for the designs designated as unbalanced, i.e. for every $+\theta$-ply there was not necessarily a $-\theta$-ply in the laminate.

Table 4.1: *Results for the horseshoe panel structure in the literature, taken from IJsselmuiden et al. (2009*a*). Failed panels are shown between brackets.*

Panel	IJsselmuiden (balanced)		IJsselmuiden (unbalanced)		Soremekun (balanced)		Adams (unbalanced)	
	Number of plies	$\lambda_{\min}$	Number of plies	$\lambda_{\min}$	Number of plies	$\lambda_{\min}$	Number of plies	$\lambda_{\min}$
1	34	1.052	34	1.114	34	1.029	34	1.153
2	30	1.093	30	1.173	30	1.127	28	1.005
3	22	1.321	22	1.308	22	1.304	22	1.219
4	18	1.042	18	1.048	20	1.433	18	1.038
5	18	1.721	16	1.206	16	1.221	16	1.204
6	22	1.187	22	1.176	22	1.172	22	1.095
7	20	1.385	18	1.016	20	1.372	18	1.005
8	26	1.242	26	1.235	24	1.033	26	1.110
9	40	1.098	38	1.028	40	1.047	38	1.042
10	36	1.025	36	1.104	36	1.006	36	1.129
11	34	1.451	30	1.011	32	1.182	30	1.082
12	30	1.089	30	1.168	30	1.122	28	1.000
13	22	1.242	22	1.231	22	1.227	22	1.146
14	18	1.105	18	1.112	20	1.502	18	1.101
15	26	1.204	26	1.197	24	1.000	26	1.076
16	34	1.318	32	1.032	32	1.219	38	1.781
17	18	1.024	18	1.029	20	1.391	18	1.020
18	22	1.076	22	1.066	22	1.063	22	(0.993)
Total	**470**		**458**		**466**		**460**	

The number of plies and the buckling load multiplier λ for the unblended case and the definitions of inner, outer, generalised and relaxed generalised blending are presented in table 4.2 for the case with only a constraint on the buckling load of each panel.

The results obtained for the case in which the horseshoe panel configuration was designed as a single laminate and for the case that each panel of the configuration was designed independently were as expected. The total ply count for the unblended design was very close to the result found in the literature (Soremekun et al. 2002), 436 plies.[1] The stacking sequence of the of the thickest of the individually designed panels, panel 9, was found to be identical to that of the single laminate design case.The single laminate design was thus clearly designed for the

[1]The result of (Soremekun et al. 2002) allows for mid-plane symmetric plies, or half plies, which gives an advantage over the formulation chosen here.

Table 4.2: *Obtained results for the 18-panel horseshoe configuration.*

Panel	single lay-up		unblended design		inner blending		outer blending		generalised blending		relaxed generalised blending	
	Number of plies	$\lambda_{\min}$	Number of plies	$\lambda_{\min}$	Number of plies	$\lambda_{\min}$	Number of plies	$\lambda_{\min}$	Number of plies	$\lambda_{\min}$	Number of plies	$\lambda_{\min}$
1	38	1.703	32	1.017	36	1.282	36	1.310	36	1.292	36	1.308
2	38	2.728	28	1.091	32	1.363	32	1.467	40	2.576	34	1.774
3	38	4.069	20	1.004	28	1.781	32	2.788	32	2.501	32	3.319
4	38	5.923	18	1.057	36	5.260	28	2.794	26	2.313	26	2.684
5	38	9.783	16	1.121	20	1.392	28	4.615	40	13.31	28	5.484
6	38	3.657	22	1.202	28	1.601	28	1.725	32	2.248	24	1.108
7	38	5.738	18	1.020	24	2.020	24	1.769	32	3.527	32	3.102
8	38	2.468	24	1.045	40	2.503	32	1.691	32	1.420	28	1.399
9	38	1.096	38	1.096	44	1.440	44	1.538	40	1.035	42	1.332
10	38	1.400	34	1.003	36	1.054	40	1.479	40	1.322	36	1.090
11	38	2.350	30	1.156	32	1.175	32	1.264	40	2.219	34	1.524
12	38	2.716	28	1.087	36	2.045	32	1.460	40	2.565	34	1.744
13	38	3.828	22	1.253	24	1.348	24	1.219	30	2.452	30	2.643
14	38	6.283	18	1.128	20	1.284	20	1.181	32	5.073	26	2.675
15	38	2.392	24	1.024	28	1.047	28	1.129	28	1.047	32	1.930
16	38	1.328	30	1.108	40	1.347	36	1.268	40	1.807	34	1.227
17	38	5.820	18	1.030	32	3.695	20	1.093	24	2.010	24	2.010
18	38	3.317	22	1.093	32	2.105	24	1.022	28	1.584	36	3.661
Total	**684**		**442**		**568**		**540**		**612**		**562**	

most severely loaded panel.

The designs obtained for inner and outer blending had, as expected, a higher ply count than the unblended design, however, their ply counts were also higher than those found in the literature (IJsselmuiden et al. 2009*a*). This signalled that the there might be something wrong with the chosen blending implementation, or that the implementation was not suited for the problem at hand.

It was suggested that the poor performance of the blending implementation proposed here resulted from the relatively large number of constraints on the problem, i.e. one buckling constraint for each panel. All these constraints were enforced using a single augmented objective function value, Eq. 2.21. Likewise, the design objective was caught in this single objective function value. IJsselmuiden et al. (2009*a*) use a two-step design method instead, in which for each guide, the ply counts of all panels in the structure are minimised individually, subject to the buckling load constraint for that specific panel.

Another observation is that the designs obtained for the definitions of generalised and relaxed generalised blending had higher, respectively similar, ply counts than the designs obtained for the definitions of inner and outer blending. The repair strategies that were used to implement these blending definitions, see section 3.4.4, render the GA more insensitive to variations in the genetic coding, because a change in a chromosome due to the genetic operations can be countered (partially) by the repair operations required to come to an acceptably blended laminate design. Therefore, it becomes harder for the GA to converge to an optimal result and premature convergence may occur.

The results of a modified objective function and the use of the repair strategy are discussed in section 4.3 for a problem in which the number of segments can be varied. These results were obtained to study the effect of the number of segments in a structure with respect to the results obtained using the proposed blending implementation.

4.2 Panel with two concentric lay-ups

The panels used in the 18-panel horseshoe configuration problem, section 4.1, were all assumed to be mechanically independent entities, i.e. that no load redistribution occured. It is more realistic to study the performance improvements that can be obtained using a blended laminate when load redistribution due to changes in the local stiffness of the laminate are accounted for.

It has been shown that significant improvements in buckling load can be computed when multiple lay-ups are allowed in one panel, for instance using parallel lay-ups (Biggers and Srinivasan 1993). Results for concentric lay-up panels show that significant performance improvements can be achieved in shear buckling

(Papadopoulos and Kassapoglou 2007) and compression buckling (Kassapoglou 2008). A design study on a square panel with two concentric lay-ups showed that buckling load improvements are only possible for a limited range of dimensions of the centre lay-up (Van Campen et al. 2009).

In this section the design of a rectangular panel with two concentric layups is considered. The geometry of the concentric layup panel is described first, after which the buckling load of the panel is optimised for different dimensions of the centre lay-up with a constraint on the weight of the panel. The section is concluded with a discussion of the obtained trends and the effect of blending on the result of the optimisation.

4.2.1 Problem definition

Design

A rectangular panel with two concentric lay-ups, drawn in Fig. 4.2, was subjected to an in-plane compressive force in x-direction. For design purposes an aspect ratio

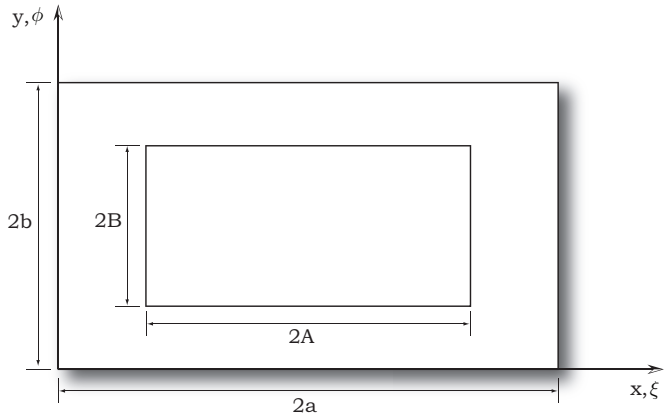

Figure 4.2: *Rectangular panel with two concentric lay-ups.*

S and a coverage ratio c of the centre patch were defined as follows:

$$S = \frac{Ab}{aB} \tag{4.3}$$

$$c = \frac{AB}{ab} \tag{4.4}$$

The aspect ratio and coverage ratio fully define the geometrical design of the panel when the outer dimensions, a and b, are specified:

$$A = \sqrt{a^2 c S} \tag{4.5}$$

$$B = \sqrt{\frac{b^2 c}{S}} \tag{4.6}$$

The weight of the panel with concentric lay-ups is given by:

$$\frac{W}{4ab} = t_p + c(t_c - t_p) \tag{4.7}$$

where W is the weight of the panel, t_p is the thickness of the perimeter lay-up and t_c is the thickness of the centre lay-up of the panel. A thickness ratio of the panel is then defined by:

$$T = \frac{t_c}{t_p} \tag{4.8}$$

Note that for a constant T the weight of the panel solely depends on c, simplifying the charting of the design space.

The constraints $0 \leq c \leq 1$, $0 \leq A \leq a$, $0 \leq B \leq b$ and $T \geq 0$ were used to define a feasible domain of all designs of the concentric panel. This domain is illustrated in Fig. 4.3. The lower bound $S = c$ corresponds to the case where the centre patch forms a vertical strip, and the upper bound $S = \frac{1}{c}$ corresponds to the case where the centre patch is a horizontal strip.

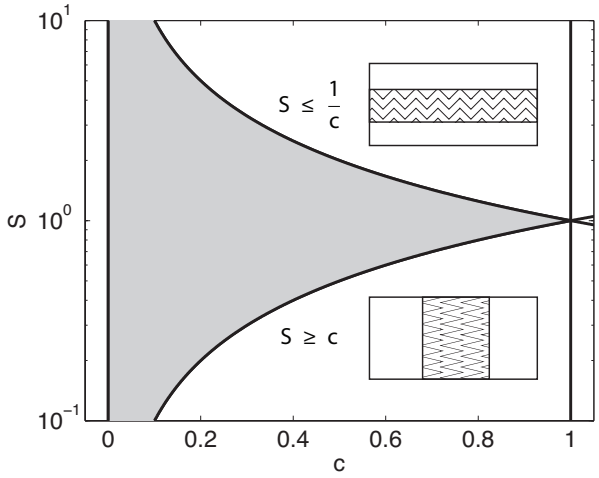

Figure 4.3: *Feasible domain of the coverage and aspect ratio.*

Analysis

Kassapoglou (2008) presents a RayleighRitz-based approach to estimate the buckling load of a panel with two concentric lay-ups as described above. The approach is designed to determine the buckling load and in-plane stresses by minimizing energy:

$$\Pi = \frac{1}{2}\int\int \left[A_{11}N_x^2 + A_{22}N_y^2 + A_{12}N_xN_y + A_{66}N_{xy}^2\right] dxdy - \int N_x(x=2a)u(x=2a)dy \tag{4.9}$$

where the in-plane forces are given by:

$$N_x = \frac{F_a}{2b} + \sum_{m=1}^{M}\sum_{n=1}^{N} H_{mn}(\cos 2m\pi\xi - 1)\cos 2\pi\phi \tag{4.10}$$

$$N_y = \frac{b^2}{a^2}\sum_{m=1}^{M}\sum_{n=1}^{N} H_{mn}\cos 2m\pi\xi(\cos 2n\pi\phi - 1) \tag{4.11}$$

$$N_{xy} = \frac{b}{a}\sum_{m=1}^{M}\sum_{n=1}^{N} H_{mn}\sin 2\pi\xi \sin 2\pi\phi \tag{4.12}$$

where F_a is the applied distributed force, H_{mn} are unknown coefficients, and M and N are the number of terms used in x- and y-direction. The normalised variables ξ and ϕ are defined as:

$$\xi = \frac{x}{2a} \tag{4.13}$$

$$\phi = \frac{y}{2b} \tag{4.14}$$

The approach of Kassapoglou (2008) has been proven to be in excellent agreement with a finite element (FE) solution for the buckling problem, and it was used for the analysis of the buckling load of the concentric lay-up panel for the work presented in this section.

4.2.2 Generated results

A panel of 1m by 1m was optimised for a range of points in the feasible domain for c and S, see Fig. 4.3. Fibre angle orientations for the optimised designs were chosen between 0° and 90° with 15° increments. The design of the thickness ratio T was left to the optimiser. Inner, outer, generalised and relaxed generalised blending were enforced. The baseline design for both optimisations was the single lay-up design $[\pm 45_4]_s$.

The buckling load analysis of the concentric lay-up panel was coded in FORTRAN

77. This programme was rewritten into a subroutine which was subsequently connected with a gateway subroutine to establish a link with MATLAB® in the form of a MEX-file. All subsequent trending studies and blending optimisation were implemented within MATLAB®.

The objective function used for the maximisation of the critical buckling load of the structure was:

$$f_{N_x} = \frac{N_x}{N_{x_0}} \tag{4.15}$$

with the constraint margin for the volume of the panel:

$$g_V = V_{\text{norm}} - 1 \tag{4.16}$$

Both the objective functions and constraint margins were implemented using an augmented objective function, Eq. 2.21, repeated on page **??** in this chapter.

The optimisation was performed using the multi-chromosomal GA described in appendix B. Ply angles were coded by integers 1 to 7, coding the fibre orientations between 0 and 90 degrees with 15-degree increments. The chromosome length was set to be 8. The number of sub-populations was 5 and the number of individuals per sub-population was 10. Every 5 iterations the best individuals of each sub-population migrated to the next sub-population. The GA was assumed to have converged after 100 iterations without improvement. The crossover rate of the GA was set to 100%, and mutation, permutation and ply swap rates were set to 5%. More details on the multi-chromosomal GA used can be found in appendix B. Equation 4.2 was used as the objective function of the optimisation, with bonus term $\varepsilon = 0.001$ and penalty term $\beta = 5$.

4.2.3 Results and discussion

The concentric panel was optimised for nine combinations of C and S, the buckling load of the panel was maximised whilst the weight of the panel was not allowed to exceed the weight of the baseline design, $[\pm 45_4]_s$. All lay-ups were required to satisfy the relaxed generalised blending definition,[2] and the thickness and lay-up of the perimeter and centre patch were considered to be variable. The resulting designs for the unblended case are plotted in table 4.3 and Fig. 4.4, for the generalised blended case in table 4.4 and Fig. 4.5, and for the relaxed generalised case in table 4.5 and Fig. 4.6.

The results obtained were similar for the unblended case and the two blended design cases. The buckling load of the panel for the different design points was not, or only slightly, affected by imposing a blended design. The simplicity of the panel with two concentric lay-ups as a blending problem was thought to

[2] No improvements in buckling load were found when using the generalised blending definition.

Table 4.3: *Optimised designs for maximum buckling load subject to a weight constraint. The designs are unblended.*

Design point	c	S	Perimeter lay-up	Centre lay-up	$\frac{N_x}{N_{x_0}}$	$\frac{V}{V_0}$
1	0.325	0.580	$[\pm 45_4]_s$	$[\pm 45_4]_s$	1.000	1.000
2	0.325	1.000	$[\pm 45_4]_s$	$[\pm 45_4]_s$	1.000	1.000
3	0.325	1.750	$[\pm 45_4]_s$	$[\pm 45_4]_s$	1.000	1.000
4	0.550	0.750	$[\pm 45_4]_s$	$[\pm 45_4]_s$	1.000	1.000
5	0.550	1.000	$[\pm 45/\pm 30/\pm 30]_s$	$[\pm 45/\pm 45/\pm 30/\pm 15/\pm 30]_s$	1.122	1.025
6	0.550	1.350	$[\pm 45/\pm 45/\pm 30]_s$	$[\pm 30/\pm 45/\pm 45/\pm 30/\pm 45]_s$	1.181	1.025
7	0.775	0.880	$[\pm 45_4]_s$	$[\pm 45_4]_s$	1.000	1.000
8	0.775	1.000	$[\pm 45_4]_s$	$[\pm 45_4]_s$	1.000	1.000
9	0.775	1.136	$[\pm 75]_s$	$[\pm 30/\pm 30/\pm 30/\pm 75/\pm 30]_s$	1.213	1.025

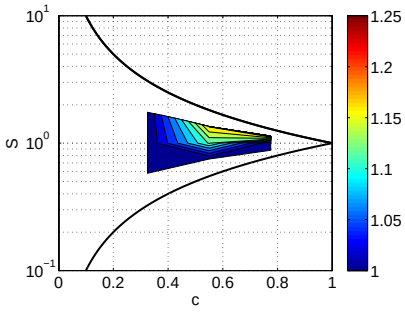

Figure 4.4: *Normalised critical buckling load* $\frac{N_x}{N_{x_0}}$ *of the unblended designs optimised for maximum buckling load subject to a weight constraint.*

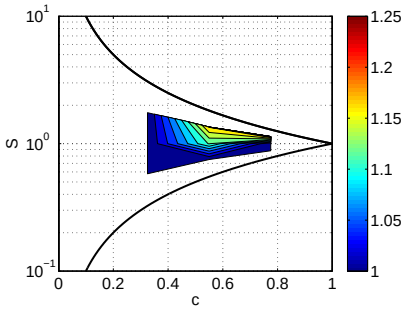

Figure 4.5: *Normalised critical buckling load* $\frac{N_x}{N_{x_0}}$ *of the generalised blended designs optimised for maximum buckling load subject to a weight constraint.*

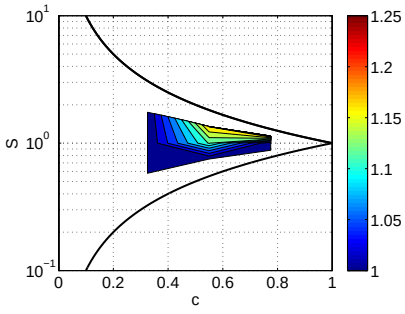

Figure 4.6: *Normalised critical buckling load* $\frac{N_x}{N_{x_0}}$ *of the relaxed generalised blended designs optimised for maximum buckling load subject to a weight constraint.*

Table 4.4: *Optimised designs for maximum buckling load subject to a weight constraint. The designs are blended following the definition for generalised blending, dropped layers are underlined.*

Design point	c	S	Perimeter lay-up	Centre lay-up	$\frac{N_x}{N_{x_0}}$	$\frac{V}{V_0}$
1	0.325	0.580	$[\pm 45_4]_s$	$[\pm 45_4]_s$	1.000	1.000
2	0.325	1.000	$[\pm 45_4]_s$	$[\pm 45_4]_s$	1.000	1.000
3	0.325	1.750	$[\pm 45_4]_s$	$[\pm 45_4]_s$	1.000	1.000
4	0.550	0.750	$[\pm 45_4]_s$	$[\pm 45_4]_s$	1.000	1.000
5	0.550	1.000	$[\pm 45/\pm 30/\pm 30]_s$	$\left[\pm 45/\underline{\pm 45/\pm 30}/\pm 30/\pm 30\right]_s$	1.120	1.025
6	0.550	1.350	$[\pm 45/\pm 45/\pm 30]_s$	$[\underline{\pm 30 \pm 45}/\pm 45/\pm 45/\pm 30]_s$	1.177	1.025
7	0.775	0.880	$[\pm 45_4]_s$	$[\pm 45_4]_s$	1.000	1.000
8	0.775	1.000	$[\pm 45_4]_s$	$[\pm 45_4]_s$	1.000	1.000
9	0.775	1.136	$[\pm 75]_s$	$\left[\underline{\pm 30/\pm 30/\pm 30}/\pm 75\right]_s$	1.213	1.025

Table 4.5: *Normalised critical buckling load $\frac{N_x}{N_{x_0}}$ of the generalised blended designs optimised for maximum buckling load subject to a weight constraint.*

Design point	c	S	Perimeter lay-up	Centre lay-up	$\frac{N_x}{N_{x_0}}$	$\frac{V}{V_0}$
1	0.325	0.580	$[\pm 45_4]_s$	$[\pm 45_4]_s$	1.000	1.000
2	0.325	1.000	$[\pm 45_4]_s$	$[\pm 45_4]_s$	1.000	1.000
3	0.325	1.750	$[\pm 45_4]_s$	$[\pm 45_4]_s$	1.000	1.000
4	0.550	0.750	$[\pm 45_4]_s$	$[\pm 45_4]_s$	1.000	1.000
5	0.550	1.000	$[\pm 45/\pm 30/\pm 30]_s$	$\left[\pm 45/\underline{\pm 45/\pm 15}/\pm 30/\pm 30\right]_s$	1.120	1.025
6	0.550	1.350	$[\pm 45/\pm 45/\pm 30]_s$	$[\underline{\pm 30}/\pm 45/\pm 45/\pm 30/\underline{\pm 45}]_s$	1.181	1.025
7	0.775	0.880	$[\pm 45_4]_s$	$[\pm 45_4]_s$	1.000	1.000
8	0.775	1.000	$[\pm 45_4]_s$	$[\pm 45_4]_s$	1.000	1.000
9	0.775	1.136	$[\pm 75]_s$	$\left[\underline{\pm 30/\pm 30}/\pm 75/\underline{\pm 30/\pm 30}\right]_s$	1.213	1.025

be the reason for this observed behaviour. Blending required only minor or no modification of the unblended design. The optimiser performed equally well for the generalised and the relaxed generalised blending definitions.

Improvements in buckling were only obtained for $c \geq 0.550$ and $S \geq 1.000$. At the same time, the normalised load at which material failure will occur was reduced, though the panel remained critical in buckling for all designs obtained.

The thickness of the centre lay-up for all three design points for which improvements were obtained in the buckling load of the panel was found to be larger than that of perimeter lay-up. The largest difference was found for design point 9, with only one layer for the perimeter lay-up. The variation in lay-up properties was also largest for design point 9, which suggests that both thickness and stiffness variation are of importance for improving the buckling load of a panel loaded in uni-axial compression.

Variation in thickness and lay-up appeared to improve the failure load of a panel with concentric lay-ups. The blending implementation proposed in chapter 3 in combination with the definitions of generalised and relaxed generalised blending worked well for the concentric panel problem. Possibly a larger difference between the results obtained for the two blending definitions would be found if the design case under consideration were extended to a panel with a generic number of concentric lay-ups.

4.3 Variable stiffness laminates

Variable stiffness (VS) laminate design is realised by varying the stacking sequence from point to point in a structure. Such stacking sequence variation can be achieved in two ways: (i) using fibre steering, varying the fibre orientation angle per ply of the laminate, and (ii) using laminate blending, dropping and adding plies to the laminate locally rather than varying the fibre orientation angle within a ply.

The design of VS composite laminates using fibre steering is described in chapters 5 to 7 of this thesis, the design of a VS composite laminate using laminate blending is demonstrated in this section. Additionally, the design of a blended VS composite laminate can be used to study the effect the number of segments in a structure have on the performance of the chosen blending implementation.

4.3.1 Problem definition

A square plate of 1m $\times$ 1m loaded in uni-axial compression, see Fig. 4.7, was used to demonstrate the stacking sequence design of a VS composite laminate

for which the optimal lamination parameter (LP) distribution was assumed to be known, see Fig. 4.8, based on the material properties: $E_1 = 181$GPa (26.25Msi), $E_2 = 10.3$GPa (1.49Msi), $G_{12} = 7.17$GPa (1.04Msi) and $\nu_{12} = 0.28$. The buckling load of the optimum LP distribution is 173.7% better than that of the best known constant stiffness design for the uni-axially loaded plate, $[\pm 45^\circ_n]_s$.

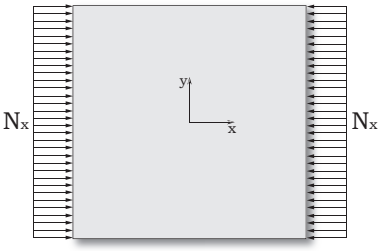

Figure 4.7: *Simply supported square plate under uni-axial compression.*

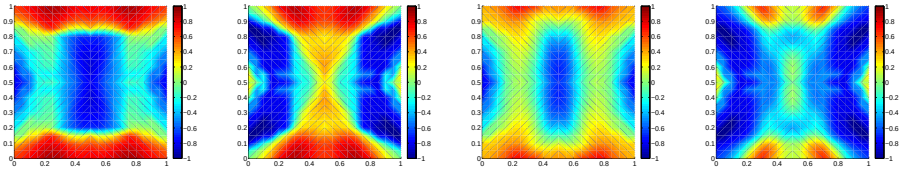

(a) $V_1^{\mathbf{A}}$ (b) $V_3^{\mathbf{A}}$ (c) $V_1^{\mathbf{D}}$ (d) $V_3^{\mathbf{D}}$

Figure 4.8: *Optimum spatial LP distribution for the VS square plate (IJsselmuiden, Abdalla and Gürdal 2010*a*).*

The objective of the demonstration was to approach the buckling load of the optimum LP distribution by matching the optimum LP distribution as closely as possible. The LP distribution was given on the finite element grid used to analyse the buckling load of the structure. Matching the LP distribution was achieved by minimising the sum of the least square errors in LPs for all nodes in the structure, Eq. 2.20:

$$\min_{\theta} f = \frac{1}{f_0} \sum_{i=1}^{n^2} |\mathbf{V}_i^* - \mathbf{V}_i| \tag{2.20}$$

where $\mathbf{V}_i^*$ denotes the optimum LPs for node i, $\mathbf{V}_i$ denotes the LPs for the same node for the design for which the objective function is evaluated, f_0 is the objective function value for the baseline single segment design, and n^2 is the total number of nodes in the structure.

The number of segments in the square plate was set to be variable to study the effect of the discretisation of the problem in the final outcome of the optimisation.

The segments for the blending problem were defined to contain a discrete number of nodes, see Fig. 4.9, and the LPs for the lay-up of a segment were ascribed to all nodes within that segment.

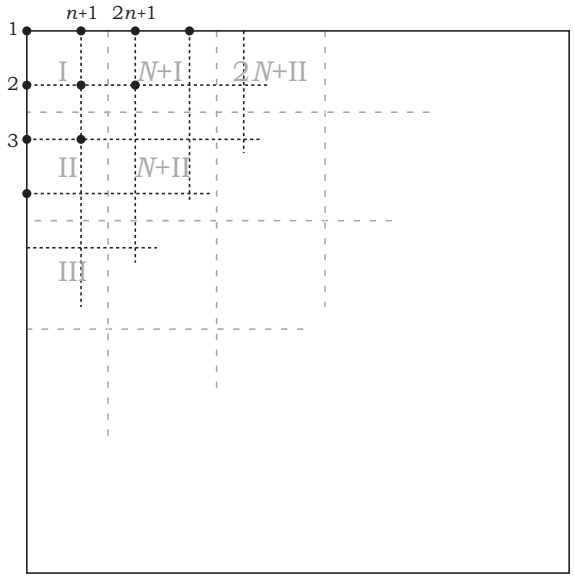

Figure 4.9: *Segment and node numbering used for the design of the VS square plate. Each segment, drawn in grey, contains a discrete number of nodes, drawn in black.*

The plate model used consisted of 21×21 nodes. The restriction that each segment had to contain a discrete number of nodes, i.e. nodes were not allowed to be on the boundary of two segments, affected the way the panel could be divided into segments in the x- and y-directions. All possible combinations for dividing the panel into segments are given in table 4.6.

Only a quarter of the plate was used to define the blended structure, making use of the symmetry of the plate; the plate and its loading were symmetric in both the x- and y-direction. The total number of segments used to define the blended structure was thereby greatly reduced, see table 4.6, this reduced the computational time required to solve the problem, and improved the likelihood of finding an optimal solution. Up to 4 by 4 segments for the quarter of the plate were considered.

4.3.2 Generated results

The lamination parameter (LP) design used as input for the blending demonstration described here, was obtained under the assumption that the plate had a

constant thickness. To keep the thickness of the plate constant, only the relaxed generalised blending definition could be adopted, because it is the only definition which allows for two different lay-ups of the same thickness to be considered blended. Another consequence was that a constraint margin for the thickness of the laminate had to be defined, such that the equality constraint $h(t) = 0$ could be satisfied:

$$\mathbf{g} = \left\{ \begin{array}{c} 1 - \frac{t}{t_c} \\ \frac{t}{t_c} - 1 \end{array} \right\} \tag{4.17}$$

where t is the thickness of the laminate and t_c is the constant thickness value.

A balanced symmetric lay-up of the form $[\pm\theta_1/\pm\theta_2/\pm\theta_3/\pm\theta_4]_s$ was assumed to generate results for this example. The optimisation was performed using the multi-chromosomal GA, appendix B. Integers 1 to 7 were used to code the fibre orientations between 0 and 90 degrees at 15-degree increments. The chromosome length for GA was chosen to be 8. The GA was set to use 5 sub-populations of 50 individuals each. After every 5 iterations the best individuals of each sub-population were migrated to the next sub-population. The solution was considered to have converged after 500 iterations without improvement. The crossover rate of the GA was set to 100%, and mutation, permutation and ply swap rates were set to 5%.

The proposed blending implementation was found to produce designs with larger ply counts for the 18-panel horseshoe configuration described in section 4.1, where the objective was to minimize ply count, than are reported in the literature (IJsselmuiden et al. 2009*a*). It was suggested that this outcome was a product of the chosen implementation. The reasoning was that the augmented objective function, Eq. 2.21, only takes into account the most severe constraint violation, effectively removing part of the selective pressure of the GA from other panels in the structure. Therefore a second augmented objective function was proposed:

$$\Phi = (1 + h_{max}) \prod_{i=1}^{n_s} \phi_i \tag{4.18}$$

with:

$$\phi_i = \left\{ \begin{array}{l} f_i + \varepsilon g_{max_i} \\ f_i + \beta g_{min_i} \end{array} \right. \tag{4.19}$$

where f_i and g_i are the local objective function and constraint margin of each individual panel, ε and β are a bonus and penalty terms as before, and h are the global constraint margins which are normalised in the same way as the constraint margins reported before in this thesis. The value of the new objective function depends on the design of all panels, and ensures that the selective pressure of the GA act fully on all the structures in the panel.

The local objective function was defined as the average error in LP-distance for

the nodes within the segment:

$$f_i = \frac{1}{n_i} \sum j = 1^{n_i} |\mathbf{V}_i - \mathbf{V}_j^*| \tag{4.20}$$

where n_i is the number of nodes in segment i and $\mathbf{V}_i$ and $\mathbf{V}_j^*$ are the lamination parameters obtained for the segment and the desired lamination parameters for the nodes in the segment respectively.

The repair strategy was identified as another possible cause of the the unexpectedly high ply counts obtained for the 18-panel horseshoe problem. Therefore, results were generated for both augmented objective functions, Eqs. 2.21 and 4.18. Results for the new augmented objective function 4.18 were generated with and without using the repair strategy, section 3.4.4. The number of butted edges was introduced as a constraint margin for the results generated without repair of the genetic coding to enforce blending.

4.3.3 Results and discussion

The objective function values and the required number of iterations for the optimisation are presented in tables 4.7 to 4.11. These results have been normalised such that, for the case of a single segment, $\Phi = 1$.

The first observation is that the results given in tables 4.7 and 4.8 are identical. This verified that the results obtained using the proposed implementation are consistent, and that the changes made to the objective function did not change the obtained results.

The normalised objective function value can be seen to decrease as the number of segments in x- or y-direction increased, as expected. The only exception is the design with four segments in the x- and y-direction. The objective function value for this design case is larger than that of design cases with less segments and the number of required iterations is smaller. This supports the hypothesis stated earlier in section 4.1 that the chosen implementation breaks down when the number of segments in a structure becomes too large, in the present example 16 segments is too large.

The results given in table 4.9, obtained using Eq. 2.21 as the objective function, show how enforcement of the relaxed generalised blending definition results in an increase of the objective function value for all design cases except that of 4 by 4 segments. The results given in tables 4.10 and 4.11 also show a higher objective function value for most cases. The objective function value for the new objective function, Eq. 4.18 for the design case where the panel was divided into 4 by 4 segments is also higher than that for the unblended design, in contrast to the same case for the original objective function.The objective function value for 4

Table 4.6: *Possible combinations of segments in x- and y-direction*

full plate			quarter plate		
direction		number of	direction		number of
x	y	segments	x	y	segments
1	1	1	1	1	1
1	3	3	1	2	2
1	7	7	1	4	4
1	21	21	1	11	11
3	1	3	2	1	2
3	3	9	2	2	4
3	7	21	2	4	8
3	21	63	2	11	22
7	1	7	4	1	4
7	3	21	4	2	8
7	7	49	4	4	16
7	21	147	4	11	44
21	1	21	11	1	11
21	3	63	11	2	22
21	7	147	11	4	44
21	21	441	11	11	121

Table 4.7: *Normalised objective function values for Eq. 2.21 for the case no blending definition was imposed.*

	segments in x-direction					
segments in	1		2		4	
y-direction	Φ	iterations	Φ	iterations	Φ	iterations
1	1.0000	505	0.8711	555	0.8537	1501
2	0.9103	765	0.8171	676	0.7704	2166
4	0.7122	1281	0.6286	3064	0.8074	1578

Table 4.8: *Normalised objective function values for Eq. 4.18 for the unblended case.*

	segments in x-direction					
segments in	1		2		4	
y-direction	Φ	iterations	Φ	iterations	Φ	iterations
1	1.0000	505	0.8711	555	0.8537	1501
2	0.9103	765	0.8171	676	0.7704	2166
4	0.7122	1281	0.6286	3064	0.8074	1578

Table 4.9: *Normalised objective function values for Eq. 2.21 for the unblended case.*

segments in y-direction	segments in x-direction: 1		2		4	
	Φ	iterations	Φ	iterations	Φ	iterations
1	1.0000	505	1.0000	679	0.8611	733
2	0.9103	509	0.9056	1382	0.8509	1285
4	0.7866	664	0.9103	1821	0.6604	3956

Table 4.10: *Normalised objective function values for Eq. 4.18 for the case blending was imposed and the repair strategy was used.*

segments in y-direction	segments in x-direction: 1		2		4	
	Φ	iterations	Φ	iterations	Φ	iterations
1	1.0000	505	0.9024	660	0.8707	658
2	0.8991	560	0.8738	671	0.8526	1589
4	0.7899	1060	0.8231	1661	0.9072	1695

Table 4.11: *Normalised objective function values for Eq. 4.18 for the case blending was imposed and no repair strategy was used.*

segments in y-direction	segments in x-direction: 1		2		4	
	Φ	iterations	Φ	iterations	Φ	iterations
1	1.0000	505	0.8907	535	0.8745	1191
2	0.9212	581	0.8570	1024	0.8898	1766
4	0.7731	1178	0.7684	2102	1.057	1794

by 4 segments becomes larger than the objective function value for the 1-segment case when the repair strategy to enforce blending is not applied.

The results obtained for a division of the panel in 4 by 4 segments contradicted the assumption that using the new objective function would improve the result of the optimisation for a larger number of segments. Nonetheless, in general the objective function values for the blended designs are lower for the new objective function than for the original objective function. It was proposed that the optimiser overall performed better for the new objective function than it did for the original objective function, because every segment in the structure contributes to its value. The relatively high value for 4 by 4 segments follows the trend seen for the unblended designs. The low objective function value that was found using the original objective function needs further investigation.

The number of iterations per case in table 4.10 and the number of iterations per case in table 4.11 confirms the hypothesis that the repair strategy causes the GA to converge sooner than would be the case when the genetic coding is interpreted without modification, and blending is enforced in the form of a constraint. The objective function value appears to be largely unaffected by the use of the repair strategy, and even to be affected negatively for a larger number of segments when no repair is used.

The results presented in this section suggest that a single step optimisation implementation is not suitable for larger blending problems with many segments to be blended. It is therefore recommended that in follow-up research, implementations with two or more steps for the generalised and relaxed generalised blending definitions, presented in this thesis, are researched. Several multi-step optimisation methods are described in the literature (De Wit and Van Keulen 2007).

4.4 Discussion

The results obtained using the new blending definitions introduced in chapter 3 were presented in this chapter. The first structure considered was an 18-panel horseshoe configuration for which several blended designs are available in the literature. This made the 18-panel horseshoe panel problem a suitable example to use to compare the proposed blending implementation with existing blending implementations. Note that the horseshoe panel problem does not account for any changes in load distribution due to changes in local stiffness of the laminate in a segment.

A rectangular plate with two concentric lay-ups was used to study the efficacy of the proposed blending implementation for a structure in which load redistribution due to the changes in local stiffness of the laminate in each segment were taken into account. Design trends for this problem were generated to chart the effect of

geometrical features on the outcome of the blending optimisation for this specific problem.

The final example considered in this chapter was the design of a variable stiffness (VS) panel using laminate blending rather than fibre steering, this will be considered further in chapters 5 to 7. Both unblended designs and designs for the case where relaxed generalised blending was enforced were obtained. Relaxed generalised blending was chosen, because it is the only blending definition, of the newly proposed blending definitions presented in this thesis, that allows for the blending of two different lay-ups of equal thickness. The problem was also used to study the effect of the number of segments in a structure on the outcome of the optimisation for blending.

The chosen blending implementation did not perform as expected for the horseshoe panel configuration. The obtained results were heavier than the results found in the literature. It was suggested that this could be an artefact of the chosen single-step implementation of the blending problem, catching the entire design of the structure to be blended in a single objective function. The repair strategy used to enforce blending was also considered as a possible cause. The results obtained for the VS panel, which was progressively divided into more segments, could be used to verify that the performance of the optimiser deteriorates when the number of segments in the structure is increased. A negative effect of the repair strategy of the genetic coding to enforce blending could not be verified.

The obtained results could not be used to reach meaningful conclusions about the relative performance of the generalised and relaxed generalised blending definitions and blending definitions found in the literature. It is therefore recommended that in follow-up research, implementations with two or more steps for the generalised and relaxed generalised blending definitions should be researched.

I've always been in the right place and time.
Of course, I steered myself there.

Bob Hope (1903 – 2003)

5

VARIABLE STIFFNESS LAMINATE DESIGN

The stress state in a structure can only be considered to be uniform under special conditions. In general the stress state in a structure varies spatially. Thus locally, fibres in laminates are not subjected to the same load combination for a structure with the same lay-up throughout. Consequently, effective use of the composite material is at best limited to one or a few points in the structure. It is expected that the mechanical behaviour of a laminate can be improved and/or the weight of the structure reduced, when a larger fraction of the composite material is used effectively. Adjustment of the local design of a laminate to improve one or more performance measures is called laminate tailoring.

Multi-segment blended laminates are one way to tailor a laminate, this has been discussed in chapter 3. Varying the in-plane fibre orientation angles within a laminate is another way to tailor a laminate, this gives a variable stiffness (VS) laminate. Variable stiffness laminate design is a more refined form of composite tailoring than laminate blending.

Early studies on VS composite laminates (Hyer and Lee 1991, Gürdal and Olmedo 1993) consider the theoretical improvements that can be achieved, and show that it is possible to tailor the stress distribution in a composite plate by introducing a curvilinear fibre angle format. Indeed, testing shows these predictions to be correct (Wu et al. 2002) and that significant improvements over constant stiffness (CS) design can be achieved. The tested VS panels are found to perform better than the analysis predicted. The thermal effect of curing plays an important role in the improvements found during testing (IJsselmuiden, Abdalla and Gürdal 2010*b*).

VS composites can be designed by using only a hand full of parameters when parametric tow-path definitions are used (Blom et al. 2008). Alternatively, fibre angles can be used as design variables directly point by point, where the increase

in design variables can be accommodated by adopting a cellular automaton (CA) framework (Setoodeh, Abdalla and Gürdal 2005).

A separable reciprocal approximation is introduced by Setoodeh et al. (2009) for the design of VS laminated composites using the fibre angles at the nodes of an FE model as design variables. This approach is adapted by Setoodeh, Abdalla and Gürdal (2006*b*) to use lamination parameters (LP) as design variables instead. One main advantage is that the number of design variables can be greatly reduced using LPs and that the design space in terms of LPs is convex. A method has been developed to design generic structures described by triangular element FE meshes (IJsselmuiden, Abdalla, Pilaka and Gürdal 2010, IJsselmuiden et al. 2011, Van Campen and IJsselmuiden 2011). A more detailed account on VS composite laminate design can be found in section 1.4.

The usage of LPs as design variables requires the conversion of LP designs to fibre angles designs (Setoodeh, Blom, Abdalla and Gürdal 2006, Van Campen et al. 2011). A further development of the method to convert a spatial distribution of LP into a spatial distribution of fibre angles developed by (Van Campen et al. 2011) is presented in this chapter. The first step in this method is to convert the LPs into a fibre angle design for a predefined laminate configuration, as discussed in chapter 2. Conversion of the distribution of LPs over a surface results in one or several possible distributions of fibre angles per ply in the laminate. These distributions have two important shortcomings: the interdependence of design points which must define a continuous path is not accounted for, and the manufacturability of the fibre orientations in terms of curvature constraints is not accounted for. Both these shortcomings will be treated in this chapter.

This chapter is structured as follows: section 5.1 consists of an in-depth discussion of the design of variable stiffness laminates as part of the framework presented in this thesis. Automated fibre placement (AFP), described in section 1.5, is an enabling technology for in-plane fibre steering, and was the manufacturing technology of choice for the research reported here. A manufacturing constraint associated with fibre steering technology, minimum steering radius, will be discussed in section 5.2. The mathematical implementation of this manufacturing constraints will be discussed in section 5.3. The conversion to fibre angles and subsequent implementation of manufacturing constraints are combined into a unified approach in section 5.4. Finally, the proposed method is verified in section 5.5.

5.1 VARIABLE STIFFNESS DESIGN

According to Svanberg (1984) most lay-up optimization problems become convex when choosing LPs as design variables. Therefore, it becomes attractive to design

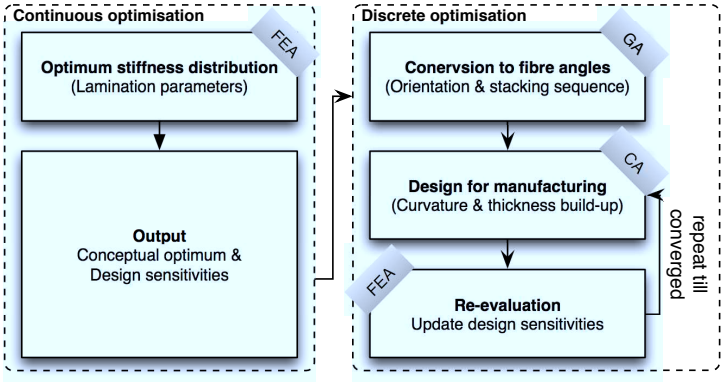

Figure 5.1: *Proposed process flow for optimisation of VS laminates, adopted from Van Campen and IJsselmuiden (2011).*

a VS structure in terms of LPs, and a two-step design methodology has been developed, see Fig. 5.1 (Van Campen and IJsselmuiden 2011).

The first step consists of the optimisation of a given design problem in terms of lamination parameters. Efficient computation of the optimum stiffness distribution is achieved by constructing an approximation of the local stiffness matrix. The optimisation in terms of LPs can be subjected to design constraints on maximum compliance, minimum strength, buckling, natural frequencies and buckling (Setoodeh et al. (2009) , IJsselmuiden et al. (2008), IJsselmuiden, Abdalla and Gürdal (2010*a*), and IJsselmuiden, Abdalla, Pilaka and Gürdal (2010)). The result of the first optimisation step is a conceptual stiffness design in terms of LPs that best satisfies the prescribed structural performance requirements.

A consequence of designing a laminate in terms of LPs is that the obtained optimum design must be converted into a laminate configuration; this is done in the second step of the two-step process. The optimum in terms of LPs (IJsselmuiden, Abdalla and Gürdal 2010*a*) was used as starting point for the work described here.

A robust method to convert a point in lamination parameter space into a laminate configuration was presented in chapter 2. This method can be applied to an FE mesh for which the optimal LPs are given at each node, and results in a distribution of fibre angles over the mesh for each layer in the structure. The stacking sequence at each node results in the global minimum of the local objective function used in the conversion process. This can either be the least-square distance in lamination parameter space, Eq. 2.20 given below:

$$f = |\mathbf{V}^* - \mathbf{V}| \tag{2.20}$$

or an objective function that resembles the objective for which the LP distribution was optimised, e.g. the inverse of the critical buckling load of the structure:

$$f = \frac{1}{\lambda(\mathbf{V})} \tag{5.1}$$

There are two drawbacks to such a fibre angle design which satisfies local optimality conditions: either (i) the effect of the objective function for which the LPs were optimised is not accounted for when Eq. 2.20 is used or, (ii), when the objective used to convert the LPs into fibre angles does reflect the objective function for which the LP distribution was optimised, local minimisation of the objective does not necessarily result in a global minimisation, as the sensitivities of the objective may change in the conversion process, see section 2.2.

Apart from the two drawbacks mentioned above, the manufacturability of the obtained fibre angle distributions must be considered. Not every distribution of fibre angles can be manufactured, because manufacturing processes like automated fibre placement (AFP) require fibre angle continuity. The degree of fibre angle continuity required depends on the manufacturing process of choice, e.g. for automated tow-placement the steering radius is a limiting factor, as will be elaborated in section 5.3. A result of fibre angle continuity is that local fibre angle designs are coupled, and a change in local fibre angles will affect the global design of the laminate. Another factor coupling local fibre angle designs is the change in load distribution within the structure that will result from a local change in stiffness, i.e. fibre angle orientation. Conversion of a variable stiffness LP design into a variable stiffness fibre angle design, thus, combines local through-the-thickness stacking sequence design of the laminate with global design for fibre angle continuity in each layer of the laminate and mechanical performance of the entire laminate.

In summary, the global design of a variable stiffness laminate is dependent on the local stacking sequence design at every point within the laminate. This global/local dependency is depicted in Fig. 5.2. All conversion studies of VS LP designs into fibre angle designs that will be presented further on in this work, were initialised by a locally optimised fibre angle distribution, before constraints on continuity were applied, as will be explained in section 5.4.

5.2 Constraint on fibre steering radius

Automated fibre placement (AFP), described in detail in section 1.5, is an enabling technology used for in-plane fibre steering, and was the manufacturing technology of choice used in the work presented here. As such, it imposes certain limitations on the nature of fibre paths that have to math the local fibre orientation angles.

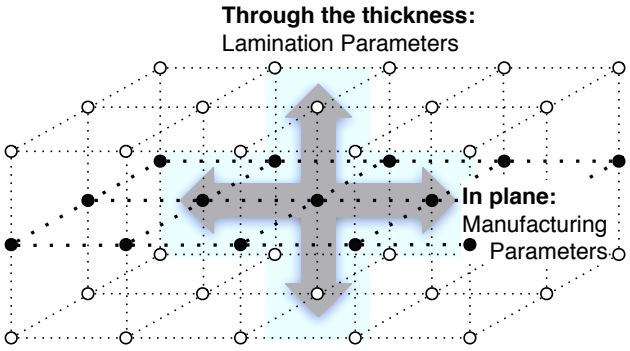

Figure 5.2: *Through-the-thickness and in-plane design.*

An overview of manufacturing constraints that are associated with AFP was given in section 1.5, here a brief summary is given. Manufacturing constraints aim to prevent structural defects, which may occur during production. Three different sources for manufacturing constraints were distinguished:

- the part geometry
- the tow material
- the fibre placement machine (FPM)

Constraints often find their origin in more than one of the sources mentioned. Nevertheless, a distinction can be made between constraints stemming from state-of-the-art manufacturing technology and those stemming from physical limitations. It is assumed that the optimal LP distribution has been obtained beforehand. Hence, constraints resulting from part geometry will not be considered in this thesis, and neither will FPM constraints, as they coincide with geometrical constraints. Fibre steering radius is one of the most important generic constraints associated with AFP. Fibrous tows can only accommodate a certain amount of in-plane curvature depending on the material system used. The curvature constraint will be discussed below.

Each tow has a given, finite width. The width of a course being placed is a multiple of this width, i.e. the width of a course with k tows is k times the tow width. When steering a course along a circular arc of given radius it becomes apparent that as tows are further away from the centre point of the circle they will have to cover a longer distance, and thus require a higher feeding rate from the tow placement machine.

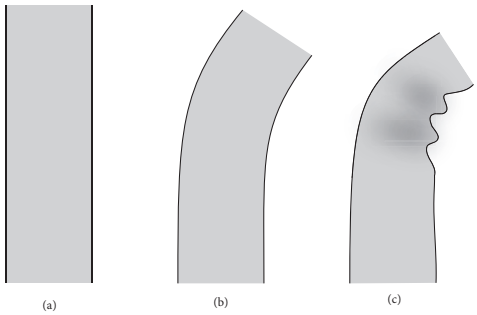

Figure 5.3: *Curvature constraint of a single tow: (a) straight tow (b) curved tow (c) tow curved beyond curvature constraint, wrinkling occurs*

The same holds true for a single tow, however, material feed cannot be adjusted as a function of radial coordinate. Instead the side of the tow furthest away from the centre point will be loaded in tension, whereas the side closest to the centre point will be in compression. The tow can only accommodate such in-plane bending up to a certain limit before starting to show out-of-plane deformations.

As soon as the curvature of the innermost tow of a course becomes too severe, the compressed side of the tow will show local buckling and wrinkle. This is detrimental to the mechanical properties of the finished product and should be avoided.

5.3 Constraint estimation

From the above discussion it can be concluded that fibre steering radius of the nodal distribution of laminate configurations needs to be constrained to obtain meaningful designs for production. Fibre steering radius is the inverse of in-plane fibre curvature, the estimation of which will be explained in this section.

So far the lamination parameter distribution has been considered as a continuous distribution over the structure. This assumption is not practical for finite element (FE) structural analysis, and consequently it is not applicable to structural optimisation of generic shell structures modelled with finite elements in terms of lamination parameters. Instead the LP distributions used for demonstration purposes in this thesis (see section 5.5 and chapter 7) were obtained on an FE grid, with optimal LPs given for each node of the structure. Conversion of such a discrete LP distribution into fibre angles will thus result in a nodal distribution of laminate configurations.

The method presented here is intended for the design of generic VS composite structures. A triangulated mesh is one of the most flexible ways to approximate a

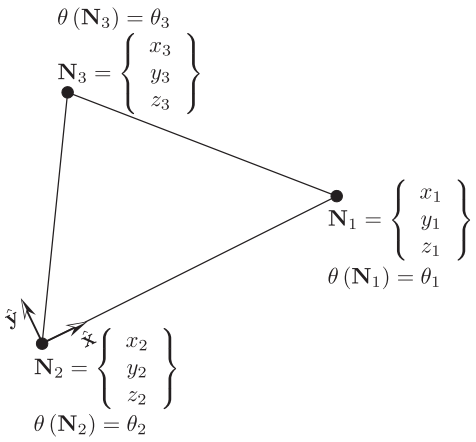

Figure 5.4: *Triangular element*

generic shell structure. Therefore, in the following triangular elements (shown in Fig. 5.4) will be used to derive the mathematical framework needed to compute in-plane fibre curvature due to fibre steering from a nodal distribution of laminate configurations.

5.3.1 Curvature computation

The local fibre steering radius is not directly obtained from a fibre angle distribution, yet in-plane fibre curvature is. The fibre steering radius is defined as the inverse of the in-plane curvature:

$$r = \frac{1}{\kappa} \tag{5.2}$$

In-plane curvature is defined as:

$$\kappa(\mathbf{x}) = |\nabla\theta(\mathbf{x})| \tag{5.3}$$

where $\mathbf{x}$ is the spatial coordinate vector.

Equation 5.3 requires the computation of the partial derivatives of $\theta(\mathbf{x})$. The computation of these partial derivatives for the general triangular element presented in Fig. 5.4 follows the method of computation posited by Winslow (2009):

$\mathbf{N}_1$, $\mathbf{N}_2$ and $\mathbf{N}_3$ are the vectors that define the location of the three local nodes

of the element in global coordinates. The area of the triangle is calculated as:

$$\mathbf{n} = (\mathbf{N}_1 - \mathbf{N}_2) \times (\mathbf{N}_3 - \mathbf{N}_2) \tag{5.4}$$

$$A_T = 0.5\,|\mathbf{n}| \tag{5.5}$$

The local coordinate system for general triangle T is defined by:

$$\mathbf{x}_T = \mathbf{N}_{T_1} - \mathbf{N}_{T_2} \tag{5.6}$$

$$\hat{\mathbf{x}}_T = \frac{\mathbf{x}_T}{|\mathbf{x}_T|} \tag{5.7}$$

$$\hat{\mathbf{y}}_T = \hat{\mathbf{n}}_T \times \hat{\mathbf{x}}_T \tag{5.8}$$

where $\hat{\mathbf{n_T}}$ is defined as the unit surface normal of the triangle:

$$\hat{\mathbf{n}}_T = \frac{\mathbf{n_T}}{2A_T} \tag{5.9}$$

Linear interpolation of fibre angles between the vertices of the triangular element is assumed. Therefore, the partial derivatives of $\theta(\mathbf{x})$ are constant for any point in the element and defined by:

$$(\nabla\theta) = \begin{bmatrix} P_{T_{11}} & P_{T_{12}} & P_{T_{13}} \\ P_{T_{21}} & P_{T_{22}} & P_{T_{23}} \\ P_{T_{31}} & P_{T_{32}} & P_{T_{33}} \end{bmatrix} \begin{Bmatrix} \theta_{T_1} \\ \theta_{T_2} \\ \theta_{T_3} \end{Bmatrix} \tag{5.10}$$

where

$$\begin{Bmatrix} P_{T_{22}} \\ P_{T_{21}} \\ P_{T_{31}} \end{Bmatrix} = \frac{1}{|\mathbf{N}_{T_1} - \mathbf{N}_{T_2}|} \left(\hat{\mathbf{x}}_T - \frac{(\mathbf{N}_{T_3} - \mathbf{N}_{T_2}) \cdot \hat{\mathbf{x}}_T}{(\mathbf{N}_{T_3} - \mathbf{N}_{T_2}) \cdot \hat{\mathbf{y}}_T} \hat{\mathbf{y}}_T \right) \tag{5.11}$$

$$\begin{Bmatrix} P_{T_{12}} \\ P_{T_{22}} \\ P_{T_{32}} \end{Bmatrix} = \frac{1}{|\mathbf{N}_{T_1} - \mathbf{N}_{T_2}|} \left(-\hat{\mathbf{x}}_T + \frac{(\mathbf{N}_{T_3} - \mathbf{N}_{T_2}) \cdot \hat{\mathbf{x}}_T - |\mathbf{N}_{T_1} - \mathbf{N}_{T_2}|}{(\mathbf{N}_{T_3} - \mathbf{N}_{T_2}) \cdot \hat{\mathbf{y}}_T} \hat{\mathbf{y}}_T \right) \tag{5.12}$$

$$\begin{Bmatrix} P_{T_{13}} \\ P_{T_{23}} \\ P_{T_{33}} \end{Bmatrix} = \left(\frac{1}{(\mathbf{N}_{T_3} - \mathbf{N}_{T_2}) \cdot \hat{\mathbf{y}}_T} \hat{\mathbf{y}}_T \right) \tag{5.13}$$

The **P**-matrices for a structure, which compute the partial fibre angle derivatives of an element, can be assembled in a global **P**-matrix. The assembly operation is the same as that used to assemble, for instance, the global stiffness matrix of a structure. Once the global **P**-matrix has been assembled the curvature is computed as follows:

$$\kappa = |\mathbf{P}\theta| \tag{5.14}$$

Note, the nodal curvature values computed this way are the average of the

curvature values of the elements sharing that node.

5.3.2 Mesh convergence study

To demonstrate the method used to compute in-plane curvature, three nodal fibre angle distributions were used for which the in-plane curvature distributions were already known. The method was used to compute an estimate for each of the three cases and the obtained results were compared to the exact distributions. The fibre angle distributions mentioned above were considered on a square plate in the xy-plane bound by $0 \leq x \leq 1$ and $0 \leq y \leq 1$. The considered distributions were:

1. Straight fibres at an angle of $\frac{\pi}{3}$ radians: $\kappa = 0$.
2. Constant curvature in x-direction $\theta = \pi x$: $\kappa = \pi$.
3. Concentric fibre angles around the point $\mathbf{x} = -\mathbf{1}^1$: $\kappa = \frac{1}{|\mathbf{x}+\mathbf{1}|}$

The discretisation of the plate was varied between 1 and 50 elements along the edges of the plate. Both the maximum error and the average error at the nodes between the exact and the estimated curvature value were computed. For the straight fibre design and the constant curvature fibre distribution, the errors were of the order of magnitude of $1 \cdot 10^{-15}$, which was considered to be a result of numerical accuracy. The result that was obtained for the concentric fibre angle distribution is plotted in Fig. 5.5 as function of discretisation. As the number of elements increases the maximum and mean error were found to converge rapidly toward zero error. The error that was found is on the conservative side, i.e. the method presented to compute in-plane curvature consistently overestimates the curvature value. Overall good agreement between the exact and estimated curvature values was found.

5.4 Constraint inclusion

The method to convert a point in lamination parameter (LP) space into a stacking sequence design presented in chapter 2 was formulated as an optimisation problem. The objective f of this optimisation was to find the stacking sequence of which the LPs are closest to the desired LPs in a least-squared sense. This distance-based objective function can be used for the optimisation procedure that is proposed in this section. However, this may ignore mechanical effects that play an important

[1] note that vector notation is used.

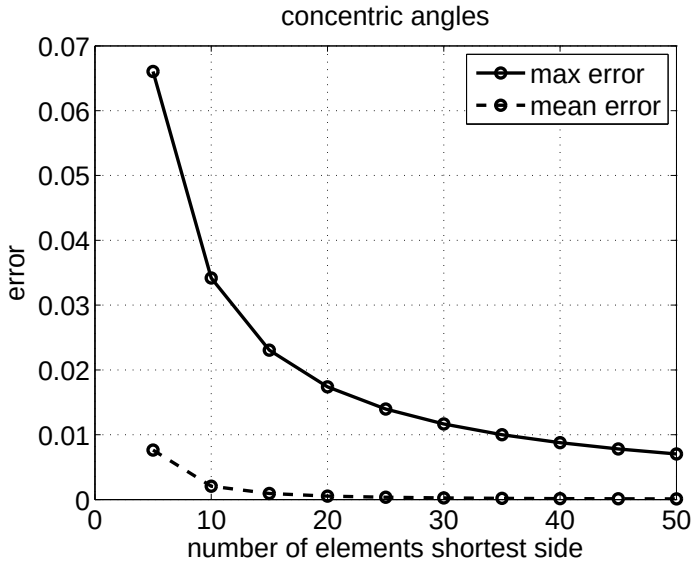

Figure 5.5: *Mesh convergence study for the estimation of in-plane fibre curvature.*

role in the obtained fibre angle distributions, because no structural analysis is carried out in the optimisation process.

Therefore, a second objective function is proposed that uses nodal sensitivity information of the optimal LP distribution. This estimate of the overall design objective is expected to give better results than the distance-based objective function.

5.4.1 Cellular automaton

Both objective functions can be evaluated locally at the level of the node rather than the structure. This makes them suited for implementation in a cellular automaton (CA) paradigm, in which the structure is updated and analysed in an iterative fashion. The CA paradigm links stacking sequence design at each node to satisfaction of manufacturing constraints for the entire structure. The computation of in-plane fibre curvature and thickness values can be seen as the analysis rule of the CA, whereas the update rule consists of changing the local fibre angle such that the augmented objective function, described later, is minimized.

The proposed optimisation procedure is presented schematically, in Fig. 5.6. The LP design at each node of the structure is converted into a fibre angle design, as discussed in chapter 2. This fibre angle design only needs to be determined once

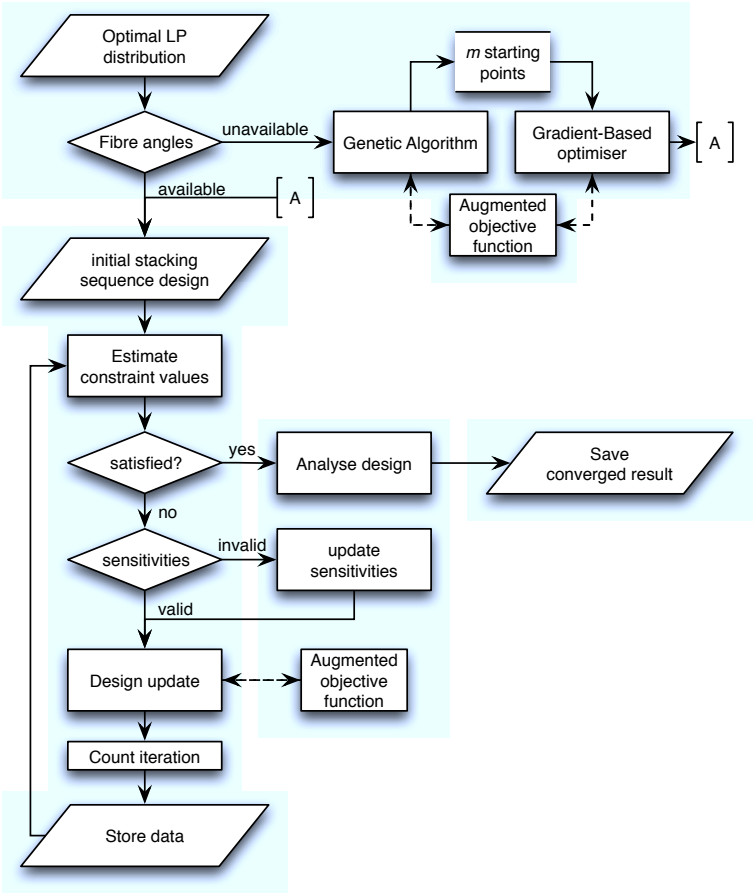

Figure 5.6: *Flow diagram of the proposed CA.*

for a given LP distribution, and can be stored for later usage. The stored fibre angle distribution is used as initial design for the CA. Here the CA is explained in qualitative terms, the numerical implementation of the CA is explained in section 5.4.2.

At the beginning of a design iteration the manufacturing parameters to be constrained or an estimate thereof are computed, see section 5.3. The obtained values are used to compute constraint margins, which are used to compute an the augmented objective function value, as is explained in section 5.4.2. Newton's method is used to update the (initial) fibre angle design. The design update rule is based on the Jacobian and (if available) the Hessian of the augmented objective function. Jacobi iteration is used to conserve the symmetry (if present) of the fibre angle design on irregular finite element meshes. The algorithm moves on to the next iteration once all fibre angle values have been updated. The CA is considered to have converged after a user-defined number of design iterations has been reached for which all constraints are satisfied and the rate of improvement has dropped below a user-defined threshold. In case the design objective is based on sensitivity information, there is the possibility to update this sensitivity data, if the lamination parameters of the updated fibre angles fall outside the user-defined trust region for the sensitivity information in LP-space. A smaller trust region for the sensitivity data is likely to result in a better outcome of the CA, but will also increase the computational effort considerably, for more sensitivity analyses are required.

5.4.2 Numerical implementation

In section 2.3.2 an augmented fitness function is proposed to include constraints in the optimisation process. Here an augmented objective function is proposed as well to simplify the update rule of the CA, as shown later. As in section 2.3.2 constraints on in-plane fibre curvature and thickness can be included using constraint margins. Here in-plane fibre curvature is used as example:

$$g_\kappa = \frac{\kappa_{\max}}{\kappa_{\text{all}}} - 1 \tag{5.15}$$

This normalization yields a value of 0.1 for 10% constraint violation, and a value of -0.1 for 10% margin. Such normalization can be applied to any constraint imposed on a structure. The augmentation procedure described here always uses the most severe constraint violation $g_{\max}$:

$$\Psi = \begin{cases} f + \varepsilon g_{\max} & \text{if} \quad g_{\max} \leq 0 \\ f + \beta g_{\max} & \text{if} \quad g_{\max} > 0 \end{cases} \tag{2.21}$$

where Ψ is to be minimized.

The update rule proposed here follows Newton's method:

$$\theta^{(k+1)} = \theta^{(k)} - \alpha_k M_k \mathbf{g}_k \tag{5.16}$$

where α_k is the allowed step size and:

$$M_k = (H_k + \mu_k I)^{-1} \tag{5.17}$$

with μ_k chosen such that the matrix M_k is always positive definite. In the case where the Hessian is not positive definite, Newton's method will move to higher function values and might stall near singular points. In such a case stabilisation is required. Alternatively, when no Hessian is available or expensive to compute one can switch to gradient descent, i.e. $H = I$ and $\mu_k = 0$. The upshot of using an augmented objective function is that it considers the constraints to be uncoupled, meaning that its Jacobian and Hessian can be assembly by summation of the Jacobians and Hessians of the objective and constraint functions of the optimisation problem.

The minimum is approached from an infeasible point in the design space when the CA would be applied directly to the stacking sequence seed, which is used to initialise it. Therefore, the danger exists that the CA might not converge or only converges very slowly. The stacking sequence seed can be regularised to circumvent this problem. This can be done by iteratively averaging the fibre orientations of each node using its own orientation and that of its direct neighbours until the maximum constraint margin value $g_{\max}$ has fallen below a preset value.

5.5 VERIFICATION

A square plate under biaxial compression, see Fig. 5.7, is considered of which the LP distribution that maximises the buckling load of the plate is known, see Fig. 5.8. Fibre angle designs were obtained for the given LP distribution for a balanced symmetric stacking sequence configuration with two distinct orientations $[\pm\theta_1/\pm\theta_2]_s$ for various dimensions of the square plate in order to demonstrate the procedure proposed in this chapter, and to investigate the consistency of the results obtained by it.

The dimension of the panel was varied in discrete steps between 0.1×0.1m to 10×10m, the normalised buckling load for each dimension is plotted as function of maximum in-plane curvature in the structure in Fig. 5.9; the buckling load is normalised using that of the best constant stiffness (CS) design, $[\pm 45_2]_s$. The stacking sequence seed[2] used to initialise the CA was obtained with the GA set to a population size of 50, a mutation probability of 5%. The GA was

[2]For more details on the conversion of LPs into fibre angle designs please see chapter 2

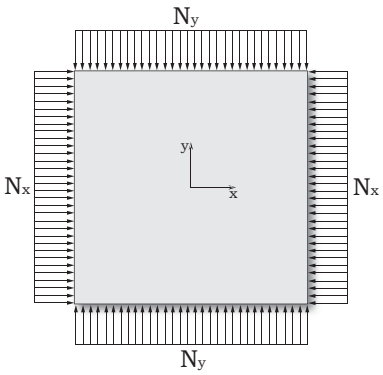

Figure 5.7: *Square plate loaded in biaxial compression.*

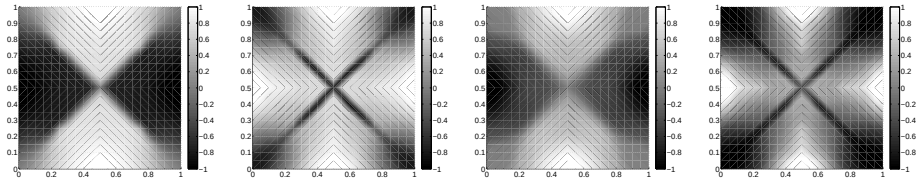

(a) $V_1^{\mathbf{A}}$ (b) $V_3^{\mathbf{A}}$ (c) $V_1^{\mathbf{D}}$ (d) $V_3^{\mathbf{D}}$

Figure 5.8: *Spatial distribution of lamination parameters to be matched (IJsselmuiden, Abdalla and Gürdal 2010*a*).*

considered to have converged after 10 iterations without improvement. The subsequent gradient-based optimiser was set to a step-size of $5 \cdot 10^{-3}$ and was considered to have converged after 10 iterations with less than 0.1% improvement. The stacking sequence seed was regularised until $g_{\max} = 0$. The CA was set to gradient descent, i.e. $M_k = I$, and used a step-size of $1 \cdot 10^{-5}$. It was considered to have converged after 50 iterations with less than 0.1% improvement.

The results for each of the studied design cases show the same trend: the buckling load is close to, but larger than, the best CS design for small curvature values (steering radii larger than 10 times the panel dimension, nearly straight fibre design) and increases as the constraint on curvature is relaxed, reaching the highest possible buckling load at steering radii larger than roughly $\frac{1}{10}$ of the dimensions of the panel. The maximum buckling load achieved for each of the designs was 44.7% higher than the buckling load of the best CS design. In comparison, the buckling load of the optimum LP design was 49.6% better than the best CS design.

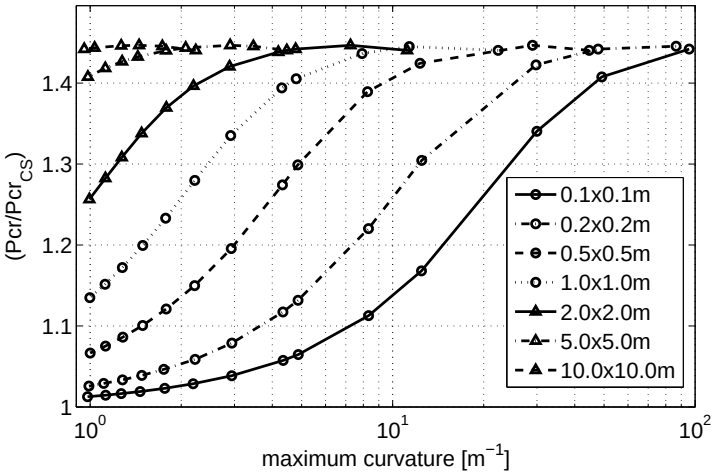

Figure 5.9: *Normalised buckling load as function of maximum in-plane curvature for a range of panel dimensions.*

The unconstrained fibre angle design for the panel dimensions 1.0×1.0m is shown in figure 5.10. The fibre angle distributions in both layers appear to be point symmetric about the centre of the panel, which is consistent with the LP distribution in Fig. 5.8. The 0°- and 90°-orientations for θ_2 reflect the stark regions where $\left\{V_1^{\mathbf{A}}, V_1^{\mathbf{A}}\right\} = \{1, 1\}$, i.e. 0°-orientation, and $\left\{V_1^{\mathbf{A}}, V_1^{\mathbf{A}}\right\} = \{-1, 1\}$, i.e. 90°-orientation. The more gradual variation for the flexural LPs, of which the values are more strongly influenced by θ_1 than θ_2, is reflected by the more gradual

distribution of fibre angles for θ_1.

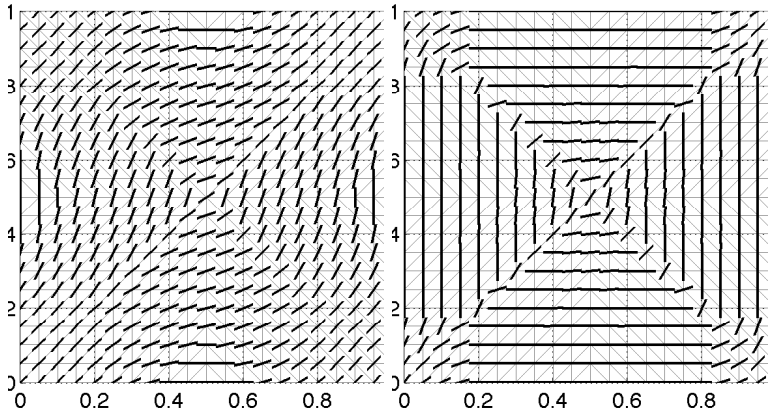

(a) θ_1 (b) θ_2

Figure 5.10: *Fibre angle design for panel dimensions* 1.0×1.0m.

It is concluded that the method to convert a VS design in terms of LPs into a fibre angle design produces consistent results for a range of structural results two orders of magnitude apart. The obtained fibre angle design was in agreement with the design that could be expected on the basis of the optimum LP distribution. The biaxial plate example will be treated in more detail in chapter 7.

Over every mountain there is a path, although it may not be seen from the valley.

Theodore Roethke (1908 – 1963)

6

Fibre path construction and thickness build-up

The design of variable stiffness (VS) laminates was discussed in chapter 5. The proposed conversion process from a VS laminate design in terms of lamination parameters (LP) into a design in terms of fibre angles results in a nodal fibre angle distribution for each layer in the laminate; and it was demonstrated how a constraint on in-plane fibre curvature could be enforced on such a nodal fibre angle distribution. However, other manufacturing parameters were not considered and the VS laminate was assumed to have constant thickness.

A VS laminate design formatted as a nodal fibre angle distribution for each layer in the laminate is not fit for production, the design needs to be converted into fibre-paths, which can be used to generate the input commands for an automated fibre-placement machine (AFP). This can be done either manually, by generating fibre paths from the nodal fibre angle distribution based on visual inspection, or automatically using a dedicated algorithm.

Once the fibre paths for a VS laminate are known the gaps and overlaps for each layer in the laminate can be determined, which allows us to estimate the thickness variation within the VS laminate in advance. When the fibre paths, and consequently thickness build-up in the laminate, are computed during the conversion process from LPs to a fibre angle distribution, thickness build-up in the laminate may also be constrained. Additionally, the mechanical properties of the laminate and its weight will change if thickness build-up is not remedied through, e.g. tow-cutting. Hence, the LPs at each point in the structure and the volume of the structure should be recomputed.

The automatic generation of fibre paths from a nodal fibre angle distribution and the estimation of thickness build-up due to gaps and overlaps are reviewed in this chapter. The methods used to describe and obtain fibre paths found in the literature are discussed, and a suitable method for the conversion of nodal fibre

angle distributions into fibre paths is identified. The discussion on fibre paths is followed by a discussion on estimation of laminate thickness build-up due to fibre steering in the laminate. A method to estimate thickness build-up in the laminate, based on the nodal fibre angle distribution, and to determine fibre paths for manufacturing is proposed based on the review of the literature on fibre path generation and thickness estimation. It is discussed how the LPs and the volume of a structure can be recomputed once the thickness distribution is known. The chapter is concluded with a demonstration of a proposed approach for estimating thickness and determining fibre paths in a VS laminate.

6.1 Fibre paths

Several methods are reported in the literature that can be used to describe fibre paths in a VS composite structure, and an overview of the methods available in the literature is given in this section. Both how to describe fibre paths and the construction of fibre paths based on a nodal fibre angle distribution are discussed. The section is concluded with a discussion of which method might best be used to generate fibre paths for a given nodal fibre angle distribution.

6.1.1 Fibre path description

The design and manufacture of variable stiffness composite laminates requires fibre paths in the plane of the laminate to be described mathematically. In early work on VS composites (Katz, Haftka and Altus 1989) structures are divided into regions of constant fibre angle. Katz et al. (1989) and Hyer and Charette (1991) use this approach to increase the load at which a panel with a hole fails, in both instances fibre angles are used directly as design variables.

A continuous variable angle fibre format is needed when automated fibre placement (AFP), see section 1.5, is considered as the manufacturing method of choice for a VS laminate. In early work, the principal material orientations were aligned with the principal stress directions (Hyer and Charette 1991), resulting in a VS composite laminate. The fibre paths and principal stress directions in the above case coincide. Note that alignment of principal material orientations with failure load will not necessarily lead to an improvement of the failure load for the laminate (Brandmaier 1970). Likewise, the strain at which a circular cylinder of a given radius buckles can be used to determine the fibre angle variation in a cylinder of elliptical cross-section in which the strain within the cross-section is constant, leading to an improvement of the buckling load of the elliptical cylinder (Lo and Hyer 2011). The fibre angle variation within a VS laminate then is a direct function of the local radius of curvature of the elliptical cylinder. Such methods, which aim to align the fibre orientation based on a desired mechanical

response from the structure, without optimising for actual structural performance are a practical way to obtain fibre path designs, but many possible optimal results are excluded taking this course. Therefore, using parametric fibre angle variation to describe fibre paths in a VS laminate is to be preferred.

Linear fibre angle variation is introduced in Gürdal and Olmedo (1993). Here the fibre angle distribution is obtained by linear interpolation between two fibre angle values, see Fig. 6.1 and Eq. 6.1:

$$\theta(x) = \frac{2(T_1 - T_0)}{a}x + T_0 \tag{6.1}$$

where the fibre angle at the mid of the panel, $x = 0$, see Fig. 6.1, and T_1

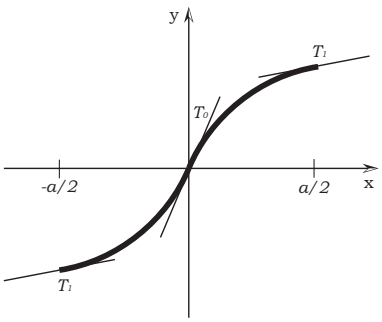

Figure 6.1: *Linear fibre angle variation.*

is the fibre angle at the panel end, $x = \frac{a}{2}$. Once the fibre angle variation is determined mathematically, the fibre path through the origin of the panel follows from (Gürdal and Olmedo 1993):

$$y = \begin{cases} \frac{a}{2(T_1-T_0)}\left\{-\ln\left[\cos\left(T_0 + \frac{2(T_1-T_0)x}{a}\right)\right] + \ln\left[\cos(T_0)\right]\right\} & \text{for} \quad 0 \le x \le \frac{a}{2} \\ \frac{a}{2(T_1-T_0)}\left\{\ln\left[\cos\left(T_1 + \frac{2(T_1-T_0)x}{a}\right)\right] - \ln\left[\cos(T_1)\right]\right\} & \text{for} \quad -\frac{a}{2} \le x < 0 \end{cases} \tag{6.2}$$

Linear fibre angle variation and similar methods like constant curvature paths are used to solve a number of problems in the literature. The in-plane response of a rectangular plate with linear fibre angle variation is proposed in Gürdal and Olmedo (1993), and discussed further in Alhajahmad, Abdalla and Gürdal (2008). Alhajahmad et al. (2008) use linear fibre angle variation for the design tailoring of aircraft fuselage panels for maximisation of the failure load under pressure pillowing. In Blom et al. (2008) it is shown that the concept of linear variation can be extended by assuming constant in-plane curvature between the two fibre angle values defining the fibre path, or by subdividing a fibre path into multiple regions each with its own fibre angle variation.

The advantage of linear fibre angle variation and other variation schemes is that only two variables, T_0 and T_1 are needed to describe a variable stiffness laminate mathematically. At the same time this poses a drawback regarding the range of fibre angle variation that can be described, which is limited to a small subset of the fibre angle variation that can be achieved using AFP, which may limit the potential performance improvements of a variable stiffness design. Therefore, a more elaborate description of variable fibre angle variation is required.

Polynomials can be used effectively to describe the fibre paths of a VS composite structure. A shape function approach can be applied to describe the fibre paths in a VS composite structure. Non-uniform rational B-splines (NURBS) are used by Nagendra, Kodiyalam, Davis and Parthasarathy (1995) to describe the base fibre paths in a structure from which all other fibre paths are derived. Mathematically NURBS are defined by interpolation through a fixed number of control points. Only four design variables are required to design a ply in a VS laminate when using Bezier curves (Parnas, Oral and Ceyhan 2003), increasing the range of laminate designs that can be described significantly, without a large increase in the total number of design variables.

Alternatively, shape functions can be used to describe the fibre angle distribution in a VS composite laminate. The fibre angle distribution in a laminate can be written as (Setoodeh, Blom, Abdalla and Gürdal 2006):

$$\theta = \sum_{m=1}^{N} a_m \phi_m = \sum_{i=0}^{p-1} \sum_{j=0}^{p-1} a_{ij} \phi_i \phi_j \tag{6.3}$$

where a_{ij} are unknown coefficients and ϕ are shape functions, which are described by Lobatto polynomials, which in turn are described by Legendre polynomials. The shape functions for a one-dimensional element are constructed using:

$$\phi_i(\xi) = \sqrt{\tfrac{2i-1}{2}} L_i(\xi) \quad \text{for} \quad i \geq 2 \tag{6.4}$$

where ξ is the normalised coordinate, and $L_i(\xi)$ is a Lobatto polynomial, which is defined by:

$$L_i(\xi) = \textstyle\int_{-1}^{\xi} P_{i-1}(\rho) d\rho \tag{6.5}$$

where P_{i-1} are the Legendre polynomials, which are defined by Rodrigues's formula:

$$P_n(\xi) = \frac{1}{2^n n!} \frac{d^n}{d\xi^n} \left[(\xi^2 - 1)^n \right] \tag{6.6}$$

The coefficients of the shape functions can be used as design variables to optimise the performance of a VS laminate (Alhajahmad et al. 2008, Klees 2009, Pilaka 2010). This gives the advantage that fibre paths can be directly determined using the streamline analogy, discussed below, and that the number of design variables,

which is dependent on the order of the Lobatto polynomials used, is small for each layer in the laminate.

6.1.2 Fibre path construction

Discrete fibre paths can be constructed using the streamline analogy, where each streamline represents the centre line of a fibre course in the laminate. For the streamline analogy it is assumed, that the width of each fibre course is made infinitely small, i.e. each streamline represents a single fibre. The solution of the stream function, Eq. 6.7, depends on the choice of boundary conditions that are set for the fibre paths (Setoodeh, Blom, Abdalla and Gürdal 2006).

$$\Psi(x, y) = C \tag{6.7}$$

The stream function connects all points for which C is equal. Note, that the streamlines for $+\theta$ and $-\theta$ will be different, because relative to the fibre orientation at a given point, the points in the structure for which a fibre orientation angle are connected differently for a negative value of the fibre orientation angle than for a positive value of equal magnitude. It has been shown in the literature that there is a direct correlation between thickness build-up in a VS laminate and the stream function (Setoodeh, Blom, Abdalla and Gürdal 2006):

$$t(x, y) \propto \frac{d\Psi}{dn}(x, y) \tag{6.8}$$

where n is the normal of the the streamline function. This can be used to define the following relationship between thickness build-up and fibre angle (Blom, Abdalla and Gürdal 2010):

$$-\mathbf{s}\nabla t = \mathbf{n}\nabla\theta \tag{6.9}$$

where $\mathbf{s}$ and $\mathbf{n}$ are the tangent vector and normal vector of the local fibre angle. The physical explanation for this equation is that change in thickness along a stream line depends on the change of fibre orientation perpendicular to that streamline. The only unknown in Eq. 6.9 is the ply thickness t; using proper boundary conditions the function can be solved. These boundary conditions are discussed in section 6.2.

Once the thickness distribution and the fibre angle distribution are known, the streamlines can be determined using (Blom et al. 2010):

$$\Psi(x, y) = -\int_0^x t(x^*, y^*)\sin\theta(x^*, y^*)dx^* + \int_0^y t(x^*, y^*)\cos\theta(x^*, y^*)dy^* \tag{6.10}$$

Then the discrete fibre courses can be calculated:

$$x_e = x_c \mp \frac{p}{2} \sin\theta_c \tag{6.11}$$

$$y_e = y_c \pm \frac{p}{2} \cos\theta_c \tag{6.12}$$

where p is the width of the course, $\langle x_c, y_c \rangle$ defines the centre line of the course, and $\langle x_e, y_e \rangle$ define the edges of the course.

6.1.3 Discussion

Of all the fibre path definitions discussed in section 6.1.1, shape functions based on Lobatto polynomials offer the most freedom to describe a VS composite laminate. Thus, the choice was made to use Lobatto polynomials when a mathematical description of the fibre angle distribution of a ply in a VS laminate was required. Curve fitting techniques can be used to determine the coefficients for the shape functions, e.g. least square fitting (Setoodeh, Blom, Abdalla and Gürdal 2006) where the objective is to minimise the average residual norm for all nodes in the structure. Note that in most cases the least square fit is an approximation of the fibre angle distribution actually desired.

The streamline analogy, as described in section 6.1.2, can be applied for any of the fibre path definitions discussed in section 6.1.1. It can also be used without any formal fibre path definition making it a suitable option for the work described in this thesis.

6.2 Thickness distribution

Thickness variations occur in VS composite structures. In this sections the causes of these thickness variations are discussed, as are the methods described in the literature that can be used to estimate the local thickness build-up in a structure. The section is concluded with a discussion of how the choice of thickness build-up estimation method was chosen for the work presented in this thesis.

6.2.1 Thickness build-up

Multiple tow courses are needed to construct a fibre-placed laminate. Here only one layer of such a laminate is considered. Assuming the tow courses in this layer are all derived from one reference curve, there are multiple options available to fill the entire layer with tow courses, two of which will be considered here (Tatting and Gürdal 2003): (i) parallel paths, and (ii) shifted paths.

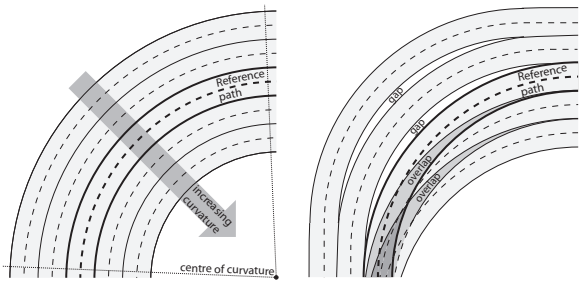

(a) Parallel paths (b) Shifted paths

Figure 6.2: *Tow paths derived from a reference curve.*

The advantage of parallel paths is that no gaps or overlaps between tows will occur, which results in a structure of uniform thickness and theoretically, without any defects. A disadvantage is that the steering radii of each parallel tow are different, which at sufficient distance from the reference path will result in violation of the maximum allowable in-plane curvature, see Fig. 6.2(a).

The in-plane curvatures of each tow course are equal when they are placed along a path which has been shifted parallel to the reference tow-path, see Fig. 6.2(b). The parallel shift results in the combination of the two most extreme cases: (i) tows fully overlapping, and (ii) gaps between the tows with no overlaps. These gaps and overlaps cause a change in the thickness of the layer under consideration, and thus in the thickness of the laminate as a whole.

6.2.2 Thickness estimation

Equation 6.9 relates the thickness build-up in of a ply of a VS laminate with the fibre angle distribution of that ply. The relation can be simplified using a change of variables $\tau = \ln t$ (Blom et al. 2010), this gives:

$$-\mathbf{s}\nabla\tau = \mathbf{n}\nabla\theta \tag{6.13}$$

and this results in a system of equations for the nodal fibre angle variation of the entire ply. Making use of the linearity of the equation this system can be rearranged in the form:

$$M\tau = \mathbf{b} \tag{6.14}$$

where M is the matrix that represents the left hand side of Eq. (6), s is the vector that represents s at every grid point and B is the vec- tor that represents the right hand side of Eq. (6), where M and $\mathbf{b}$ are left hand side and right hand side of Eq. 6.13, respectively.

Equation 6.14 is a differential equation, therefore, adequate boundary conditions are required to solve it. One option would be to define the thickness of the VS laminate along part of the boundary of the design region, after which the hyperbolic differential equation, Eq. 6.14, can be solved using a finite element scheme (Pilaka 2010). Alternatively, according to streamline theory only boundary conditions need to be defined at the inflow boundary of the design region (Blom et al. 2010), who arbitrarily define the inflow boundary as:

$$\mathbf{sN} \leq 0 \tag{6.15}$$

where $\mathbf{s}$ is the vector tangent to the fibre orientation and $\mathbf{N}$ is the outward normal vector to the design domain, see Fig. 6.3.

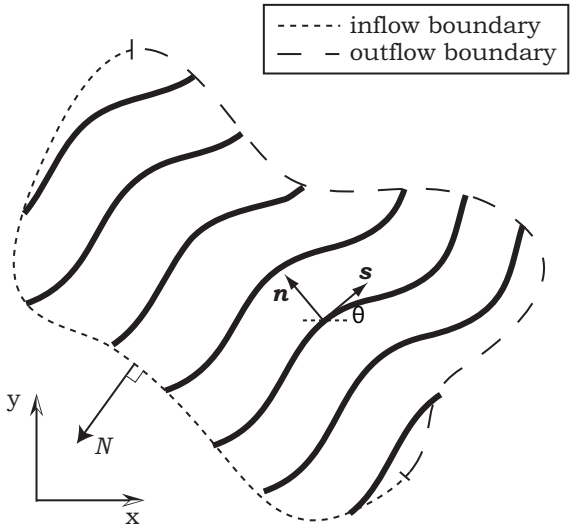

Figure 6.3: *Streamline definitions (Blom et al. 2010).*

The thickness along the inflow boundary of the design domain can then be defined such that certain, physically useful optimality criteria are fulfilled. Some possible optimality criteria are minimum thickness and maximum smoothness of the thickness distribution of the VS laminate (Blom et al. 2010). Additionally periodic boundary conditions can be enforced.

Maximum thickness can be enforced using a min-max formulation (Olhoff 1989), and smoothing is maximized by minimizing the H_1-norm of the thickness distribution:

$$\min \frac{1}{2}\tau^T \nabla^2 \tau \tag{6.16}$$

The Laplacian, ∇^2, can be discretised in the same way as the gradient operator,

see section 5.3.1. This discretisation results in matrix K. The minimum thickness and maximum smoothness objectives can be combined in one objective function using a weighting factor w (Blom et al. 2010):

$$f_{\min} = (1-w)\frac{\alpha}{\alpha^*} + w\frac{\frac{1}{2}\tau^T K\tau}{\frac{1}{2}\tau^{*T} K\tau^*} \tag{6.17}$$

where $0 \leq w \leq 1$, α is the maximum thickness in the structure, and α^* and $\frac{1}{2}\tau^{*T} K\tau^*$ are respectively the minimum maximum thickness and the maximum smoothness in the structure.

6.3 Implementation

In the first two sections of this chapter the available literature on the description and generation of tow-paths, and, on the thickness build-up in a VS was discussed. Based on this literature review the streamline analogy (Blom et al. 2010) was chosen and used for the work presented in this thesis. The implementation of the streamline analogy as implemented in the research discussed in this thesis will be described below.

6.3.1 Estimation of thickness distribution

The hyperbolic differential equation, Eq. 6.14, was solved using a finite element scheme(Pilaka 2010); for the work presented in this thesis, the QUADprog function in MATLAB® was used. The fibre course designs were optimized for smoothness, i.e. the differences in thickness between nodes were minimized.

The smeared thickness build-up obtained for a laminate is affected by the act of laminate balancing. The thickness distribution for a layer with the orientation vector $+\theta$ will differ from that obtained for the layer with orientation vector $-\theta$ because the tangent vector $\mathbf{s}$ and normal vector $\mathbf{n}$ to the fibre orientation will be different and therefore matrix M and vector $\mathbf{b}$ in Eq. 6.14 will also differ. Consequently the inflow and outflow boundaries of the design domain will be different.

The smeared thickness distribution should be obtained for every layer in a VS laminate, both in $+\theta$- and $-\theta$-orientation. The total thickness distribution for the VS laminate then follows as the sum of the thickness distributions of all layers in the laminate. Note that, for symmetric fibre angle distributions and boundary conditions the symmetry can be obtained to achieve the streamlines of the conjugate $-\theta$-layer.

6.3.2 Computation of LPs and volume

The thickness distribution changes the LPs at any given point in the structure, because the relative weight of each of the layers comprising the lay-up have changed. The new LP-values can be computed using Eq. 6.18 to Eq. 6.20:

$$\left\{V_1^{\mathbf{A}}, V_2^{\mathbf{A}}, V_3^{\mathbf{A}}, V_4^{\mathbf{A}}\right\} = \frac{1}{t_{\text{tot}}} \sum_{i=1}^{n} t_i \left\{\cos 2\theta_i, \sin 2\theta_i, \cos 4\theta_i, \sin 4\theta_i\right\} \quad (6.18)$$

$$\left\{V_1^{\mathbf{B}}, V_2^{\mathbf{B}}, V_3^{\mathbf{B}}, V_4^{\mathbf{B}}\right\} = \frac{2}{t_{\text{tot}}^2} \sum_{i=1}^{n} \left(\left(\frac{t_{\text{tot}}}{2} - \sum_{j=1}^{i-1} t_j \right)^2 - \left(\frac{t_{\text{tot}}}{2} - \sum_{j=1}^{i} t_j \right)^2 \right) \left\{\cos 2\theta_i, \sin 2\theta_i, \cos 4\theta_i, \sin 4\theta_i\right\} \quad (6.19)$$

$$\left\{V_1^{\mathbf{D}}, V_2^{\mathbf{D}}, V_3^{\mathbf{D}}, V_4^{\mathbf{D}}\right\} = \frac{4}{t_{\text{tot}}^3} \sum_{i=1}^{n} \left(\left(\frac{t_{\text{tot}}}{2} - \sum_{j=1}^{i-1} t_j \right)^3 - \left(\frac{t_{\text{tot}}}{2} - \sum_{j=1}^{i} t_j \right)^3 \right) \left\{\cos 2\theta_i, \sin 2\theta_i, \cos 4\theta_i, \sin 4\theta_i\right\} \quad (6.20)$$

where n is the number of layers in the laminate.

The LP distributions considered in this thesis were all given on a triangular finite element (FE) mesh. The volume of the entire structure could therefore be computed using:

$$V = \frac{1}{3} \sum_{i=1}^{n_e} A_{e_i} (t_{1_i} + t_{2_i} + t_{3_i}) \quad (6.21)$$

where n_e is the number of elements in the structure, A_{e_i} is the surface area of element i and t_{1_i}, t_{2_i} and t_{3_i} are the thickness values at the three nodes of element i.

6.3.3 Computation of streamlines

The smeared thickness distribution obtained for a given fibre angle distribution was then used to determine the fibre paths for the VS composite. Once the thickness distribution and the fibre angle distribution were known for a ply the streamlines for each layer could be computed using Eq. 6.10.

The exact functions for the thickness distribution and the fibre angle distribution within each layer were unknown. Therefore Eq. 6.10 was solved using numeric integration. The resulting fibre paths were then used to compute the discrete fibre courses for each layer of a VS composite laminate.

6.4 Demonstration

A square plate loaded in bi-axial compression, see Fig. 5.7, was used to demonstrate the implementation of the streamline approach (Blom et al. 2010) described in section 6.3. The optimal LP distribution for the square plate example was assumed to be known, and a fibre angle distribution for the plate was obtained in section 5.5.

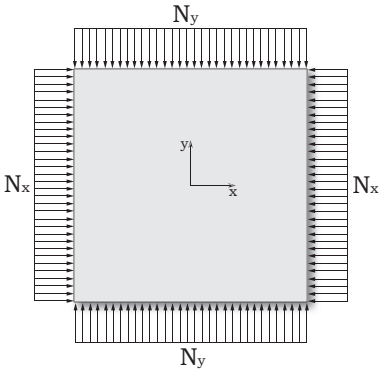

Figure 5.7: *Square plate loaded in biaxial compression.*

The fibre angle design obtained for the case of a 0.5×0.5m square panel of the balanced symmetric stacking sequence configuration $[\pm\theta_1/\pm\theta_2/\pm\theta_3/\pm\theta_4]_s$ and with a constraint on in-plane curvature of $\kappa_{\text{all}} = 4.878\text{m}^{-1}$ was used for the demonstration of the implementation of the streamline approach, see Fig. 6.5.

The estimate of the thickness distribution of each $+\theta$ and $-\theta$ layer in the laminate was computed individually, as were the fibre paths. The results that were obtained for the 0.5×0.5m square panel are plotted in Fig. 6.6. In this particular case, the thickness distributions and streamlines for the $+\theta$ and $-\theta$-layers are mirror images: the thickness distribution and streamlines can be mirrored about the horizontal or vertical centreline to arrive at the thickness distribution and streamlines of the conjugate $-\theta$-layer for a $+\theta - layer$. This symmetry is a direct result of the symmetry of the optimal LP distribution and the subsequent symmetry of the fibre angle distribution that was obtained.

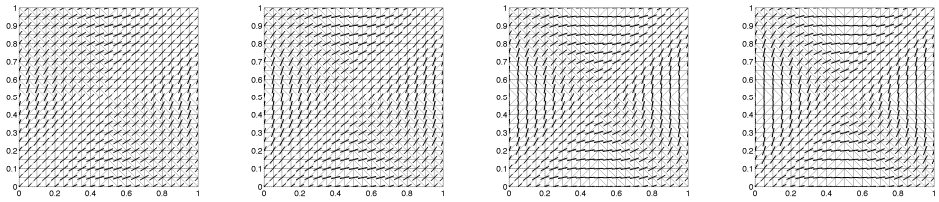

(a) θ_1 (b) θ_2 (c) θ_3 (d) θ_4

Figure 6.5: *Fibre angle distribution obtained for the square plate in biaxial compression of* $1.0 \times 1.0\text{m}$ *in dimension with an in-plane curvature constraint of* $\kappa_{all} = 4.878\text{m}^{-1}$.

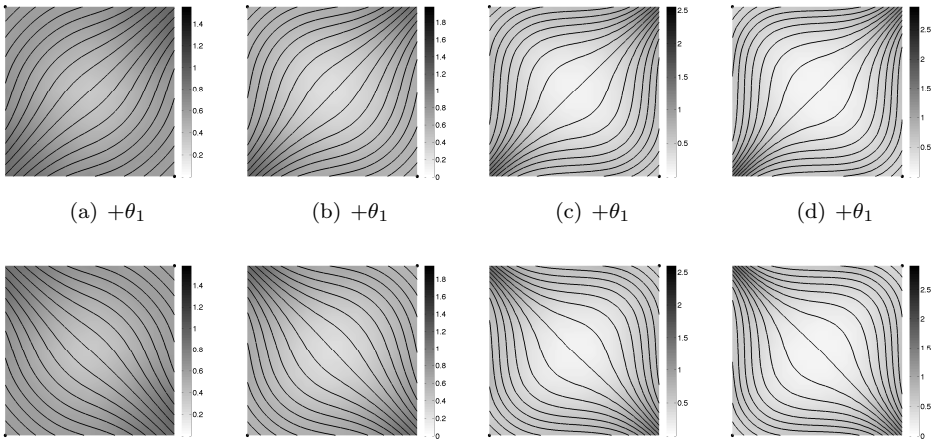

(a) $+\theta_1$ (b) $+\theta_1$ (c) $+\theta_1$ (d) $+\theta_1$

(e) $-\theta_1$ (f) $-\theta_1$ (g) $-\theta_1$ (h) $-\theta_1$

Figure 6.6: *Thickness build-up and streamlines. Thickness build-up is indicated by the shading.*

The thickness distribution and the streamlines that were obtained are smooth, and correspond well to the fibre angle distributions for which they were obtained. It was therefore concluded that is is possible to determine the thickness distribution and the streamlines for a nodal fibre angle distribution using the streamline analogy.

The volume of the obtained smeared thickness estimate was computed using Eq. 6.21, and found to be 6.1 times the volume of the case where no thickness variation due to fibre steering is considered. The increase in volume is a result of fibre paths overlapping; the fibre paths were obtained such that the smeared thickness in a ply nowhere was lower than 1.

The thickness distribution due to fibre steering of the laminate affected the buckling load of the plate. The LP distributions for the case where the thickness distribution was and was not included are plotted in Figs. 6.7 and 6.8. The distributions were very similar, it was mainly the centre of the panel that was affected. The buckling load of the panel for the case where the effect of thickness variation was included was 285 times the buckling load for the case where the thickness variation was not included. The increase was mainly attributed to the significant increase in weight.

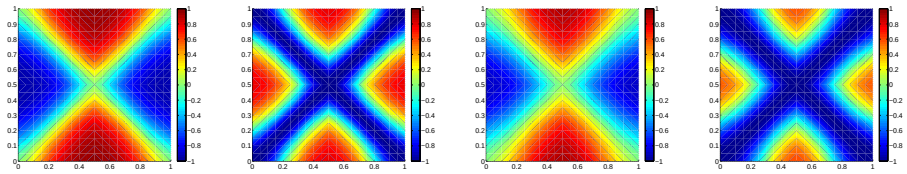

(a) $V_1^{\mathbf{A}}$ (b) $V_3^{\mathbf{A}}$ (c) $V_1^{\mathbf{D}}$ (d) $V_3^{\mathbf{D}}$

Figure 6.7: *LP distribution for the bi-axially loaded square plate without thickness build-up taken into account,* $\kappa_{all} = 4.878\text{m}^{-1}$ *and* $n = 4$.

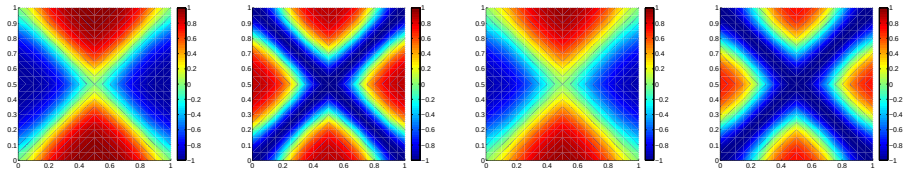

(a) $V_1^{\mathbf{A}}$ (b) $V_3^{\mathbf{A}}$ (c) $V_1^{\mathbf{D}}$ (d) $V_3^{\mathbf{D}}$

Figure 6.8: *LP distribution for the bi-axially loaded square plate with thickness build-up taken into account,* $\kappa_{all} = 4.878\text{m}^{-1}$ *and* $n = 4$.

The streamline analogy is applied to multiple example structures in chapter 7. Thickness build-up and the effect of the constraint on curvature thereon are

presented in section 7.3. Fibre angles and paths for three of the example structures are presented in section 7.4.

Facts are important, but
facts alone don't tell a story yet.
Jonathan Safran Foer

7

RESULTS VARIABLE STIFFNESS LAMINATE DESIGN

Note: Part of the results presented in this chapter have been previously published in Van Campen et al. (2011) and IJsselmuiden et al. (2011).

The work presented in this thesis forms part of a two-step design approach developed for the design of tailored variable stiffness composite laminates (Van Campen and IJsselmuiden 2011, IJsselmuiden et al. 2011). In the first step of this approach laminates are designed in terms of lamination parameters (LP), and in the second step the obtained LP design is converted into a fibre angle design for production.

The conversion of LPs to fibre angles was described and demonstrated in chapter 2. The application of the conversion process to a variable stiffness (VS) laminate design in terms of LPs and the implementation of a constraint on in-plane fibre curvature was described and demonstrated in chapter 5 using the example of a square plate loaded in-plane in bi-axial compressive for which the LP distribution, which maximises the buckling load, was assumed to be known. The estimation of thickness build-up in the laminate due to overlapping fibre paths and construction of fibre paths was discussed and demonstrated in chapter 6 using the same bi-axial plate example for which a fibre angle distribution was obtained in chapter 5.

Using the developed optimisation tools for the conversion process from LPs to a fibre angle design four exemplar structural components were studied. The results of these studies are presented in this chapter. The four components were:

- a square plate loaded in bi-axial compression
- a square plate loaded in uni-axial compression
- a curved plate with a hole loaded in compression and shear

- a wing rib loaded in shear

The optimised LP distributions for all the structures listed above were assumed to be known and given on a finite element (FE) mesh. The first three design cases were chosen to study how the constraint on in-plane fibre curvature affected the performance of the obtained fibre angle design. The structures were also used to study how the number of designed layers in the laminate affected the buckling performance of the plate, and how the constraint on in-plane fibre curvature affected the thickness build-up due to the overlapping fibre paths in the obtained fibre angle design. Additionally, the third design case served to demonstrate the developed tools performed given a more complicated three-dimensional FE mesh. The first two structural components were two-dimensional, and did not have any features like a hole, or a cut-out.

The last structural component to be studied was designed to be representative of a typical aircraft part which may be encountered in contemporary aircraft design. The component was used to demonstrate how the developed two-step design approach could be coupled with commercial FE software,[1] thereby validating the industrial applicability of the proposed two-step design process for VS composite structures.

This chapter is concluded with a discussion on the obtained results and the merits of the proposed approach for converting a VS composite design in terms of LPs into a VS composite design in terms of fibre angles, and eventually fibre paths.

7.1 Optimisation formulation

The LP distributions maximising the buckling loads of all the structures considered in this chapter were assumed to be known, and these optimum LP distributions were converted into a manufacturable fibre angle design to test the conversion process proposed in section 5.4, and subsequently to test the estimation of laminate thickness build-up due to fibre steering and the construction of fibre paths, described in chapter 6. The proposed conversion process and the objective functions used are briefly recapitulated in this section.

7.1.1 Proposed conversion from LP to fibre angle design

The optimum LP distributions for all structures under consideration were given at the nodes of an FE mesh. A genetic algorithm (GA) was used to explore the design space for each node of the FE mesh. The result of the GA was then refined

[1] The design case was established within the AUTOW project, part of the European Union Sixth Framework Programme, Project no. 030771.

using a gradient-based optimiser. Both the GA and the gradient-based optimiser minimised the least-square error in LP-space, Eq. 2.20, explained below.

Once an initial fibre angle design was obtained, constraints could be enforced on the obtained fibre angle distribution using a cellular automaton (CA) paradigm. The flow diagram of the proposed conversion process and CA paradigm is presented in Fig. 5.6, page 105. The CA could use two different objective functions which are described in what follows.

7.1.2 Design objective

The objective of all the problems described in this chapter was to maximise the buckling load for each of the respective example structure. The buckling load of the structures were obtained using a finite element (FE) routine programmed in MATLAB® (IJsselmuiden, Abdalla and Gürdal 2010*a*). This FE programme can also be used to obtain the design sensitivities of the buckling load of a structure with respect to the elements of the **A**- matrix and **D**-matrix at each node of the plate. Using these sensitivities the inverse of the buckling load λ of the plate could be estimated using (IJsselmuiden, Abdalla and Gürdal 2010*a*):

$$\frac{1}{\lambda} \cong \sum \psi_m : \mathbf{A} + \phi_b : \mathbf{D}^{-1} \tag{7.1}$$

where ψ_m and ϕ_b are matrices containing respectively the sensitivity data for the **A**-matrix and the inverse of the **D**-matrix.

Two different design objectives were used to study the proposed conversion process, shown in Fig. 5.6: the least square error in LP space and the approximation of the buckling load, Eq. 7.1. The LP-based objective function takes the form:

$$f = |\mathbf{V} - \mathbf{V}^*| \quad \text{with} \quad \mathbf{V} = \left\{V_1^{\mathbf{A}}, V_3^{\mathbf{A}}, V_1^{\mathbf{D}}, V_3^{\mathbf{D}}\right\} \tag{2.20}$$

where * denotes the given optimum lamination parameters. The minimisation of Eq. (7.1) for each point will maximize the buckling load of the panel:

$$f = \psi_m : \mathbf{A} + \phi_b : \mathbf{D}^{-1} \tag{7.2}$$

Note that the **A**- and **D**-matrix are linear functions in terms of the LPs.

7.1.3 Curvature constraint

The constraint on curvature was applied using the CA presented in chapter 5, see Fig. 5.6. The CA was designed to use an augmented objective function of the form:

$$\Psi = \begin{cases} f + \varepsilon g_{\max} & \text{if} \quad g_{\max} \leq 0 \\ f + \beta g_{\max} & \text{if} \quad g_{\max} > 0 \end{cases} \tag{2.21}$$

where f is the design objective, $g_{\max}$ is the maximum constraint margin value and ε and β are a bonus term and a penalty term respectively. It was shown in section 5.3 how in-plane curvature of the fibre angle distribution can be estimated. A constraint margin in-plane fibre angle curvature would take the form:

$$g_\kappa = \frac{\kappa_{\max}}{\kappa_{\text{all}}} - 1 \tag{5.15}$$

where κ_{all} is the allowable in-plane curvature value. The constraint margin was designed such that it will take the value 0.1 for a 10% violation of the constraint and a value of -0.1 for a 10% margin for the imposed constraint.

7.2 Buckling load and constraint on in-plane curvature

Three of the four example structures discussed in this chapter were used to study the effects of in-plane fibre angle curvature constraints on the buckling load of the plate. The lay-up of the plate was considered to be $[\pm\theta_1/\ldots/\pm\theta_n]_s$, where n was varied parametrically from 1 to 4 whilst keeping the total thickness of the laminate constant. The structures under consideration were a square plate loaded in biaxial compression, a square plate loaded in uni-axial compression and a curved panel with a hole loaded in shear. The LP distributions that maximised the respective buckling loads of the three example structures were assumed to be known.

7.2.1 Problem definition

All three structures described in this section consisted of a 1.524mm-thick (0.06in.-thick) laminate, 0.1905mm (0.0075in) ply-thickness, based on the following material properties: $E_1 = 181$GPa (26.25Msi), $E_2 = 10.3$GPa (1.49Msi), $G_{12} = 7.17$GPa (1.04Msi) and $\nu_{12} = 0.28$. The LP designs that optimised the buckling performance of the plate were assumed to be known (IJsselmuiden, Abdalla and Gürdal 2010*a*).

Square plate under bi-axial compression

A square plate of 0.5m by 0.5m in dimension loaded in bi-axial compression was considered, see Fig. 5.7, page 108. This square plate example was used in section 5.5 to study how the constraint on in-plane fibre angle curvature affects on the buckling load of the plate for the lay-up $[\pm\theta_1/\ldots/\pm\theta_n]_s$ with $n = 4$. The buckling load of the optimal LP design of the square plate loaded in bi-axial

compression was 52% higher than that of the baseline constant stiffness (CS) design, $[\pm 45_n]_s$. The optimal LP distribution for the bi-axially loaded square plate is plotted in Fig. 7.1.

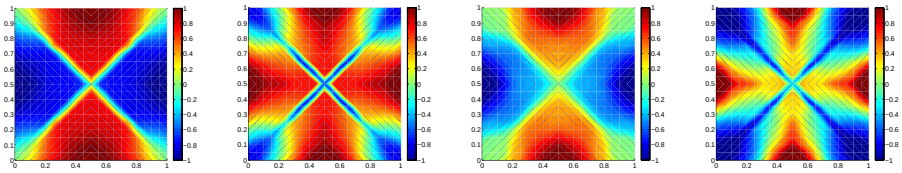

(a) $V_1^{\mathbf{A}}$ (b) $V_3^{\mathbf{A}}$ (c) $V_1^{\mathbf{D}}$ (d) $V_3^{\mathbf{D}}$

Figure 7.1: *Optimal LP distribution for the square plate loaded in bi-axial compression*

Square plate under uni-axial compression

A square plate of 1m × 1m loaded in uni-axial compression was considered, see Fig. 4.7, page 87. The example of the uni-axially loaded square plate was used in section 4.3 to study the design of a VS composite laminate using laminate blending to achieve a VS lay-up design. The buckling load of the optimum LP design of the square plate loaded in uni-axial compression, see Fig. 7.2, was 174% higher than that of the baseline CS design, $[\pm 45_n]_s$.

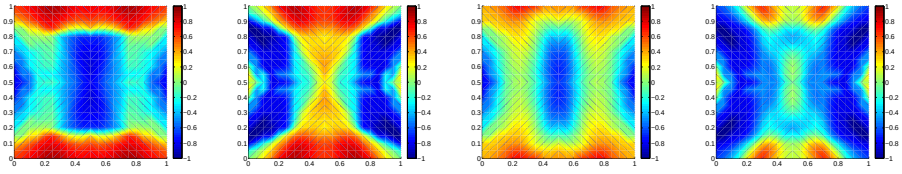

(a) $V_1^{\mathbf{A}}$ (b) $V_3^{\mathbf{A}}$ (c) $V_1^{\mathbf{D}}$ (d) $V_3^{\mathbf{D}}$

Figure 7.2: *Optimal LP distribution for the square plate loaded in uni-axial compression*

Curved panel with a hole under compression and shear

A panel curved out of plane containing a hole was considered to demonstrate the proposed conversion process from an LP distribution to a VS fibre angle design for a three-dimensional structure without a very regular mesh. The straight edges of the panel were simply supported, the curved edges were clamped, and the panel was loaded in compression and shear, see Fig. 7.3.

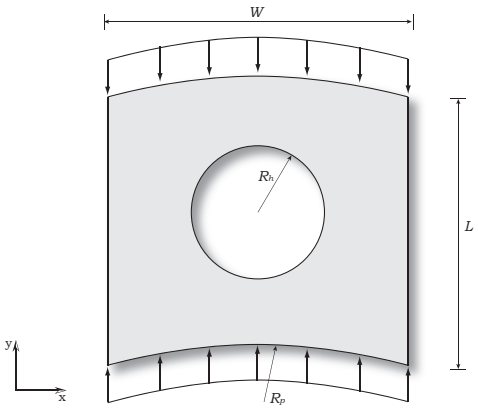

Figure 7.3: *Curved panel with a hole loaded in shear,* $L = W = 500\text{mm}$*,* $R_p = 750\text{mm}$ *and* $R_h = 120\text{mm}$

The buckling load of the LP optimum of the curved panel with a hole loaded in shear was 97% higher than that of the baseline CS design, $[\pm 45_n]_s$. The optimum LP distribution for the curved panel with a hole is plotted in Fig. 7.4.

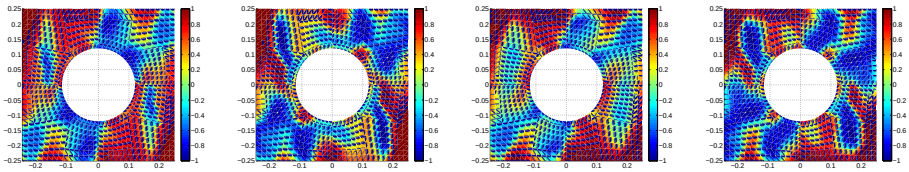

(a) $V_1^{\mathbf{A}}$ (b) $V_3^{\mathbf{A}}$ (c) $V_1^{\mathbf{D}}$ (d) $V_3^{\mathbf{D}}$

Figure 7.4: *Optimal LP distribution for the curved panel with a hole loaded in shear*

7.2.2 Generated results

The results were obtained for a lay-up $[\pm\theta_1/\pm\theta_2/\ldots/\pm\theta_n]_s$ where n was varied parametrically from 1 to 4. Note that the thickness of the laminate was kept constant. Each design was initialised by locally minimising the LP-based objective, Eq. 2.20, for every FE node of the structure, following the procedure depicted in Fig. 5.6. The GA was set to a population size of 25 with an elite population of five individuals, a crossover rate of 100%, and a mutation rate of 5%. The elite individuals were passed on to a gradient based optimizer using the same objective function eq. 2.20 after the GA converged. The initial fibre angle designs, or

fibre angle seeds, obtained were then subjected to a constraint on in-plane fibre curvature using the CA. The constraint on in-plane curvature was varied from $\kappa_{\text{all}} = 1\text{m}^{-1}$ to the maximum in-plane curvature for the unconstrained fibre angle design. The algorithm was run until convergence, i.e. the change in objective function value, Eq. 2.21, dropped below 0.1% for five consecutive iterations, or until a maximum number of iterations was reached. Results were obtained using the error in LP space, Eq. 2.20, and the buckling load estimate of the panel, Eq. 7.2, as a design objective.

7.2.3 Results and discussion

The Pareto fronts, in terms of maximum in-plane fibre curvature and normalised buckling load and in terms of maximum in-plane curvature and objective function value, obtained are presented here for each structural component. The Pareto fronts obtained using the LP-based (Eq. 2.20) and sensitivity-based (Eq. 7.2) objective functions are compared for each structure to determine whether the computationally less demanding LP-based objective function, Eq. 2.20, could be allowed to replace the sensitivity-based objective function.

Square plate under bi-axial compression

The normalised buckling load as a function of the constraint on curvature is plotted for the bi-axially loaded plate for both objective functions in Fig. 7.5. The trends obtained were nearly identical. The normalised buckling load increases as a function of the constraint on curvature, levelling off at a maximum value.

The maximum value for the case of one designed layer in the laminate, $n = 1$, i.e. $[\pm\theta]_s$, is significantly lower than that for the other n-values considered; from $n = 2$ onwards the effect of increasing the number of layers in the laminate on the maximum buckling load value is minor. The buckling load values obtained for a constraint on in-plane fibre curvature smaller than 3m^{-1} were not affected by the number of layers in the laminate.

The buckling load value obtained for the case where $n = 1$ was higher than that of the other cases when the curvature constraint was smaller than 2m^{-1} for the LP-based objective and smaller than 3m^{-1} for the sensitivity-based objective. A possible explanation would be, that each fibre angle design is initialised by a VS fibre angle seed. The fibre angle distribution of the fibre angle seed may vary strongly from layer to layer, as will be discussed in section 7.4. Such strong variation will make it harder for the CA to converge to a design where all fibre angle distributions throughout the thickness of the lay-up are nearly similar. The mechanism behind the observed behaviour might be that the load redistribution

required for a maximum buckling load are different for a small value of the constraint on curvature than for a large constrain value, this is a subject for further investigation.

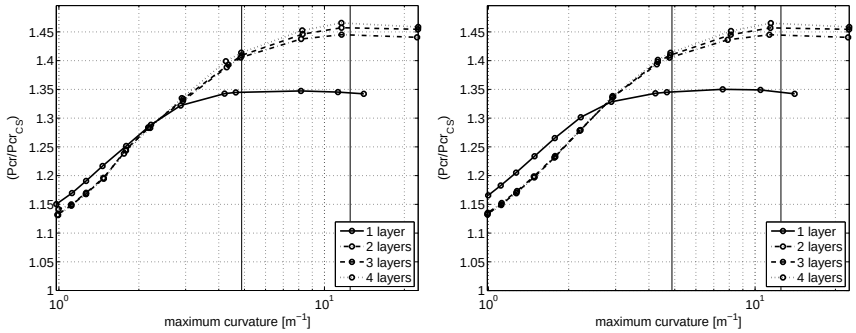

(a) Distance-based objective, Eq. 2.20 (b) Sensitivity-based objective, Eq. 7.1

Figure 7.5: *Pareto front of the example of a square plate under bi-axial compression for 1 to 4 designed layers in the laminate, buckling load normalised using the buckling load value of the best constant stiffness design. The vertical lines indicate* $\kappa = 4.878\text{m}^{-1}$ *and* $\kappa = 12.5\text{m}^{-1}$.

The average error in LP-space as a function of the constraint on curvature is plotted for the bi-axially loaded plate for both objective functions in Fig. 7.6. In contrast to the Pareto fronts for the normalised buckling load value, the trends that were obtained for both objectives are very different. The average error in LP-space is smaller for the LP-based objective than for the sensitivity-based objective. The error showed an increasing trend for larger curvature values for the sensitivity-based objective. Despite the differences in average LP-error, the fibre angle designs, see section 7.4, and the buckling performance of the structure were very similar. It was therefore concluded that, for the example of the plate loaded in bi-axial compression, the LP-based objective function can be used as a replacement for the sensitivity-based objective function.

Square plate under uni-axial compression

The normalised buckling load as function of the constraint on curvature is plotted for the uni-axially loaded plate for both objective functions in Fig. 7.7. Similarly to the bi-axially loaded plate, the trends that were obtained for both objective functions were nearly identical. All trends except that for $n = 1$ showed a monotonically increasing trend as a function of the constraint on in-plane curvature until the maximum buckling load value for the unconstrained case was reached.

Increasing the number of layers in the laminate had a significant effect on the buckling load value that was obtained, for n larger than 2 including more layers

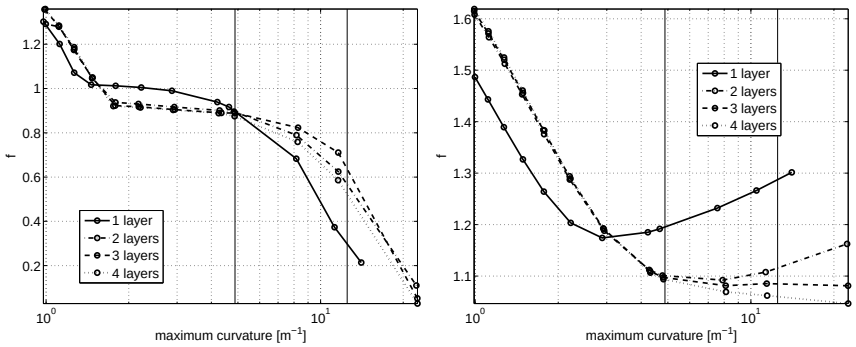

(a) Distance-based objective, Eq. 2.20 (b) Sensitivity-based objective, Eq. 7.1

Figure 7.6: *Pareto front of the example of a square plate under bi-axial compression for 1 to 4 designed layers in the laminate, average distance in LP-space f (dimensionless) per node. The vertical lines indicate $\kappa = 4.878\text{m}^{-1}$ and $\kappa = 12.5\text{m}^{-1}$.*

in the laminate positively effected the buckling load of the square plate for the entire range of curvature constraint values considered. The effect was slightly more pronounced for larger values of the curvature constraint.

The buckling load values for the case where $n = 1$ were higher than those for the other values considered up to $\kappa_{\text{all}} \approx 6\text{m}^{-1}$. The maximum buckling load for $n = 1$ was also not reached for the case where the in-plane curvature of the fibre angle distribution was not constrained. This also points to the hypothesis that the CA, depending on the fibre angle seed used, may converge to a local optimum.

The Pareto fronts for the average error are plotted in Fig. 7.8. The difference in the obtained trends is large, as was the case for the bi-axially loaded plate. The average error for the LP-based objective was also clearly lower than for the sensitivity-based objective, and increasing trends for the average error as a function of the constraint on in-plane curvature were observed for larger constraint values. The differences in the fibre angle designs, see section 7.4, and the buckling performance of the structure were minor, and it was concluded that, for the example of the plate loaded in uni-axial compression, the LP-based objective function could be used as replacement for the sensitivity-based objective function, as the buckling load of the results obtained with either objective are similar in value.

Curved panel with a hole under compression and shear

The Pareto fronts obtained for the normalised buckling load of the curved panel with a hole loaded in shear and compression for the LP-based and sensitivity-based objective functions are plotted in Fig. 7.9; the trends obtained are nearly

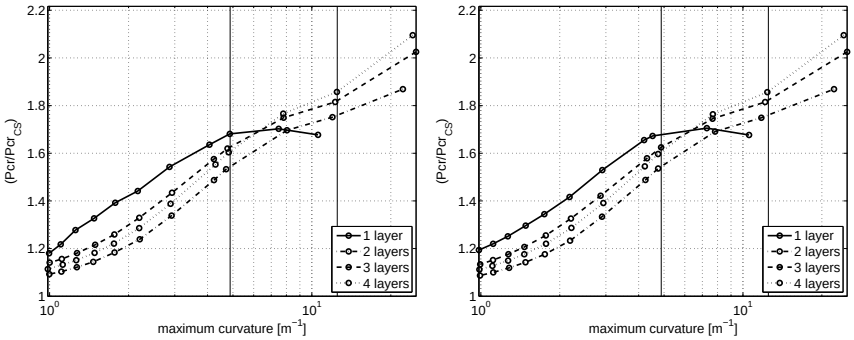

(a) Distance-based objective, Eq. 2.20 (b) Sensitivity-based objective, Eq. 7.1

Figure 7.7: *Pareto front of the example of a square plate under uni-axial compression for 1 to 4 designed layers in the laminate, buckling load normalised using the buckling load value of the best constant stiffness design. The vertical lines indicate* $\kappa = 4.878\mathrm{m}^{-1}$ *and* $\kappa = 12.5\mathrm{m}^{-1}$.

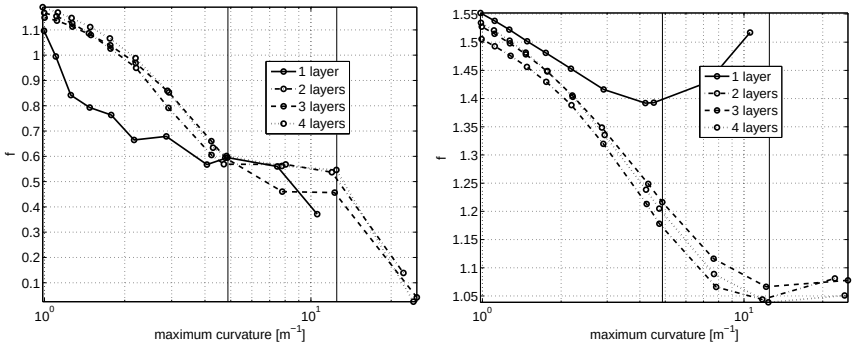

(a) Distance-based objective, Eq. 2.20 (b) Sensitivity-based objective, Eq. 7.1

Figure 7.8: *Pareto front of the example of a square plate under uni-axial compression for 1 to 4 designed layers in the laminate, average distance f (dimensionless) in LP-space per node. The vertical lines indicate* $\kappa = 4.878\mathrm{m}^{-1}$ *and* $\kappa = 12.5\mathrm{m}^{-1}$.

identical. The normalised buckling load of the panel increases monotonically as function of the constraint on in-plane curvature.

The obtained value for the buckling load was nearly insensitive to the number of layers in the laminate n up to $\kappa_{\text{all}} \approx 6\text{m}^{-1}$, from which point onward the buckling loads for $n = 1$ were clearly lower than those for the other n-values considered.

The buckling load values for the case where $n = 1$ and the constraint on in-plane curvature were slightly higher than the buckling load values obtained for the other n-values, but the difference is negligible compared to the differences found for the examples of the plate loaded in bi-axial and uni-axial compression. It was therefore concluded that the difference in performance for $n = 1$ and the other values of n depends on the mechanics of the problem under consideration.

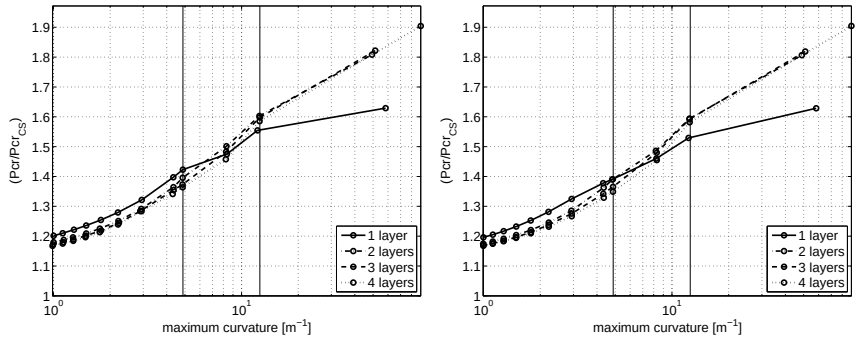

(a) Distance-based objective, Eq. 2.20 (b) Sensitivity-based objective, Eq. 7.1

Figure 7.9: *Pareto front of the example of a curved panel loaded in compression and shear for 1 to 4 designed layers in the laminate, buckling load normalised using the buckling load value of the best constant stiffness design. The vertical lines indicate* $\kappa = 4.878\text{m}^{-1}$ *and* $\kappa = 12.5\text{m}^{-1}$.

The Pareto fronts for the average error in LP-space as function of the constraint on in-plane curvature are plotted in Fig. 7.10 for the curved panel example. The trends and the range of the average error are different for the two objectives, as was found for the examples of the plate loaded in bi-axial and uni-axial compression. Based on the fibre angle distributions obtained and the trends obtained for the normalised buckling load, it was concluded that, for the example of a curved panel with a hole loaded in compression and shear, the LP-based objective function can be used as replacement for the sensitivity-based objective function.

Discussion

The trends that were obtained for the normalised buckling load value as a function of a constraint on in-plane curvature were nearly identical for both objective

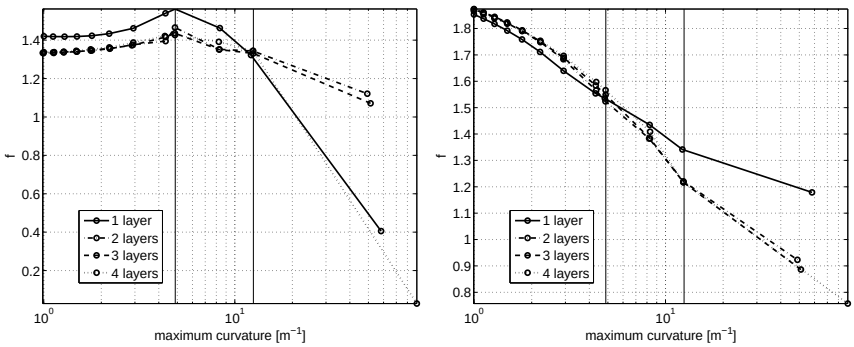

(a) Distance-based objective, Eq. 2.20 (b) Sensitivity-based objective, Eq. 7.1

Figure 7.10: *Pareto front of the example of a curved panel loaded in compression and shear for 1 to 4 designed layers in the laminate, average distance f (dimensionless) in LP-space per node. The vertical lines indicate* $\kappa = 4.878\text{m}^{-1}$ *and* $\kappa = 12.5\text{m}^{-1}$.

functions for all the three example structures considered in this section. The observed trends were also consistent between the three example structures considered. The differences between the obtained trends for the three structures can be explained by the difference in mechanical response of the respective structures, and the observed trends are expected to be found for a broad range of VS composite structures designed in terms of LPs.

The proposed conversion method could not be guaranteed to converge to the global optimum for every constraint on in-plane curvature. Therefore, it was suggested that the CA should be seeded with several fibre angle distributions. For example: if a balanced symmetric laminate of the form $[\pm\theta_1/\ldots/\pm\theta_n]_s$ was to be designed for $n = 6$, the CA could be initialised with fibre angle seeds of the form $[(\pm\theta_1)_6]_s$, $[(\pm\theta_1/\pm\theta_2)_3]_s$ and $[(\pm\theta_1/\pm\theta_2/\pm\theta_3]_s$ next to the seed $[\pm\theta_1/\pm\theta_2/\pm\theta_3/\pm\theta_4/\pm\theta_5/\pm\theta_6]_s$.

7.3 THICKNESS BUILD-UP AND CONSTRAINT ON IN-PLANE CURVATURE

The estimation of thickness build up in a laminate due to overlapping fibre paths was described in chapter 6. Here the thickness build-up in the laminate as function of the constraint on in-plane curvature of the fibre angle distribution is considered.

7.3.1 Problem definition

Thickness build-up in a VS laminate occurs due to overlapping fibre paths. It was expected that the amount and the size of overlaps[2] will increase for larger in-plane curvatures of the fibre distribution, leading to a larger variation in ply thickness and a larger maximum thickness in the ply.

The same three example problems used to study buckling load as a function of the constraint on in-plane curvature, a plate loaded in bi-axial compression, a plate loaded in uni-axial compression and a curved panel with a hole loaded in compression and shear, were used to study the effect of the constraint on in-plane curvature on the maximum thickness of the laminate and the volume of the laminate. The effect the variation in thickness had on the buckling load of the structures was also studied.

7.3.2 Results and discussion

The thickness distribution for the results generated in section 7.2.2 was determined using the method described in chapter 6. The maximum thickness of the estimated thickness distributions was determined for each design. Likewise, the volume of the thickness estimates was computed using Eq. 6.21:

$$V = \frac{1}{3}\sum_{i=1}^{n_e} A_{e_i}(t_{1_i} + t_{2_i} + t_{3_i}) \tag{6.21}$$

where n_e is the number of elements in the structure, A_{e_i} is the surface area of element i and t_{1_i}, t_{2_i} and t_{3_i} are the thickness values at the three nodes of element i, and the buckling load was evaluated accounting for the effect of the variation in thickness. The trends that were obtained are discussed below, only the results for the LP-based objective are presented.

Square plate under bi-axial compression

The normalised maximum thickness in the laminate as a function of the constraint on in-plane curvature obtained for the example of a square plate loaded in b-axial compression is plotted in Fig. 7.16. The maximum thickness of the laminate was the largest for $n = 1$ and this decreased as the number of layers in the laminate increased. The maximum thickness in the laminate occurs for the case where the in-plane curvature is not constrained, as expected.

The normalised volume of the laminate increases as function of the constraint on in-plane curvature, as depicted in Fig. 7.12. This is because all tows were

[2]Here amount refers to the total number of individual instances that fibre paths overlap, size refers to the fraction of a fibre path overlapping an other fibre path.

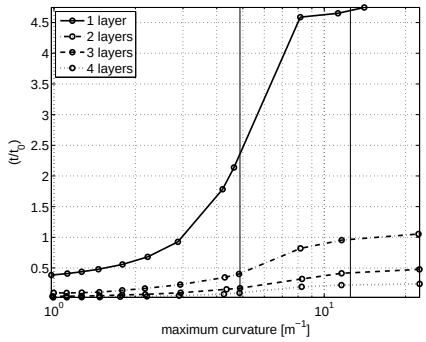

Figure 7.11: *Pareto front for 1 to 4 designed layers in the laminate, normalised maximum thickness build-up. The vertical lines indicate* $\kappa = 4.878\text{m}^{-1}$ *and* $\kappa = 12.5\text{m}^{-1}$.

assumed to fully overlap, resulting in a minimum ply thickness of 1. Constructing meaningful fibre path designs became increasingly difficult for larger values of the curvature constraint, see section 7.4, and eventually broke down for the unconstrained design, which explains the reduction in volume for $n = 1$ and $n = 4$ near the unconstrained case.

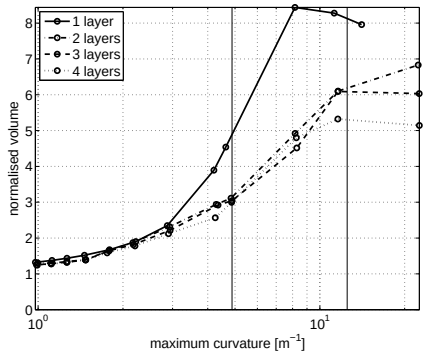

Figure 7.12: *Pareto front for 1 to 4 designed layers in the laminate, normalised volume. The vertical lines indicate* $\kappa = 4.878\text{m}^{-1}$ *and* $\kappa = 12.5\text{m}^{-1}$.

The varying thickness per layer has its effect on the LP distribution. The LPs for the structure when the affect of thickness variation is included can be computed using Eq. 6.18 and Eq. 6.20: The LP distributions for the cases with and without the thickness effect are plotted in Figs. 7.13 and 7.14, respectively, for the case where $\kappa_{\text{all}} = 12.5\text{m}^{-1}$ and $n = 4$. The distributions were similar, it was mainly the centre of the panel that was affected.

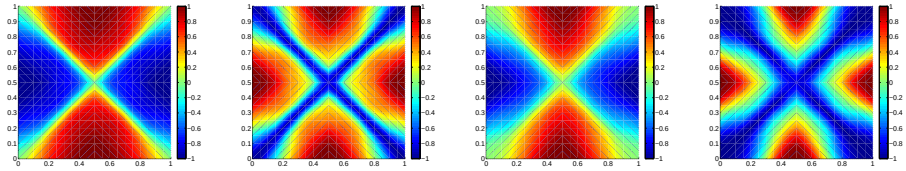

(a) $V_1^{\mathbf{A}}$ (b) $V_3^{\mathbf{A}}$ (c) $V_1^{\mathbf{D}}$ (d) $V_3^{\mathbf{D}}$

Figure 7.13: *LP distribution for the bi-axially loaded square plate without thickness build-up taken into account,* $\kappa_{all} = 12.5\text{m}^{-1}$ *and* $n = 4$.

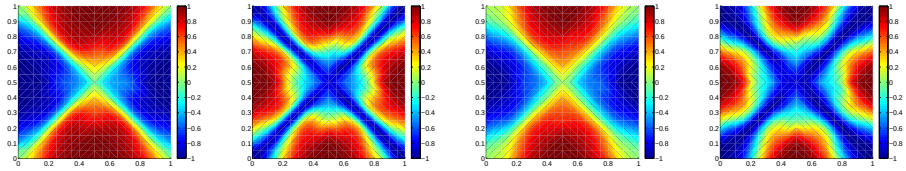

(a) $V_1^{\mathbf{A}}$ (b) $V_3^{\mathbf{A}}$ (c) $V_1^{\mathbf{D}}$ (d) $V_3^{\mathbf{D}}$

Figure 7.14: *LP distribution for the bi-axially loaded square plate with thickness build-up taken into account,* $\kappa_{all} = 12.5\text{m}^{-1}$ *and* $n = 4$.

The effect the thickness distribution and the resulting change in LP distribution had on the buckling load of the panel is plotted in Fig. 7.15. The buckling load, P_{cr}, was normalised using the buckling load obtained without assuming thickness build-up, P_{cr}^{CT}. The buckling load was positively affected by the thickness build-up in the laminate, except for the cases where the generation of fibre paths broke down. It was concluded that thickness build-up due to overlapping fibre paths positively affects the buckling load of the plate, at the cost of a (substantial) increase in weight. It was noted that the thickness build-up in the laminate was found to be most severe for $n = 1$. As the number of layers in the laminate was increased, the maximum thickness build-up dropped. The same trend was followed by the normalised volume and buckling load, but not as noticeable.

Square plate under uni-axial compression

The maximum thickness in the laminate and the volume of the laminate as function of the constraint on in-plane curvature are plotted in Figs. 7.16 and 7.17 for the example of a square plate loaded in uni-axial compression. The maximum thickness in the laminate and the volume of the laminate monotonically increased as a function of the curvature constraint for all values of n. These trends are similar to the trends found for the example of a square plate loaded in bi-axial compression.

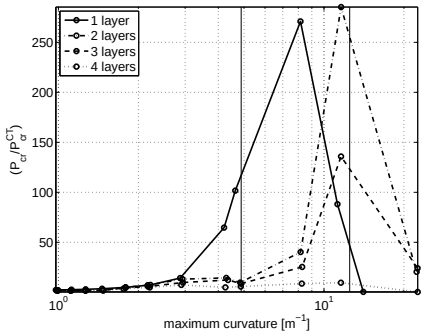

Figure 7.15: *Pareto front for 1 to 4 designed layers in the laminate, buckling load when thickness build-up was taken into account, normalised using the buckling load value of the best constant stiffness design. The vertical lines indicate* $\kappa = 4.878\mathrm{m}^{-1}$ *and* $\kappa = 12.5\mathrm{m}^{-1}$.

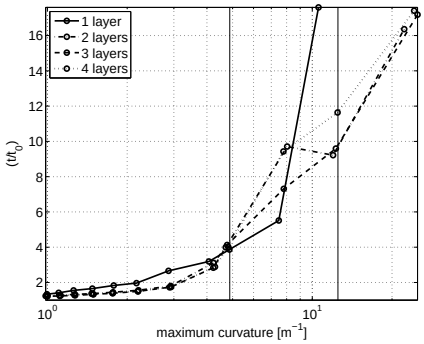

Figure 7.16: *Pareto front for 1 to 4 designed layers in the laminate, normalised maximum thickness build-up. The vertical lines indicate* $\kappa = 4.878\mathrm{m}^{-1}$ *and* $\kappa = 12.5\mathrm{m}^{-1}$.

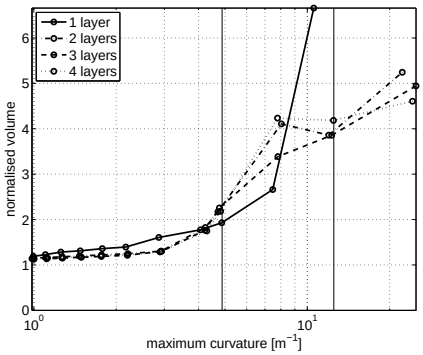

Figure 7.17: *Pareto front for 1 to 4 designed layers in the laminate, normalised volume. The vertical lines indicate* $\kappa = 4.878\text{m}^{-1}$ *and* $\kappa = 12.5\text{m}^{-1}$.

Laminate thickness build-up due to overlapping fibre paths reflects in the LP distribution of the plate when thickness variation is accounted for; the LP distribution without thickness effect is plotted in Fig. 7.18 and the LP distribution with thickness effect is plotted in Fig. 7.19 for the case where $\kappa_{\text{all}} = 12.5\text{m}^{-1}$ and $n = 4$; the LP distributions look similar.

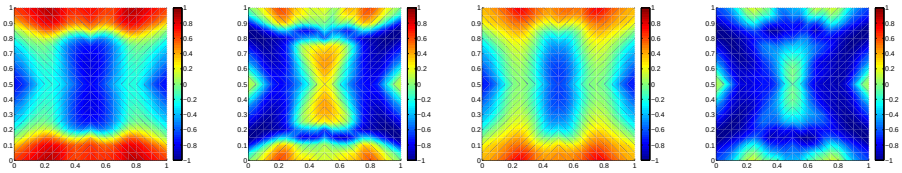

(a) $V_1^{\mathbf{A}}$ (b) $V_3^{\mathbf{A}}$ (c) $V_1^{\mathbf{D}}$ (d) $V_3^{\mathbf{D}}$

Figure 7.18: *LP distribution for the uni-axially loaded square plate without thickness build-up taken into account,* $\kappa_{all} = 12.5\text{m}^{-1}$ *and* $n = 4$.

The buckling load of the structure as function of the constraint on in-plane curvature with thickness build-up taken into account is plotted in Fig. 7.20, normalised using the constant stiffness buckling load, P_{cr}^{CT}. The buckling load values with thickness build-up taken into account are consistently higher than those without, the trend is monotonically increasing. It was concluded that for the square plate in uni-axial compression there is a positive effect of thickness build-up due to course overlaps on the buckling load of the plate.

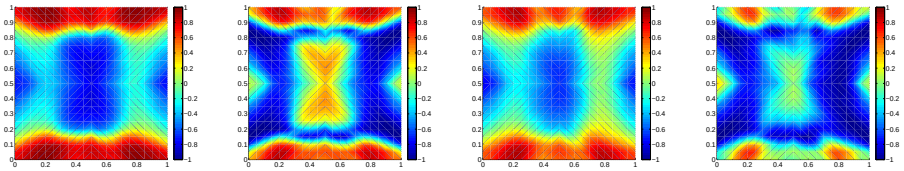

(a) $V_1^{\mathbf{A}}$ (b) $V_3^{\mathbf{A}}$ (c) $V_1^{\mathbf{D}}$ (d) $V_3^{\mathbf{D}}$

Figure 7.19: *LP distribution for the uni-axially loaded square plate with thickness build-up taken into account,* $\kappa_{all} = 12.5\text{m}^{-1}$ *and* $n = 4$.

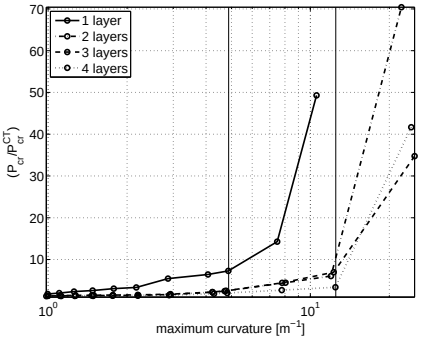

Figure 7.20: *Pareto front for 1 to 4 designed layers in the laminate, buckling load when thickness build-up was taken into account, normalised using the buckling load value of the best constant stiffness design. The vertical lines indicate* $\kappa = 4.878\text{m}^{-1}$ *and* $\kappa = 12.5\text{m}^{-1}$.

CURVED PANEL WITH A HOLE UNDER COMPRESSION AND SHEAR

The maximum thickness in the laminate and the volume of the laminate as a function of the constraint on in-plane curvature are plotted in Figs. 7.21 and 7.22 for the example problem of a curved panel with a hole loaded in compression and shear. The trend found for the maximum thickness in the laminate and the volume of the laminate monotonically increased as a function of the curvature constraint. These trends are similar to the trends found for the examples of a square plate loaded in bi-axial and uni-axial compression. The largest maximum thickness was found for the case where in-plane curvature was not constrained for $n = 1$, as was the maximum volume.

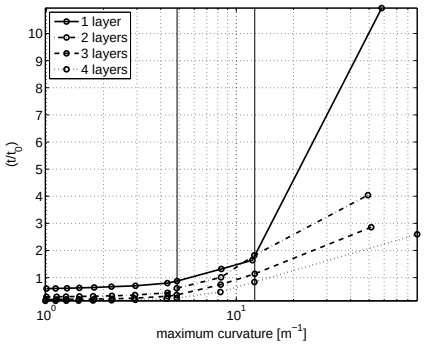

Figure 7.21: *Pareto front for 1 to 4 designed layers in the laminate, normalised maximum thickness build-up. The vertical lines indicate* $\kappa = 4.878\text{m}^{-1}$ *and* $\kappa = 12.5\text{m}^{-1}$.

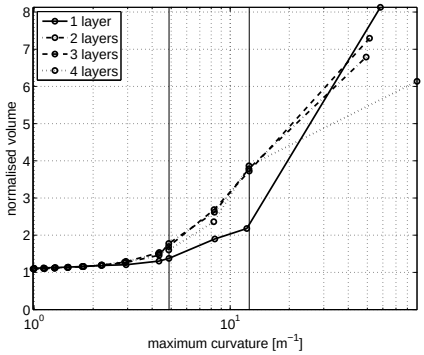

Figure 7.22: *Pareto front for 1 to 4 designed layers in the laminate, normalised volume. The vertical lines indicate* $\kappa = 4.878\text{m}^{-1}$ *and* $\kappa = 12.5\text{m}^{-1}$.

The increase in local thickness as function of the constrained on curvature affected the LP distribution for the case where the thickness build-up was taken into account. Again, upon visual inspection, similar LP distributions were found, Figs. 7.23 and 7.24, for the case where $\kappa_{\text{all}} = 12.5\text{m}^{-1}$ and $n = 4$.

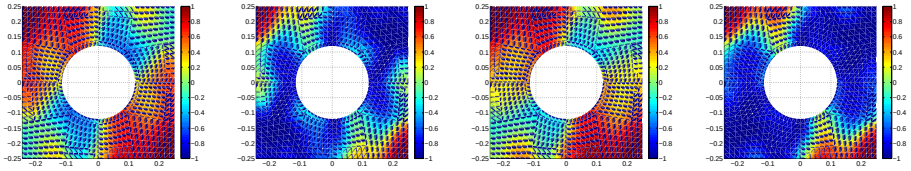

(a) $V_1^{\mathbf{A}}$ (b) $V_3^{\mathbf{A}}$ (c) $V_1^{\mathbf{D}}$ (d) $V_3^{\mathbf{D}}$

Figure 7.23: *LP distribution for the curved panel with a hole without thickness build-up taken into account,* $\kappa_{all} = 12.5\text{m}^{-1}$.

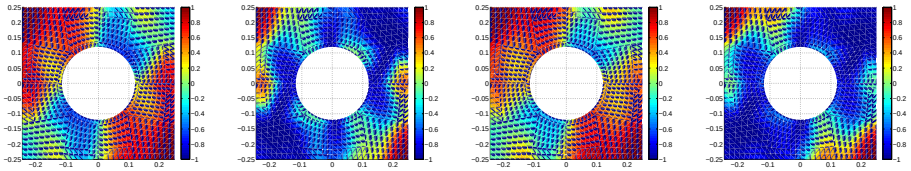

(a) $V_1^{\mathbf{A}}$ (b) $V_3^{\mathbf{A}}$ (c) $V_1^{\mathbf{D}}$ (d) $V_3^{\mathbf{D}}$

Figure 7.24: *LP distribution for the curved panel with a hole with thickness build-up taken into account,* $\kappa_{all} = 12.5\text{m}^{-1}$.

The buckling load for the case where thickness build-up was taken into account as function of the constraint on curvature is plotted in Fig.7.25. Up to $\kappa_{\text{all}} = 12.5\text{m}^{-1}$ the thickness variation was found to have a positive effect on the buckling load of the panel except for the unconstrained case for $n = 1$ and $n = 4$. It was concluded that thickness build-up in the laminate has a positive effect on the buckling load for the example of a curved panel with a hole loaded in compression and shear.

Discussion

The trends for maximum thickness in the laminate and volume of the laminate found were similar for the three example structures considered. All three structures showed an increase in the maximum thickness that occurs in the laminate as the constraint on curvature is relaxed.

All results showed a volume that was larger than that of the nominal constant stiffness structure, which was thought to be a direct effect of constraining the minimum thickness of each ply to 1.

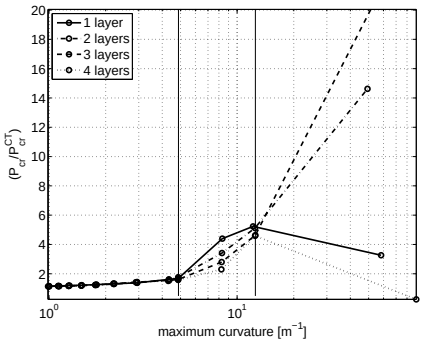

Figure 7.25: *Pareto front for 1 to 4 designed layers in the laminate, buckling load when thickness build-up was taken into account, normalised using the buckling load value of the best constant stiffness design. The vertical lines indicate* $\kappa = 4.878\text{m}^{-1}$ *and* $\kappa = 12.5\text{m}^{-1}$.

Improvements in buckling load were found for nearly all curvature constraint values. The cases where a deterioration, or a reduced improvement, of the buckling load were found, were limited to designs without a constraint on in-plane curvature for which, as a result, the fibre path generation and estimation of the smeared thickness in the laminate broke down. Overall it was concluded that thickness build-up due to overlapping fibre courses has a positive effect on the buckling load of a thin-walled variable stiffness composite structure at the expense of a (considerable) increase in structural weight.

Having more plies in the laminate was found to spread the thickness build-up more evenly throughout the structure, resulting in a lower maximum thickness of the laminate. The same effect was less noticeable for the normalised volume of the laminate.

7.4 Fibre angle design and fibre paths

A number of the fibre angle distributions, curvature distributions, smeared thickness distribution estimates and fibre path designs obtained for the trend studies presented in this chapter are plotted and discussed in this section. The particular cases considered are for the laminate $[\pm\theta_1/\pm\theta_2]_s$ designed for the allowable curvatures κ_{all} of 12.5m^{-1} and 4.878m^{-1}.

The fibre angle design, curvature distribution, thickness distribution and fibre paths are plotted for the example of the square plate in bi-axial compression for the LP-based and the sensitivity-based objectives. Only the results for the LP-based objective are plotted for the other two example structures. More results

are presented in appendix C for all three structures, the mentioned constraints on curvature and n ranging from 1 to 4.

7.4.1 Square plate under bi-axial compression

The fibre angle distribution, curvature distribution, thickness estimate and fibre paths for each layer in the laminate are plotted in Figs. 7.26 to 7.31 for the cases with $\kappa_{\text{all}} = 12.5\text{m}^{-1}$ and $\kappa_{\text{all}} = 4.878\text{m}^{-1}$, respectively, for both objective functions. Note that on visual inspection the distributions that were obtained for the LP-objective are nearly identical to the results obtained for the sensitivity-based objective, Figs. 7.26 and 7.27, Figs. 7.28 and 7.29, and Figs. 7.30 and 7.31.

The fibre angle distribution for the square plate under bi-axial compression is point symmetric about the centre of the plate for both layers for the unconstrained case and the two curvature constraint values considered. The maximum curvature value of the outer ply, θ_1, is lower than that of the inner ply, θ_2. This reflects the gradual variation of the flexural LPs of the optimum LP-distribution for this example, see Fig. 7.1, which are affected most by the outermost ply/plies in the laminate. The in-plane LP-distribution, which for the optimum LP-distribution for this example locally shows strong variation, see Fig. 7.1, is affected equally by all plies in the laminate. To satisfy both the requirements on in-plane and flexural LPs, the strong variations in the in-plane LPs manifest in the inner ply upon fibre angle retrieval.

The large in-plane curvature for the inner ply resulted in a breakdown of the fibre path creation and the thickness estimation for the case where no constraint on in-plane curvature was considered. Large part of the structure was not covered by a fibre path and one fibre path closed in on itself, see Figs. 7.26(g) and 7.26(h).

The thickness distribution estimates and fibre paths for $\kappa_{\text{all}} = 12.5\text{m}^{-1}$ and $\kappa_{\text{all}} = 4.878\text{m}^{-1}$ were overall smooth and appeared to be manufacturable, though part of the plate was still not covered by a tow path for $\kappa_{\text{all}} = 12.5\text{m}^{-1}$, resulting in a low value for the smeared ply thickness at the centre of the panel.

7.4.2 Square plate under uni-axial compression

The fibre angle distribution, curvature distribution, thickness estimate and fibre paths for each layer in the laminate are plotted in Figs. 7.32 to 7.34 for the where curvature was not constrained, the case where $\kappa_{\text{all}} = 12.5\text{m}^{-1}$ and $\kappa_{\text{all}} = 4.878\text{m}^{-1}$, respectively, for the LP-based objective function only.

The fibre angle distributions for all three cases, no constraint on curvature, $\kappa_{\text{all}} = 12.5\text{m}^{-1}$ and $\kappa_{\text{all}} = 4.878\text{m}^{-1}$ were found to be point symmetric. The in-plane

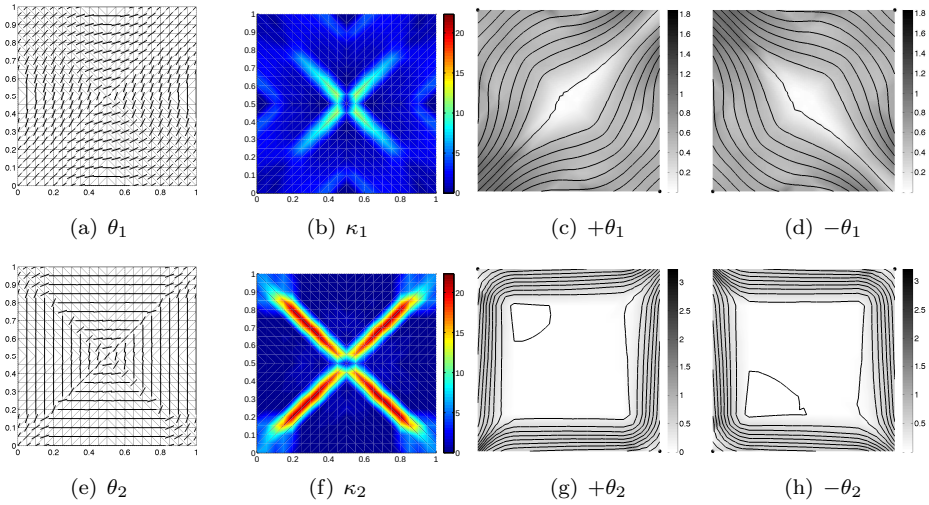

(a) θ_1 (b) κ_1 (c) $+\theta_1$ (d) $-\theta_1$

(e) θ_2 (f) κ_2 (g) $+\theta_2$ (h) $-\theta_2$

Figure 7.26: *Square plate in bi-axial compression: fibre angle distribution, curvature distribution, fibre paths and thickness distributions for $+\theta$ and $-\theta$, $n = 2$ no constraint on curvature, LP-based objective.*

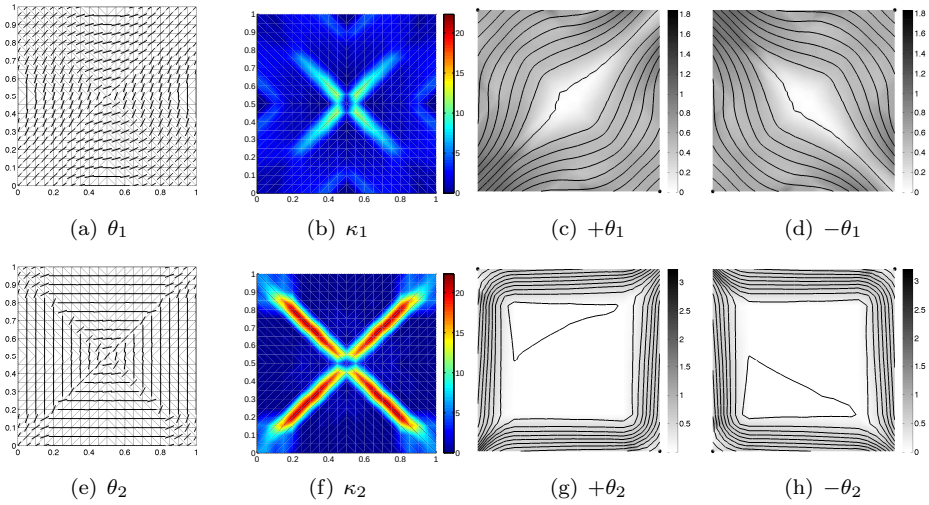

(a) θ_1 (b) κ_1 (c) $+\theta_1$ (d) $-\theta_1$

(e) θ_2 (f) κ_2 (g) $+\theta_2$ (h) $-\theta_2$

Figure 7.27: *Square plate in bi-axial compression: fibre angle distribution, curvature distribution, fibre paths and thickness distributions for $+\theta$ and $-\theta$, $n = 2$ no constraint on curvature, sensitivity-based objective.*

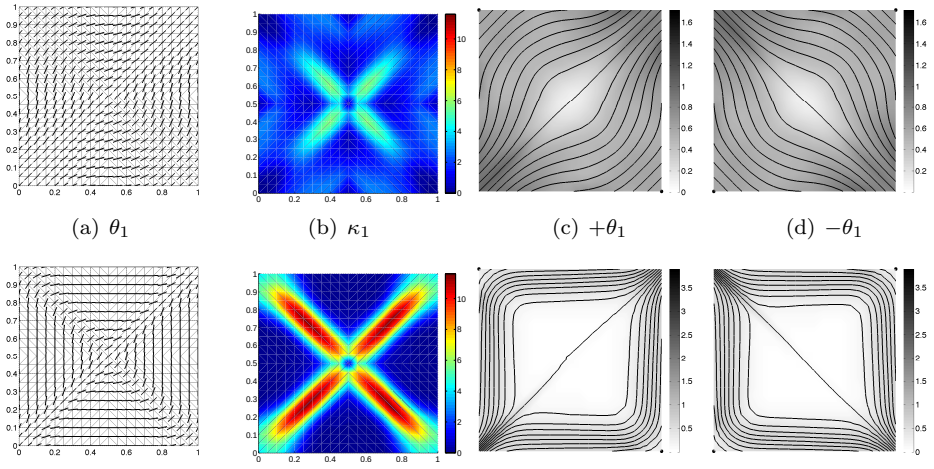

(a) θ_1 (b) κ_1 (c) $+\theta_1$ (d) $-\theta_1$

(e) θ_2 (f) κ_2 (g) $+\theta_2$ (h) $-\theta_2$

Figure 7.28: *Square plate in bi-axial compression: fibre angle distribution, curvature distribution, fibre paths and thickness distributions for* $+\theta$ *and* $-\theta$*,* $n = 1$*,* $\kappa_{all} = 12.5\text{m}^{-1}$*, LP-based objective.*

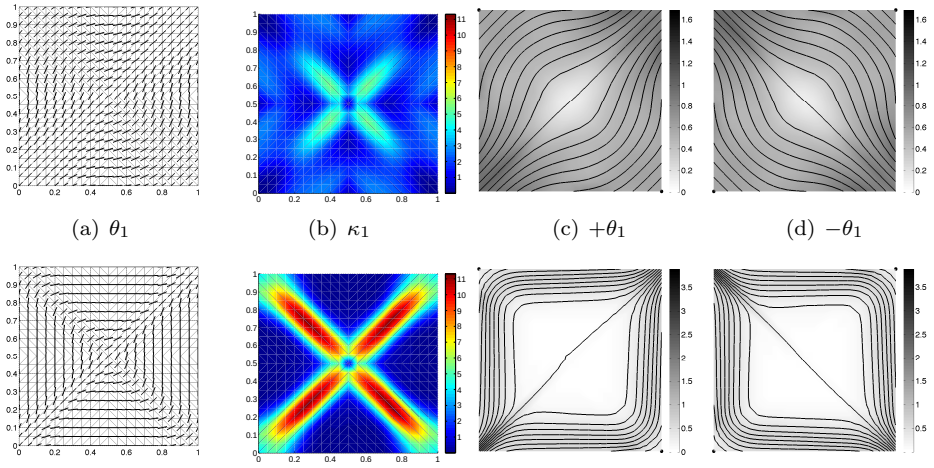

(a) θ_1 (b) κ_1 (c) $+\theta_1$ (d) $-\theta_1$

(e) θ_2 (f) κ_2 (g) $+\theta_2$ (h) $-\theta_2$

Figure 7.29: *Square plate in bi-axial compression: fibre angle distribution, curvature distribution, fibre paths and thickness distributions for* $+\theta$ *and* $-\theta$*,* $n = 1$*,* $\kappa_{all} = 12.5\text{m}^{-1}$*, sensitivity-based objective.*

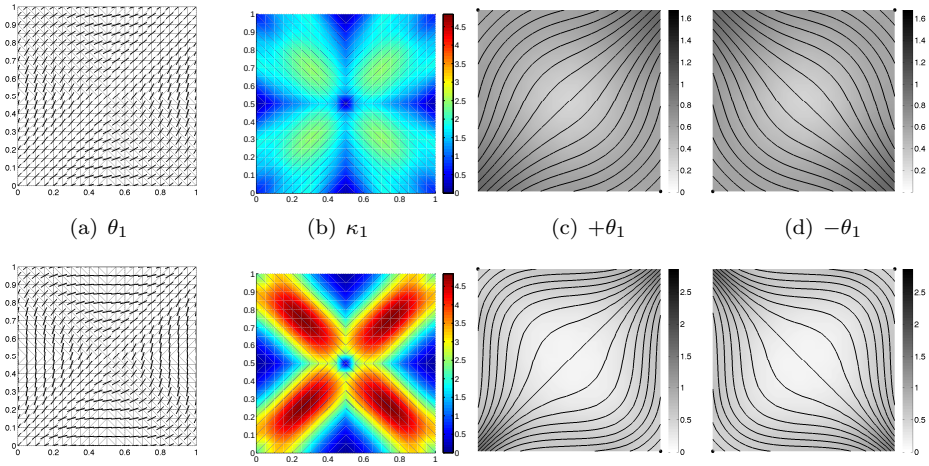

(a) θ_1 (b) κ_1 (c) $+\theta_1$ (d) $-\theta_1$

(e) θ_2 (f) κ_2 (g) $+\theta_2$ (h) $-\theta_2$

Figure 7.30: *Square plate in bi-axial compression: fibre angle distribution, curvature distribution, fibre paths and thickness distributions for $+\theta$ and $-\theta$, $n = 1$, $\kappa_{all} = 4.878\text{m}^{-1}$, LP-based objective.*

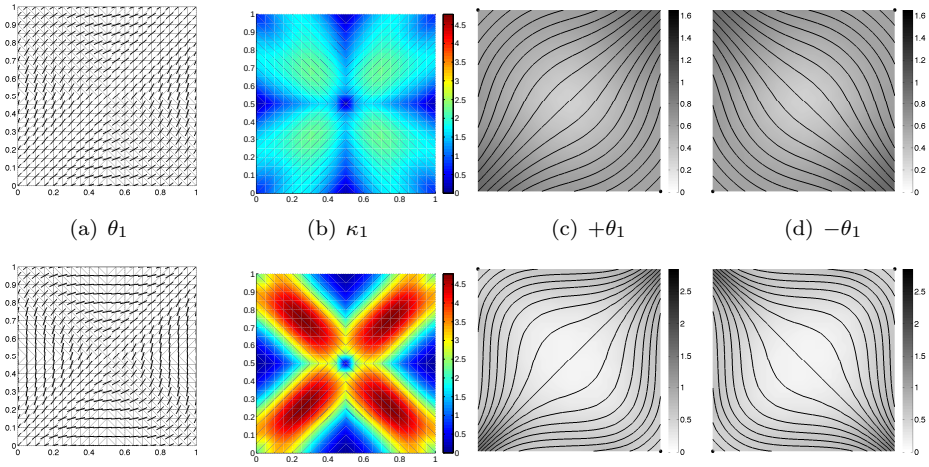

(a) θ_1 (b) κ_1 (c) $+\theta_1$ (d) $-\theta_1$

(e) θ_2 (f) κ_2 (g) $+\theta_2$ (h) $-\theta_2$

Figure 7.31: *Square plate in bi-axial compression: fibre angle distribution, curvature distribution, fibre paths and thickness distributions for $+\theta$ and $-\theta$, $n = 1$, $\kappa_{all} = 4.878\text{m}^{-1}$, sensitivity-based objective.*

fibre curvature was found to be more pronounced for the inner ply, as was the case for the example of a plate under bi-axial compression. The maximum gradient for the optimum LP distribution was also found to be larger for the in-plane LPs than for the out-of-plane LPs, see Fig. 7.2, which confirms the conclusion that a relatively stronger variation in the in-plane LPs compared to the flexural LPs will manifest in the form of higher in-plane curvature for the more inward plies of the laminate.

The fibre paths for the case where no constraint on curvature was enforced, see Fig. 7.32 were considered to be unrealistic, leaving large parts of the plate uncovered by fibre paths. The fibre paths and smeared thickness estimates for $\kappa_{\text{all}} = 12.5\text{m}^{-1}$ and $\kappa_{\text{all}} = 4.878\text{m}^{-1}$ appeared to be manufacturable. Note, that the fibre paths that were obtained were no longer anti-symmetric with respect to the vertical centreline of the plate due to the boundary conditions used for fibre path construction, see chapter 6.

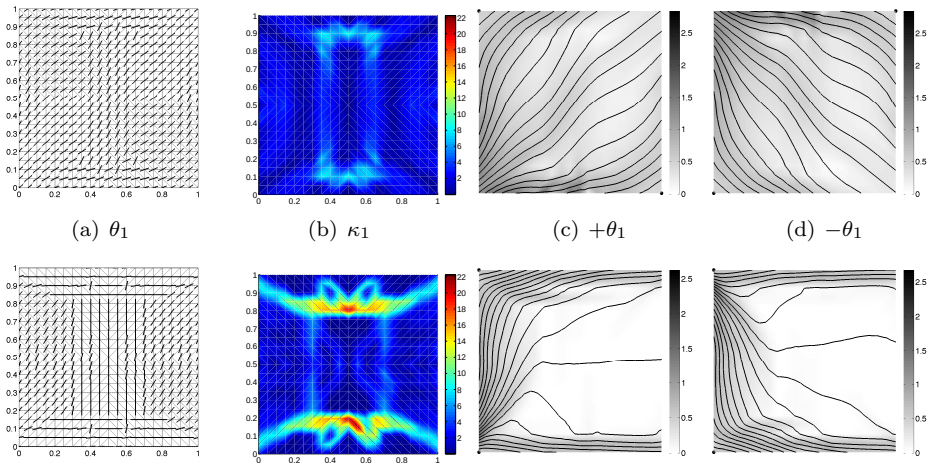

(a) θ_1 (b) κ_1 (c) $+\theta_1$ (d) $-\theta_1$

(e) θ_2 (f) κ_2 (g) $+\theta_2$ (h) $-\theta_2$

Figure 7.32: *Square plate in uni-axial compression: fibre angle distribution, curvature distribution, fibre paths and thickness distributions for $+\theta$ and $-\theta$, $n = 2$ no constraint on curvature.*

7.4.3 Curved panel with a hole under compression and shear

The fibre angle distribution, curvature distribution, thickness estimate and fibre paths for each layer in the laminate are plotted in Figs. 7.35 to 7.37 for the unconstrained case, and the cases of $\kappa_{\text{all}} = 12.5\text{m}^{-1}$ and $\kappa_{\text{all}} = 4.878\text{m}^{-1}$, respectively,

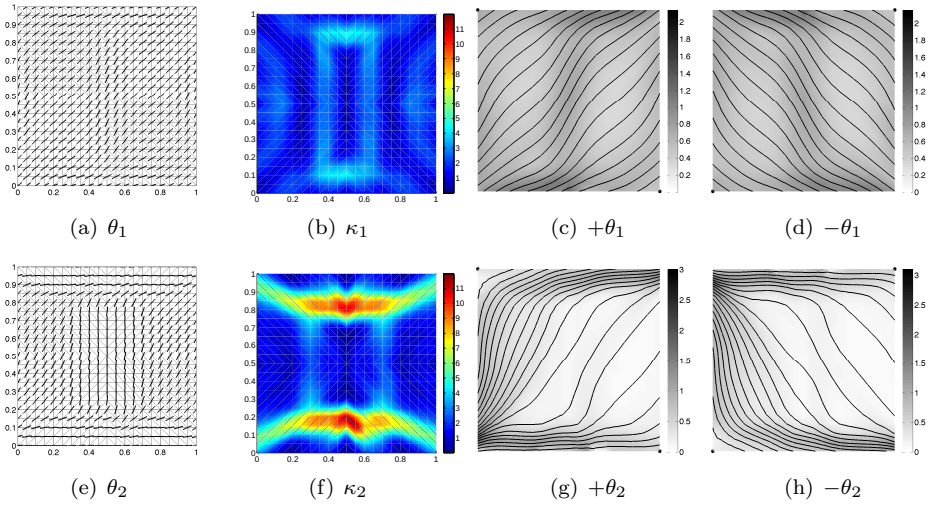

(a) θ_1 (b) κ_1 (c) $+\theta_1$ (d) $-\theta_1$

(e) θ_2 (f) κ_2 (g) $+\theta_2$ (h) $-\theta_2$

Figure 7.33: *Square plate in uni-axial compression: fibre angle distribution, curvature distribution, fibre paths and thickness distributions for $+\theta$ and $-\theta$, $n = 1$, $\kappa_{all} = 12.5\text{m}^{-1}$.*

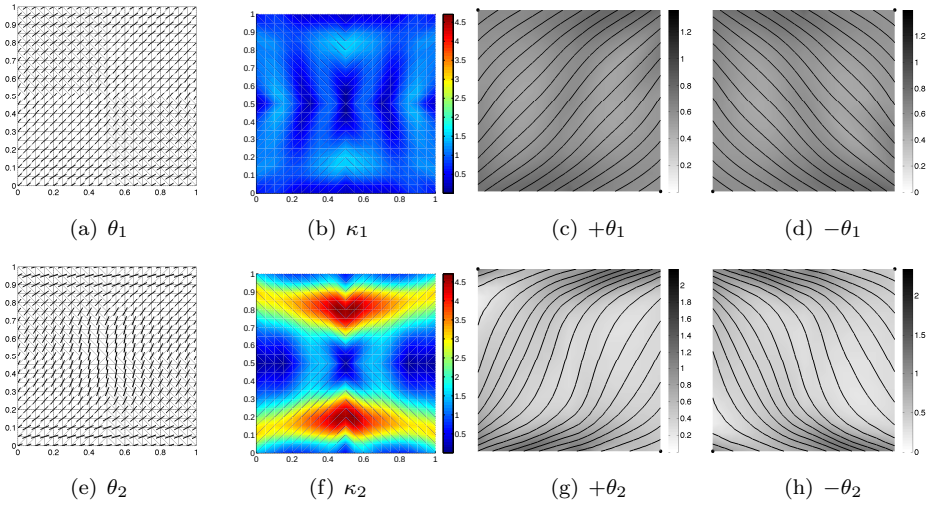

(a) θ_1 (b) κ_1 (c) $+\theta_1$ (d) $-\theta_1$

(e) θ_2 (f) κ_2 (g) $+\theta_2$ (h) $-\theta_2$

Figure 7.34: *Square plate in uni-axial compression: fibre angle distribution, curvature distribution, fibre paths and thickness distributions for $+\theta$ and $-\theta$, $n = 1$, $\kappa_{all} = 4.878\text{m}^{-1}$.*

for the LP-based objective function only.

The fibre angle distributions for all three cases, no constraint on curvature, $\kappa_{\text{all}} = 12.5\text{m}^{-1}$ and $\kappa_{\text{all}} = 4.878\text{m}^{-1}$ were found to be point symmetric about the centre of the panel. The in-plane fibre angle curvature was found to be in the same range for both plies, in contrast to the previous two example structures. It was concluded that this was a result of the similar gradients for the in-plane and flexural LPs of the optimum LP design, see Fig. 7.4, which confirms the previous conclusion that a relative difference in variation between the in-plane and flexural LPs manifests in the relative amount of curvature of the inward layers compared to the curvature of the outward layers of the laminate.

Seemingly manufacturable fibre paths and smeared thickness estimates were only obtained for $\kappa_{\text{all}} = 12.5\text{m}^{-1}$ and $\kappa_{\text{all}} = 4.878\text{m}^{-1}$. The fibre paths appeared to be point symmetric.

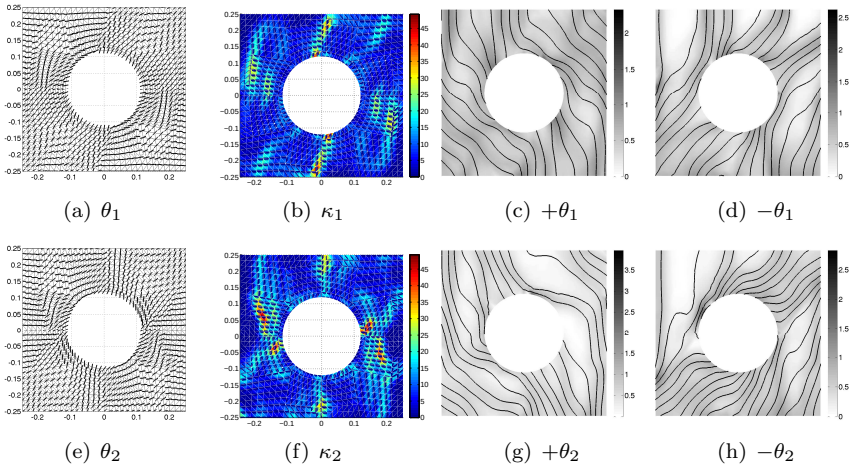

(a) θ_1 (b) κ_1 (c) $+\theta_1$ (d) $-\theta_1$

(e) θ_2 (f) κ_2 (g) $+\theta_2$ (h) $-\theta_2$

Figure 7.35: *Curved panel with a hole under a shear load: fibre angle distribution, curvature distribution, fibre paths and thickness distributions for $+\theta$ and $-\theta$, $n = 2$ no constraint on curvature.*

7.4.4 Discussion

It was concluded for the example of a square plate loaded in bi-axial compression that the fibre angle distribution, curvature distribution, smeared thickness distribution and fibre paths are nearly identical for both the LP-based and the sensitivity- based objective.

The maximum in-plane curvature value found was higher for plies closer to the mid-plane of the laminate for the examples of a plate loaded in bi-axial compres-

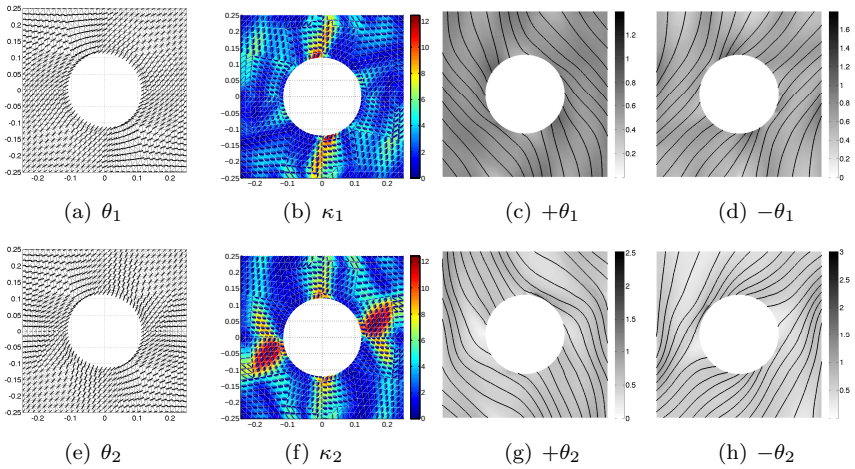

(a) θ_1 (b) κ_1 (c) $+\theta_1$ (d) $-\theta_1$

(e) θ_2 (f) κ_2 (g) $+\theta_2$ (h) $-\theta_2$

Figure 7.36: *Curved panel with a hole under a shear load: fibre angle distribution, curvature distribution, fibre paths and thickness distributions for $+\theta$ and $-\theta$, $n = 1$, $\kappa_{all} = 12.5\text{m}^{-1}$.*

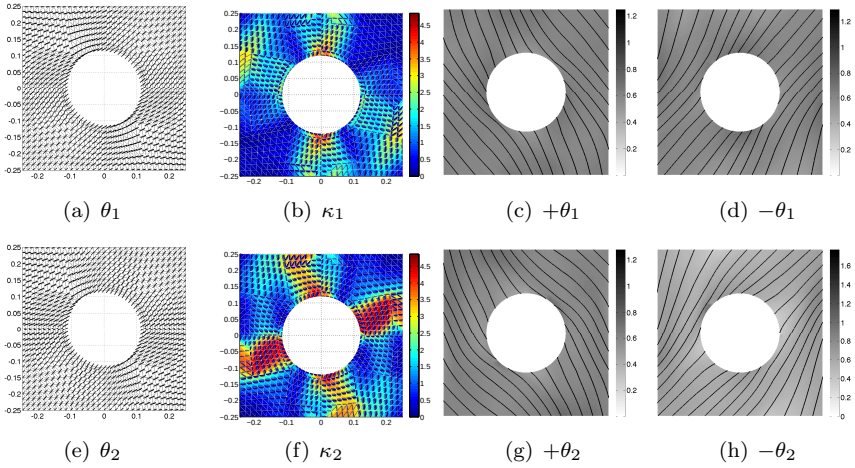

(a) θ_1 (b) κ_1 (c) $+\theta_1$ (d) $-\theta_1$

(e) θ_2 (f) κ_2 (g) $+\theta_2$ (h) $-\theta_2$

Figure 7.37: *Curved panel with a hole under a shear load: fibre angle distribution, curvature distribution, fibre paths and thickness distributions for $+\theta$ and $-\theta$, $n = 1$, $\kappa_{all} = 4.878\text{m}^{-1}$.*

sion and of a plate loaded in uni-axial compression for all results obtained, see appendix C. The maximum in-plane curvature values found for the example of a curved panel with a hole loaded in compression and shear did not show such an increase for plies closer to the mid-plane of the laminate. The conclusion was that relative differences between the in-plane distributions of the in-plane and flexural LPs manifest in the relative amount of curvature of the more inward plies in the laminate compared to the curvature of the more outward plies of the laminate, because the in-plane LPs are equally affected by all layers in the laminate, whereas the flexural LPs are more strongly affected by the outward plies of the laminate.

No realistic fibre path designs were found for the cases where no constraint on in-plane curvature was considered, but the fibre paths obtained for $\kappa_{\text{all}} = 12.5\text{m}^{-1}$ and $\kappa_{\text{all}} = 4.878\text{m}^{-1}$ appeared to be manufacturable. Nonetheless, the symmetry of the fibre angle distribution may be lost during the construction of fibre paths, and it was suggested that using different boundary conditions should investigated as this might help to solve this problem.

7.5 Wing-rib loaded in shear

An integrated design engineering approach was developed for dry tow-placement for the AUTOW project, European Union Sixth Framework Programme Project no. 030771. Part of this design engineering approach, which supports the fabrication of dry tow-placed preforms by optimising designs whilst taking into account manufacturing constraints and design specifications, was presented in chapters 5 and 6 of this thesis.

The design of a wing rib was considered (IJsselmuiden et al. 2011) to demonstrate the integrated design approach. Originally designing a test article to be manufactured for the AUTOW project was envisioned, but due to the geometrical complexity of this sine-wave rib, in the end a simpler flat rib model was used. Nonetheless, the results obtained for the flat rib model were compared to those for the sine-wave rib design.

The results described in deliverable 15 of the AUTOW project (IJsselmuiden et al. 2011) are repeated in what follows. The fibre angle designs were derived from the optimised lamination parameter designs, as was done for the other examples described in this chapter. Designs were obtained for several constraints on in-plane curvature, and the affect of thickness build-up and coupling terms on the mechanical behaviour of the wing rib designs was considered. Note that the results for thickness build-up differ from those described in deliverable 15, because minor changes were made to the estimation of thickness build-up in the structure, see chapter 6, after deliverable 15 was completed.

7.5.1 Problem definition

The initial objective was to design the same article as was used for full-scale testing in the AUTOW-project, a sine-wave wing rib (Fig. 7.38). The test article was designed as a conventional constant stiffness composite laminate. However, the geometry of the sine-wave rib was geometrically complex. Therefore, the decision was made to investigate the possibility of developing a competitive and geometrically less complex design by making use of fibre steering to improve the structural performance of the flat rib design.

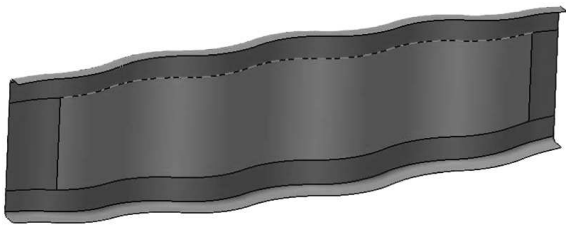

Figure 7.38: *Sine-wave rib test article designed for the AUTOW project.*

The design of the flat rib was based on that of the sine-wave rib. The height profile, length and loading conditions were kept the same, and only the rib web was modified to be parallel to the x-axis of the aircraft at any given point. The flat rib design is shown in Fig. 7.39.

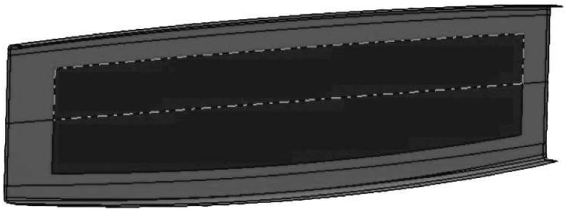

Figure 7.39: *Flat rib design modified from the sine-wave rib.*

Only the lay-up of the web of the rib could be designed, see Fig. 7.40, the lay-up of the flanges of the rib were assumed to be given and fixed, LP distributions were obtained for both the flat rib and the sine-wave rib to maximise the buckling load of the rib. The objective of the flat-rib design was to achieve a buckling load equal to or higher than that of the baseline design for the sine-wave rib, $[0/90/45/90/-45/0/90/\underline{0}]_s$, where the underlined ply is not mirrored about the mid-plane of the lay-up. Another design requirement was that the buckling load of the rib design should exceed the ultimate load of the rib by 1.5 times or more.

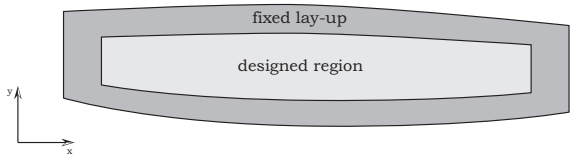

Figure 7.40: *Lay-up design region.*

Both the sine-wave rib and the flat rib design were modelled using the FE software package NASTRAN. The NASTRAN models were used to compute the buckling load of the sine-wave rib and the flat rib. The NASTRAN models were also used to obtain the design sensitivities of the two rib designs with respect to the entries of the **A**- and the **D**-matrices at each node of the model. These sensitivities were used in the optimisation of the LP distribution for the flat rib and the sine-wave rib, and were later also used in the conversion from the LP distribution to a manufacturable fibre angle design. The buckling load values for the base line sine-wave rib design and the feasible optimised VS designs in terms of LPs for the flat rib and the sine-wave rib are given in table 7.1.

Table 7.1: *First and second buckling mode and weight difference compared to the base line design for the optimised LP distributions.*

Design	Number of plies	Mode 1	Mode 2	% weight difference
Sine-wave rib baseline	15	2.8947	3.0752	0.0
Sine-wave rib optimum	15	3.7192	3.7997	0.0
Flat rib optimum	24	1.6460	1.7070	15.2

Fibre angle distributions were obtained for both the optimised LP distribution for the sine-wave rib and the optimised LP distribution for the flat rib. Results were obtained for the case where no constraint on in-plane curvature was considered, and for the cases where the allowable curvature κ_{all} was constrained to 12.5m^{-1} and 4.878m^{-1}. Results were also obtained for both the LP-based and the sensitivity-based objective functions, and the effect of thickness build-up due to overlapping tows, and the effect of neglecting the coupling terms $V_2^{\mathbf{A}}$, $V_4^{\mathbf{A}}$, $V_2^{\mathbf{D}}$ and $V_4^{\mathbf{D}}$.

7.5.2 Results flat rib

The fibre angle designs of the flat rib that were obtained for the lay-up $[\pm\theta_1/\pm\theta_2/\pm\theta_3/\pm\theta_4/\pm\theta_5/\pm\theta_6]_s$ and for a constraint on in-plane fibre curvature

of 12.5m^{-1} and 4.878m^{-1} are plotted in Figs. 7.41 and 7.42, respectively. The fibre angle designs for both curvature constraints were obtained using the LP-based objective function, Eq. 2.20, repeated on page 127.

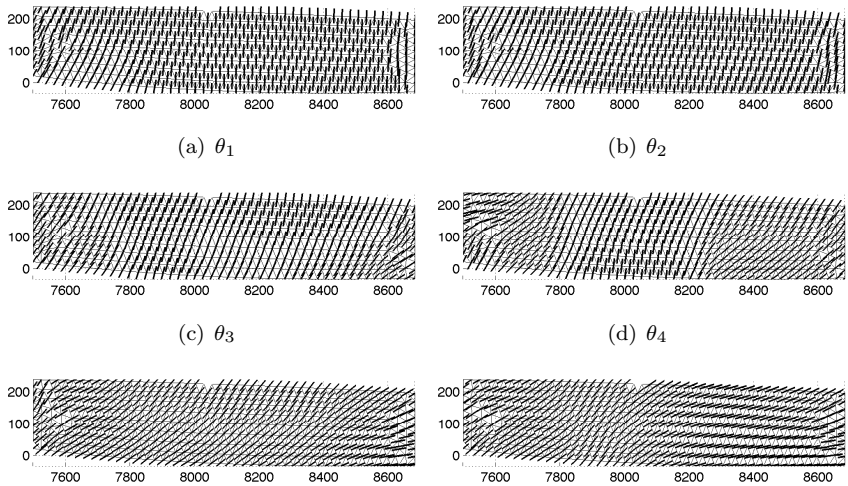

(a) θ_1 (b) θ_2

(c) θ_3 (d) θ_4

(e) θ_5 (f) θ_6

Figure 7.41: *Fibre angle design flat rib for* $\kappa_{all} = 12.5\text{m}^{-1}$.

The curvature distributions of the fibre angle designs for a constraint on in-plane fibre curvature of 12.5m^{-1} and 4.878m^{-1}, see Figs. 7.43 and 7.44, show that most steering occurs towards the front of the rib for plies 4 and 5 for $\kappa_{textrmall} = 12.5\text{m}^{-1}$. The maximum curvature values for the other plies are considerably lower. More regions in more plies were found to be close to the curvature constraint for $\kappa_{textrmall} = 4.878\text{m}^{-1}$.

The fibre paths and thickness distributions that were obtained for the cases considered are plotted in Figs. 7.45 and 7.46. The fibre paths that were obtained for both curvature constraint values do not resemble the respective fibre angle distributions very well. This was attributed to the boundary conditions used in the chosen implementation to generate fibre paths and estimated smeared thickness. The inflow boundary is arbitrarily defined, Eq. 6.15, see chapter 6:

$$\mathbf{sN} \leq 0 \tag{6.15}$$

where $\mathbf{s}$ is the vector tangent to the fibre orientation and $\mathbf{N}$ is the outward normal vector to the design domain, see Fig. 6.3. As a result the inflow region was relatively small for the given example, only the short left-hand side of the design region. Hence the fibre paths came out almost straight and were discarded. A more apt formulation of the in- and outflow boundaries might yield a more desirable result

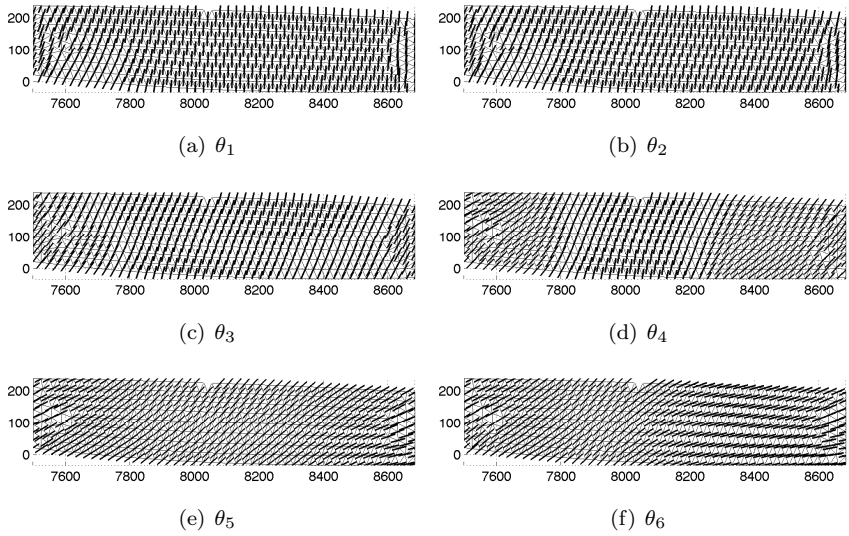

(a) θ_1 (b) θ_2

(c) θ_3 (d) θ_4

(e) θ_5 (f) θ_6

Figure 7.42: *Fibre angle design flat rib for* $\kappa_{all} = 4.878\text{m}^{-1}$.

for the fibre paths.

The buckling load multipliers for the results that were obtained for the optimum LP distribution for the flat rib are presented in table 7.2 . The buckling load multipliers were normalised using those of the LP optimum and given as a percentage, the buckling load multipliers presented were computed using NASTRAN.

It can be seen from the results shown in table 7.2 that allowing for thickness build-up in the laminate increases the value of the buckling load multiplier of the VS flat rib design, it is even necessary to satisfy the design requirement for the first buckling mode when a constraint on curvature was implied. However, the reliability of the obtained thickness distribution is questionable, as the fibre paths for which it was obtained do not correspond very well to the fibre angle distribution they were obtained for, as discussed above. Therefore, the results in which thickness build-up was taken into consideration were discarded. It was concluded that without accounting for thickness build-up no design satisfying the design requirement for the first buckling mode could be found.

7.5.3 Results sine-wave rib

Fibre angle designs of the sine-wave rib were obtained for the lay-up $[\pm\theta_1/\pm\theta_2/\pm\theta_3/90/\underline{0}]_s$, where the underlined ply is not mirrored about the mid-plane of the laminate. The fibre angle design for a constraint on in-plane fibre

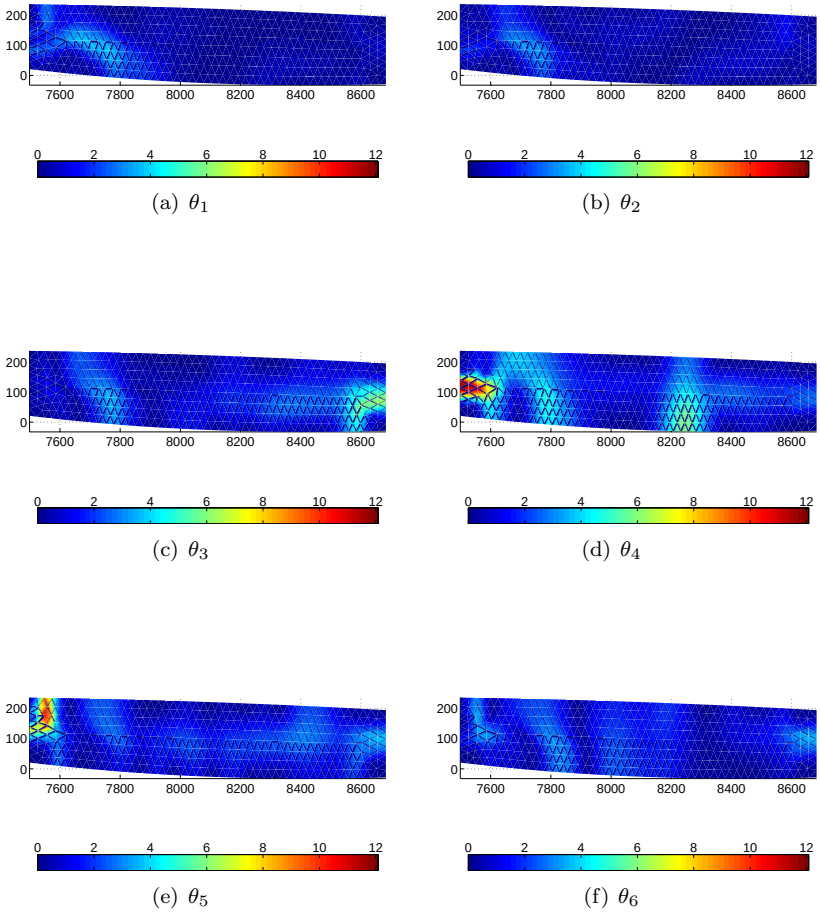

(a) θ_1 (b) θ_2

(c) θ_3 (d) θ_4

(e) θ_5 (f) θ_6

Figure 7.43: *Curvature distribution flat rib for* $\kappa_{all} = 12.5\text{m}^{-1}$.

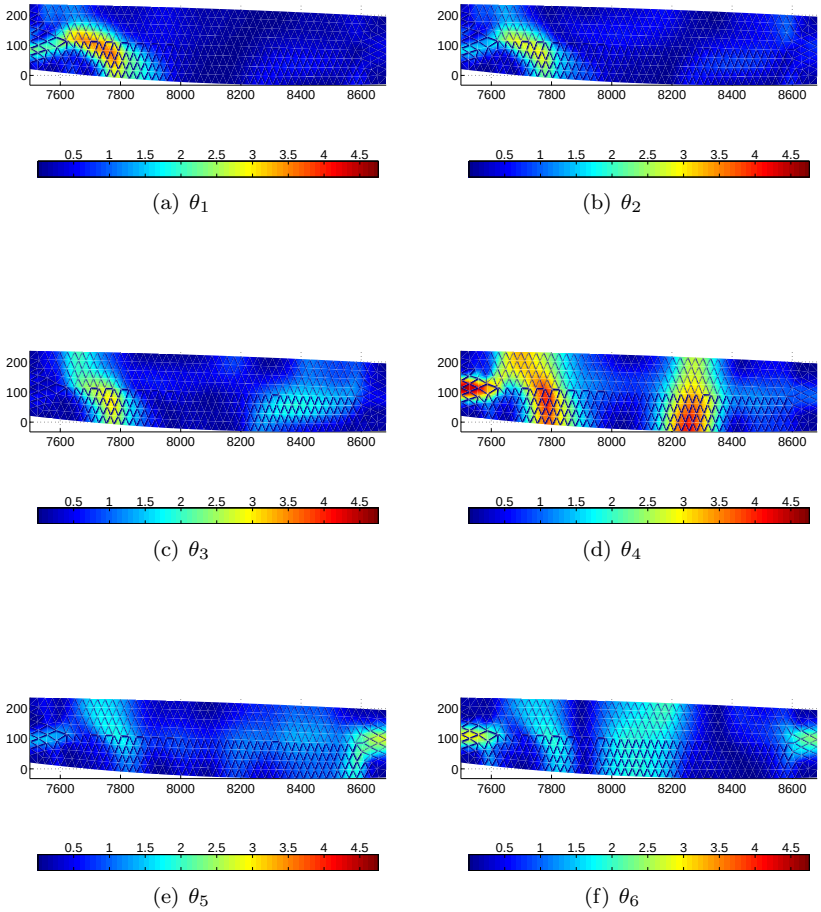

(a) θ_1 (b) θ_2

(c) θ_3 (d) θ_4

(e) θ_5 (f) θ_6

Figure 7.44: *Curvature distribution flat rib for* $\kappa_{all} = 4.878\text{m}^{-1}$.

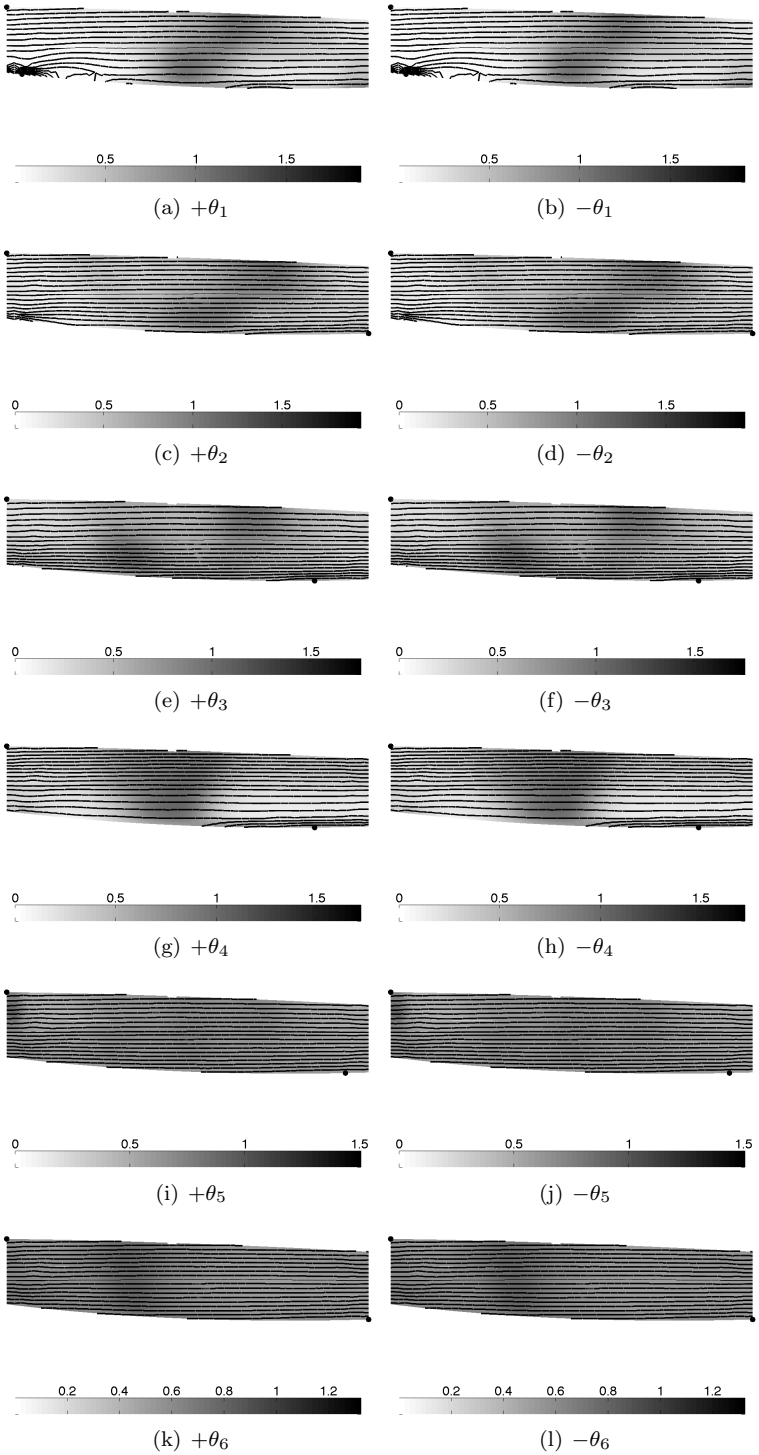

Figure 7.45: *Fibre paths and thickness distribution distribution flat rib for* $\kappa_{all} = 12.5\text{m}^{-1}$.

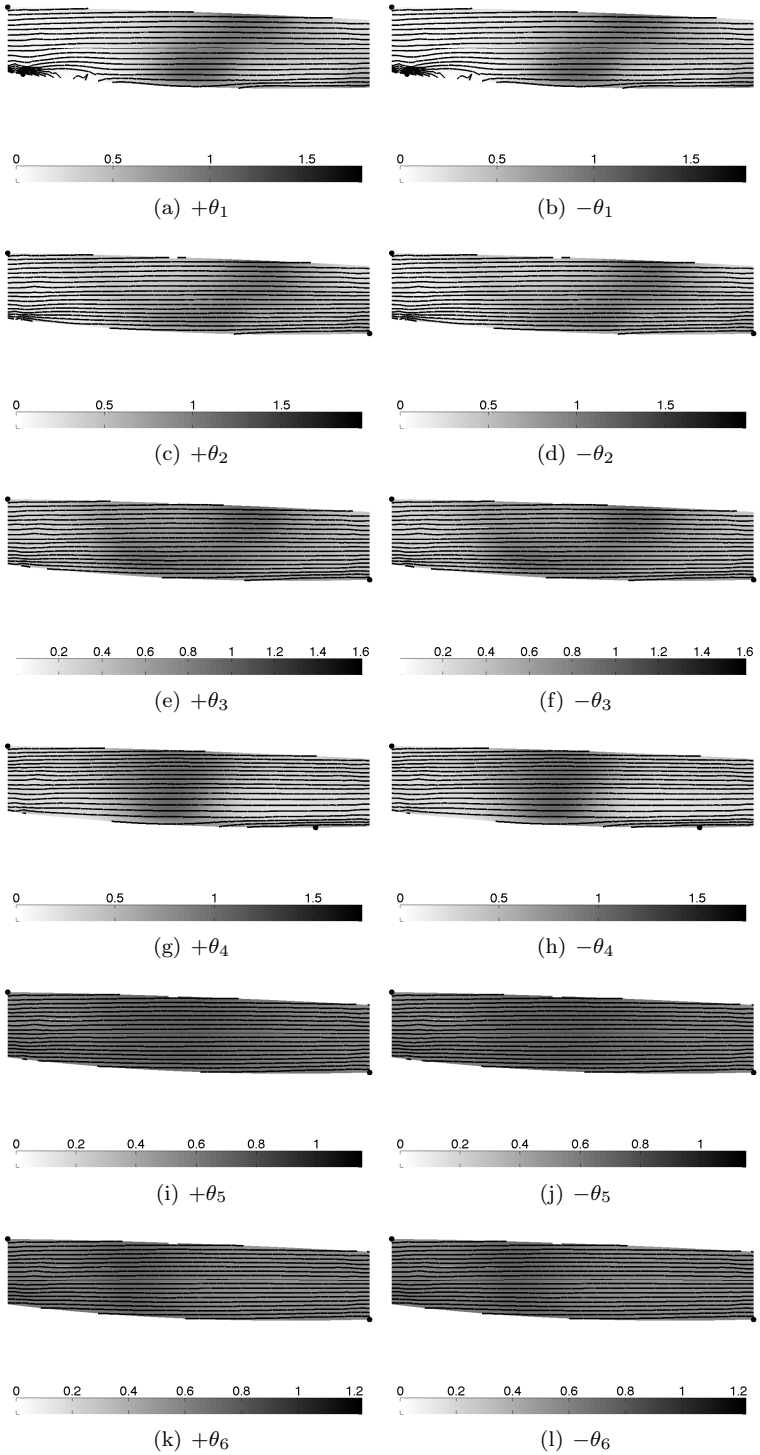

Figure 7.46: *Fibre paths and thickness distribution flat rib for* $\kappa_{all} = 4.878\text{m}^{-1}$.

Table 7.2: *Buckling load multiplier values obtained using the LP-based objective, eq. 2.20, for the cases with and without thickness variation taken into account and with and without coupling terms taken into account. The values in grey do not meet the design requirement for the first buckling load.*

Constraint	Thickness build-up	λ_o (LP optimum) mode 1	mode 2	λ (percentage of λ_o) mode 1	mode 2
none	no	1.646	1.707	89.14	99.64
	yes			110.43	119.67
$\kappa_{\text{all}} = 12.5\text{m}^{-1}$	no			91.08	99.79
	yes			111.19	119.52
$\kappa_{\text{all}} = 4.878\text{m}^{-1}$	no			86.26	99.92
	yes			89.59	103.55

curvature of 12.5m^{-1} and 4.878m^{-1} are plotted in Figs. 7.47 and 7.48, respectively.The fibre angle designs for both curvature constraints were obtained using the LP-based objective function.

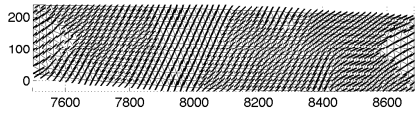

(a) θ_1

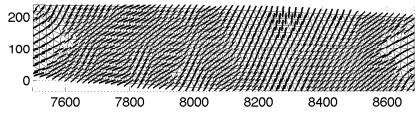

(b) θ_2

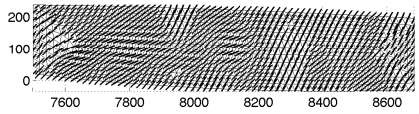

(c) θ_3

Figure 7.47: *Fibre angle design sine-wave rib for* $\kappa_{all} = 12.5\text{m}^{-1}$.

The range of curvature values for all three plies in the laminate was found to be similar for both curvature constraint values, see Figs. 7.49 and 7.50. The peaks in curvature were also spread much more evenly throughout the design region than was the case for the flat rib design. A likely cause of the observed difference in curvature distribution between the flat rib design and the sine-wave rib design is

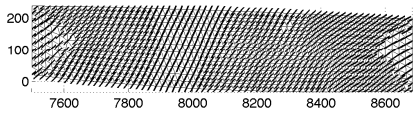

(a) θ_1

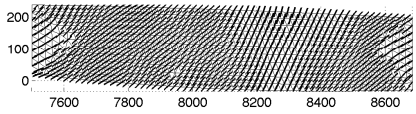

(b) θ_2

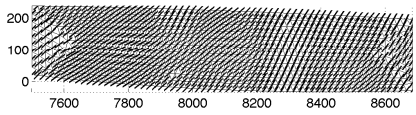

(c) θ_3

Figure 7.48: *Fibre angle design sine-wave rib for* $\kappa_{all} = 4.878\text{m}^{-1}$.

the difference in load redistribution mechanisms between the two structures which leads to an increase in the buckling load.

The fibre paths and thickness distributions obtained for the two curvature constraint cases are plotted in Figs. 7.51 and 7.52. The fibre paths obtained for both curvature constraint values did not resemble the respective fibre angle distributions very well, as was the case for the flat rib design. The boundary conditions used in the process to generate the fibre paths were thought to be the cause of the observed difference.

The buckling load multipliers, computed using NASTRAN, for the results that were obtained for the optimum LP distribution for the flat rib are presented in table 7.3 The buckling load multipliers were normalised using those of the LP optimum and given as a percentage.

The results presented in table 7.3 show that all the fibre angle designs obtained satisfy the design requirement on the first buckling mode of the structure, with and without including thickness build-up in the buckling analysis. Thickness variation can be seen to have a negative effect on the buckling load of the sine-wave rib, contrary to the results that were found for the flat rib design, table 7.2. The reliability of the obtained thickness distribution was questionable, and therefore, the results with thickness build-up were discarded. Note that the fibre paths found were nearly parallel, but not completely; hence thickness build-up still occurred.

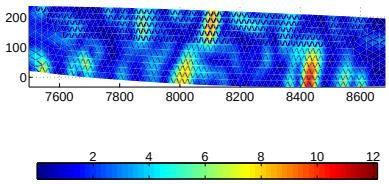

(a) θ_1

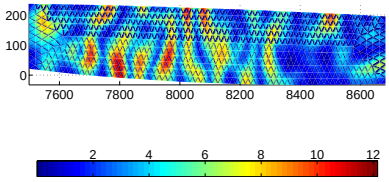

(b) θ_2

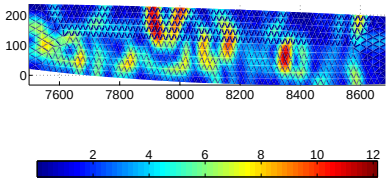

(c) θ_3

Figure 7.49: *Curvature distribution sine-wave rib for* $\kappa_{all} = 12.5\text{m}^{-1}$.

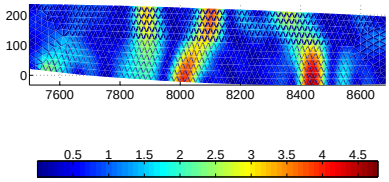

(a) θ_1

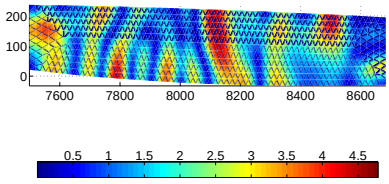

(b) θ_2

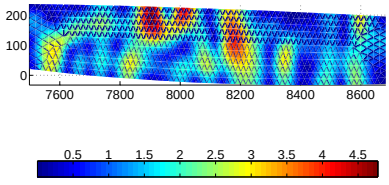

(c) θ_3

Figure 7.50: *Curvature distribution sine-wave rib for* $\kappa_{all} = 4.878\text{m}^{-1}$.

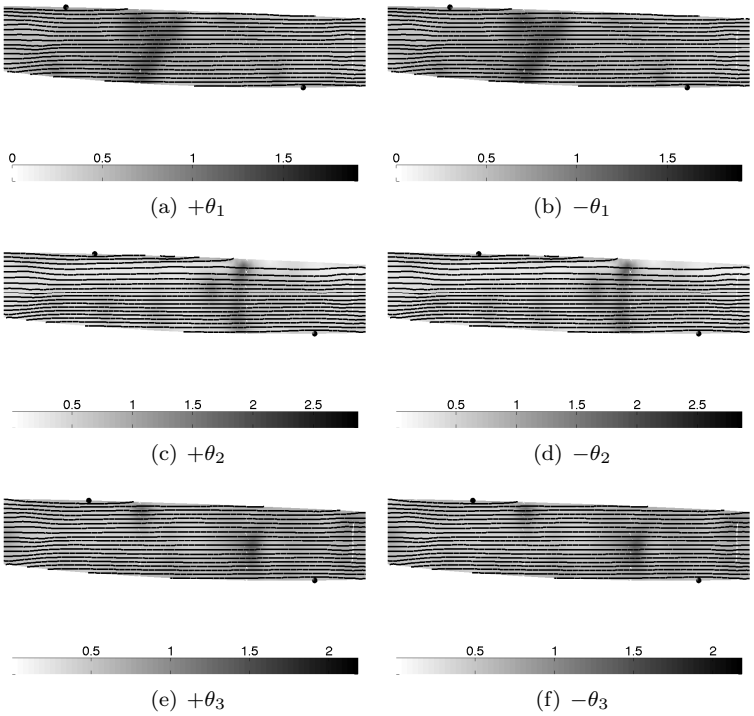

(a) $+\theta_1$ (b) $-\theta_1$

(c) $+\theta_2$ (d) $-\theta_2$

(e) $+\theta_3$ (f) $-\theta_3$

Figure 7.51: *Fibre paths and thickness distribution distribution sine-wave rib for* $\kappa_{all} = 12.5\text{m}^{-1}$.

Table 7.3: *Buckling load multiplier values obtained using the LP-based objective, eq. 2.20, for the cases with and without thickness variation taken into account and with and without coupling terms taken into account. The values in grey do not meet the design requirement for the first buckling load.*

Constraint	Thickness build-up	λ_o (LP optimum) mode 1	mode 2	λ (percentage of λ_o) mode 1	mode 2
none	no	3.719	3.800	90.08	92.96
	yes			84.31	86.55
$\kappa_{\text{all}} = 12.5\text{m}^{-1}$	no			90.52	93.51
	yes			85.42	88.13
$\kappa_{\text{all}} = 4.878\text{m}^{-1}$	no			86.26	93.22
	yes			89.59	82.59

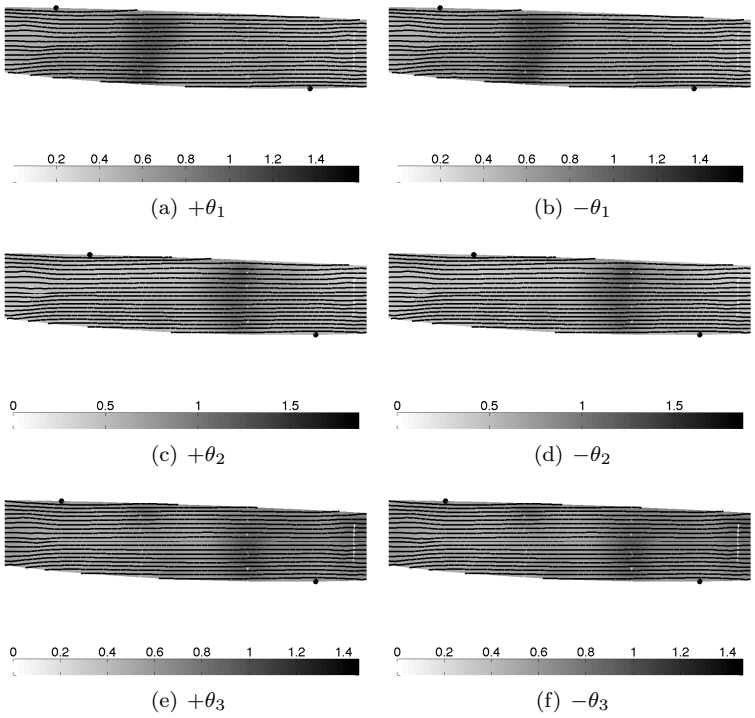

(a) $+\theta_1$ (b) $-\theta_1$

(c) $+\theta_2$ (d) $-\theta_2$

(e) $+\theta_3$ (f) $-\theta_3$

Figure 7.52: *Fibre paths and thickness distribution sine-wave rib for* $\kappa_{all} = 4.878\text{m}^{-1}$.

7.5.4 Discussion

The results obtained for the flat rib and sine-wave rib validated coupling the of the developed two-step design approach with commercial FE software. However, none of the fibre angle designs of the flat rib with a constraint on in-plane fibre angle curvature met all of the design guide-lines set, despite a weight increase of 15.2% compared to the sine-wave rib, assuming constant thickness of the laminate. It was concluded that it is not possible to replace the sine-wave rib design with a flat rib design without a considerable increase in the weight of the structure.

One cause for concern is that the method used to generate fibre paths based on the fibre angle distribution per ply in the laminate does not yield proper fibre path designs for either the flat rib or the sine-wave rib. It is suggested that the boundary conditions used to generate fibre paths should be reconsidered.

7.6 Conclusion

The conversion of a variable stiffness (VS) lamination parameter (LP) design into a VS fibre angle design with a constraint on in-plane curvature was discussed for four structural components for which an optimal LP design was available in this chapter. Two different design objectives, namely based on the least-square error in LP space and based on sensitivity information, were used. The results show that the proposed conversion process generated consistent results for different geometries and loading conditions. Nearly identical results were found for both design objectives, and it was found that relative differences between the in-plane distributions of the in-plane and flexural LPs manifest in the relative amount of curvature of the plies. The flexural LPs are mostly affected by the outer plies of the laminate, whereas the in-plane LPs are equally affected by all plies of the laminate. The modest spatial variation of the desired flexural LP distribution reflected in the in-plane fibre angle curvature of the outer plies of the laminate, and the strong spatial variation of the desired in-plane LP distribution manifested in comparatively high in-plane curvature values for the more inward plies of the laminate.

The buckling load of the first three example structures considered in this chapter showed an increasing trend as a function of the constraint on in-plane curvature of the fibre angle distribution per ply. The maximum thickness of the thickness build-up due to overlapping fibre paths showed a similar trend, whereas the overall volume of the structure reduced as a function of curvature constraint value, which was attributed to the choice of boundary conditions used for the construction of the fibre paths and computations of the smeared thickness estimate.

The buckling loads of the structures were re-evaluated for the obtained thickness distribution. Improvements in buckling load were found for the example of a

square plate in uni-axial compression, a square plate in bi-axial compression and a curved panel with a hole under compression and shear when the thickness build-up in the laminate was accounted for during analysis. It was concluded that laminate thickness build-up will lead to an improvement in buckling performance at the cost of an increase of structural weight. The maximum thickness-build in the laminate was found to decrease as function of the number of designed layers in the laminate.

The proposed conversion method can not be guaranteed to converge to the global optimum for every constraint on in-plane curvature. Therefore, it was suggested that the CA should be seeded with several fibre angle distributions.

The method used to generate fibre paths based on the fibre angle distribution per ply in the laminate gave cause for concern. The symmetry of the fibre angle distribution was lost for the example of a square plate loaded in uni-axial compression, and no realistic fibre path designs were found for either the flat rib or the sine-wave rib examples. It is suggested that the boundary conditions used to generate fibre paths should be reconsidered, such that they will preserve symmetry of the fibre angle distribution and such that they will be applicable to a large range of geometries.

If I had more time, I would have written a shorter letter.
T.S. Eliot (1888 – 1965)

8

CONCLUSIONS AND RECOMMENDATIONS

The work presented in this thesis forms part of a larger research effort being carried out at the Aerospace Structures and Computational Mechanics (ASCM) group of the faculty of Aerospace Engineering of the Delft University of Technology (the Netherlands), to develop design and optimisation techniques for variable stiffness (VS) fibre-placed composite laminates. One of the techniques under development is a two-step optimisation approach for VS composite structures. The first step of this approach is to optimise a VS composite structure in terms of lamination parameters (LP), in the second step the LP design is converted into a lay-up design. A possible second step, to convert an LP design into a lay-up design, is presented in this thesis.

The objective of the work presented here was to investigate the methods available in literature and to develop new methods to obtain the optimal VS lay-up design for a given LP design of a VS composite laminate that satisfies prescribed manufacturing constraints. The work presented in this thesis was divided into three parts to fulfill this objective:

- the conversion of LPs into a lay-up design
- the design of blended composite lay-ups
- the design of steered composite lay-ups

The reasoning behind this division is that, after a design in terms of LPs was converted into a design in terms of fibre angles, there are two possible ways to arrive at a variable stiffness laminate design: laminate blending or fibre steering. Eventually laminate blending and fibre steering might be combined, but this was beyond the scope of the present work.

The conversion from a set of lamination parameters into a lay-up design is discussed in chapter 2 and new tools for the conversion from LPs to a lay-up design are developed in this chapter. The design of multi-segment blended composite laminates using a guide-based optimisation procedure is described in chapter 3. The results obtained using the new blending definitions introduced in chapter 3 are compared to results obtained using two pre-existing blending definitions for a benchmark problem taken from the literature in chapter 4. An in-depth discussion of the design of variable stiffness laminates as part of the framework presented in this thesis is given in chapter 5, and one of the manufacturing constraints associated with fibre steering technology, minimum steering radius, and its mathematical implementation are discussed in this chapter. A unified approach for the conversion of LPs into a fibre angle design and the implementation of one or multiple manufacturing constraints is presented on the basis of this discussion in chapter 5. The unified conversion approach presented produces a VS lay-up design on a finite element grid. How this nodal fibre angle distribution per ply in the laminate is converted into fibre paths fit for production using automated fibre placement technology was discussed in chapter 6. The estimation of thickness build-up due to gaps and overlaps is also reviewed in this chapter. Four example structures were studied using the developed optimisation tools for the conversion process from LPs to a fibre angle design is discussed in chapter 7. The effect of the constraint on in-plane curvature of the fibre distribution of a ply has on the buckling performance of the four structures considered, and the thickness build-up in the laminate of these structures was studied. The effect thickness variation due fibre steering has on the buckling load of the four structures was also studied.

The conclusions that were drawn based on the work described in the above are grouped per part of the work, i.e. the conversion of LPs into a lay-up design, the design of blended composite lay-ups, and the design of blended composite lay-ups. The conclusions are followed by recommendations for future work on the subject of this thesis and future challenges are identified. Finally, overall conclusions for the work done for this research are given based on the conclusions per part of the work and the recommendations made.

Note that part of the work presented in this thesis was developed as part of the AUTOW project, European Union Sixth Framework Programme Project no. 030771, in which the design and engineering of composite parts manufactured using dry tow-placement has been investigated.

8.1 LAMINATION PARAMETERS AND LAMINATE CONFIGURATION

Composite lay-ups with a discrete number of equally thick layers were considered in this thesis. The mathematical description of the lamination parameters is

presented in chapter 2. This description was used to determine which part of the feasible LP domain could be described by a laminate of a given discrete number of equally thick layers and a lay-up configuration. It was shown that the part of the feasible LP domain converges to the full theoretical feasible domain as the number of layers in the laminate n goes to infinity. The rate of convergence towards the full feasible domain was found to be larger for the flexural LPs $V_1^{\mathbf{D}}$ and $V_3^{\mathbf{D}}$ than for the in-plane LPs $V_1^{\mathbf{A}}$ and $V_3^{\mathbf{A}}$. For the lay-up $[\pm\theta_1/\ldots/\theta_n]_s$ it was proven the the part of the feasible domain that can be described by this lay-up is a fractal, which is additional proof that the part of the feasible domain described by such a practical laminate converges to the full theoretical feasible LP envelope. Note that to the author's knowledge to date (2011) no exact analytical description of the feasible LP domain has been made.

The conversion process from LPs to a fibre angle design was also discussed in chapter 2. In the literature it is shown that, using a maximum of three layers in the laminate, any combination of the lamination parameters $V_1^{\mathbf{A}}$, $V_3^{\mathbf{A}}$, $V_1^{\mathbf{D}}$ and $V_3^{\mathbf{A}}$ can be matched. However, this observation is only valid for laminates where ply thickness is a continuous variable. Since, for the work done for this thesis, only laminates with a discrete number of equally thick plies were considered, this observation was not used to convert an LP design into a lay-up design. A semi-analytical approach was developed to convert LPs into a lay-up design, but it was concluded that this approach could not be expanded to more than two design fibre orientations in the laminate, which would exclude a larger part of the feasible LP domain from the conversion process. Therefore, a two-step approach was developed which could be expanded to any arbitrary number of designed fibre orientation in the laminate. The developed two-step approach consisted of a genetic algorithm (GA) used to explore the design space and a gradient-based optimiser to converge to a final lay-up design. The design objective used for the GA and the gradient-based optimiser was the least-squared distance in LP-space between the desired set of LP-values and the LP-values computed for the laminate. Constraints on e.g. the 10%-rule for robustness of the laminate design, could be implemented using an augmented objective function formulation. The two-step approach was proven to be able to match any set of up to all 12 LP values with a laminate design, provided the number of layers in the laminate is chosen to be large enough. The approach was tested for several combinations of LPs, and consistently better results were found for larger values of the number of layers in the laminate n. It was therefore concluded, that the proposed two-step approach provides a robust and flexible method to convert LPs into an optimal lay-up design in a least-squared sense.

8.2 Multi-segment blended laminate design

One way to create a variable stiffness laminate is to divided a structure into several segments for each of which the optimum lay-up is determined. The design of such multi-segment laminates is discussed in chapter 3. The manufacturing constraints which are quintessential to multi-segment laminate design are discussed and the concept of laminate blending is presented, laminate blending is needed to guarantee the structural integrity of the laminate design. The implementations of laminate blending found in the literature were divided into four categories:

- implementations where lay-ups are not intrinsically blended and the blending process is enforced through a single optimisation step
- implementations where lay-ups are not intrinsically blended and the blending process is enforced through multiple optimisation steps
- implementations where lay-ups are intrinsically blended and the blending process is enforced through a single optimisation step
- implementations where lay-ups are intrinsically blended and the blending process is enforced through multiple optimisation steps

The advantages and disadvantages of all four categories are discussed and a choice was made to develop an not intrinsically blended, multi-step blending implementation for two new blending definitions: generalised blending and relaxed generalised blending. The first step of the implementation was considered to be the optimisation of a structure in terms of LPs, after which, in a second step, an optimal blended lay-up design was obtained. This second step was implemented in the form of a multi-chromosomal GA, following the principal of guide-based blending. A guiding laminate stack was encoded using one chromosome. Which plies are taken from the guiding stack is determined by an additional chromosome for each segment in the structure. The fact that the designs could be represented using the multi-chromosomal GA, which are not blended, made the implementation non-intrinsically blended. Therefore, it was proposed that a repair strategy was implemented to guarantee that fully blended laminate designs would be obtained.

The results obtained using the new blending definitions introduced in chapter 3 are presented in chapter 4. Three structures were considered, an 18-panel horseshoe configuration for which blended laminate results are available in the literature, a panel with two concentric lay-ups, and a square panel for which the best variable stiffness lamination parameter distribution was assumed known.

No satisfactory results were found for the horseshoe panel configuration. The suggestions was made that this could be an artefact of the use of a single objective function value to capture a laminate design with many segments. The repair

strategy used to enforce laminate blending also was identified as a likely cause of the observed behaviour. The results obtained for the VS panel could be used to verify that the performance of the optimiser deteriorates when the number of segments in the structure was increased. A negative effect of the repair strategy of the genetic coding to enforce blending could not be verified. No meaningful conclusions could be reached about the relative performance of the generalised and relaxed generalised blending definitions.

8.3 VARIABLE STIFFNESS LAMINATE DESIGN

Varying the in-plane fibre orientation angles within a laminate is a more refined way to design VS composite structures than using laminate blending. The conversion of a spatial LP-distribution an in-plane fibre angle distribution that satisfied a constraint on in-plane fibre angle curvature is discussed in chapter 5. All the LP distributions considered for conversion into a lay-up design discussed in this thesis were defined on a finite element (FE) grid. Direct conversion from LPs into stacking sequence designs, discussed in chapter 2, as a result led to a stacking sequence design for each node of the FE grid. Therefore, a method was developed to estimate the in-plane curvature of such a nodal fibre angle distribution, such that fibre angle curvature could be subsequently constrained.

A cellular automaton (CA) was developed to enforce manufacturing constraints, like the the constraint on in-plane curvature, on the initial fibre angle design obtained by converting a given optimum LP distribution into a least-square optimal stacking sequence distribution. The CA used Jacobi iteration to conserve the possible symmetry of the initial fibre angle design, or seed. Two objective functions were used in combination with the CA, the average least-square error in LP space between the obtained VS lay-up and the optimum LP distribution, and an objective function based on an estimate of the buckling load of the structure obtained via sensitivity information, if available. Manufacturing constraints were entered into the CA via an augmented objective function formulation. The results that were obtained using the CA were found to be consistent and scalable, and that, for small values of the constraint on curvature, the design would converge towards the best-known constant stiffness (CS) design.

How the nodal fibre angle distribution per ply in the laminate can be converted into fibre paths which are fit for production using automated fibre placement (AFP) technology is discussed in chapter 6. A streamline approach was adopted for the work presented in this thesis after a survey of the available literature on the subject of path generation. The advantage of the streamline analogy was that it also provides an estimate of the smeared thickness of the laminate, based on the notion that thickness variation in the laminate results from overlapping fibre paths. It was shown how the LP distribution of the laminate, including the effect

of thickness variation and the change in volume of the laminate due to thickness variation, could be computed. The fibre path designs that were obtained appeared to be manufacturable.

The developed method to convert an optimum LP design for a structure into an optimum VS lay-up design that satisfies a constraint on curvature is discussed using four exemplar structures, in chapter 7:

- a square plate loaded in bi-axial compression
- a square plate loaded in uni-axial compression
- a curved plate with a hole loaded in compression and shear
- a wing rib loaded in shear

Results were generated for two different design objectives: the average least-square error in LP-space and a sensitivity-based estimate of the buckling load of the structure. The results showed that the proposed conversion process generated consistent designs for different geometries and loading conditions, and early identical results were found for either design objective. It was concluded that relative differences between the in-plane distributions of the in-plane and flexural LPs manifest in the relative amount of curvature of the more inward plies in the laminate compared to the curvature of the more outward plies of the laminate, because the in-plane LPs are equally affected by all layers in the laminate, whereas the flexural LPs are more strongly affected by the outward plies of the laminate. The effect the constraint on in-plane fibre curvature had on the performance of the structure, the maximum thickness of the structure due to overlapping fibre paths, the volume of the structure, and the buckling load of the structure when thickness variation due to overlapping fibre paths was taken into account was studied. The buckling load of a structure was found, as expected, to show an increasing trend, as the constraint on in-plane curvature was relaxed. Increasing the number of layers in the laminate also had a positive effect on the buckling load value, which became more pronounced when the constraint on in-plane curvature was relaxed further.

The maximum thickness of the laminate also increased when the constraint on in-plane curvature was relaxed, as did the volume of the laminate. Similarly significant improvements in buckling load value were found when the thickness variation due to overlapping fibre paths was taken into account. There were a few exceptions to this trend for design cases without a constraint on in-plane curvature.

The case where only one designed layer in the laminate was considered, consistently showed slightly different trends from the cases where multiple designed layers in the laminate were considered. The buckling load values that were obtained for small values of the curvature constraint were found to be higher. It was

concluded that this was a result of the CA converging to a local optimum, rather than to a global optimum, for the designs where multiple layers were considered.

8.4 Recommendations for future work and future challenges

8.4.1 Recommendations for future work

The proposed conversion method outlined in chapter 5 could not be guaranteed to converge to the global optimum for every constraint on in-plane curvature of the fibre angle distribution per ply. Therefore, it was suggested that the CA should be seeded with several fibre angle distributions. For example: if a balanced symmetric laminate of the form $[\pm\theta_1/\ldots/\pm\theta_n]_s$ was required to be designed for $n = 6$, the CA could be initialised with fibre angle seeds of the form $[(\pm\theta_1)_6]_s$, $[(\pm\theta_1/\pm\theta_2)_3]_s$ and $[(\pm\theta_1/\pm\theta_2/\pm\theta_3]_s$ next to the seed $[\pm\theta_1/\pm\theta_2/\pm\theta_3/\pm\theta_4/\pm\theta_5/\pm\theta_6]_s$.

The method used to generate fibre paths based on the fibre angle distribution per ply in the laminate, see chapter 6, gave a reason for concern. The symmetry of fibre angle distributions was lost in some of the cases considered, and no realistic fibre path designs were found for other cases. It is suggested that the boundary conditions that are used to generate fibre paths should be reconsidered, such that they will preserve symmetry of the fibre angle distribution, and such that they are applicable for a large range of geometries.

8.4.2 Future challenges

It has been proved that the part of the feasible LP domain that can be described by a laminate of a given number of equally thick layers and lay-up configuration is a fractal, see section 8.1. This proof might prove to be a useful step towards producing a compact analytical description of the feasible LP domain, such an analytical description to the author's knowledge, not being available to date, 2011.

Ideally the conversion of LPs into a lay-up design would be known in a closed analytical form. Currently, no such formulation is known, except for designs where layer thickness is considered to be a continuous variable. It is therefore recommended that describing the feasible LP domain using fractals should be investigated further, as should using fractals when converting a point in LP-space into a laminate design. When making a comparison with fractal image compression (Mandelbrot 1999), a LP distribution of a structure may be seen as a compressed version of its layup design.

Two methods to design a variable stiffness laminate were discussed in this thesis: laminate blending and fibre steering. A long term goal would be to combine these

two techniques into a unified design approach. Such a unified approach would give the designer more control over the thickness distribution of a steered variable stiffness composite lay-up.

8.5 Final conclusions

A method was developed, and presented in this thesis, to convert the optimum design of a variable stiffness composite laminate, in terms of lamination parameters, into an optimum lay-up design of a variable stiffness composite laminate. It was concluded that it is possible to convert any given combination of lamination parameters successfully into a lay-up design, provided the number of equally thick plies in the laminate is chosen large enough. Converting the LP distribution for a VS laminate, the structural performance of the lay-up design obtained was found to be very close to the structural performance of the LP optimum.

It was shown how the different lay-ups in a VS composite structure could be combined to form a coherent whole using laminate blending. It was proved to be more successful to achieve a coherent lay-up design using fibre steering, though the design of fibre paths, such that the performance of the laminate was not negatively affected by thickness build-up in the laminate due to gaps and overlaps between neighbouring tows, remains an issue, and further research is required. A long-term goal would be to combine fibre steering and laminate blending into a unified design approach.

The overall conclusion is that a flexible computational tool set has been developed which can be used to convert a variable stiffness composite design given in terms of lamination parameters into an optimal variable stiffness lay-up design. The results that were obtained using the developed tools showed that it is possible to convert a lamination parameter design into a fibre angle design which very closely approaches the mechanical properties of the optimum lamination parameter design.

BIBLIOGRAPHY

Abdalla, M. M., Kassapoglou, C. and Gürdal, Z. (2009), Formulation of composite laminate robustness constraint in lamination parameters space, Proceedings of the 50^{th} AIAA/ASME/ASCE/AHS/ASC Structures, Structural Dynamics and Materials Conference, Palm Springs, CA.

Adams, D. B., Watson, L. T. and Gürdal, Z. (2003), 'Optimization and blending of composite laminates using genetic algorithms with migration', *Mechanics of Advanced Materials and Structures* **10**(3), 183–203.

Adams, D. B., Watson, L. T., Gürdal, Z. and Anderson-Cook, C. M. (2004), 'Genetic algorithm optimization and blending of composite laminates by locally reducing laminate thickness', *Advances in Engineering Software* **35**, 35–45.

Ahn, C. W. (2006), *Advances in Evolutionary Algorithms: Theory, Design and Practice*, Vol. 18 of *Studies in Computational Intelligence*, Springer-Verlag Berlin Heidelberg, Samsung Advanced Institute of Technology (SAIT), Republic of Korea.

Alhajahmad, A., Abdalla, M. M. and Gürdal, Z. (2008), 'Design tailoring for pressure pillowing using tow-placed steered fibers', *Journal of Aircraft* **45**(2), 630 – 640.

Ashby, M. F. (1992), *Materials selection in mechanical design*, second edition edn, Butterworth-Heinemann.

Autio, M. (2000), 'Determining the real lay-up of a laminate corresponding to optimal lamination parameters by genetic search', *Structural and Multidisciplinary Optimization* **20**, 301–310.

Autio, M. (2001), 'Optimization of coupled thermal-structural problems of laminated plates with lamination parameters', *Structural and Multidisciplinary Optimization* **21**(1), 40–51.

Biggers, S. B. and Srinivasan, S. (1993), 'Compression buckling response of tailored rectangular composite plates', *AIAA journal* **31**(3), 590–596.

Blom, A. W. (2010), Structural Performance of Fiber-Placed Variable Stiffness Composite Conical and Cylindrical Shells, PhD thesis, Delft Universtiy of Technology.

Blom, A. W., Abdalla, M. M. and Gürdal, Z. (2010), 'Optimization of course locations in fiber-placed panels for general fibre angle distributions', *Composites Science and Technology* **70**(4), 564 – 570.

Blom, A. W., Lopes, C. S., Kromwijk, P. J., Gürdal, Z. and Camanho, P. (2009), 'A theoretical model to study the influence of tow-drop areas on the stiffness and strength of variable-stiffness laminates', *Journal of Composite Materials* **43**(5), 403 – 425.

Blom, A. W., Setoodeh, S., Hol, J. M. A. M. and Gürdal, Z. (2008), 'Design of variable-stiffness conical shells for maximum fundamental eigenfrequency', *Computers and Structures* **86**(9), 870–878.

Blom, A. W., Tatting, B. F., Hol, J. M. A. M. and Gürdal, Z. (2009), 'Fiber path definitions for elastically tailored conical shells', *Composites Part B: Engineering* **40**, 77 – 84.

Brandmaier, H. E. (1970), 'Optimum filament orientation criteria', *Journal of Composite Materials* **4**(3), 422–425.

Caprino, G. and Crivelli Visconti, I. (1982), 'A note on specially orthotropic laminates', *Journal of Composite Materials* **16**, 395 – 399.

De Wit, A. and Van Keulen, F. (2007), Numerical comparison of multi-level optimization techniques, *in* '48$^{\text{th}}$ AIAA/ASME/ASCE/AHS Structures, Structural Dynamics, and Materials Conference', American Institute of Aeronautics and Astronautics, Honolulu, Hawaii.

Diaconu, C. G., Sato, M. and Sekine, H. (2002*a*), 'Feasible region in general design space of lamination parameters for laminated composites', *AIAA Journal* **40**(3), 559 – 565.

Diaconu, C. G., Sato, M. and Sekine, H. (2002*b*), 'Layup optimization of symmetrically laminated thick plates for fundamental frequencies using lamination parameters', *Structural and Multidisciplinary Optimization* **24**(4), 302–311.

Diaconu, C. G. and Sekine, H. (2004), 'Layup optimization for buckling of laminated composite shells with restricted layer angles', *AIAA Journal* **42**(10), 2153–2163.

Fagiano, C. (2010), Computational modeling of tow-placed composite laminates with fabrication features, PhD thesis, Delft Universtiy of Technology, Kluyverweg 1, 2629 HS Delft, the Netherlands.

Fukunaga, H. and Sekine, H. (1992), 'Stiffness design method of symmetric laminates using lamination parameters', *AIAA Journal* **30**(11), 2791 – 2793.

Fukunaga, H., Sekine, H., Sato, M. and Iino, A. (1995), 'Buckling design of symmetrically laminated plates using lamination parameters', *Computers & Structures* **57**(4), 643 – 649.

Fukunaga, H. and Vanderplaats, G. N. (1991), 'Stiffness optimization of orthotropic laminated composites using lamination parameters', *AIAA Journal* **29**(4), 641–646.

Ghiasi, H., Pasini, D. and Lessard, L. (2009), 'Optimum stacking sequence design of composite materials part i: Constant stiffness design', *Composite Structures* **90**(1), 1–11.

Giger, M., Keller, D. and Ermanni, P. (2007), 'A graph-based parameterization concept for global laminate optimization', *Structural and Multidisciplinary Optimization* .

Grenestedt, J. and Gudmundson, P. (1993), Layup optimization of compoiste material structures, *in* P. Pedersen, ed., 'Optimal Design with Advanced Materials', Elsevier Science, pp. 311 – 336.

Gürdal, Z., Haftka, R. T. and Hajela, P. (1999), *Design and Optimization of Laminated Composite Materials*, Wiley, New York.

Gürdal, Z., IJsselmuiden, S. T. and Campen, J. M. V. (2010), Composite laminate optimization with discrete variables, *in* R. Blockley and W. Shyy, eds, 'Encyclopedia of Aerospace Engineering', Vol. 8, Wiley, New York, chapter 432.

Gürdal, Z. and Olmedo, R. (1993), 'In-plane response of laminates with spatially varying fiber orientations: Variable stiffness concept', *AIAA Journal* **31**(4), 751 – 758.

Hammer, V., Bendsøe, M., Lipton, R. and Pedersen, P. (1997), 'Parametrization in laminate design for optimal compliance', *International Journal of Solids and Structures* **34**(4), 415 – 434.

Holland, J. H. (1975), *Adaptation in Natural and Artificial Systems*, first mit press edition, 1992 edn, MIT Press/ Bradford Books, Camebridge Massachusetts.

Hyer, M. and Lee, H. (1991), 'The use of curvilinear fiber format to improve buckling resistance of composite plates with central circular holes', *Composite Structures* **18**(3), 239–261.

Hyer, M. W. and Charette, R. (1991), 'Use of curvilinear fiber format in composite structure design', *AIAA Journal* **29**(6), 1011 – 1015.

IJsselmuiden, S. T., Abdalla, M. M. and Gürdal, Z. (2008), 'Implementation of strength-based failure criteria in the lamination parameter design space', *AIAA Journal* **46**(7), 1826 – 1834.

IJsselmuiden, S. T., Abdalla, M. M. and Gürdal, Z. (2010*a*), 'Optimization of variable-stiffness panels for maximum buckling load using lamination parameters', *AIAA Journal* **48**(1), 134 – 143.

IJsselmuiden, S. T., Abdalla, M. M. and Gürdal, Z. (2010*b*), 'Thermomechanical design optimization of variable stiffness composite panels for buckling', *Journal of Thermal Stresses* **33**(10), 977 – 992.

IJsselmuiden, S. T., Abdalla, M. M., Pilaka, V. K. and Gürdal, Z. (2010), Design of variable stiffness composite structures for advanced fibre placement technology, *in* 'SAMPE 2010, New Materials and Processes for a New Economy'.

IJsselmuiden, S. T., Abdalla, M. M., Seresta, O. and Gürdal, Z. (2009*a*), 'Multi-step blended stacking sequence design of panel assemblies with buckling constraints', *Composites Part B: Engineering* **40**(4), 329–336.

IJsselmuiden, S. T., Abdalla, M. M., Seresta, O. and Gürdal, Z. (2009*b*), 'Multi-step stacking sequence design of panel assemblies with buckling constraints', *Composites Part B: Engineering* **doi:10.1016/j.compositesb.2008.12.002**.

IJsselmuiden, S. T., Campen, J. M. V., Schön, A. and Carosella, S. (2011), Deliverable 15 - design full-scale component, Technical report, AUTOW, Automated Preform Fabrication by Dry Tow Placement, EU Sixth Framework Programme, Thematic Priority Aeronautics and Space, Project no. 030771.

Jegley, D. C., Tatting, B. F. and Gürdal, Z. (2003), Optimization of elastically tailored tow-placed plates with holes, *in* '44$^{\text{th}}$ AIAA/ASME/ASCE/AHS Structures, Structural Dynamics, and Materials Conference', American Institute of Aeronautics and Astronautics, Norfolk, VA.

John D. Anderson, J. (2001), *Fundamentals of Aerodynamics*, 3rd edition edn, McGraw Hill.

Jones, R. M. (1999), *Mechanics of Composite Materials*, second edition edn, Taylor and Francis, Philadelphia.

Kassapoglou, C. (2008), 'Composite plates with two concentric layups under compression', *Composites Part A: Applied Science and Manufacturing* **39**(1), 104–112.

Kassapoglou, C. (2010), *Design and Analysis of Composite Structures with Applications to Aerospace Structures*, John Wiley & Sons Ltd.

Katz, Y., Haftka, R. and Altus, E. (1989), Optimization of fiber directions for increasing the failure load of a plate with a hole, Proceedings of the ASC 4^{th} Technical Conference on Composite Materials, pp. 62 – 71.

Keedwell, E. and Narayanan, A. (2005), *Intelligent Bioinformatics*, John Wiley & Sons Ltd.

Keller, D. (2011), 'Global laminate optimization on geometrically partitioned shell structures', *Structural and Multidisciplinary Optimization* **43**(3), 353 – 368.

Klees, J. C. (2009), Fibre angle orientation optimisation for variable stiffness laminates, Master's thesis, Delft Universtiy of Technology, Kluyverweg 1, 2629 HS Delft, the Netherlands.

Kratmann, K., Sutcliffe, M., Lilleheden, L., Pyrz, R. and Thomsen, O. (2009), 'A novel image analysis procedure for measuring fibre misalignment in unidirectionnal fibre composites', *Composites Science and Technology* **69**, 228 – 238.

Kristinsdottir, B. P. and Zabinsky, Z. B. (1994), 'Including manufacturing tolerances in composite design', Monthly technical progress report, under contracts NAS1-18889 (report No. 58) and NAS1-20013, task 2 (report 4).

Kristinsdottir, B. P., Zabinsky, Z. B., Tuttle, M. E. and Neogi, S. (2001), 'Optimal design of large composite panels with varying loads', *Composite Structures* **51**, 93–102.

Levenstein, V. (1966), 'Binary codes capable of correcting insertions and reversals', *Sov. Phys. Dokl.* **10**, 707 – 710.

Lipton, R. P. (1994), 'On optimal reinforcement of plates and choice of design parameters', *Control and Cybernetics* **23**(3), 481 – 493.

Liu, B. and Haftka, R. T. (2001), Composite wing structural design optimization with continuity constraints, Proceedings of the 42^{nd} AIAA/ASME/ASCE/AHS/ASC Structures, Structural Dynamics, and Materials Conference, Seattle, WA, USA.

Liu, D., Toropov, V., Querin, O. M. and Barton, D. C. (2009*a*), Bilevel optimization of blended composite panels, Proceedings of the 50^{th} AIAA/ASME/ASCE/AMS/ASC Structures, Structural Dynamics, and Maerials Conference, Palm Springs, CA.

Liu, D., Toropov, V., Querin, O. M. and Barton, D. C. (2009*b*), Stacking sequence optimization of composite panels for blending characteristics using lamination parameters, Proceedings of the 8^{th} World Congress on Structural and Multidisciplinary Optimization, Lisbon, Portugal.

Liu, W. and Butler, R. (2007), Optimum buckling design of composite wing cover panels with manufacturing constraints, Proceedings of the 48^{th} AIAA/ASME/ASCE/AHS/ASC Structures, Structural Dynamics, and Materials Conference, Honolulu, Hawaii.

Lo, H.-C. and Hyer, M. W. (2011), Fundamental vibration frequencies of circular and elliptical composite cylinders with circumferentially varying fibre orientation, Proceedings of the 52^{nd} AIAA/ASME/ASCE/AHS/ASC Structures Dynamics and Materials Conference.

Mandelbrot, B. B. (1999), *The Fractal Geometry of Nature, Updated and Augmented*, W.H. Freemand and Company, New York.

Marsh, G. (2009), 'Boeing's 787: trails, tribulations, and restoring the dream', *Reinforced Plastics* **53**(8), 16–21.

Matsuzaki, R. and Todoroki, A. (2007), 'Stacking-sequence optimization using fractal branch-and-bound method for unsymmetrical laminates', *Composite Structures* **78**, 537 – 550.

McMahon, M. T. and Watson, L. T. (2000), 'A distributed genetic algorithm with migration for the design of composite laminate structures', *Parallel algorithms and Applications* **14**, 329–362.

McMahon, M. T., Watson, L. T., Soremekun, G. A., Gürdal, Z. and Haftka, R. T. (1998), 'A fortran 90 genetic algorithm module for composite laminate structure design', *Engineering with Computers* **14**(3), 260–273.

Miki, M. (1982), Material design of composite laminates with required in-plane elastic properties, Progress in Science and Engineering of Composites, ICCM-IV, Tokyo, pp. 1725 – 1731.

Miki, M. and Sugiyama, Y. (1993), 'Optimum design of laminated composite plates using lamination parameters', *AIAA Journal* **31**, 921 – 922.

Nagendra, S., Kodiyalam, S., Davis, J. E. and Parthasarathy, V. (1995), Optimization of tow fiber paths for composite design, number AIAA-95-1275-CP.

Narita, Y. (2003), 'Layerwise optimization for the maximum fundamental frequency of laminated composite plates', *Journal of Sound and Vibration* **263**(5), 1005–1016.

Narita, Y. and Hodgkinson, J. (2005), 'Layerwise optimisation for maximising the fundamental frequencies of point-supported rectangular laminated composite plates', *Composite Structures* **69**(2), 127–135.

Nieto, F., Hernández, S. and Jurado, J. (2009), 'Optimum design of long-span suspension bridges considering aeroelastic and kinematic constraints', *Structural and Multidisciplinary Optimization* **39**, 133 – 151.

Niu, M. C.-Y. (1992), *Composite Airframe Structures*, Practical Design Information and Data, second edition (1993) edn, Conmilit Press LTD.

Olhoff, N. (1989), 'Multicriterion structural optimization via bound formulation and mathematical programming', *Structural Optimization* **1**, 11 – 17.

Papadopoulos, L. and Kassapoglou, C. (2007), 'Shear buckling of rectangular composite plates composed of concentric layups', *Composites Part A: Applied Science and Manufacturing* **38**, 1425 – 1430.

Parnas, L., Oral, S. and Ceyhan, Ü. (2003), 'Optimum design of composite structures with curved fiber courses', *Composites Science and Technology* **63**, 1071 – 1082.

Pilaka, V. K. (2010), Design of realistic variable stiffness composites, Master's thesis, Delft Universtiy of Technology.

Rédei, G. P. (1982), *Genetics*, Macmillan Publishing Co. Inc.

Schatzberg, E. (1994), 'Ideology and technical choice: The decline of the wooden airplane in the united states, 1920-1945', *Technology and Culture* **35**(1), 34 – 69.

Seresta, O., Gürdal, Z., Adams, D. B. and Watson, L. T. (2007), 'Optimal design of composite wing structures with blended laminates', *Composites Part B: Engineering* **38**, 469–480.

Setoodeh, S., Abdalla, M. M. and Gürdal, Z. (2005), 'Combined topology and fiber path design of composite layers using cellular automata', *Structural and Multidisciplinary Optimization* **30**(6), 413–421.

Setoodeh, S., Abdalla, M. M. and Gürdal, Z. (2006*a*), 'Approximate feasible regions for lamination parameters', *Collection of Technical Papers - 11th AIAA/ISSMO Multidisciplinary Analysis and Optimization Conference* **2**, 814–822.

Setoodeh, S., Abdalla, M. M. and Gürdal, Z. (2006*b*), 'Design of variable-stiffness laminates using lamination parameters', *Composites Part B: Engineering* **37**(4–5), 301–309.

Setoodeh, S., Abdalla, M. M., Gürdal, Z. and Tatting, B. F. (2005), Design of variable-stiffness composite laminates for maximum in-plane stiffness using lamination parameters, number AIAA 2005-2083, Proceedings of the 46th AIAA/ASME/ASCE/AHS/ASC Structure, Structural Dynamics and Materials Conference, Austin, Texas.

Setoodeh, S., Abdalla, M. M., IJsselmuiden, S. T. and Gürdal, Z. (2009), 'Design of variable-stiffness composite panels for maximum buckling load', *Composite Structures* **87**(1), 109–117.

Setoodeh, S., Blom, A. W., Abdalla, M. M. and Gürdal, Z. (2006), 'Generating curvilinear fiber paths from lamination parameters distribution', *AIAA-2006-1875, 47th AIAA/ASME/AHS/ASC Structures, Structural Dynamics and Material Conference* .

Setoodeh, S., Gürdal, Z. and Watson, L. T. (2006), 'Design of variable-stiffness composite layers using cellular automata', *Computer methods in applied mechanics and engineering* **195**(9–12), 836–851.

Soremekun, G. A., Gürdal, Z., Kassapoglou, C. and Toni, D. (2002), 'Stacking sequence blending of multiple composite laminates using genetic algorithm', *Composite Structures* **56**(1), 53–62.

Svanberg, K. (1984), On local and global minima in structural optimization, *in* 'New Directions in Optimum Structural Design (Proceedings of the Second International Symposium on Optimum Structural Design)', Tuscon, AZ.

Tatting, B. F. and Gürdal, Z. (2003), Automated finite element analysis of elastically-tailored plates, Contractor Report NASA/CR-2003-212679, National Aeronautics and Space Administration.

Tatting, B. F., Setoodeh, S. and Gürdal, Z. (2005), Enhancements of tow-steering design techniques design of rectangular panel under combined loads, Contractor Report NASA CR-2005-213911, National Aeronautics and Space Administration, Langley Research Center, Hampton, Virginia 23681-2199.

Terada, Y., Todoroki, A. and Shimamura, Y. (2001), 'Stacking sequence optimizations using fractal branch and bound method for laminated composites', *JSME International Journal, Series A* **44**(4), 490 – 498.

Todoroki, A. and Sekishiro, M. (2008), 'Stacking sequence optimization to maximize the buckling load of blade-stiffened panels with strength constraints using the iterative fractal branch and bound method', *Composites Part B: Engineering* **39**, 842 – 850.

Tsai, S. W. and Hahn, H. T. (1980), *Introduction to Composite Materials*, Technomic Publishing Co., Inc.

Tsai, S. W. and Pagano, N. J. (1968), *Invariant properties of composite materials, composite material workshop*, Technomic.

Van Campen, J. M. and Gürdal, Z. (2009), Retrieving variable stiffness laminates from lamination parameters distribution, Proceedings of the 50^{th} AIAA/ASME/ASCE/AHS/ASC Structures, Structural Dynamics and Materials Conference, Palm Springs, CA.

Van Campen, J. M. and IJsselmuiden, S. T. (2011), Deliverable 25 - optimization, Technical report, AUTOW, Automated Preform Fabrication by Dry Tow Placement, EU Sixth Framework Programme, Thematic Priority Aeronautics and Space, Project no. 030771.

Van Campen, J. M., Kassapoglou, C. and Gürdal, Z. (2009), Blended designs for composite plates with two concentric lay-ups under compression, *in* '17$^{\text{th}}$ International Conference on Composite Materials', The British Composites Society.

Van Campen, J. M., Kassapoglou, C. and Gürdal, Z. (2011), Generating realistic laminate fiber angle distributions for optimal variable stiffness laminates. Submitted to Composites Part B: Engineering, Ref. No.: JCOMB-D-11-00115.

Van Campen, J. M., Seresta, O., Abdalla, M. M. and Gürdal, Z. (2008), General blending definition for stacking sequence design of composite laminate structures, Proceedings of the 49^{th} AIAA/ASME/ASCE/AHS/ASC Structures, Structural Dynamics and Materials Conference, Schaumburg, IL, USA.

Warner, E. P. (1922), Metal construction of aircraft, Technical memorandum 153, NACA.

Weaver, P. M. and Nemeth, M. P. (2007), 'Bounds on flexural properties and buckling response for symmetrically laminated composite plates', *Journal of Engineering Mechanics* **133**(11), 1178 – 1191.

Winslow, P. (2009), Synthesis and Optimisation of Free-Form Grid Structures, PhD thesis, University of Cambridge, Trinity Hall.

Wu, K. C., Gürdal, Z. and Starnes, Jr., J. H. (2002), Structural response of compression-loaded,tow-placed, variable stiffness panels, number AIAA 2002-1512, Proceedings of the 43^{rd} AIAA/ASME/ASCE/AHS/ASC Structures, Structural Dynamics and Materials Conference, Denver, CO.

Zabinsky, Z. B. (1994), 'Global optimization for composite structural design', Monthly technical progress report, under contracts NAS1-18889 (report No. 58) and NAS1-20013, task 2 (report 4).

A

MATERIAL INVARIANTS

Material properties of a laminate given in terms of lamination parameters can be computed using the matrices of material invariants:

$$\Gamma_0 = \begin{bmatrix} U_1 & U_4 & 0 \\ U_4 & U_1 & 0 \\ 0 & 0 & U_5 \end{bmatrix}, \Gamma_1 = \begin{bmatrix} U_2 & 0 & 0 \\ 0 & -U_2 & 0 \\ 0 & 0 & 0 \end{bmatrix}, \Gamma_2 = \begin{bmatrix} 0 & 0 & \frac{1}{2}U_2 \\ 0 & 0 & \frac{1}{2}U_2 \\ \frac{1}{2}U_2 & \frac{1}{2}U_2 & 0 \end{bmatrix}$$

$$\Gamma_3 = \begin{bmatrix} U_3 & -U_3 & 0 \\ -U_3 & U_3 & 0 \\ 0 & 0 & -U_3 \end{bmatrix}, \Gamma_4 = \begin{bmatrix} 0 & 0 & U_3 \\ 0 & 0 & -U_3 \\ U_3 & -U_3 & 0 \end{bmatrix}$$

The material invariants, U_i $(i = 1, \ldots, 5)$, are defined in terms of lamina reduced stiffnesses by(**?**):

$$U_1 = \frac{1}{8}(3S_{11} + 3S_{22} + 2S_{12} + 4S_{66})$$

$$U_2 = \frac{1}{2}(S_{11} - S_{22})$$

$$U_3 = \frac{1}{8}(S_{11} + S_{22} - 2S_{12} - 4S_{66})$$

$$U_4 = \frac{1}{8}(S_{11} + S_{22} + 6S_{12} - 4S_{66})$$

$$U_5 = \frac{1}{8}(S_{11} + S_{22} - 2S_{12} + 4S_{66})$$

In turn the lamina reduced stiffnesses in terms are given by:

$$S_{11} = \frac{E_1}{1-\mu_{12}\mu_{21}} \tag{A.1}$$

$$S_{12} = \frac{\mu_{12}E_2}{1-\mu_{12}\mu_{21}} \tag{A.2}$$

$$S_{22} = \frac{E_2}{1-\mu_{12}\mu_{21}} \tag{A.3}$$

$$S_{66} = G_{12} \tag{A.4}$$

$$\tag{A.5}$$

where $\mu_{12} = \frac{E_2}{E_1}\mu_{12}$.

B

MULTI-CHROMOSOMAL GENETIC ALGORITHM

In the research presented in this thesis a multi-chromosomal genetic algorithm (GA) is used, which is described in this appendix. The GA was developed on the basis of the multi-chromosomal GA by McMahon et al. (1998). The GA is suited for the design of composite laminates in terms of discrete fibre orientation angles, and it can use a user-defined number of encoded integer strings to represent a laminate design. The algorithmic representation of composite laminates using integer strings is presented first. Then the reproduction mechanism and the genetic operators of the GA are described.

B.1 ALGORITHMIC REPRESENTATION

A genetic algorithm (GA) is a stochastic and population-based search and optimisation heuristic, GAs are designed to mimic the process of natural selection found in nature. The design space is explored by a population of individuals where the better designs, i.e. the fitter individuals, have a better chance of reproduction and of passing on their genetic coding, i.e. design characteristics, to the next generation.

GAs are a powerful search heuristic in the sense that they can cover the full design space, and are not dependent on a single initial design point. However, GAs require a large number of function evaluations making them only computationally viable for problems that require relatively little computing time. Convergence rates tend to be high using a GA, but because GAs are a probabilistic search heuristic there is a chance they will not converge to the global optimum.

Designs can take the form of one or more integer coded strings called *chromosomes* and the characters in the integer string are called *genes* (Keedwell and

Narayanan 2005, Ahn 2006). A set of chromosomes describing one design is called an *individual*. Multiple individuals are grouped to form one sub-population, and the entire population is formed by a collection of one or more sub-populations. This multi-chromosomal representation, shown in Fig. B.1, is based on the multi-chromosomal representation introduced by (McMahon et al. 1998).

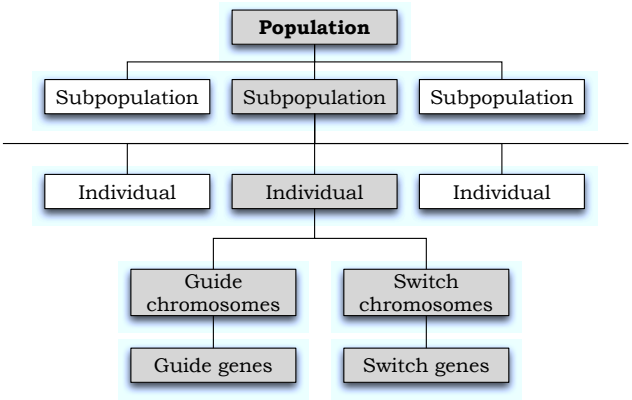

Figure B.1: *Structure of a population with multi-chromosomal individuals after McMahon et al. (1998).*

Two types of chromosomes are distinguished in the implementation of the multi-chromosomal GA described here: *guide*-chromosomes and *switch*-chromosomes. These chromosome types are in every respect identical except for the set of integer values they use for the encoding of the design. The number of guide- and switch chromosomes that constitute one individual is user-determined.

The workings of the multi-chromosomal GA are described using the logical flow of a main programme that implements the GA. User input is used to initialise the population, i.e. the sub-populations and the individuals within. The individuals of each sub-population are then evaluated and ranked according to a fitness function value.

Individuals are selected for reproduction based on a fitness ranking, see section B.2, and a child sub-population is created by applying genetic operators, see section B.3, to the selected individuals. The child sub-population is evaluated, and based on their fitness function value child individuals are passed on to form a new parent sub-population.

The possibility exists to retain a predefined number of the best individuals of the previous parent sub-population; this is known as elitist selection. When multiple sub-populations are used the elite individuals of one sub-population are migrated from one sub-population to the next to diversify the genetic search and prevent

the algorithm from converging towards a local optimum. The creation of child individuals and the construction of new parent populations is repeated until convergence criteria are met, i.e. there is not improvement in the best fitness function value for a user-defined number of iterations.

The flow diagram of the multi-chromosomal GA, as described above, is depicted in Fig. B.2. The GA was implemented in MATLAB® R2009b using a class definition for the work presented in this thesis.

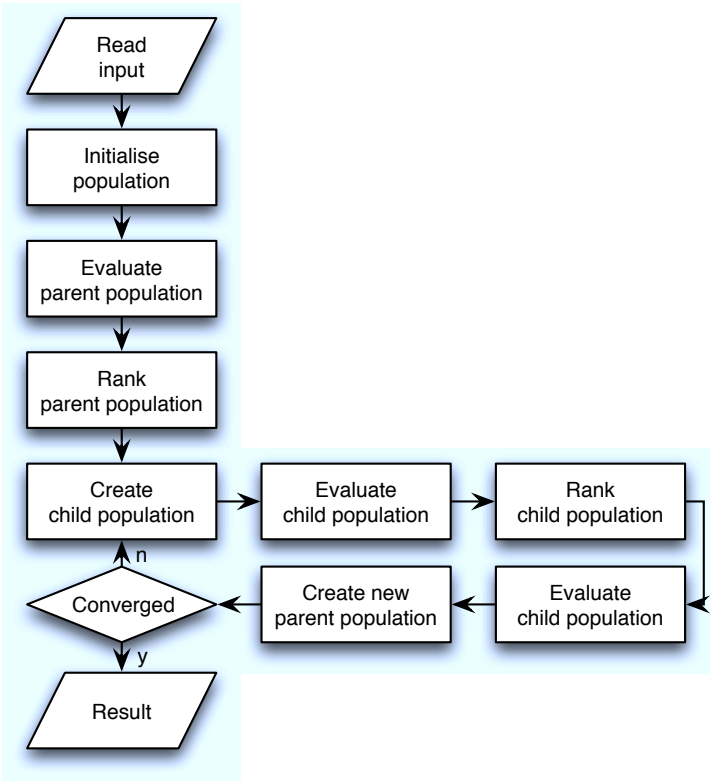

Figure B.2: *Logical flow of the multi-chromosomal GA.*

B.2 FITNESS AND REPRODUCTION

Reproduction is established using the crossover operator, see section B.3. The chance of an individual being selected for reproduction to construct the child

population depends on its fitness function value. The implementation of the multi-chromosomal GA described here uses roulette-wheel selection[1] to determine this chance.

All individuals in the sub-population are ranked according to a fitness function value, the best individual with the best fitness value gets rank 1, and the individual with the worst fitness function value gets rank n, assuming there are n individuals in the sub-population. The probability of the individual to be selected for reproduction is inversely proportional to its rank, and is computed by:

$$p_i = \frac{n - i + 1}{n(n+1)} \tag{B.1}$$

This way the better designs are more likely to propagate into the new generation. Note that individuals cannot be crossed with themselves. After reproduction using the crossover operator, child individuals may be subjected to one of the other genetic operators described in section B.3. The chance of each of these operations is user defined. All child individuals are evaluated and ranked once they have been generated.

A small, user-defined number m of the parent sub-population is retained in the new parent sub-population. The retained individuals are called elite individuals and are the m lowest ranked individuals. The new parent sub-population is completed by the $n - m$ lowest ranked individuals of the generated child individuals. The reproduction cycle is repeated for the new parent sub-population, see Fig. B.2.

Optionally the probability can be defined of k random individuals to migrate from one parent sub-population to the next. The immigrant individuals replace the k least fit individuals of a sub-population. A ring topology is used to structure the migration process (McMahon and Watson 2000).

B.3 GENETIC OPERATORS

Here chromosomes are defined as coded integer strings, where each integer value in the string is referred to as a gene. The multi-chromosomal GA described was designed such that all chromosomes within an individual and throughout the population are of the same length, and such that all individuals contain the same number of chromosomes of each chromosome type. The genetic operators described in this section are applied to individual (pairs) of chromosomes, i.e. crossover location and mutation location differ from chromosome to chromosome.

[1] Each individual is assigned a part of a fictitious roulette wheel proportional to its fitness function value.

All the genetic operators described in this section are assigned a probability of occurrence, which usually is a relatively small value, e.g. 5%. The only exception is the crossover operator which is applied to all individuals to create the child population. All child individuals have a chance that one or more of the genetic operators is applied to them according to the specified probabilities.

Crossover

The crossover operator works on a pair of chromosomes. When two individuals are crossed over the crossover operator is applied sequentially to all chromosome pairs, i.e. the first chromosome of individual A is crossed over with the first chromosome of individual B, the second with the second, etc.

The crossover operator is modelled after the crossover as found to occur in natural chromosomes, see Fig. B.3, during prophase I of meioisis (Rédei 1982). Parts of the chromosomes are exchanged as the crossed chromosomes are moved apart. Crossover can naturally occur at multiple places along two chromosomes, however, here crossover was modelled as a single point event.

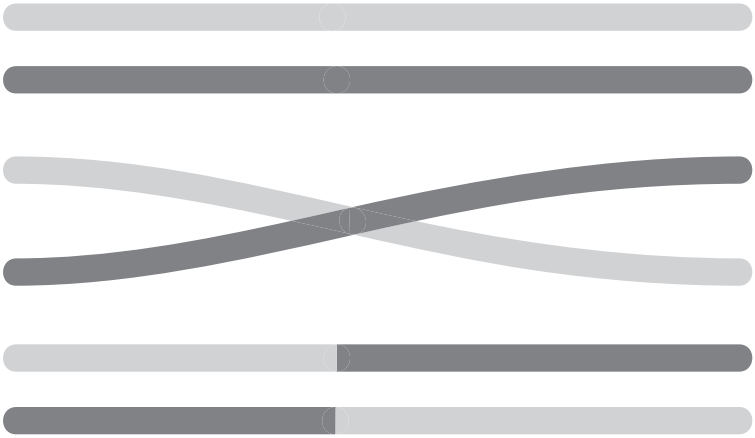

Figure B.3: *Crossover.*

Two chromosomes are considered to demonstrate the crossover procedure as shown:

				Parent A											Parent B						
3	7	5	2	1	4	2	1	3	5	×	7	7	2	4	3	5	1	2	2	1
										⇓											
				Child A						&					Child B						
3	7	5	2	3	5	1	2	2	1		7	7	2	4	1	4	2	1	3	5

A random location for the crossover is determined, in the above example between the 4^{th} and 5^{th} gene, and the parts of the two chromosomes after the crossover location are exchanged.

Permutation

Permutation can be explained as self-crossover over of a chromosome, see Fig. B.4, i.e. the chromosome forms a loop. The chromosome is broken at the location where it crosses itself and the severed parts are recombined. The genetic order of the looped part of the chromosome is reversed, as a result.

Figure B.4: *Permutation.*

Permutation is modelled by determining two random locations along the chromosome. The order of the part between these two chromosomes is reversed as demonstrated:

Before permutation											After permutation									
3	7	5	2	1	4	2	1	3	5	⇒	3	7	2	4	1	2	5	1	3	5

MUTATION

Mutation targets a random single gene of the chromosome. This gene is replaced by a random integer taken from the encoding alphabet used. The mutation procedure is demonstrated as shown below, where the underlined gene is mutated:

Before mutatation											After mutation									
3	7	5	2	1	4	2	1	3	5	⇒	3	7	5	2	1	4	7	1	3	5

PLY-SWAP

The ply-swap operator interchanges two random genes of a chromosome. The ply-swap procedure is demonstrated as shown below, where the swapped genes are underlined:

Before ply-swap											After ply-swap									
3	7	5	2	1	4	2	1	3	5	⇒	3	7	2	2	1	4	5	1	3	5

C

Fibre paths and smeared thickness distribution

In chapter 7 the results that fibre angle results and thickness distribution and fibre path designs that were obtained for several example problems were discussed. The designs that were obtained for three example structures are presented in this appendix: a square plate subjected to bi-axial in-plane compressive load, a square plate subjected to a uni-axial in-plane compressive load, and a curved panel with a hole subjected to a shear load.

Results are presented for the unconstrained case, for the case where the allowable curvature κ_{all} was constrained to 12.5m^{-1} and the case where the allowable curvature was constrained to 4.878m^{-1}. Results were obtained for the objective minimising the minimum least-square error in terms of lamination parameters (LP), Eq. 2.20.

$$f = |\mathbf{V} - \mathbf{V}^*| \quad \text{with} \quad \mathbf{V} = \left\{V_1^{\mathbf{A}}, V_3^{\mathbf{A}}, V_1^{\mathbf{D}}, V_3^{\mathbf{D}}\right\} \tag{2.20}$$

where * denotes the given optimum lamination parameters.Results were obtained for the lay-up $[\pm\theta_1/\ldots/\pm\theta_n]_s$, for n ranging from 1 to 4.

C.1 Square plate in bi-axial compression

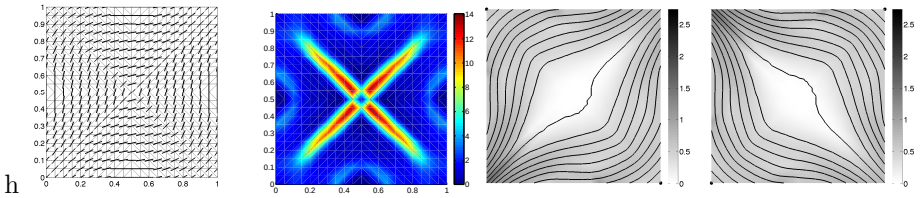

h

(a) θ_1 (b) κ_1 (c) $+\theta_1$ (d) $-\theta_1$

Figure C.1: *Square plate in bi-axial compression: fibre angle distribution, curvature distribution, fibre paths and thickness distributions for $+\theta$ and $-\theta$, $n = 1$ no constraint on curvature.*

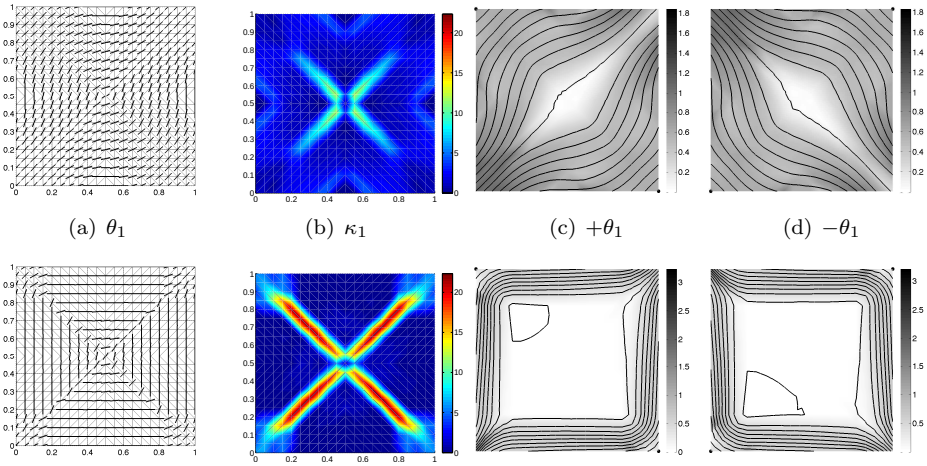

(a) θ_1 (b) κ_1 (c) $+\theta_1$ (d) $-\theta_1$

(e) θ_2 (f) κ_2 (g) $+\theta_2$ (h) $-\theta_2$

Figure C.2: *Square plate in bi-axial compression: fibre angle distribution, curvature distribution, fibre paths and thickness distributions for $+\theta$ and $-\theta$, $n = 2$ no constraint on curvature.*

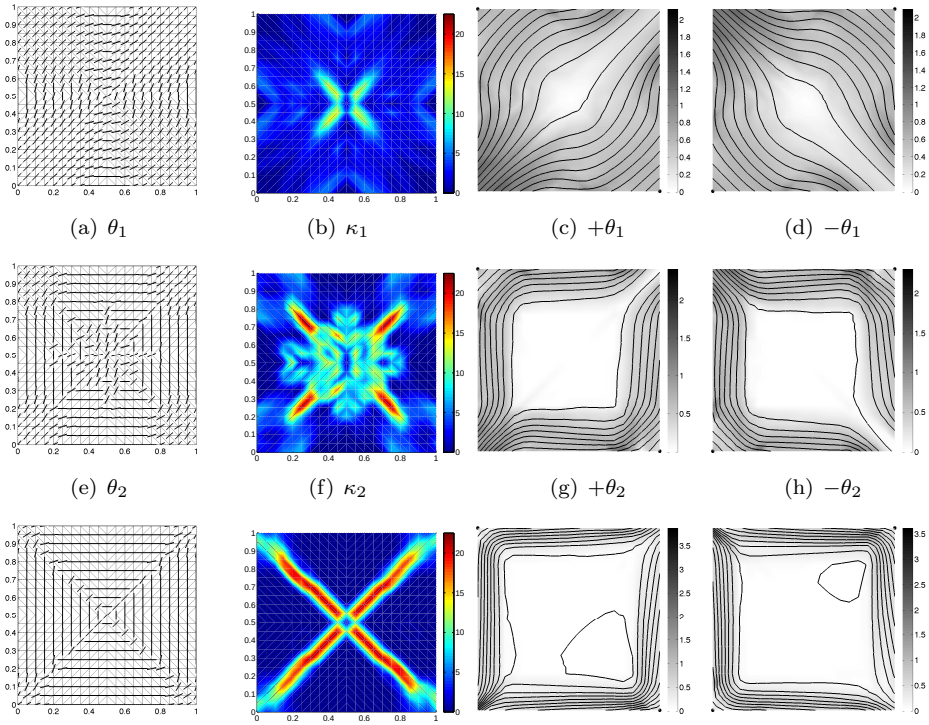

(a) θ_1 (b) κ_1 (c) $+\theta_1$ (d) $-\theta_1$

(e) θ_2 (f) κ_2 (g) $+\theta_2$ (h) $-\theta_2$

(i) θ_3 (j) κ_3 (k) $+\theta_3$ (l) $-\theta_3$

Figure C.3: *Square plate in bi-axial compression: fibre angle distribution, curvature distribution, fibre paths and thickness distributions for $+\theta$ and $-\theta$, $n = 3$ no constraint on curvature.*

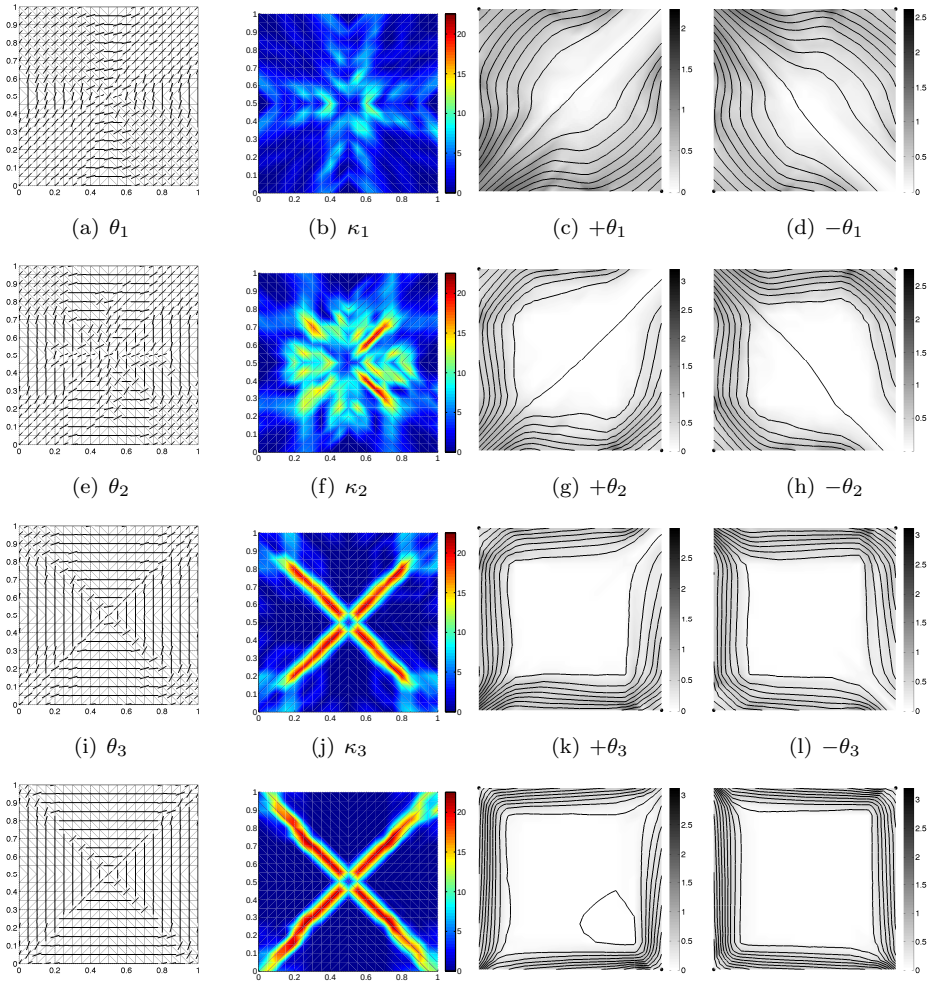

(a) θ_1 (b) κ_1 (c) $+\theta_1$ (d) $-\theta_1$

(e) θ_2 (f) κ_2 (g) $+\theta_2$ (h) $-\theta_2$

(i) θ_3 (j) κ_3 (k) $+\theta_3$ (l) $-\theta_3$

(m) θ_4 (n) κ_4 (o) $+\theta_4$ (p) $-\theta_4$

Figure C.4: *Square plate in bi-axial compression: fibre angle distribution, curvature distribution, fibre paths and thickness distributions for $+\theta$ and $-\theta$, $n = 4$ no constraint on curvature.*

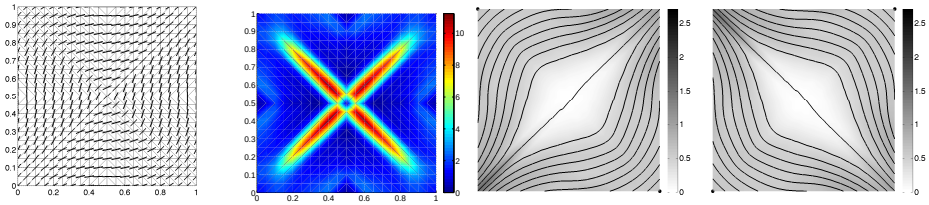

(a) θ_1 (b) κ_1 (c) $+\theta_1$ (d) $-\theta_1$

Figure C.5: *Square plate in bi-axial compression: fibre angle distribution, curvature distribution, fibre paths and thickness distributions for* $+\theta$ *and* $-\theta$*,* $n = 1$*,* $\kappa_{all} = 12.5\text{m}^{-1}$*.*

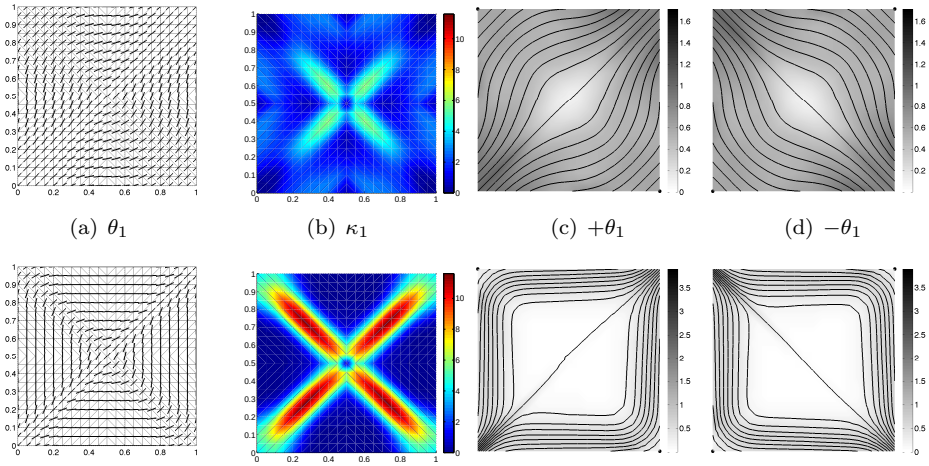

(a) θ_1 (b) κ_1 (c) $+\theta_1$ (d) $-\theta_1$

(e) θ_2 (f) κ_2 (g) $+\theta_2$ (h) $-\theta_2$

Figure C.6: *Square plate in bi-axial compression: fibre angle distribution, curvature distribution, fibre paths and thickness distributions for* $+\theta$ *and* $-\theta$*,* $n = 1$*,* $\kappa_{all} = 12.5\text{m}^{-1}$*.*

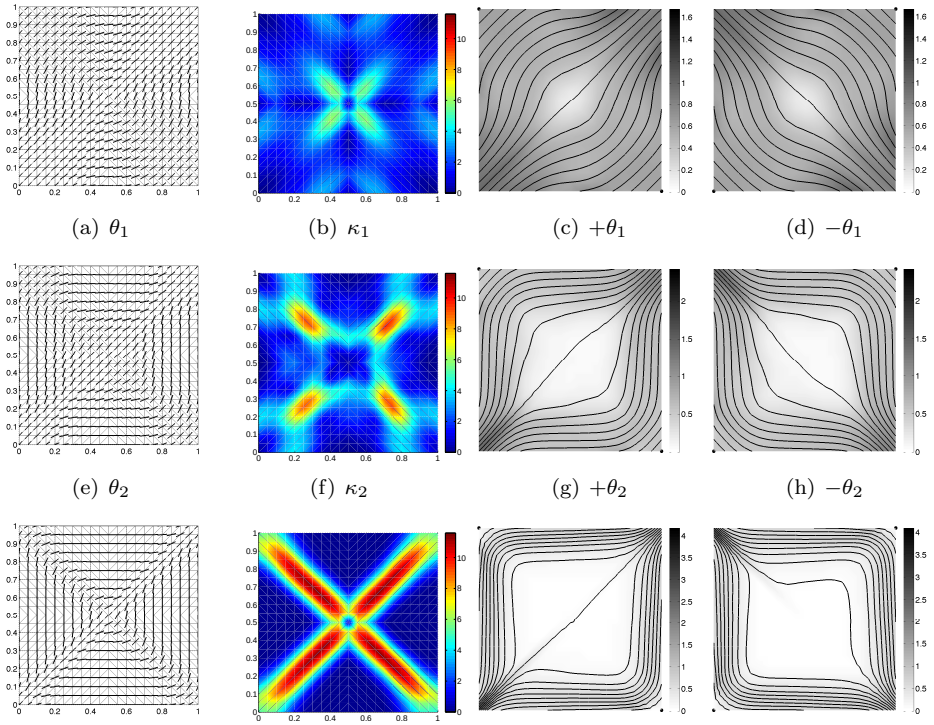

(a) θ_1 (b) κ_1 (c) $+\theta_1$ (d) $-\theta_1$

(e) θ_2 (f) κ_2 (g) $+\theta_2$ (h) $-\theta_2$

(i) θ_3 (j) κ_3 (k) $+\theta_3$ (l) $-\theta_3$

Figure C.7: *Square plate in bi-axial compression: fibre angle distribution, curvature distribution, fibre paths and thickness distributions for $+\theta$ and $-\theta$, $n = 1$, $\kappa_{all} = 12.5\mathrm{m}^{-1}$.*

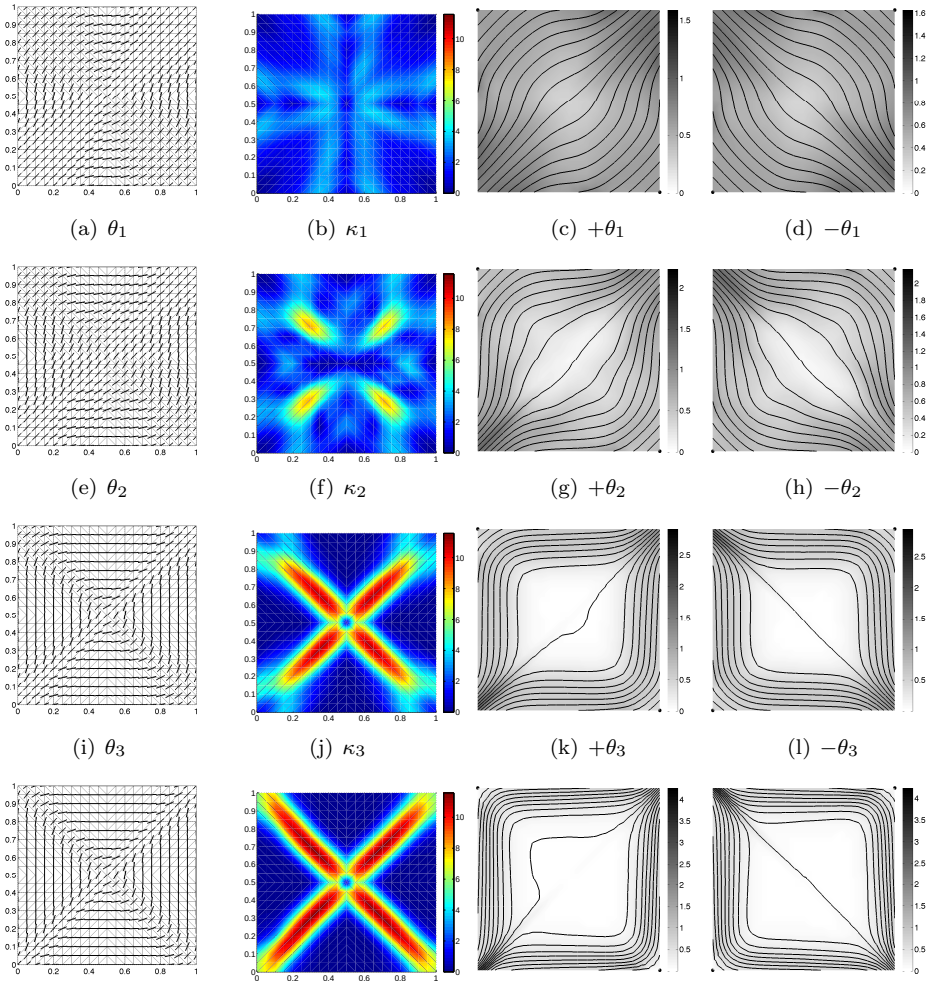

(a) θ_1 (b) κ_1 (c) $+\theta_1$ (d) $-\theta_1$

(e) θ_2 (f) κ_2 (g) $+\theta_2$ (h) $-\theta_2$

(i) θ_3 (j) κ_3 (k) $+\theta_3$ (l) $-\theta_3$

(m) θ_4 (n) κ_4 (o) $+\theta_4$ (p) $-\theta_4$

Figure C.8: *Square plate in bi-axial compression: fibre angle distribution, curvature distribution, fibre paths and thickness distributions for* $+\theta$ *and* $-\theta$*,* $n = 1$*,* $\kappa_{all} = 12.5\text{m}^{-1}$*.*

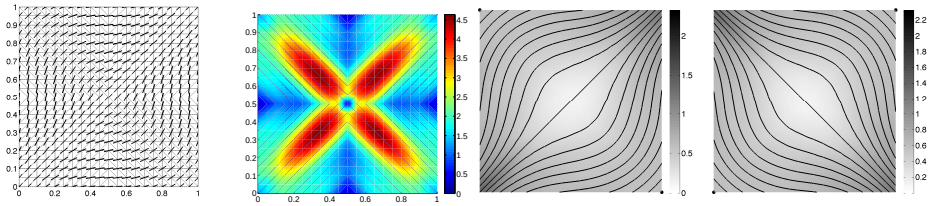

(a) θ_1 (b) κ_1 (c) $+\theta_1$ (d) $-\theta_1$

Figure C.9: *Square plate in bi-axial compression: fibre angle distribution, curvature distribution, fibre paths and thickness distributions for* $+\theta$ *and* $-\theta$*,* $n = 1$*,* $\kappa_{all} = 4.878\text{m}^{-1}$.

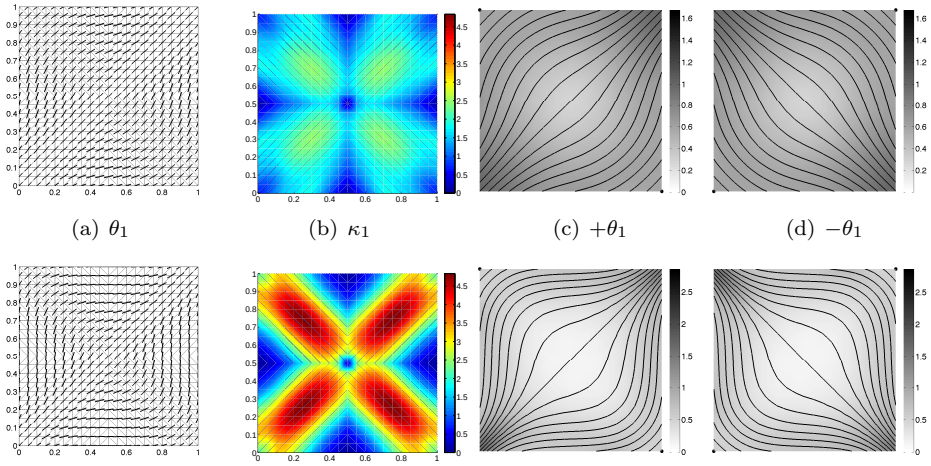

(a) θ_1 (b) κ_1 (c) $+\theta_1$ (d) $-\theta_1$

(e) θ_2 (f) κ_2 (g) $+\theta_2$ (h) $-\theta_2$

Figure C.10: *Square plate in bi-axial compression: fibre angle distribution, curvature distribution, fibre paths and thickness distributions for* $+\theta$ *and* $-\theta$*,* $n = 1$*,* $\kappa_{all} = 4.878\text{m}^{-1}$.

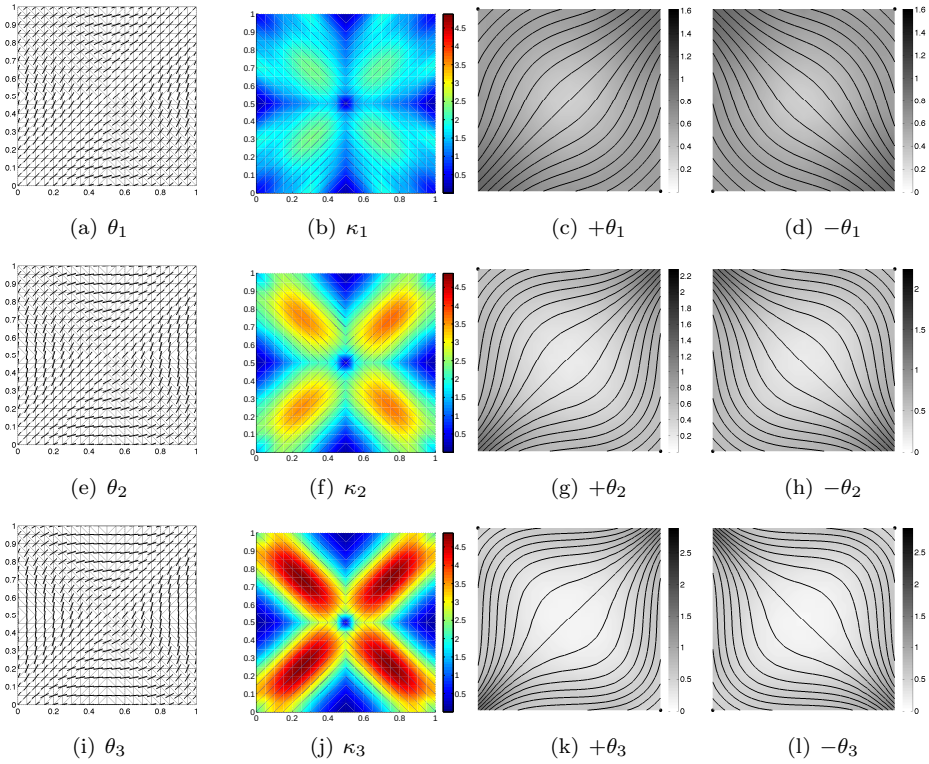

(a) θ_1 (b) κ_1 (c) $+\theta_1$ (d) $-\theta_1$

(e) θ_2 (f) κ_2 (g) $+\theta_2$ (h) $-\theta_2$

(i) θ_3 (j) κ_3 (k) $+\theta_3$ (l) $-\theta_3$

Figure C.11: *Square plate in bi-axial compression: fibre angle distribution, curvature distribution, fibre paths and thickness distributions for* $+\theta$ *and* $-\theta$*,* $n = 1$*,* $\kappa_{all} = 4.878\text{m}^{-1}$.

C.2 SQUARE PLATE IN UNI-AXIAL COMPRESSION

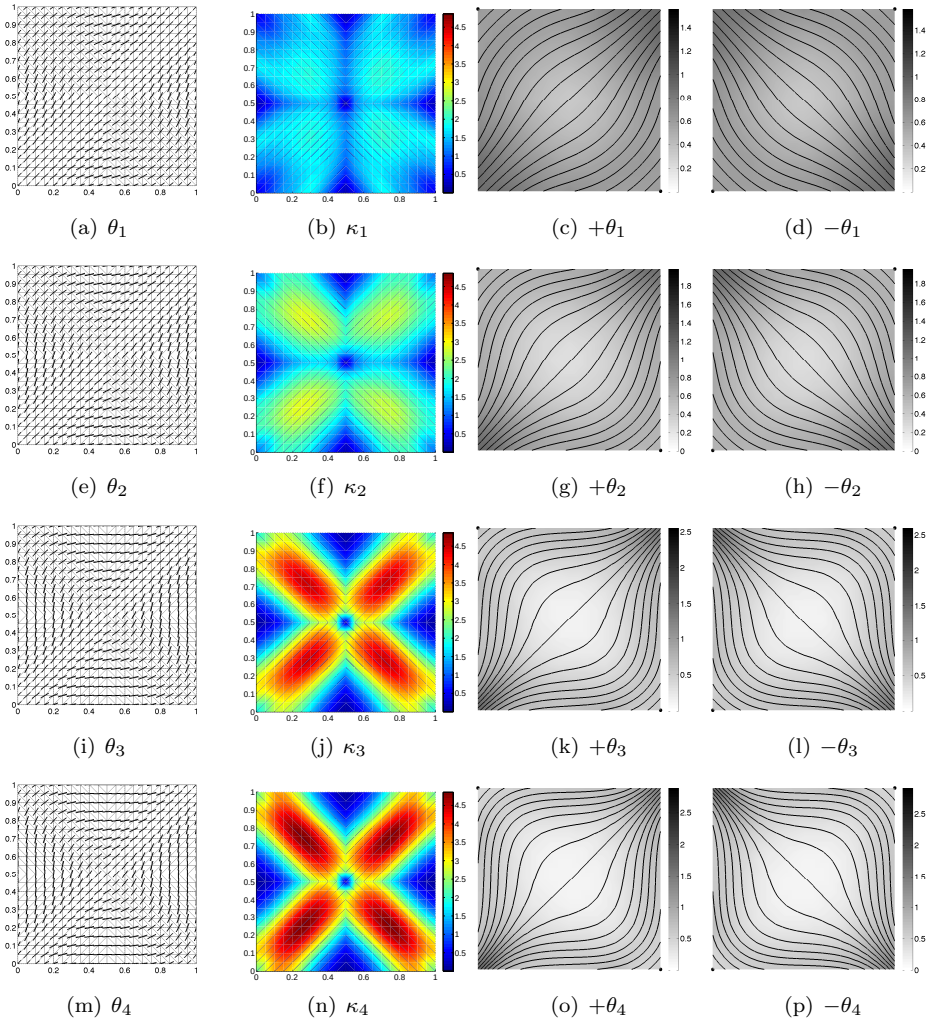

(a) θ_1 (b) κ_1 (c) $+\theta_1$ (d) $-\theta_1$

(e) θ_2 (f) κ_2 (g) $+\theta_2$ (h) $-\theta_2$

(i) θ_3 (j) κ_3 (k) $+\theta_3$ (l) $-\theta_3$

(m) θ_4 (n) κ_4 (o) $+\theta_4$ (p) $-\theta_4$

Figure C.12: *Square plate in bi-axial compression: fibre angle distribution, curvature distribution, fibre paths and thickness distributions for* $+\theta$ *and* $-\theta$*,* $n = 1$*,* $\kappa_{all} = 4.878\text{m}^{-1}$.

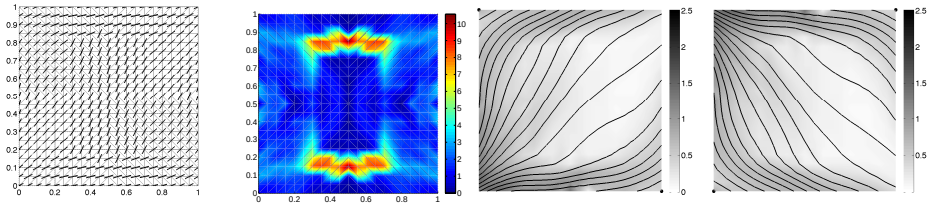

(a) θ_1 (b) κ_1 (c) $+\theta_1$ (d) $-\theta_1$

Figure C.13: *Square plate in uni-axial compression: fibre angle distribution, curvature distribution, fibre paths and thickness distributions for $+\theta$ and $-\theta$, $n = 1$ no constraint on curvature.*

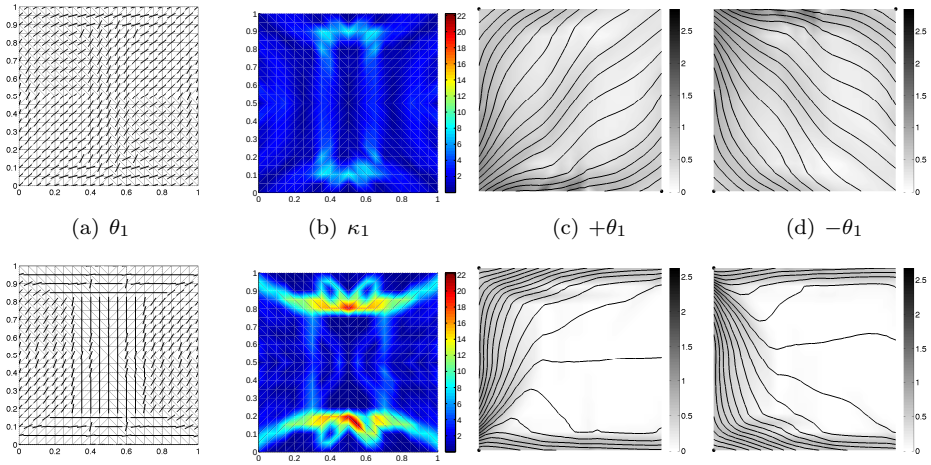

(a) θ_1 (b) κ_1 (c) $+\theta_1$ (d) $-\theta_1$

(e) θ_2 (f) κ_2 (g) $+\theta_2$ (h) $-\theta_2$

Figure C.14: *Square plate in uni-axial compression: fibre angle distribution, curvature distribution, fibre paths and thickness distributions for $+\theta$ and $-\theta$, $n = 2$ no constraint on curvature.*

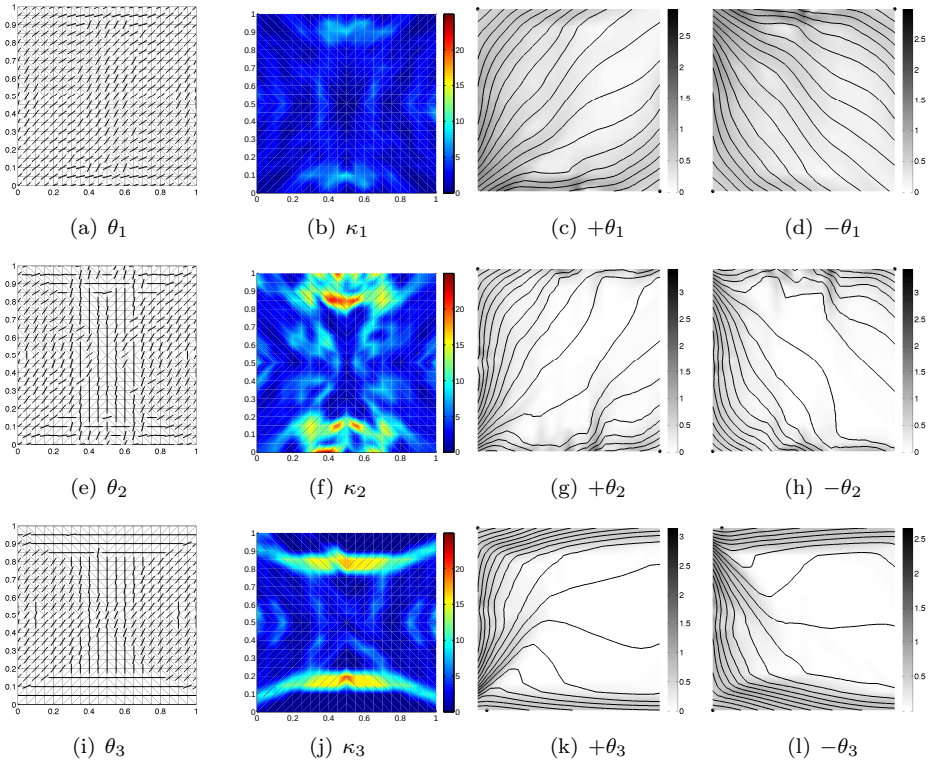

(a) θ_1 (b) κ_1 (c) $+\theta_1$ (d) $-\theta_1$

(e) θ_2 (f) κ_2 (g) $+\theta_2$ (h) $-\theta_2$

(i) θ_3 (j) κ_3 (k) $+\theta_3$ (l) $-\theta_3$

Figure C.15: *Square plate in uni-axial compression: fibre angle distribution, curvature distribution, fibre paths and thickness distributions for $+\theta$ and $-\theta$, $n = 3$ no constraint on curvature.*

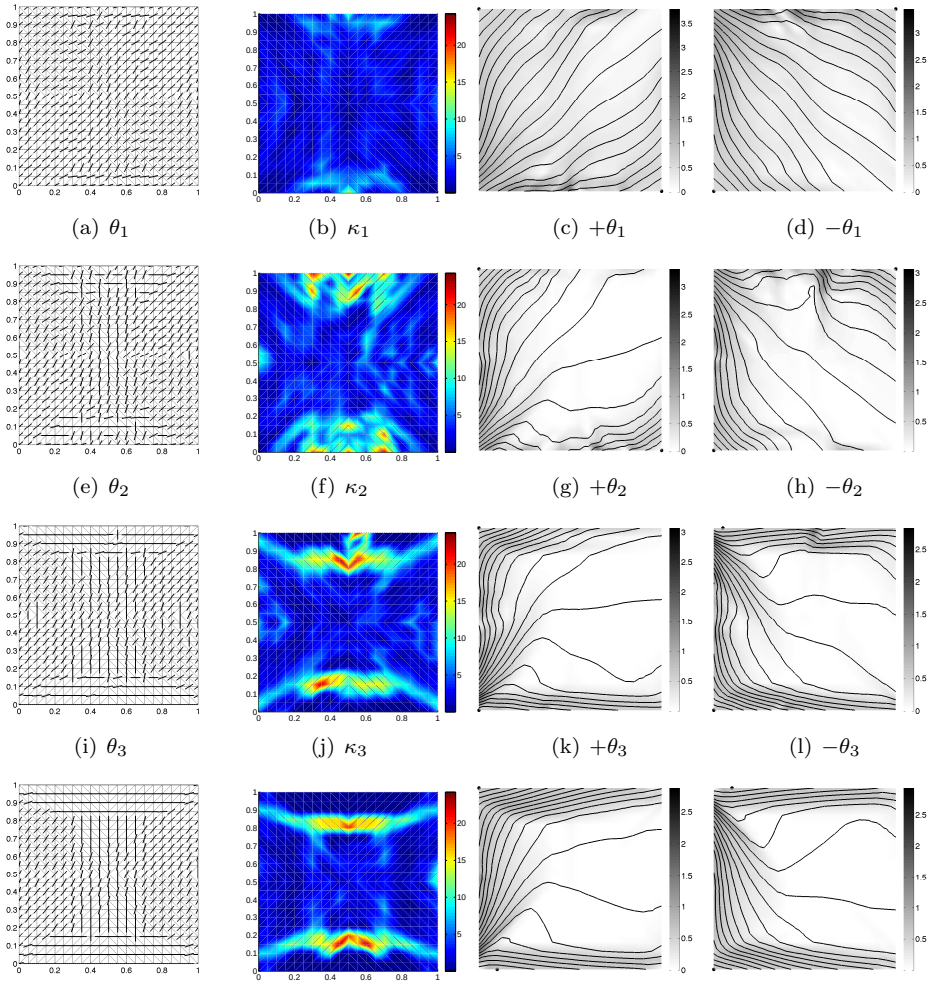

(a) θ_1 (b) κ_1 (c) $+\theta_1$ (d) $-\theta_1$

(e) θ_2 (f) κ_2 (g) $+\theta_2$ (h) $-\theta_2$

(i) θ_3 (j) κ_3 (k) $+\theta_3$ (l) $-\theta_3$

(m) θ_4 (n) κ_4 (o) $+\theta_4$ (p) $-\theta_4$

Figure C.16: *Square plate in uni-axial compression: fibre angle distribution, curvature distribution, fibre paths and thickness distributions for $+\theta$ and $-\theta$, $n = 4$ no constraint on curvature.*

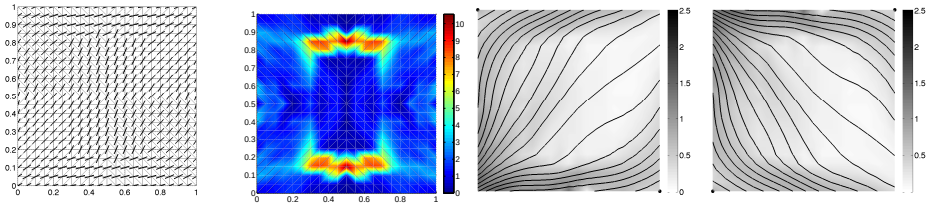

(a) θ_1 (b) κ_1 (c) $+\theta_1$ (d) $-\theta_1$

Figure C.17: *Square plate in uni-axial compression: fibre angle distribution, curvature distribution, fibre paths and thickness distributions for* $+\theta$ *and* $-\theta$*,* $n = 1$*,* $\kappa_{all} = 12.5\text{m}^{-1}$.

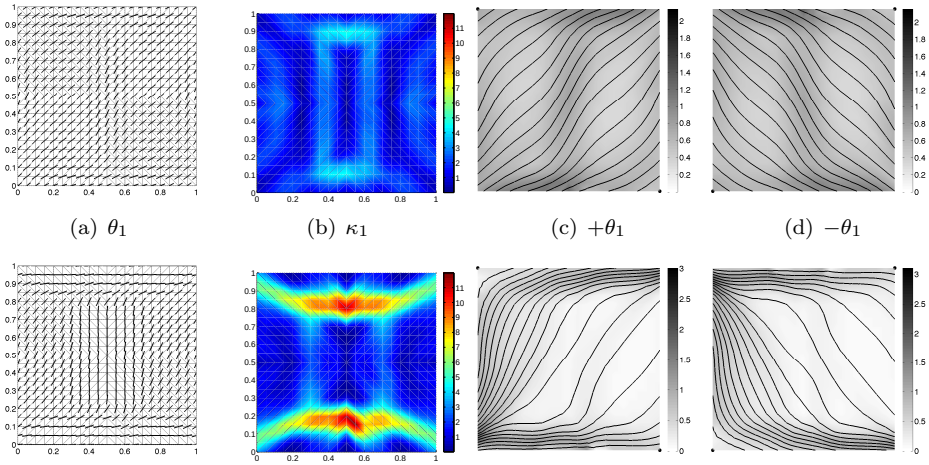

(a) θ_1 (b) κ_1 (c) $+\theta_1$ (d) $-\theta_1$

(e) θ_2 (f) κ_2 (g) $+\theta_2$ (h) $-\theta_2$

Figure C.18: *Square plate in uni-axial compression: fibre angle distribution, curvature distribution, fibre paths and thickness distributions for* $+\theta$ *and* $-\theta$*,* $n = 1$*,* $\kappa_{all} = 12.5\text{m}^{-1}$.

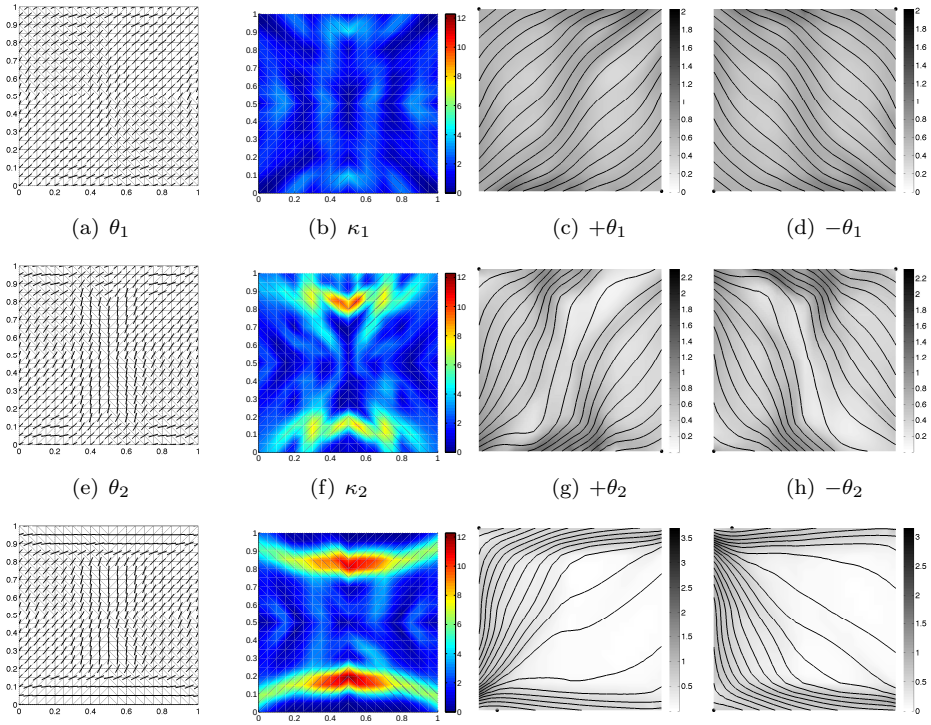

(a) θ_1 (b) κ_1 (c) $+\theta_1$ (d) $-\theta_1$

(e) θ_2 (f) κ_2 (g) $+\theta_2$ (h) $-\theta_2$

(i) θ_3 (j) κ_3 (k) $+\theta_3$ (l) $-\theta_3$

Figure C.19: *Square plate in uni-axial compression: fibre angle distribution, curvature distribution, fibre paths and thickness distributions for* $+\theta$ *and* $-\theta$*,* $n = 1$*,* $\kappa_{all} = 12.5\text{m}^{-1}$.

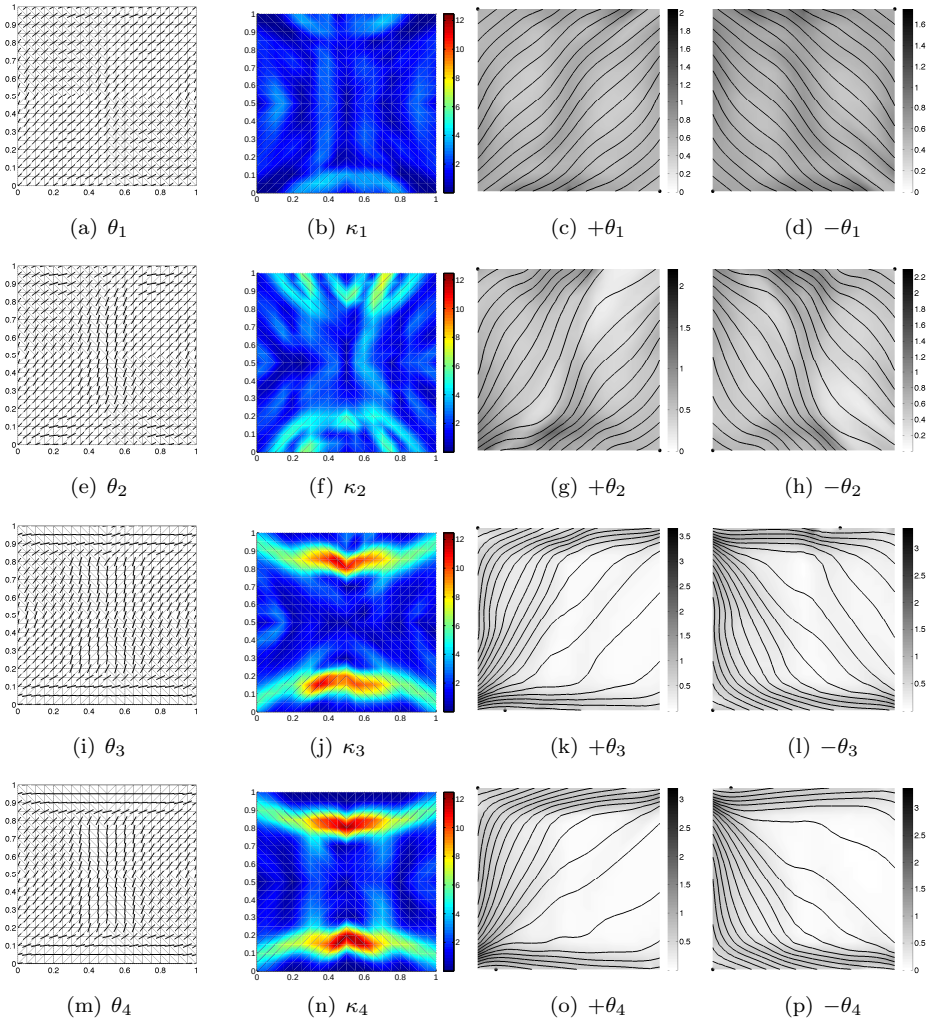

(a) θ_1 (b) κ_1 (c) $+\theta_1$ (d) $-\theta_1$

(e) θ_2 (f) κ_2 (g) $+\theta_2$ (h) $-\theta_2$

(i) θ_3 (j) κ_3 (k) $+\theta_3$ (l) $-\theta_3$

(m) θ_4 (n) κ_4 (o) $+\theta_4$ (p) $-\theta_4$

Figure C.20: *Square plate in uni-axial compression: fibre angle distribution, curvature distribution, fibre paths and thickness distributions for* $+\theta$ *and* $-\theta$*,* $n = 1$*,* $\kappa_{all} = 12.5\text{m}^{-1}$.

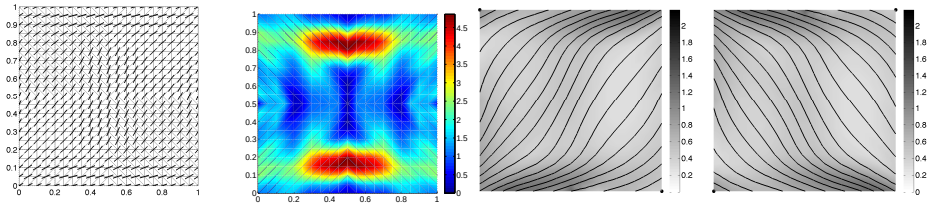

(a) θ_1 (b) κ_1 (c) $+\theta_1$ (d) $-\theta_1$

Figure C.21: *Square plate in uni-axial compression: fibre angle distribution, curvature distribution, fibre paths and thickness distributions for* $+\theta$ *and* $-\theta$*,* $n = 1$*,* $\kappa_{all} = 4.878\text{m}^{-1}$*.*

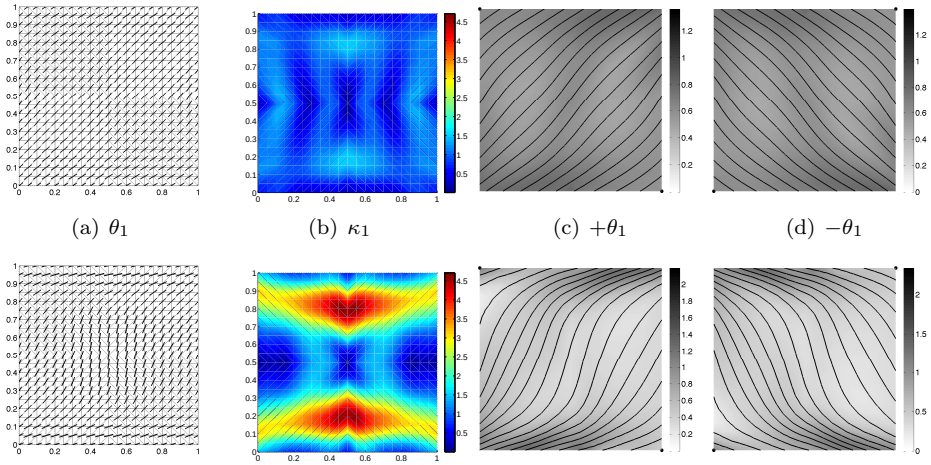

(a) θ_1 (b) κ_1 (c) $+\theta_1$ (d) $-\theta_1$

(e) θ_2 (f) κ_2 (g) $+\theta_2$ (h) $-\theta_2$

Figure C.22: *Square plate in uni-axial compression: fibre angle distribution, curvature distribution, fibre paths and thickness distributions for* $+\theta$ *and* $-\theta$*,* $n = 1$*,* $\kappa_{all} = 4.878\text{m}^{-1}$*.*

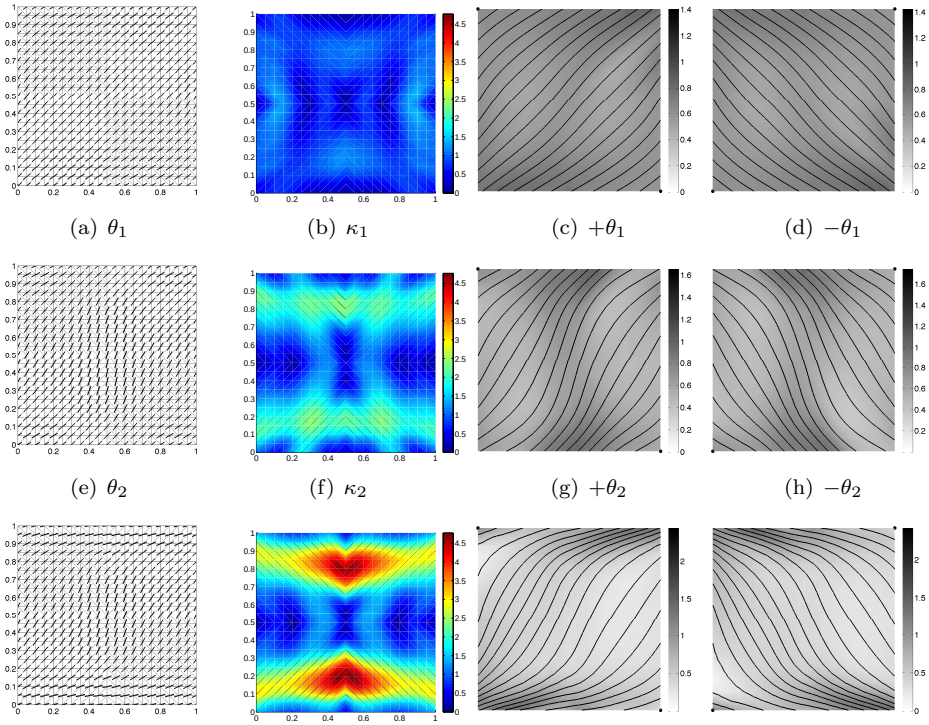

(a) θ_1 (b) κ_1 (c) $+\theta_1$ (d) $-\theta_1$

(e) θ_2 (f) κ_2 (g) $+\theta_2$ (h) $-\theta_2$

(i) θ_3 (j) κ_3 (k) $+\theta_3$ (l) $-\theta_3$

Figure C.23: *Square plate in uni-axial compression: fibre angle distribution, curvature distribution, fibre paths and thickness distributions for* $+\theta$ *and* $-\theta$*,* $n = 1$*,* $\kappa_{all} = 4.878\text{m}^{-1}$.

C.3 CURVED PANEL WITH A HOLE LOADED IN COMPRESSION AND SHEAR

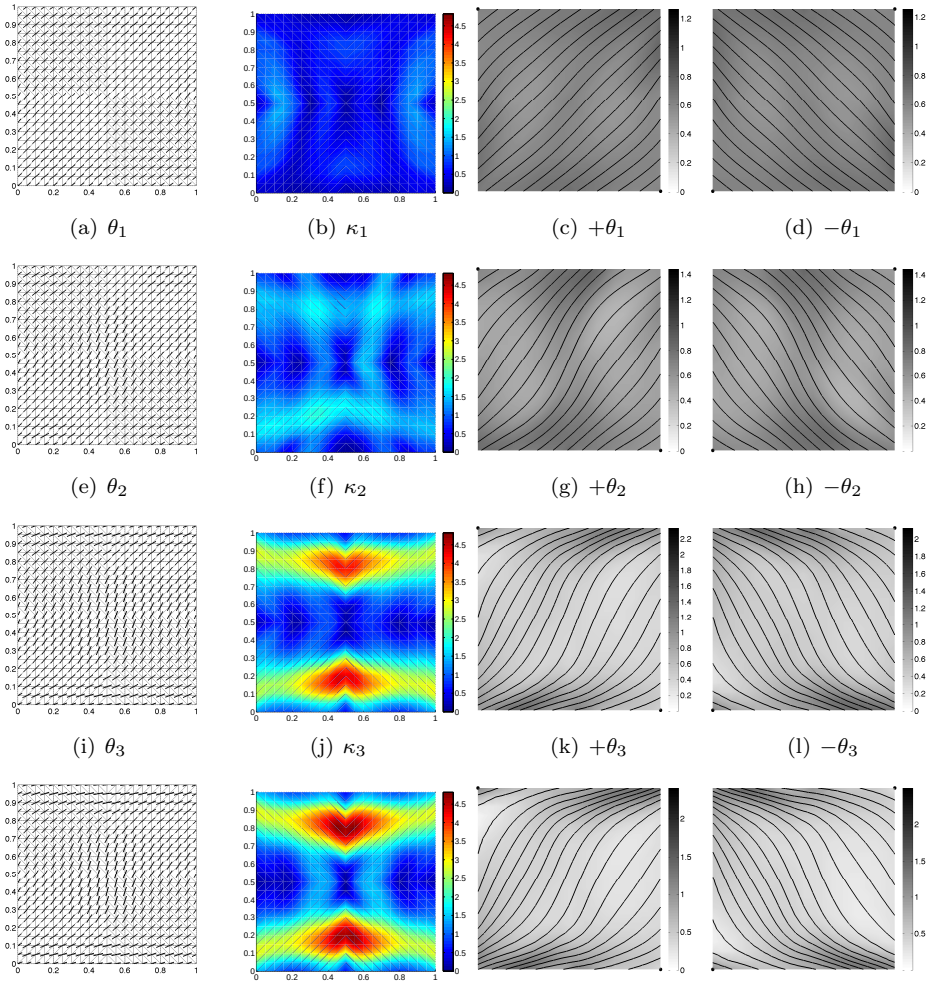

(a) θ_1 (b) κ_1 (c) $+\theta_1$ (d) $-\theta_1$

(e) θ_2 (f) κ_2 (g) $+\theta_2$ (h) $-\theta_2$

(i) θ_3 (j) κ_3 (k) $+\theta_3$ (l) $-\theta_3$

(m) θ_4 (n) κ_4 (o) $+\theta_4$ (p) $-\theta_4$

Figure C.24: *Square plate in uni-axial compression: fibre angle distribution, curvature distribution, fibre paths and thickness distributions for* $+\theta$ *and* $-\theta$*,* $n = 1$*,* $\kappa_{all} = 4.878\text{m}^{-1}$.

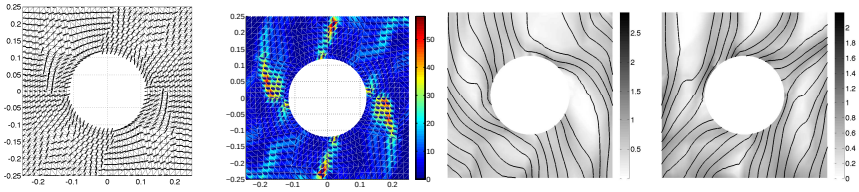

(a) θ_1 (b) κ_1 (c) $+\theta_1$ (d) $-\theta_1$

Figure C.25: *Curved panel with a hole loaded in compression and shear: fibre angle distribution, curvature distribution, fibre paths and thickness distributions for* $+\theta$ *and* $-\theta$*,* $n = 1$ *no constraint on curvature.*

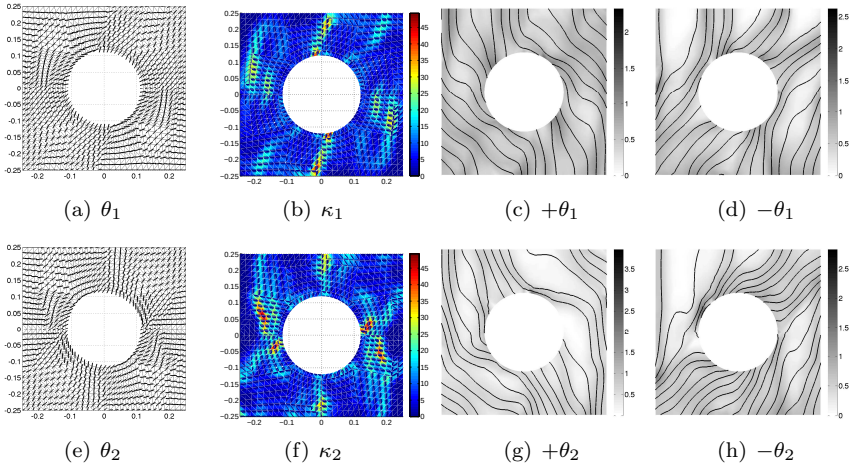

(a) θ_1 (b) κ_1 (c) $+\theta_1$ (d) $-\theta_1$

(e) θ_2 (f) κ_2 (g) $+\theta_2$ (h) $-\theta_2$

Figure C.26: *Curved panel with a hole loaded in compression and shear: fibre angle distribution, curvature distribution, fibre paths and thickness distributions for* $+\theta$ *and* $-\theta$*,* $n = 2$ *no constraint on curvature.*

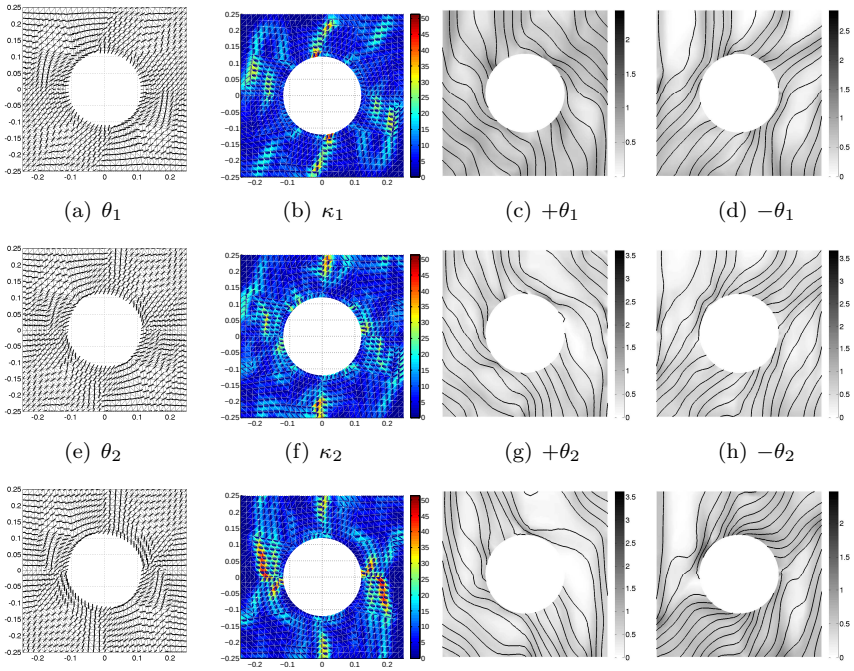

(a) θ_1 (b) κ_1 (c) $+\theta_1$ (d) $-\theta_1$

(e) θ_2 (f) κ_2 (g) $+\theta_2$ (h) $-\theta_2$

(i) θ_3 (j) κ_3 (k) $+\theta_3$ (l) $-\theta_3$

Figure C.27: *Curved panel with a hole loaded in compression and shear: fibre angle distribution, curvature distribution, fibre paths and thickness distributions for $+\theta$ and $-\theta$, $n = 3$ no constraint on curvature.*

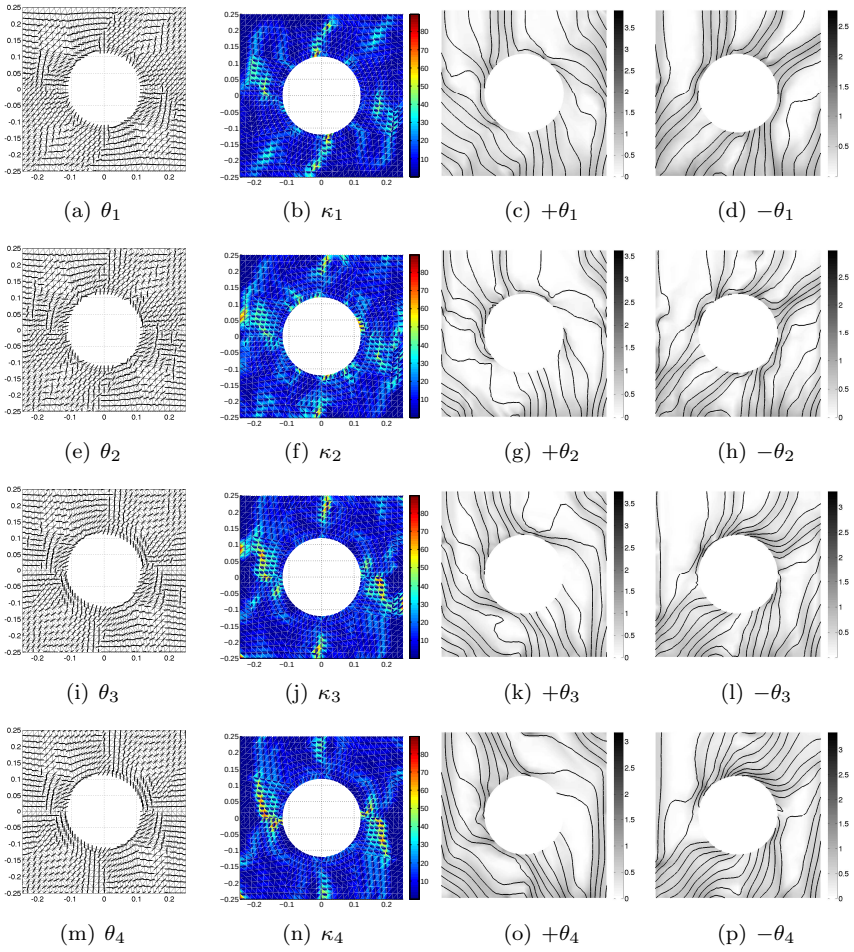

(a) θ_1 (b) κ_1 (c) $+\theta_1$ (d) $-\theta_1$

(e) θ_2 (f) κ_2 (g) $+\theta_2$ (h) $-\theta_2$

(i) θ_3 (j) κ_3 (k) $+\theta_3$ (l) $-\theta_3$

(m) θ_4 (n) κ_4 (o) $+\theta_4$ (p) $-\theta_4$

Figure C.28: *Curved panel with a hole loaded in compression and shear: fibre angle distribution, curvature distribution, fibre paths and thickness distributions for* $+\theta$ *and* $-\theta$*,* $n = 4$ *no constraint on curvature.*

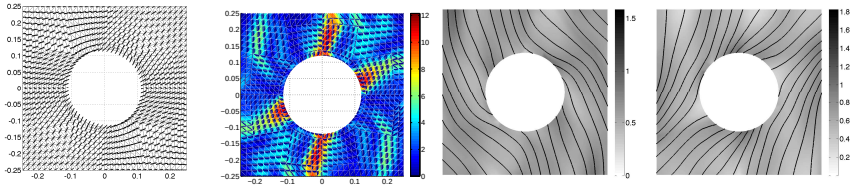

(a) θ_1 (b) κ_1 (c) $+\theta_1$ (d) $-\theta_1$

Figure C.29: *Curved panel with a hole loaded in compression and shear: fibre angle distribution, curvature distribution, fibre paths and thickness distributions for* $+\theta$ *and* $-\theta$*,* $n = 1$*,* $\kappa_{all} = 12.5\text{m}^{-1}$*.*

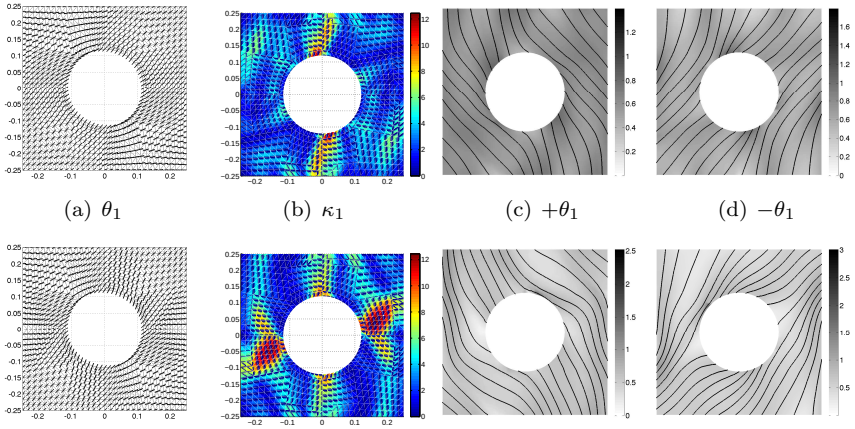

(a) θ_1 (b) κ_1 (c) $+\theta_1$ (d) $-\theta_1$

(e) θ_2 (f) κ_2 (g) $+\theta_2$ (h) $-\theta_2$

Figure C.30: *Curved panel with a hole loaded in compression and shear: fibre angle distribution, curvature distribution, fibre paths and thickness distributions for* $+\theta$ *and* $-\theta$*,* $n = 1$*,* $\kappa_{all} = 12.5\text{m}^{-1}$*.*

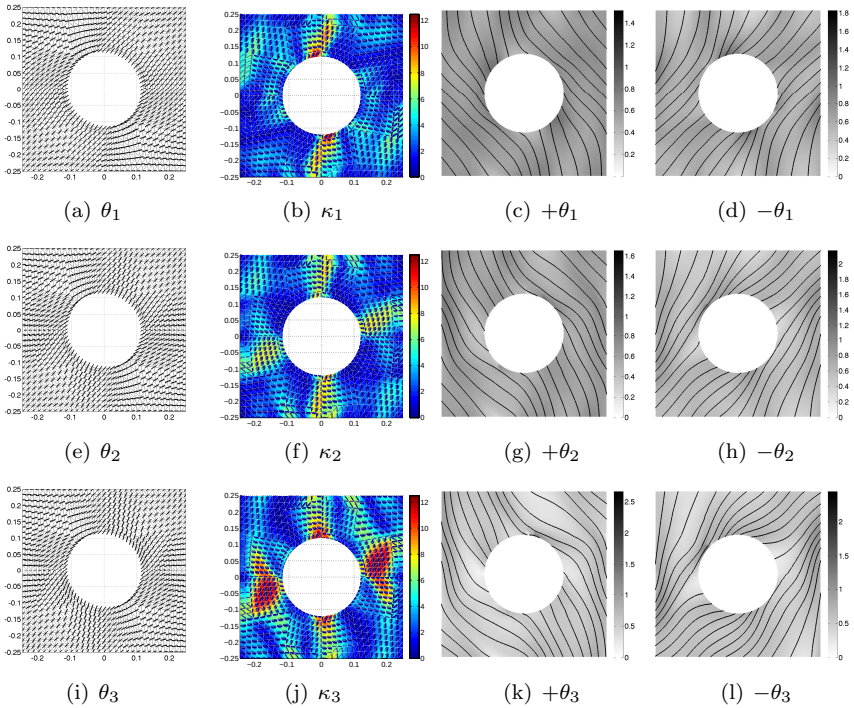

(a) θ_1 (b) κ_1 (c) $+\theta_1$ (d) $-\theta_1$

(e) θ_2 (f) κ_2 (g) $+\theta_2$ (h) $-\theta_2$

(i) θ_3 (j) κ_3 (k) $+\theta_3$ (l) $-\theta_3$

Figure C.31: *Curved panel with a hole loaded in compression and shear: fibre angle distribution, curvature distribution, fibre paths and thickness distributions for* $+\theta$ *and* $-\theta$*,* $n = 1$*,* $\kappa_{all} = 12.5\text{m}^{-1}$.

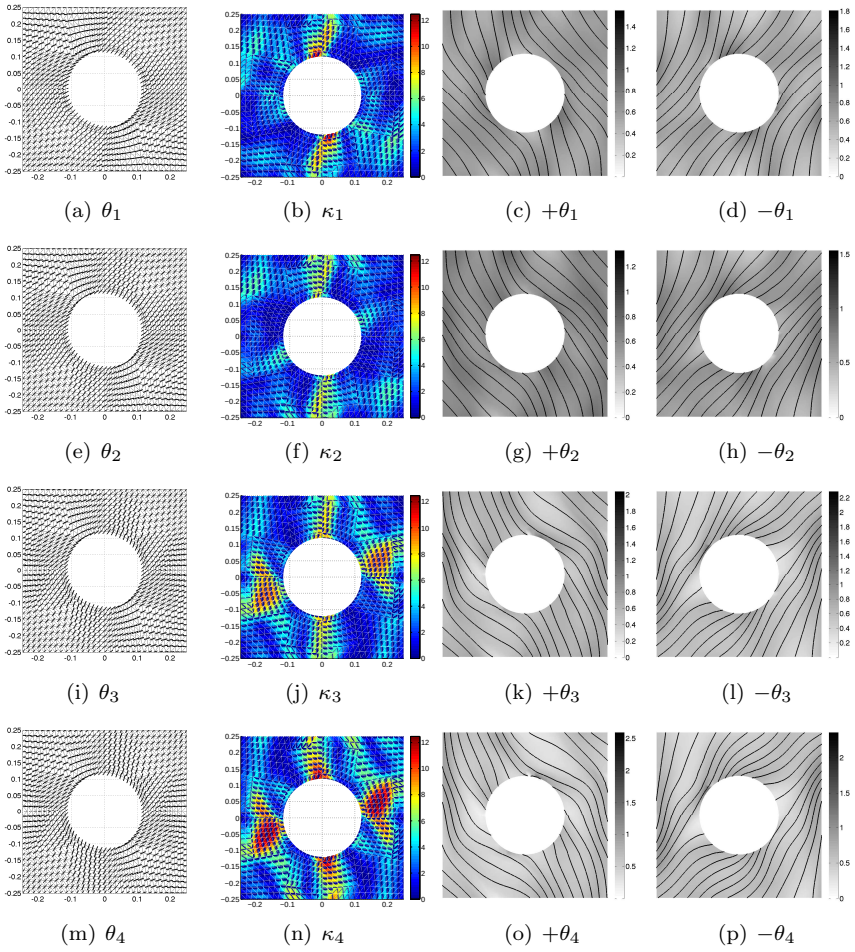

(a) θ_1 (b) κ_1 (c) $+\theta_1$ (d) $-\theta_1$

(e) θ_2 (f) κ_2 (g) $+\theta_2$ (h) $-\theta_2$

(i) θ_3 (j) κ_3 (k) $+\theta_3$ (l) $-\theta_3$

(m) θ_4 (n) κ_4 (o) $+\theta_4$ (p) $-\theta_4$

Figure C.32: *Curved panel with a hole loaded in compression and shear: fibre angle distribution, curvature distribution, fibre paths and thickness distributions for* $+\theta$ *and* $-\theta$*,* $n = 1$*,* $\kappa_{all} = 12.5\text{m}^{-1}$.

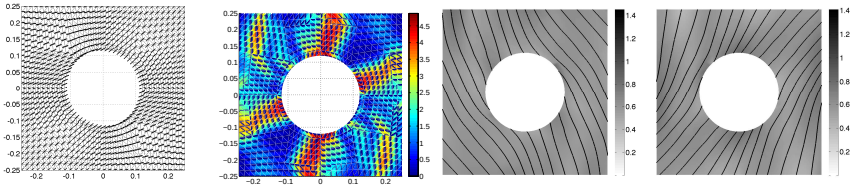

(a) θ_1 (b) κ_1 (c) $+\theta_1$ (d) $-\theta_1$

Figure C.33: *Curved panel with a hole loaded in compression and shear: fibre angle distribution, curvature distribution, fibre paths and thickness distributions for* $+\theta$ *and* $-\theta$*,* $n = 1$*,* $\kappa_{all} = 4.878\text{m}^{-1}$*.*

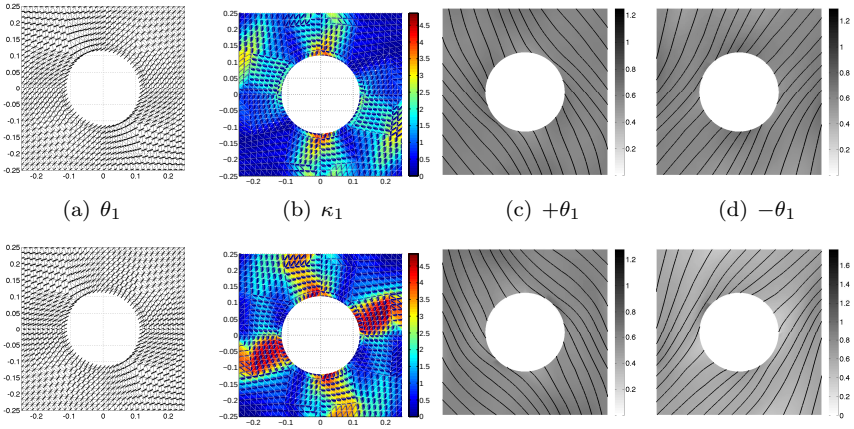

(a) θ_1 (b) κ_1 (c) $+\theta_1$ (d) $-\theta_1$

(e) θ_2 (f) κ_2 (g) $+\theta_2$ (h) $-\theta_2$

Figure C.34: *Curved panel with a hole loaded in compression and shear: fibre angle distribution, curvature distribution, fibre paths and thickness distributions for* $+\theta$ *and* $-\theta$*,* $n = 1$*,* $\kappa_{all} = 4.878\text{m}^{-1}$*.*

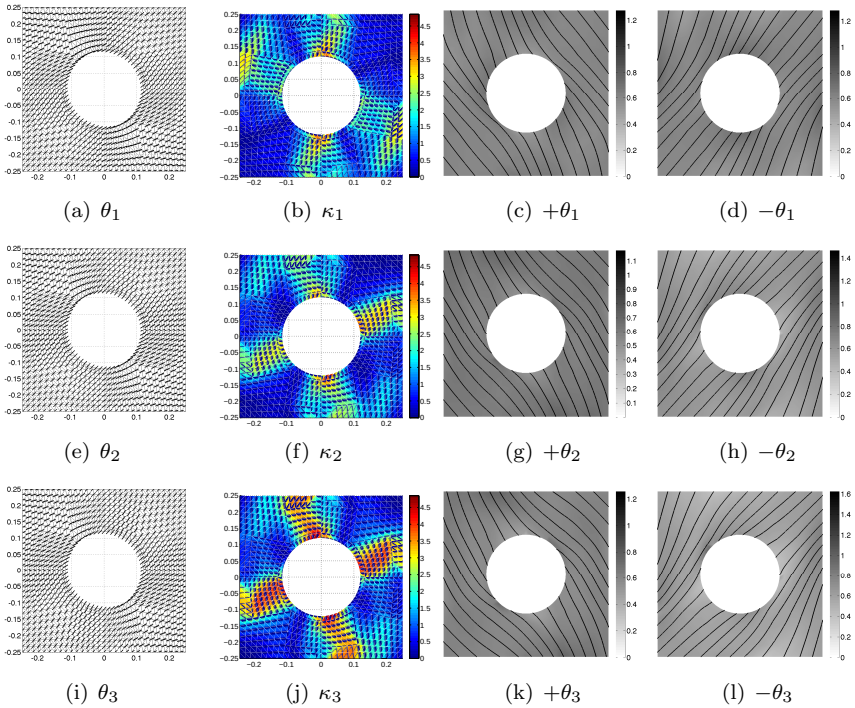

(a) θ_1 (b) κ_1 (c) $+\theta_1$ (d) $-\theta_1$

(e) θ_2 (f) κ_2 (g) $+\theta_2$ (h) $-\theta_2$

(i) θ_3 (j) κ_3 (k) $+\theta_3$ (l) $-\theta_3$

Figure C.35: *Curved panel with a hole loaded in compression and shear: fibre angle distribution, curvature distribution, fibre paths and thickness distributions for* $+\theta$ *and* $-\theta$*,* $n = 1$*,* $\kappa_{all} = 4.878\text{m}^{-1}$.

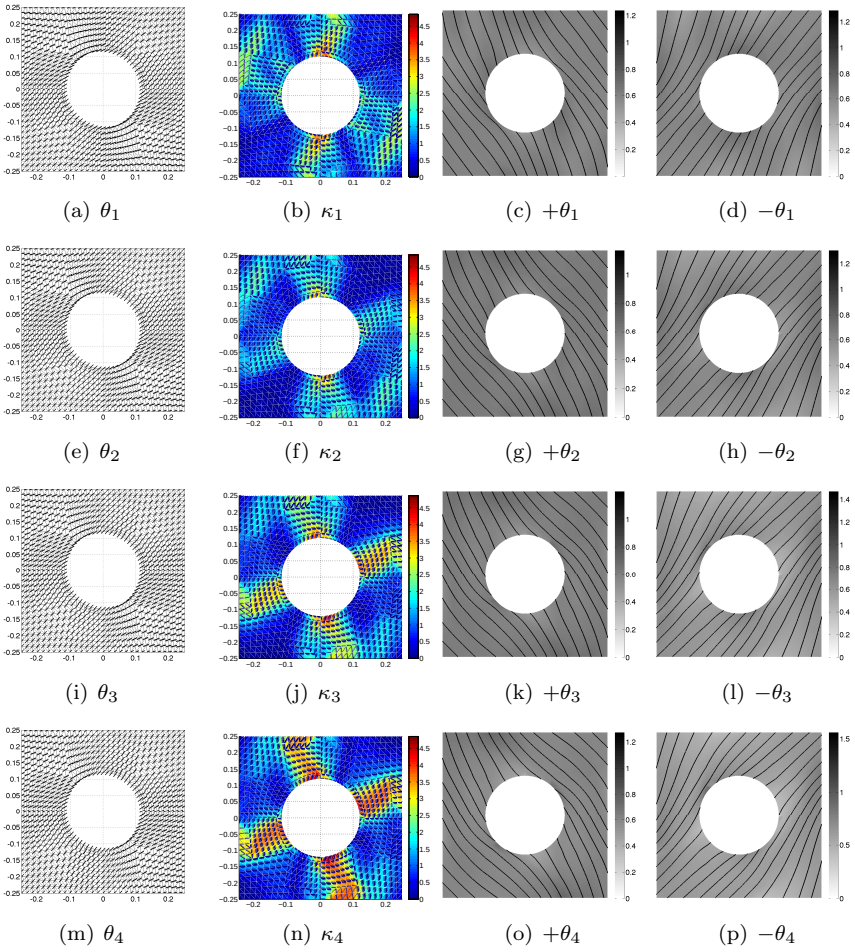

(a) θ_1 (b) κ_1 (c) $+\theta_1$ (d) $-\theta_1$

(e) θ_2 (f) κ_2 (g) $+\theta_2$ (h) $-\theta_2$

(i) θ_3 (j) κ_3 (k) $+\theta_3$ (l) $-\theta_3$

(m) θ_4 (n) κ_4 (o) $+\theta_4$ (p) $-\theta_4$

Figure C.36: *Curved panel with a hole loaded in compression and shear: fibre angle distribution, curvature distribution, fibre paths and thickness distributions for* $+\theta$ *and* $-\theta$*,* $n = 1$*,* $\kappa_{all} = 4.878\text{m}^{-1}$.

Curriculum vitae

Julien Marie Jan Ferdinand van Campen was born on 9 July 1982 in Nijmegen, the Netherlands. He attended Gymnasium Bernrode in Heeswijk-Dinther, the Netherlands from which he obtained a Gymnasium diploma in 2000. In the fall of 2000 he enrolled at the Faculty of Aerospace Engineering at Delft University of Technology from which he graduated with a B.Sc. degree in 2004 and an M.Sc. degree in 2006. His Master thesis project was a feasibility study for a light-weight floor concept done as part of the SuperLIGHT-CAR project, a European Union Sixth Framework Programme project. The thesis work was carried out at the Aerospace Structures and Computational Mechanics Group of the Faculty of Aerospace Engineering in cooperation with the DaimlerChrysler Research and Development Center in Ulm, Germany. In early 2007 he started working on a Ph.D. in Variable Stiffness Composite laminate design under the direction of Professor Zafer Gürdal. He was also co-responsible for the second year project for Aerospace Engineering students, familiarising students with the structural design of aerospace control systems and the use of Piezo-electric materials in such systems; in this he assisted Dr. ir. Roeland De Breuker. In 2008 he supervised a student group in the Design Synthesis Exercise at the Faculty of Aerospace engineering that researched the possibility of Delft University of Technology participating in the Google Lunar X-Prize. Julien is also a car enthusiast, which led to him becomming an active team member of the Delft University of Technology Formula Student Team, DUT Racing, from 2004 till 2009. In the fall of 2009 Julien became a member of the Operative Team of Formula Student Germany which is responsible for the organisation of the Formula Student event at the Hockenheim Ring in Germany each year in August. Julien has accepted a fixed position as a research and development engineer at Daimler where he will both work at the Daimler Research and Development Center in Ulm and the Mercedes-Benz Technology Center in Sindelfingen, Germany. In his new position he will continue to work on the design and optimisation of composite lay-ups.